

TABLE OF CONTENTS

	Page
INTRODUCTION	1
0.1 Objectives and originality	5
0.2 Background theory on aircraft modelling	7
0.3 DATCOM method	14
0.4 FDerivatives code: Description and improvements	17
0.5 Stability analysis method	42
0.6 Continuity algorithm: application on High Incidence Research Model aircraft	52
 CHAPTER 1 LITERATURE REVIEW	 71
1.1 Methods used by semi-empirical codes to calculate the aerodynamics coefficients and their stability derivatives	71
1.2 Computational Fluid Dynamics (CFD) methods	78
1.3 Weight Functions Method	80
1.4 Other methods in the literature	81
 CHAPTER 2 ARTICLE 1: NEW METHODOLOGY AND CODE FOR HAWKER 800XP AIRCRAFT STABILITY DERIVATIVES CALCULATIONS FROM GEOMETRICAL DATA	 85
2.1 Introduction	86
2.2 Brief description of the DATCOM method	88
2.3 Aircraft model	89
2.4 FDerivatives' new code	90
2.5 DATCOM improvements for stability derivatives calculations	94
2.6 Validation results obtained for the entire Hawker 800XP aircraft	105
2.7 Conclusions	111
 CHAPTER 3 ARTICLE 2: STABILITY DERIVATIVES FOR X-31 DELTA-WING AIRCRAFT VALIDATED USING WIND TUNNEL TEST DATA	 113
3.1 Introduction	114
3.2 FDerivatives' code description	116
3.2.1 FDerivatives: Logical scheme and graphical interface	117
3.2.2 FDerivatives: functions' description	121
3.2.3 FDerivatives: Improvements of DATCOM method	122
3.3 Testing with the X-31 aircraft model	124
3.4 Validation of the results obtained with the X-31 aircraft	126
3.5 Longitudinal motion analysis	135
3.6 Conclusions	142
 CHAPTER 4 ARTICLE 3: THE WEIGHT FUNCTIONS METHOD APPLICATION ON A DELTA-WING X-31 CONFIGURATION	 145
4.1 Introduction	146

4.2 Weight Functions Method description..... 147
 4.3 Application on X-31 aircraft..... 148
 4.3.1 Aircraft longitudinal motion analysis 149
 4.3.2 Aircraft lateral analysis motion..... 153
 4.4 Root Locus Map..... 156
 4.5 Conclusions..... 160

CHAPTER 5 ARTICLE 4: WEIGHT FUNCTIONS METHOD FOR STABILITY
 ANALYSIS APPLICATIONS AND EXPERIMENTAL VALIDATION
 FOR HAWKER 800XP AIRCARFT 161
 5.1 Introduction..... 162
 5.2 The Weight Functions Method 164
 5.3 Description of the model..... 166
 5.3.1 Longitudinal motion..... 166
 5.3.2 Lateral motion..... 167
 5.4 Results obtained using the weight functions method for the
 Hawker 800XP aircraft 168
 5.4.1 Results obtained for longitudinal motion using the weight functions
 method..... 169
 5.4.2 Results obtained for lateral motion using the weight functions method. 175
 5.5 Eigenvalues stability analysis of linear small-perturbation equations 180
 5.5.1 Longitudinal motion results 181
 5.5.2 Lateral motion results 184
 5.6 Conclusions..... 186

CHAPTER 6 APPLICATION OF THE WEIGHT FUNCTIONS METHOD ON A HIGH
 INCIDENCE REASEARCH AIRCRAFT MODEL 189
 6.1 Introduction..... 190
 6.2 The HIRM: Model Description and its Implementation in Admire Code 192
 6.3 The Weight Functions Method 196
 6.3.1 Longitudinal aircraft model 197
 6.3.2 Lateral aircraft model..... 198
 6.4 Results..... 201
 6.4.1 Longitudinal motion..... 201
 6.4.2 Lateral motion..... 206
 6.5 Conclusions..... 210

GENERAL CONCLUSION..... 213

RECOMMANDATIONS 217

APPENDIX A: GEOMETRICAL PARAMETERS OF THE AIRCRAFT PRESENTED IN
 REFERENCE NACA-TN-4077 219

APPENDIX B: LONGITUDINAL AND LATERAL AERODYNAMIC DERIVATIVES 221

BIBLIOGRAPHY.....225

LIST OF TABLES

	Page
Table 0.1	Notations for speeds, positions, moments of inertia, forces and moments in an aircraft's reference axis8
Table 0.2	Hawker 800XP wing characteristics10
Table 0.3	Geometrical parameters.....11
Table 0.4	Summary of the HIRM aircraft's geometrical data, along with aircraft mass and mass distribution data13
Table 0.5	DATCOM method limitations16
Table 0.6	Inputs for Wing/Canard and Horizontal/Vertical Tail's geometry21
Table 0.7	Inputs for fuselage parameters22
Table 0.8	Leading edge radius calculated versus experimental40
Table 0.9	Validation of the method presented above for the leading edge radius estimation41
Table 0.10	Airplanes classification47
Table 0.11	Levels of flying qualities.....47
Table 0.12	Flight phase categories48
Table 0.13	Points of equilibrium; initial conditions of continuity algorithm.....59
Table 1.1	Outputs of Digital DATCOM code.....74
Table 2.1	Outputs for Wing – Body – Tail configuration94
Table 2.2	Wing characteristics97
Table 2.3	Basic model geometrical characteristics98
Table 3.1	Geometrical parameters.....125
Table 3.2	Relative errors of lift coefficient variation with angle of attack127
Table 3.3	Relative errors of drag coefficient variation with angle of attack.....129

Table 3.4	Short-period motion.....	136
Table 3.5	Phugoid motion	138
Table 3.6	Static values for short-period approximation	141
Table 6.1	HIRM geometrical data.....	195

LIST OF FIGURES

	Page
Figure 0.1	The main methods used for aircraft analysis.....2
Figure 0.2	Body axis system of the aircraft.....8
Figure 0.3	Three views of the Hawker 800XP aircraft.....10
Figure 0.4	Body axes system of an HIRM aircraft.....13
Figure 0.5	Logical diagram of the new FDerivatives code19
Figure 0.6	Main window of the graphical interface for the FDerivatives code.....20
Figure 0.7	Root directory of the FDerivatives code23
Figure 0.8	Fuselage effect on the zero lift pitching moment coefficient for the wing-body configuration (median position of the wing)28
Figure 0.9	Effect of compressibility on the wing or wing-body zero lift pitching moment coefficient.....29
Figure 0.10	Pitching moment coefficient versus angle of attack estimated with FDerivatives and Digital DATCOM codes, compared with the experimental results provided by Thomas et al. (1957).....33
Figure 0.11	Pitching moment coefficient versus angles of attack for WB and WBT configurations estimated with the FDerivatives code and compared with experimental results provided by Thomas et al. (1957).....33
Figure 0.12	The ellipse that approximates the leading edge radius for the NACA 65A008 airfoil40
Figure 0.13	Logical diagram for the weight functions method44
Figure 0.14	Difference between Handling Qualities and Flying Qualities45
Figure 0.15	Diagram for developing Handling Qualities criteria.....46
Figure 0.16	Cooper-Harper rating scale49
Figure 0.17	Steps of the continuity algorithm52
Figure 0.18	Flight envelope of the HIRM aircraft.....53

Figure 0.19	ADMIRE: Main graphical window simulation and the aircraft response.....	55
Figure 0.20	Angle of attack, elevon angle and thrust variation versus airspeed V , starting at the initial conditions presented in Table 5.4 for $H = 20$ m and $M = 0.22$	64
Figure 0.21	Angle of attack, elevon angle and thrust variation versus airspeed V , starting at the initial conditions presented in Table 5.4 for $H = 3000$ m and $M = 0.22$	66
Figure 0.22	Angle of attack, elevon angle and thrust variation versus airspeed V , starting at the initial conditions presented in Table 5.4 for $H = 6000$ m and $M = 0.55$	68
Figure 0.23	The flight envelope for HIRM aircraft stabilized with control laws.....	69
Figure 1.1	3D aircraft's visualization in Digital DATCOM code.....	76
Figure 1.2	Drag coefficient due to elevator deflection results obtained with <i>aircraft_name.xml</i> command for A-380 aircraft, presented in the example given by Digital DATCOM code.....	76
Figure 1.3	Other modality to view the results for each coefficient in Digital DATCOM code.....	77
Figure 2.1	Three views of the Hawker 800XP aircraft.....	89
Figure 2.2	Logical scheme of FDerivatives code.....	91
Figure 2.3	Graphical interface of the FDerivatives code.....	93
Figure 2.4	Fuselage represented as a body of revolution.....	94
Figure 2.5	Lift coefficient distribution for the W configuration at $Re = 3.49 \cdot 10^6$	98
Figure 2.6	C_L versus α (experimental versus calculated) for WB configuration.....	99
Figure 2.7	C_m versus α (experimental and calculated), WB configuration.....	101
Figure 2.8	C_{Lq} and C_{mq} versus α , Hawker 800XP, WBT configuration.....	102
Figure 2.9	C_{Dq} versus α at the altitude $H = 30$ ft and $q = 5$ deg/s.....	102
Figure 2.10	$C_{y\beta}$ versus α at the altitude $H = 30$ ft.....	103
Figure 2.11	$C_{y\beta}$ versus α at the altitude $H = 30$ ft.....	104

Figure 2.12 $C_{n\beta}$ versus α at the altitude $H = 30$ ft104

Figure 2.13 C_L versus α at $M = 0.4$105

Figure 2.14 C_D versus α at $M = 0.4$ 106

Figure 2.15 C_L versus α at $M = 0.5$106

Figure 2.16 C_D versus α at $M = 0.5$ 107

Figure 2.17 C_m versus α at Mach number = 0.3108

Figure 2.18 $C_{y\beta}$ versus α at Mach number = 0.3108

Figure 2.19 $C_{l\beta}$ versus α at Mach number $M = 0.3$ 109

Figure 2.20 $C_{n\beta}$ versus α at Mach number $M = 0.3$ 109

Figure 2.21 C_{yp} versus α at Mach number $M = 0.3$110

Figure 2.22 C_{np} versus α at Mach number $M = 0.3$ 110

Figure 2.23 C_{lp} versus α at Mach number $M = 0.3$ 111

Figure 2.24 C_{nr} versus α at Mach number $M = 0.3$111

Figure 3.1 FDerivatives' logical scheme118

Figure 3.2 Main window.....119

Figure 3.3 Wing and Canard parameters119

Figure 3.4 Fuselage parameters120

Figure 3.5 Vertical Tail parameters120

Figure 3.6 Wing geometry for X-31 model aircraft122

Figure 3.7 Twisted nonlinear wing for the X-31 aircraft.....123

Figure 3.8 Three-views of the X-31 model125

Figure 3.9 Lift coefficient variations with angle of attack127

Figure 3.10 Drag coefficient variations with angle of attack128

Figure 3.11 X-31 aircraft fuselage, modeled as a revolution body129

Figure 3.12	Pitching moment coefficient variations with angles of attack	130
Figure 3.13	Lift and pitch moment coefficients due to the pitch rate (C_{Lq}, C_{mq}) versus the angle of attack	131
Figure 3.14	Yawing, side force and rolling moments due to the roll-rate derivatives' variations with the angle of attack.....	132
Figure 3.15	Side force, yawing and rolling moments due to the sideslip angle derivatives' variations with the angle of attack.....	133
Figure 3.16	Side force, rolling and yawing moment coefficients variation with angle of attack	135
Figure 3.17	Short-period response to phasor initial condition	138
Figure 3.18	Phugoid response to phasor initial condition	140
Figure 3.19	Short-period response to elevator step input	142
Figure 4.1	Coefficients a_i and d_j variation with the angle of attack	150
Figure 4.2	Weight functions chosen for longitudinal dynamics.....	151
Figure 4.3	Stability analyses with the weight functions method for different values of constant w_4 as a function of angle of attack	152
Figure 4.4	The c_i and b_j coefficients' variation with the angle of attack	154
Figure 4.5	Weight functions chosen for the lateral dynamics	155
Figure 4.6	Lateral-Directional stability analysis with the weight functions method for different values of constant w_3 as a function of angle of attack	156
Figure 4.7	Root locus map longitudinal motion of the X-31 aircraft	158
Figure 4.8	Root locus map for lateral motion.....	159
Figure 5.1	The a_i and d_j coefficients' variation with the angle of attack for Mach numbers $M = 0.4$ at altitude $H = 3,000$ m and $M = 0.5$ at $H = 8,000$ m.....	170
Figure 5.2	Weight functions w_{1long} , w_{2long} and w_{3long} chosen for longitudinal dynamics at Mach numbers $M = 0.4$ and 0.5 corresponding to altitudes $H = 3,000$ and $8,000$ m (left and right diagrams, respectively).....	172
Figure 5.3	Stability analysis with the WFM for different values of constant w_{4long} as a function of angle of attack for Mach number $M = 0.4$	173

Figure 5.4	Stability analysis with the WFM for different values of constant $w_{4\text{long}}$ as a function of angle of attack for Mach number $M = 0.5$	174
Figure 5.5	Weight functions variation with the angle of attack for lateral-directional motion for $M = 0.4$ and $H = 3,000$ m (left) and $M = 0.5$ and $H = 8,000$ m (right).....	176
Figure 5.6	Lateral-directional stability analysis with the WFM for different values of constant w_4 as a function of the angle of attack for $M = 0.4$	177
Figure 5.7	Lateral-directional stability analysis with the WFM for different values of constant $w_{4\text{lat}}$ as a function of the angle of attack for $M = 0.5$	180
Figure 5.8	Root locus plot (Imaginary vs. Real eigenvalues) longitudinal motion representation for $M = 0.4$ and 0.5	183
Figure 5.9	Root locus plot (Imaginary vs. Real eigenvalues) lateral directional motion representation for $M = 0.4$ and 0.5	186
Figure 6.1	ADMIRE: Main graphical window simulation and Aircraft response	194
Figure 6.2	Total weight function W for a complete range angle of attack/elevon deflection, with a null canard deflection for longitudinal motion.....	202
Figure 6.3	Stability/instability fields for longitudinal motion using the Weight Functions Method with $w_2 = 1$	203
Figure 6.4	Equilibrium curves for elevon and canard deflection angles versus angle of attack	204
Figure 6.5	Weight function W without/ with a control law at equilibrium for longitudinal motion	205
Figure 6.6	Total weight function W for a complete range of angle of attack/elevon deflection, for lateral motion.....	207
Figure 6.7	Equilibrium curves for elevon and rudder deflection angles versus angle of attack	208
Figure 6.8	Weight function W with and without a control law at equilibrium for lateral motion.....	209

LIST OF ABBREVIATIONS AND ACRONYMS

ADMIRE	Aero-Data Model in Research Environment
AG	Action Group
AOA	Angle of attack
AVT	Applied Vehicle Technology
CRIAQ	Consortium for Research and Innovation in Aerospace in Quebec
DLR	German Aerospace Center (Deutsches Zentrum für Luft-und Raumfahrt e.V.)
DNW–NWB	Low–Speed Wind Tunnel of the German–Dutch Wind Tunnels
GARTEUR	Group for Aeronautical Research and Technology in EUROpe
FM	Flight Mechanics
FOI	Swedish Defence Research Agency
HIRM	High Incidence Research Aircraft Model
HQM	Handling Qualities Method
NATO	North Atlantic Treaty Organization
LARCASE	Laboratory of Research in Active Controls, Aeroservoelasticity and Avionics
PIO	Pilot-Involved (Pilot-Induced) (Pilot-In-the-loop) Oscillations
RTO	Research and Technology Organization
SAAB	Saab AB
WFM	Weight Functions Method

LIST OF SYMBOLS

b	Wing span
\bar{c}	MAC (Mean Aerodynamic Chord)
C_A	Axial-force coefficient
C_D	Drag coefficient
$C_{D\alpha}$	Drag due to the angle of attack derivative
C_{Dq}	Drag due to the pitch rate derivative
$C_{D\dot{\alpha}}$	Drag due to the angle of attack rate derivative
$(CH)A$	Control-surface hinge moment derivative due to angle of attack
$(CH)D$	Control-surface hinge moment derivative due to control deflection
c_L	Local airfoil section lift coefficient
C_L	Lift coefficient
$(CLA)D$	Lift-curve slope of the deflected, translated surface
c_{Lmax}	Maximum airfoil section lift coefficient
C_{Lmax}	Wing maximum lift-coefficient
$C_{L\alpha}$	Lift due to the angle of attack derivative
C_{Lq}	Lift due to the pitch rate derivative
$C_{m\dot{\alpha}}$	Lift due to the angle of attack rate derivative
C_m	Pitching moment coefficient
C_{m0}	Zero pitching moment coefficient
$C_{m\alpha}$	Static longitudinal stability moment with respect to the angle of attack derivative
C_{mq}	Pitching moment due to the pitch rate derivative

$C_{m\dot{\alpha}}$	Pitching moment due to the angle of attack rate derivative
CN	Normal-force coefficient
C_{lp}	Rolling moment due to the roll rate derivative
C_{lr}	Rolling moment due to the yaw rate derivative
$C_{l\beta}$	Rolling moment due to the sideslip angle derivative
$C_{l\dot{\beta}}$	Rolling moment due to the sideslip angle rate derivative
C_{np}	Yawing moment due to the roll rate derivative
C_{nr}	Yawing moment due to the yaw rate derivative
$C_{n\beta}$	Yawing moment due to the sideslip angle derivative
$C_{n\dot{\beta}}$	Yawing moment due to the sideslip angle rate derivative
C_T	Tangential force coefficient
C_{yp}	Side force due to the roll rate derivative
C_{yr}	Side force due to the yaw rate derivative
$C_{y\beta}$	Side force due to the sideslip angle derivative
$C_{y\dot{\beta}}$	Side force due to the sideslip angle rate derivative
DELTA	Control-surface streamwise deflection angle
DELTA T	Trimmed control-surface streamwise deflection angle
D(CDI)	Incremental induced-drag coefficient due to flap deflection
D(CD MIN)	Incremental minimum drag coefficient due to control or flap deflection
D(CL)	Incremental lift coefficient in the linear-lift angle of attack range due to deflection of control surface
D(CL MAX)	Incremental maximum lift coefficient

$D(CM)$	Incremental pitching moment coefficient due to control surface deflection valid in the linear lift angle of attack
f_k	Functions used for weight functions method
g	Gravity acceleration constant
H	Altitude
I_x, I_y, I_z	Moment of inertia about the X, Y and Z body axes, respectively
I_{xz}	Product of inertia
I_{xy}	x-y body axis product of inertia
l_β	Rolling moment due to the sideslip angle derivative
$l_{\alpha\dot{\beta}}$	Rolling moment due to the roll rate derivative and alpha derivative
$l_{\alpha\delta a}$	Rolling moment due to the aileron derivative and alpha derivative
$l_{\delta a}$	Rolling moment due to the aileron derivative
$l_{\delta r}$	Rolling moment due to the rudder derivative
l_r	Rolling moment due to the yaw rate derivative
l_p	Rolling moment due to the roll rate derivative
L_p	Rolling moment due to roll rate
L_r	Rolling moment due to yaw rate
L_β	Rolling moment due to sideslip
L_δ	Roll control derivative
m	Aircraft mass
M	Mach number
M_q	Pitching moment due to pitch rate
M_u	Pitching moment increment with increased speed

XXVIII

M_α	Pitching moment due to incidence
$M_{\dot{\alpha}}$	Pitching moment due to the rate of change of the incidence
M_δ	Pitching moment due to flaps deflection
n_β	Yawing moment due to the sideslip angle derivative
$n_{\alpha p}$	Yawing moment due to the roll rate derivative and alpha derivative
$n_{\alpha \delta a}$	Yawing moment due to the aileron derivative and alpha derivative
$n_{\delta a}$	Yawing moment due to the aileron derivative
$n_{\delta r}$	Yawing moment due to the rudder derivative
n_r	Yawing moment due to the yaw rate derivative
n_p	Yawing moment due to the roll rate derivative
N_p	Yawing moment due to roll rate
N_r	Yawing moment due to yaw rate
N_β	Yawing moment due to sideslip
N_δ	Yawing moment due to flap deflection
p	Roll rate
p, q, r	Angular rates about the X, Y and Z body axes, respectively
$\dot{p}, \dot{q}, \dot{r}$	Time rate of change of p, q, r
q	Pitch rate
q/q_∞	Dynamic pressure ratio
q_∞	Dynamic pressure
r	Yaw rate
S	Wing area
t	Time

T	Thrust
T_p	Phugoid mode period
u	Forward velocity
\dot{u}	Time rate of change of u
V	Airspeed
w_k	Weight functions
W	Total Weight functions
x_{CG}	Distance between the centre of gravity of the aircraft and the quarter-chord point of wing MAC, parallel to MAC, positive for CG aft of MAC
x_{eng}	x-position of the engine's center of gravity
x_k	Unknown of the system used for weight functions method
XCP	Distance between the aircraft moment reference centre and the centre of pressure divided by the longitudinal reference length
X_u	Drag increment with increased speed
X_α	Drag due to incidence
X_δ	Drag due to flap deflection
y_β	Side force due to the sideslip angle derivative
$y_{\delta a}$	Side force due to the aileron derivative
$y_{\delta r}$	Side force due to the rudder derivative
y_r	Side force due to the yaw rate derivative
y_p	Side force due to the roll rate derivative
Y_p	Side force due to roll rate
Y_r	Side force due to yaw rate
Y_β	Side force due to sideslip

Y_{δ}	Side force control derivative
Z_q	Lift due to pitch rate
Z_u	Lift increment due to speed increment
Z_{α}	Lift due to incidence
$Z_{\dot{\alpha}}$	Lift due to the rate of change of incidence
Z_{δ}	Lift due to flap deflection
α	Angle of attack
$\dot{\alpha}, \dot{\beta}, \dot{\theta}$	Time rate of change of α, β, θ
β	Sideslip angle
δ	Control deflection
δ_a	Aileron deflection
δ_c	Canard deflection
δ_e	Elevator deflection
δ_{LEi}	Wing, leading-edge inner flaps
δ_{LEo}	Wing, leading-edge outer flaps
δ_{TE}	Wing, trailing-edge flaps
δ_r	Rudder deflection
Λ_{LE}	Quarter-chord sweep angle at Leading Edge
κ_{Ls}	Stall factor in the relation for maximum lift coefficient
$\kappa_{L\Lambda}$	Sweep factor in the relation for maximum lift coefficient
$\kappa_{L\theta}$	Twist factor in the relation for maximum lift coefficient
$\kappa_{\Lambda 1}, \kappa_{\Lambda 2}$	Sweep coefficients

λ_p	Phugoid eigenvalues
ϕ	Roll angle
Φ	Bank angle
ω_{nsp}	Short-period modal damping
ω_{np}	Phugoid modal damping
θ	Total twist (geometrical and aerodynamic)
θ	Pitch angle
ψ	Heading angle
ζ_{sp}	Short-period natural frequency
ζ_p	Phugoid natural frequency

Index

<i>B</i>	Body (Fuselage)
<i>CG</i>	Centre of Gravity
<i>LE</i>	Leading Edge
<i>H</i>	Horizontal Tail
<i>k</i>	Number of weight functions
<i>p</i>	Phugoid
<i>sp</i>	Short period
<i>TE</i>	Trailing Edge
<i>V</i>	Vertical Tail
<i>W</i>	Wing

XXXII

WB Wing Body

WBH Wing Body Horizontal Tail

WBT Wing Body Tail

INTRODUCTION

For airplanes, one of the main concerns is that the vehicle is easily controllable and maneuverable. Two different aspects are important: controllability and stability, concepts which are not equivalent. A high number of airplanes considered excellent in terms of their characteristics (dimensions, weights and performances) show a slight lateral instability called divergence spiral. Instability is no longer a problem thanks to the fly-by-wire system which replaces the conventional manual flight control. The automatic signals sent by the aircraft's computers allows to perform functions without needing the pilot's input, as in systems that automatically help stabilize the aircraft.

Today, generation of mathematical models needed to represent the various dynamics phenomena are very important in the aerospace field. Such mathematical models are conceived in many disciplines related to aerospace engineering. Major aerospace companies have developed their own codes to estimate the aerodynamics characteristics and aircraft stability in conceptual phase.

In parallel, universities have developed various codes for educational and research purpose. At LARCASE laboratory, where the projects are focused mainly in aeronautical field, a code called FDerivatives was dedicated to the analytical and numerical calculations of the aerodynamics coefficients and their corresponding stability derivatives. This code is written in MATLAB and has a user friendly graphical interface. Strongly linked to the aircraft geometry and flight conditions, the aerodynamic derivatives are needed for its stability and control analysis. Given the complexity and the scope of this project, the research was performed on the aircraft flying in the subsonic regime. Presagis gave the « Best Simulation Award » to the LARCASE laboratory for FDerivatives and data FLSIM applications.

This code can be used as a design tool, and new methods for aircraft's analysis have been added, to be able to complete the aim of this thesis. The weight functions method was applied

to study the stability and a numerical application of the continuity algorithm is presented to improve the flight envelope for minimum airspeeds.

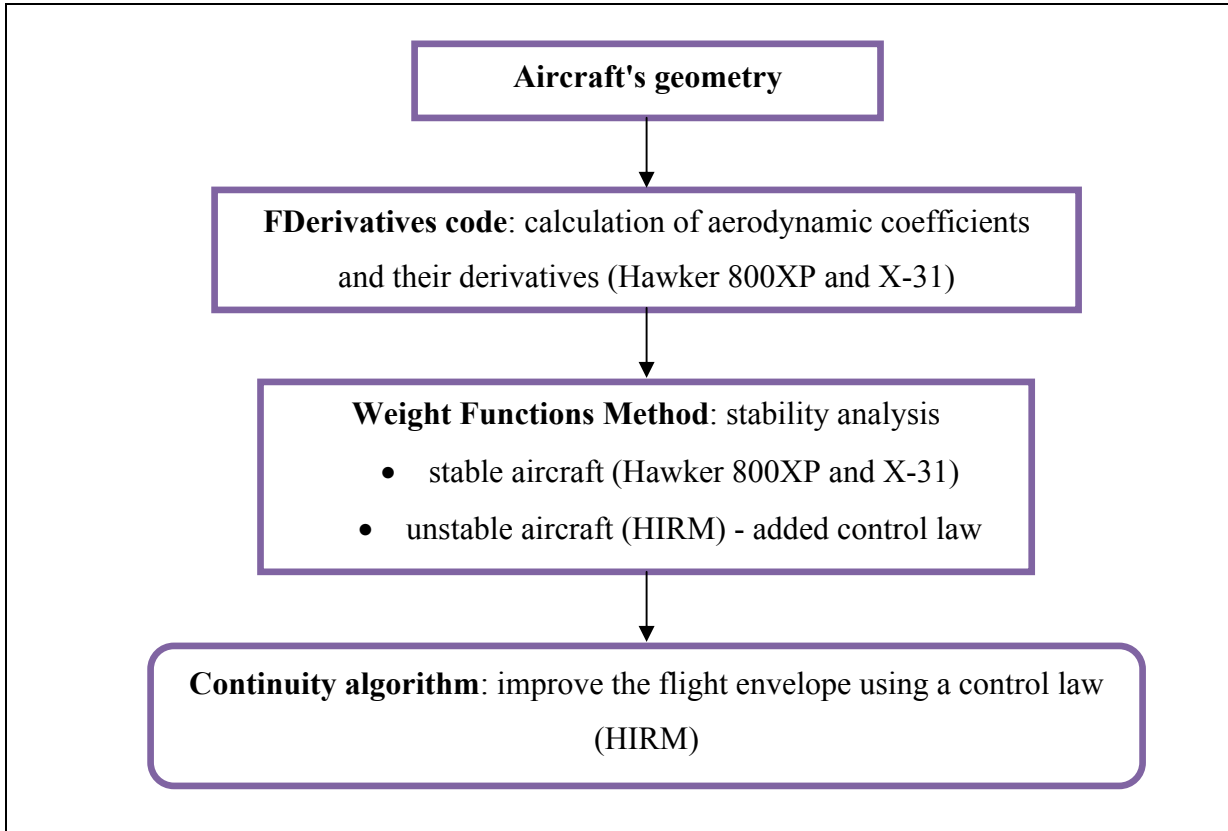


Figure 0.1 The main methods used for aircraft analysis

This research thesis is part of two projects. The first project was initiated by CAE Inc. and the Consortium for Research and Innovation in Aerospace in Quebec (CRIAQ) and the second project was funded by NATO in the frame of the NATO RTO AVT-161 program, «Assessment of Stability and Control Prediction Methods for NATO Air and Sea Vehicles ». The latter project was awarded the « RTO Scientific Achievement Award 2012 », the most prestigious award that has been offered to the AVT-161 NATO research team.

Three aircraft models were analyzed in this paper:

- The Hawker 800XP, a midsize twin-engine corporate aircraft with low swept-back one-piece wing, a high tail plane and rear-mounted engines;

- The X-31 aircraft, designed to break the « stall barrier », which allows it to fly at angles of attack that would typically cause an aircraft to stall resulting in loss of control; and
- The High Incidence Research Model (HIRM) of a generic fighter aircraft implemented in Aero-Data Model In Research Environment (ADMIRE) code, developed by the Swedish Defense Research Agency.

Four of the five journal papers presented in this thesis use the in-house results obtained with FDerivatives code. The first two papers were written in collaboration with my colleagues at the LARCASE laboratory. My contributions as main author, as well as the contributions of colleagues to each article, are specified in the Objectives and Originality section. As Ph.D. advisor, Dr. Botez is the co-author of these papers.

In the first paper, the aerodynamics and stability coefficients are estimated based for the Hawker 800XP, a mid-size corporate aircraft, using the new in-house FDerivatives code. These coefficients were further validated with the geometrical and experimental flight test data provided by CAE Inc.

The second paper was also realized by use of the same in-house code, but for a different aircraft configuration. The X-31 aircraft is a delta-wing configuration that was tested in the Low-Speed Wind Tunnel of the German-Dutch Wind Tunnels (DNW-NWB). By taking into account a minimum number of geometrical parameters delivered by German Aerospace Center (DLR), the remaining geometrical data were calculated to complete the database of the aircraft's geometry. The aerodynamics and their stability coefficients, as well as the total side force, rolling and yawing moments' coefficients were validated with wing tunnel test data. The longitudinal behavior of the aircraft about the pitch-axis reference frame was also analyzed.

We began with a code based on the geometrical parameters of an airplane, and built on that with a new method called the weight functions method. This method was applied for

longitudinal and lateral–directional dynamics studies in the last three papers. This method extends the FDerivatives code so that it can produce a complex analysis of aircraft stability, as a design tool, completed with the continuity algorithm used to estimate flight envelope minimum airspeeds.

The development of a new interface that can unify FDerivatives code with the weight functions method and a continuity algorithm could be a future project at LARCASE. Before embarking on this new project it will be necessary to validate how to choose the weight functions for similar aircraft configurations (classical configuration wing-body-tail, as in the Hawker 800XP, a wing-delta configuration, as in the X-31, and a wing-delta configuration equipped with thrust vectoring capability, as with the HIRM). Therefore, a minimum of three different aircraft will be analyzed with the weight functions method.

The weight functions method presented here is similar to the Lyapunov method, except for how the weight functions are defined. In the Lyapunov method the functions are chosen simultaneously, while for the weight functions method each weight function is selected step by step. Numerical results are presented in the last three papers.

The continuity algorithm is described in this thesis as the last step in our analysis, and numerical results are presented for HIRM aircraft in order to estimate the minimum airspeeds of the flight envelope for the model stabilized by using the control law.

This thesis is organized as follows: A literature review is presented in Chapter 1 after a detailed Introduction. An introduction to the first paper and to the FDerivatives code is provided in Chapter 2, including the detailed results and description of the FDerivatives code for the Hawker 800 XP configuration. The second paper is fully presented in Chapter 3. The weight function and the handling qualities methods are introduced and presented in Chapter 4 (for the X-31 aircraft), Chapter 5 (for the Hawker 800 XP) and Chapter 6 (for HIRM model aircraft). General conclusions and further work recommendations complete this thesis.

The following sections explain the objectives and the originality of the proposed work and the applied theory is also summarized. A detailed introduction to the FDerivatives code, how it works and its structure is presented. Stability analysis is covered in Section 0.5, where the theory is developed for the weight functions method, the handling qualities method and the continuity algorithm, with numerical results applied to HIRM aircraft.

0.1 Objectives and originality

The main objective of this thesis is to perform a more complete analysis of an aircraft in subsonic regime as a design tool, based on geometrical parameters. Its originality lies in the methods chosen to analyze the stability of three real aircraft, sustained with numerical results. In order to accomplish this task, this research treats three categories:

- The new in-house FDerivatives code, developed at LARCASE laboratory, designed to calculate the aerodynamic coefficient values and their derivatives. The results have been validated numerically for two different aircraft configurations: the Hawker 800XP and X-31 aircraft.
- The Weight Functions Method (WFM) is used as a design tool to determine an aircraft's stability. The method was applied on the Hawker 800XP, the X-31 and a High Incidence Research Aircraft Model (HIRM) aircraft.
- A continuity algorithm is used to estimate the minimum airspeeds for longitudinal dynamics of the HIRM aircraft, stabilized with the control law.

To achieve this goal, the flight test data provided by CAE Inc for the Hawker 800XP and the experimental results provided by the Low-Speed Wind Tunnel of the German-Dutch Wind Tunnels (DNW-NWB) for the X-31 model have been invaluable. With their data, along with the real airfoils' coordinates, the FDerivatives code could be validated. The High Incidence Research Aircraft Model (HIRM) developed by the Swedish Defense Research Agency and implemented in Aero-Data Model In Research Environment (ADMIRE) code was used to validate the WFM and the continuity algorithm. The flight configurations were selected because they are among the flight conditions for Cat. II Pilot Induced Oscillation (PIO)

criteria validation, performed on the FOI aircraft model presented in the PIO Handbook by the Group for Aeronautical Research and Technology in Europe, Flight Mechanics/Action Group 12.

The first step was to help to define and complete the FDerivatives code, conceived and developed to calculate the aerodynamic coefficients and static/dynamic stability derivatives of an aircraft in subsonic regime, based on its geometrical data. FDerivatives is an implementation in MATLAB of the DATCOM method, improved for estimating the pitching moment coefficient, the lift curve slope, and for the calculus of the aerodynamic parameters for airfoils specified by NACA. This will be detailed in Section 0.4, with the code description and its improvements.

The first model implemented and tested in FDerivatives code was the geometry of a Hawker 800XP, thoroughly checked and verified for missing data (such as airfoils, fuselage coordinates, among others). Each function contained in the DATCOM method was then implemented in MATLAB with the relevant improvements. The task required teamwork, and a large part of the implementation of the methods in FDerivatives code was accomplished by Mr. Dumitru Popescu.

The checking and completing of the geometry in order to implement it in Digital DATCOM and validate its first phase with flight test data was part of my work. Once the geometry was validated I switched to the MATLAB code. I first verified all the functions written earlier by my team, and then I continued to implement the derivatives functions regarding the sideslip, the roll rate and the pitch moment coefficient.

While the FDerivatives code was being completed for a typical wing-body-tail configuration, the canard model was implemented. The graphical interface was radically changed; this change can be seen in the second journal publication. The results were validated using the X-31 aircraft geometry and the wind tunnel experimental data for Mach number 0.18 at Sea

Level. This model was also tested in Digital DATCOM, where the wing was implemented as a horizontal tail and the canard as the wing parameters.

Once the code was completed and validated for two real aircraft, with different configurations, the second step was to choose and apply a new stability method called the Weight Functions Method. This new method replaces the classical Lyapunov stability criterion based on finding a Lyapunov function. Finding a Lyapunov function is not simple task and it is not always guaranteed. The Lyapunov method is very useful, however, when the linearization around the point of equilibrium leads to a matrix of evolution with eigenvalues having zero real parts.

The difference between these two methods is that the WFM finds one function at a time, with their number equal to the number of the first-order differential equations. The WFM's basic principle is to find three positive weight functions for a system with four first-order differential equations, where the fourth weight function is a constant, imposed by the user. Aircraft stability is determined from the sign of the total weight function; this sign should be negative for a stable aircraft. The Root Locus method was used to validate this new method.

The first two aircraft models were stable, and so a third, nonlinear model was used. For HIRM aircraft the WFM was applied to the original aerodynamics model implemented in ADMIRE code, as well as for the model stabilized with control laws, defined for longitudinal and lateral motions. Starting with its flight envelope, which has a non-typical shape, the continuity algorithm was chosen to improve this envelope for a HIRM model stabilized with the control law.

0.2 Background theory on aircraft modelling

The theoretical concepts on which the subsequent chapters are based are next described. An aircraft is represented in Figure 0.2 in the body axis system, which is fixed in the aircraft's

centre of gravity. The x - axis is positive forward through the nose, the y - axis is positive out through the right wing and the z - axis is positive upward.

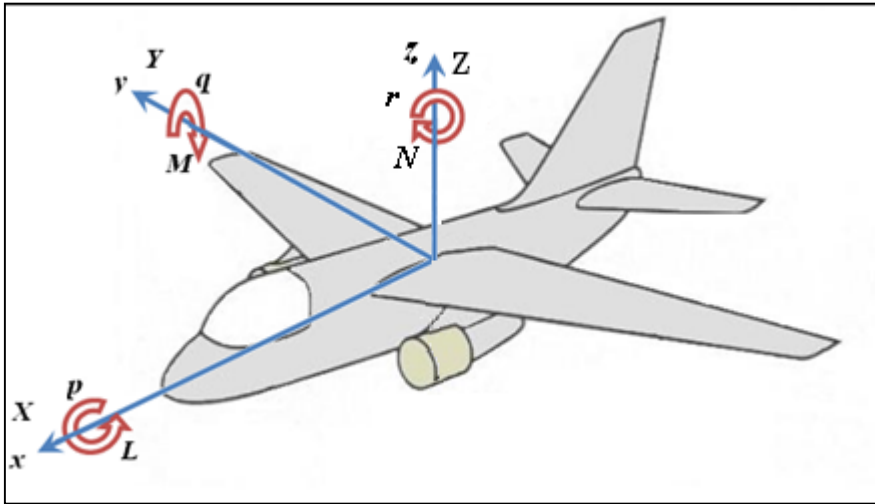


Figure 0.2 Body axis system of the aircraft

Table 0.1 presents the applied forces and moments, as well as the angular velocities and positions found in the reference axis system.

Table 0.1 Notations for speeds, positions, moments of inertia, forces and moments in an aircraft's reference axis

Axis	Linear speed	Angular speed	Angular position	Moment of inertia	Moment applied	Force applied
x	u	p roll rate	ϕ roll angle	I_x roll inertia	L	X
y	v	q pitch rate	θ pitch angle	I_y pitch inertia	M	Y
z	w	r yaw rate	ψ yaw angle	I_z yaw inertia	N	Z

The six equations of forces and moments (Etkin et al., 1996) used to analyze the Hawker 800XP and X-31 aircrafts are given by eq.(0.1):

$$\begin{aligned}
X &= m(\dot{u} + qw - rv - g \sin \theta) \\
Y &= m(\dot{v} + ru - pw - g \cos \theta \sin \phi) \\
Z &= m(\dot{w} + pv - qu - g \cos \theta \cos \phi) \\
L &= I_x \dot{p} + qr(I_z - I_y) - (\dot{r} + qp)I_{xz} \\
M &= I_y \dot{q} + (p^2 - r^2)I_{xz} + pr(I_x - I_z) \\
N &= I_z \dot{r} + (qr - \dot{p})I_{xz} + pq(I_y - I_x)
\end{aligned} \tag{0.1}$$

Three other equations are required to relate the angular rates p , q and r to the Euler angles: ϕ , θ and ψ (see eq.(0.2)).

$$\begin{aligned}
p &= \dot{\phi} - \dot{\psi} \sin \theta \\
q &= \dot{\theta} \cos \phi + \dot{\psi} \cos \theta \sin \phi \\
r &= \dot{\psi} \cos \phi \cos \theta - \dot{\theta} \sin \phi
\end{aligned} \tag{0.2}$$

The Euler rates are defined in eq.(0.3)

$$\begin{aligned}
\dot{\phi} &= p + q \sin \phi \tan \theta + r \cos \phi \tan \theta \\
\dot{\theta} &= q \cos \phi - r \sin \phi \\
\dot{\psi} &= (q \sin \phi + r \cos \phi) \sec \theta
\end{aligned} \tag{0.3}$$

The model described by eqs (0.1), (0.2) and (0.3) was used to study the stability of two different aircraft configurations, for the Hawker 800XP and the X31.

The first aircraft studied in this paper is the Hawker 800XP, a midsize twin-engine corporate aircraft with low swept-back one-piece wings, a high tailplane and rear-mounted engines, for which the maximum Mach number is equal to 0.9. This aircraft operates in the subsonic and transonic regimes. Three views of the Hawker 800XP aircraft are represented in the OXYZ reference system (Figure 0.3).

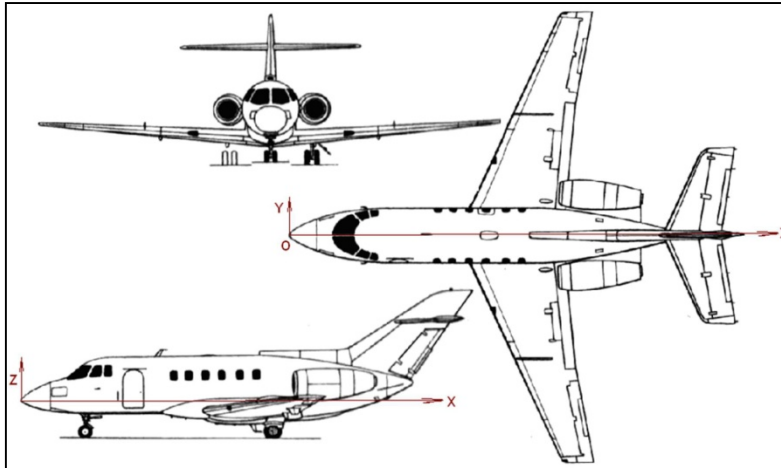


Figure 0.3 Three views of the Hawker 800XP aircraft

Table 0.2 Hawker 800XP wing characteristics

Airfoils	Root section	NACA 4420
	Tip section	NACA 4412
Taper ratio		2.5
Aspect ratio		10.05
Span		15 [ft]
Area		22.39 [ft ²]
Root chord		2.143 [ft]
MAC		1.592 [ft]
Tip chord		0.8572 [ft]
Geometrical twist		-3.5 ⁰
Aerodynamical twist		-3.4 ⁰
Sweepback angle of leading edge		12 ⁰
Dihedral angle		2 ⁰
Reynolds number		3490000

The study proposed in the present thesis is mainly based on the geometry of tested aircraft. Because the number of the parameters defining the inputs to estimate the aerodynamic and

stability coefficients in FDerivatives code is very large, it was sometimes necessary to estimate the missing geometrical data. These parameters are detailed in the next section.

The X-31 aircraft, the second aircraft analyzed, was designed to break the « stall barrier », allowing it to fly at angles of attack that would typically cause an aircraft to stall resulting in loss of control. The X-31 employs thrust vectoring paddles which are placed in the jet exhaust, allowing the aircraft's aerodynamic surfaces to maintain their control at very high angles. For its control, the aircraft has a small canard, a single vertical tail with a conventional rudder, and wing leading-edge and trailing-edge flaps.

The X-31 aircraft also uses computer controlled canard wings to stabilize the aircraft at high angles of attack. The stall angle at low Mach numbers is $\alpha = 30^0$. The X-31 model geometry (Henne et al., 2005) was given by the DLR, at the scale 1:5.6 (Table 0.3) at the AVT-161 meeting.

Table 0.3 Geometrical parameters

Fuselage length	1.725 m
Wing span	1.0 m
Wing Mean Aerodynamic Chord (MAC)	0.51818 m
Wing reference area	0.3984 m ²
Wing sweep angle, inboard	57 deg
Wing sweep angle, outboard	45 deg
Canard span	0.36342 m
Canard reference area	0.04155 m ²
Canard sweep angle	45 deg
Vertical Tail reference area	0.0666 m ²
Vertical Tail sweep angle	58 deg

The main part of the X-31 model is a wing-fuselage section with eight servo-motors for changing the angles of the canard (δ_c), the wing Leading-Edge inner/outer flaps (δ_{LEi} / δ_{LEo}), wing Trailing-Edge flaps (δ_{TE}) and the rudder (δ_r) (Rein et al., 2008). The variation of these angles, for each control surface, is given as:

- Canard: $-70^0 \leq \delta_c \leq 20^0$,
- Wing inner Leading-Edge flaps: $-70^0 \leq \delta_{LEi} \leq 0^0$,
- Wing outer Leading-Edge flaps: $-40^0 \leq \delta_{LEo} \leq 0^0$,
- Wing Trailing-Edge flaps: $-30^0 \leq \delta_{TE} \leq 30^0$,
- Rudder: $-30^0 \leq \delta_r \leq 30^0$.

The wing parameters were introduced in Digital DATCOM for the horizontal tail and the canard as a wing.

The third model in this study is the HIRM (High Incidence Research Model) (Admirer4p1), (Lars et al., 2005), (Terlouw, 1996) of a generic fighter aircraft. This aircraft model has an envelope defined by a Mach number between 0.15 and 0.5 and altitude of between 100 and 20,000 ft for the following angles: the angle of attack $\alpha = [-10 \text{ to } 30]$ degrees, sideslip angle $\beta = [-10 \text{ to } 10]$ degrees, elevon angle $\delta_e = [-30 \text{ to } 30]$ degrees, canard angle $\delta_c = [-55 \text{ to } 25]$ degrees, and rudder angle $\delta_r = [-30 \text{ to } 30]$ degrees.

The aerodynamics coefficients were obtained based on wind tunnel and flight tests (Admirer4p1) for a model « ... *originally designed to investigate flight at high angles of attack ... but [that] does not include compressibility effects resulting from high subsonic speeds.* » (Terlouw, 1996, p 21).

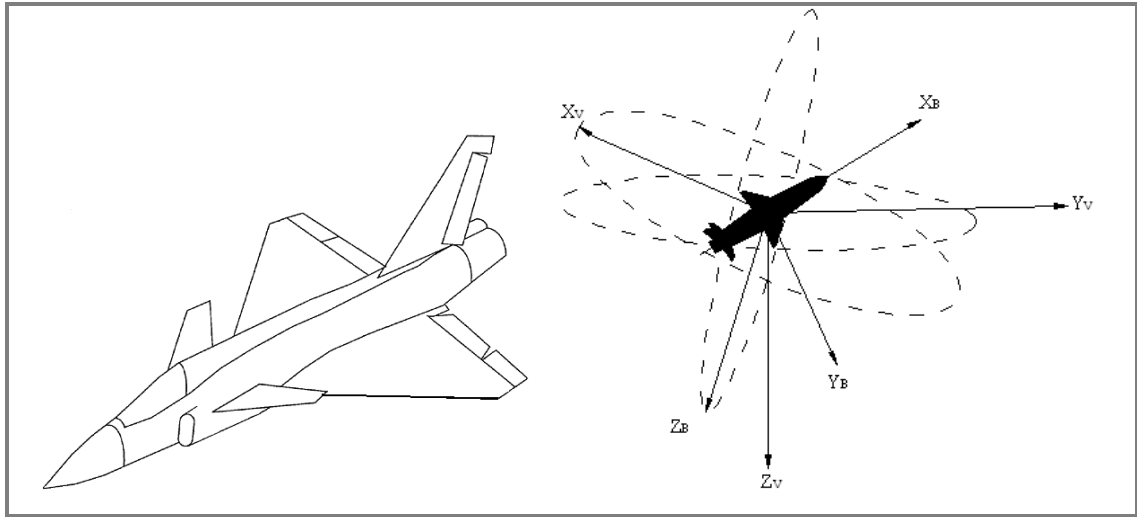


Figure 0.4 Body axes system of an HIRM aircraft

Table 0.4 Summary of the HIRM aircraft's geometrical data, along with aircraft mass and mass distribution data

Parameters	Numerical values [Units]
Wing area S	45 m^2
Wing span b	10 m
Wing Mean Aerodynamic Chord \bar{c}	5.2 m
Mass m	9100 kg
x -body axis moment of inertia I_x	21000 kgm^2
y -body axis moment of inertia I_y	81000 kgm^2
z -body axis moment of inertia I_z	101000 kgm^2
xz -body axis product of inertia I_{xz}	2500 kgm^2
z_{eng}	-0.15 m
x_{cg}	$0.25 \bar{c}$

The HIRM aircraft was evaluated (see Figure 0.4 and Table 0.4) based on the nonlinear system of equations given by eq.(0.4):

$$\left\{ \begin{array}{l}
\bar{q} S C_D - mg \sin \theta + F_{E0} \frac{\rho}{\rho_0} = m(\dot{u} + qw - rv) \\
-\bar{q} S C_Y + mg \sin \phi \cos \theta = m(\dot{v} + ru - pw) \\
\bar{q} S C_L + mg \cos \phi \cos \theta = m(\dot{w} + pv - qu) \\
-\bar{q} S b C_l = I_x \dot{p} - I_{xz} (\dot{r} + pq) - (I_y - I_x) qr \\
-\bar{q} S \bar{c} C_m + (Z_{ATP1} + Z_{ATP2}) F_{Ex} = I_y \dot{q} - I_{xz} (r^2 - p^2) - (I_z - I_x) rp \\
-\bar{q} S b C_n - (Y_{ATP1} + Y_{ATP2}) F_{Ex} = I_z \dot{r} - I_{xz} (\dot{p} - qr) - (I_x - I_y) pq \\
\dot{\phi} = p + (q \sin \phi + r \cos \phi) \tan \theta \\
\dot{\theta} = q \cos \phi - r \sin \phi \\
\dot{\psi} = \frac{(q \sin \phi + r \cos \phi)}{\cos \theta} \\
\dot{x} = u \cos \psi \cos \theta + v (\cos \psi \cos \theta \sin \phi - \sin \psi \cos \phi) + \\
\quad + w (\cos \psi \sin \theta \cos \phi + \sin \psi \sin \phi) \\
\dot{y} = u \sin \psi \cos \theta + v (\sin \psi \sin \theta \sin \phi + \cos \psi \cos \phi) + \\
\quad + w (\sin \psi \sin \theta \cos \phi - \cos \psi \sin \phi) \\
\dot{z} = -u \sin \theta + v \cos \theta \sin \phi + w \cos \theta \cos \phi
\end{array} \right. \quad (0.4)$$

0.3 DATCOM method

The aircraft geometrical parameters are: wing span, Mean Aerodynamic Chord (MAC), sweep back angle of the leading edge, reference surface, weights, thrust, speeds (minimum control speed on the ground (VMC Ground), take-off safety speed (V2) and landing reference speed or threshold crossing speed (VREF), length, height, position of the gravitational centre, position and number of the engines, among numerous others.

The required inputs are estimated as a function of the airfoils' coordinates, while the aircraft geometrical data is given in 3D coordinates.

A. Digital DATCOM limitations (Finck et al., 1978)

An aircraft's stability is measured in terms of its derivatives - the rate of change of one variable with respect to another variable. The DATCOM method, implemented in FORTRAN and called the Digital DATCOM code presents several operational limitations (Finck et al., 1978), (Williams et al., 1979a) (see Table 0.5).

- « The forward lifting surface is always input as the wing and the aft lifting surface as the horizontal tail. This convention is used regardless of the nature of the configuration.
- Twin vertical tail methods are only applicable to lateral stability parameters at subsonic speeds.
- Airfoil section characteristics are assumed to be constant across the airfoil span, or as an average for the panel. Inboard and outboard panels of a cranked or double-delta planform can have their individual panel leading edge radii and maximum thickness ratios specified separately.
- If airfoil sections are simultaneously specified for the same aerodynamic surface by an NACA designation and by coordinates, the coordinate information will take precedence.
- Jet and propeller power effects are only applied to the longitudinal stability parameters at subsonic speeds. Jet and propeller power effects cannot be applied simultaneously.
- Ground effect methods are only applicable to longitudinal stability parameters at subsonic speeds.
- Only one high lift or control device can be analyzed at a time. The effect of high lift and control devices on downwash is not calculated. The effects of multiple devices can be calculated by using the experimental data input option to supply the effects of one device and allowing Digital DATCOM to calculate the incremental effects of the second device.
- Jet flaps are considered to be symmetrical high lift and control devices. The methods are only applicable to the longitudinal stability parameters at subsonic speeds.
- The program uses the input namelist names to define the configuration components to be synthesized. For example, the presence of namelist HTPLNF causes

B. Classical aircraft configurations Wing – Body – Tail and Canard

This DATCOM reference treats the classical body–wing–tail stability and geometry including control effectiveness for a variety of high–lift/control devices. The outputs for the high–lift/control devices are usually expressed in terms of incremental effects due to control surface deflections.

Digital DATCOM code is applied to the classical aircraft, including canard configurations, in order to estimate the following characteristics:

- *Static stability characteristics.* In Digital DATCOM, where the semi–empirical DATCOM methods are computed, the longitudinal and the lateral–directional stability derivatives have been calculated in the stability axis system. The outputs are: the normal force C_N and the axial force C_A coefficients, the lift, drag and moment coefficients C_L , C_D , and C_m , as well as their corresponding longitudinal derivatives $C_{L\alpha}$, $C_{m\alpha}$, $C_{y\beta}$, $C_{n\beta}$ and $C_{l\beta}$.
- *Dynamic stability lift, pitch, roll and yaw derivatives* C_{Lq} , C_{mq} , C_{lp} , C_{np} , C_{lr} , C_{nr} , $C_{L\dot{\alpha}}$, and $C_{m\dot{\alpha}}$.
- *High–lift and control characteristics* including jet flaps, split, plain, single slotted, double slotted, fowler and leading edge flaps and slats, trailing edge flap controls and spoilers.
- *Trim data*, which can be calculated only for subsonic speeds, where $C_m = 0$. The trim option is available for the first mode configurations, as they have a trim control device on the wing or horizontal tail, and for the second mode configurations, where the horizontal tail is all–movable.

0.4 FDerivatives code: Description and improvements

With its projects focused mainly in the aerospace field, LARCASE identified the need to develop a new code for educational and research purposes. This new code, called FDerivatives, is dedicated to the analytical and numerical calculation of the aerodynamics

coefficients and their corresponding stability derivatives. FDerivatives is written in MATLAB and has a user-friendly graphical interface. Strongly linked to aircraft geometry and flight conditions, the aerodynamic coefficients and derivatives are needed for aircraft stability and control analysis. Given the complexity and scope of this project, the research was limited to aircraft flying in the subsonic regime.

C. Description of the FDerivatives code

The model implemented in the new FDerivatives code is based on the methodology used in the DATCOM procedure (Williams et al., 1979a) for calculating the aerodynamic coefficients and their stability derivatives for an aircraft. The main advantage of this new code is the estimation of the lift, drag and moment coefficients and their corresponding stability derivatives by use of relatively few aircraft geometrical data: area, aspect ratio, taper ratio and sweepback angle for the wing and for the horizontal and vertical tails. In addition, the airfoils for the wing, the horizontal and vertical tails, as well as the fuselage and nacelle parameters, are designed in a three-dimensional plane.

A logical block diagram is presented in Figure 0.5, which shows how the code works, as a function of the chosen configuration. The methods presented as a function of Mach number for a WBT configuration are also given for the other two configurations WB and W in the same four regimes: low-speed, subsonic, transonic and supersonic. The graphical interface is designed to allow the user to select the desired configuration for the calculation of the aerodynamic coefficients and stability derivatives.

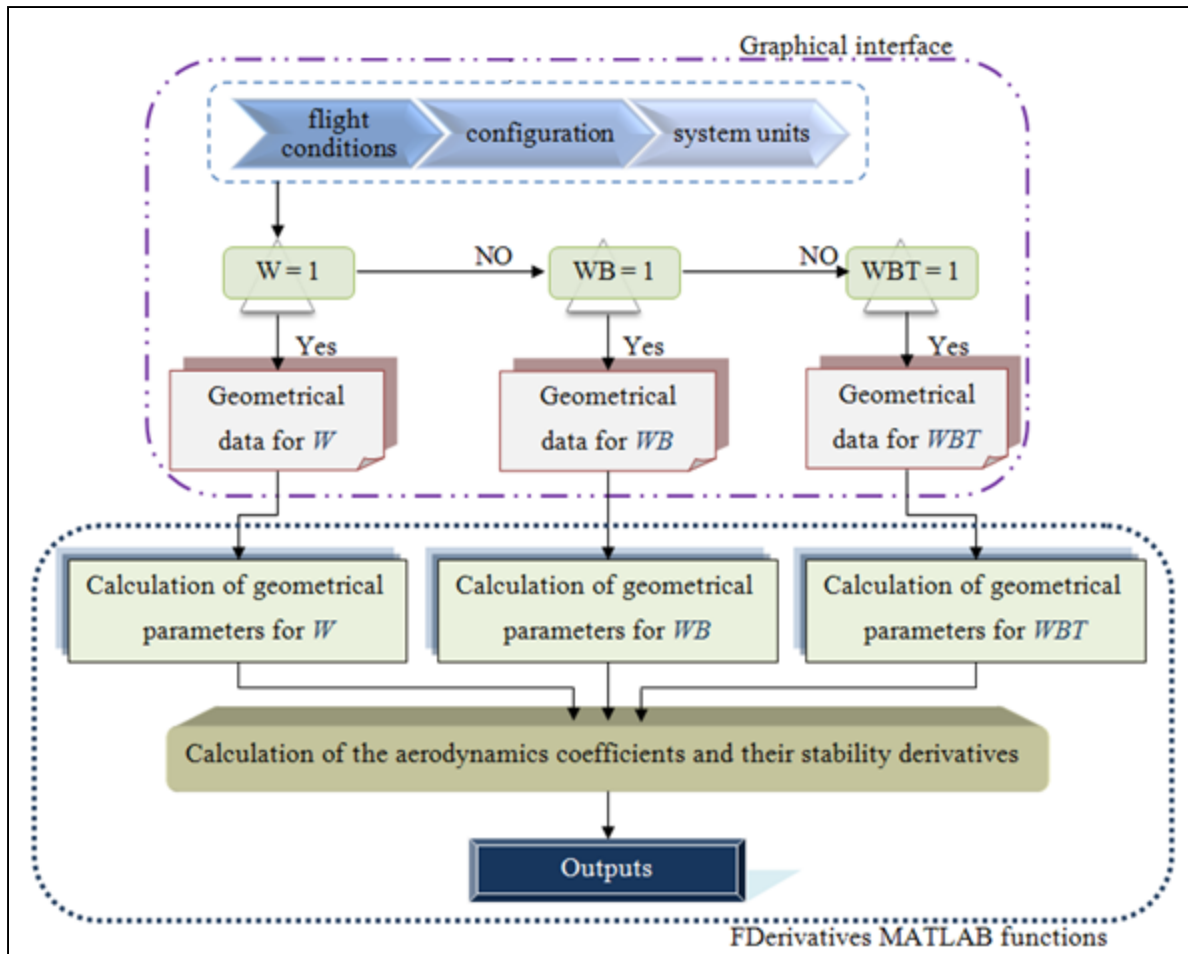


Figure 0.5 Logical diagram of the new FDerivatives code

In the FDerivatives code, the Reynolds number and the airflow speed over the aircraft are calculated by considering a theoretical atmospheric model such as the model defined by the International Civil Aviation Organization (ICAO). This model is an ideal one, in which the atmosphere is divided into seven different layers, with a linear distribution of temperature.

The main window of the graphical interface is presented in Figure 0.6. The flight characteristics (altitude, Mach number and angle of attack), the type of the platform (straight-tapered or non-straight-tapered wing or canard) and the configuration, Wing, Wing-Body or Wing-Body-Tail must be defined before the outputs can be calculated.

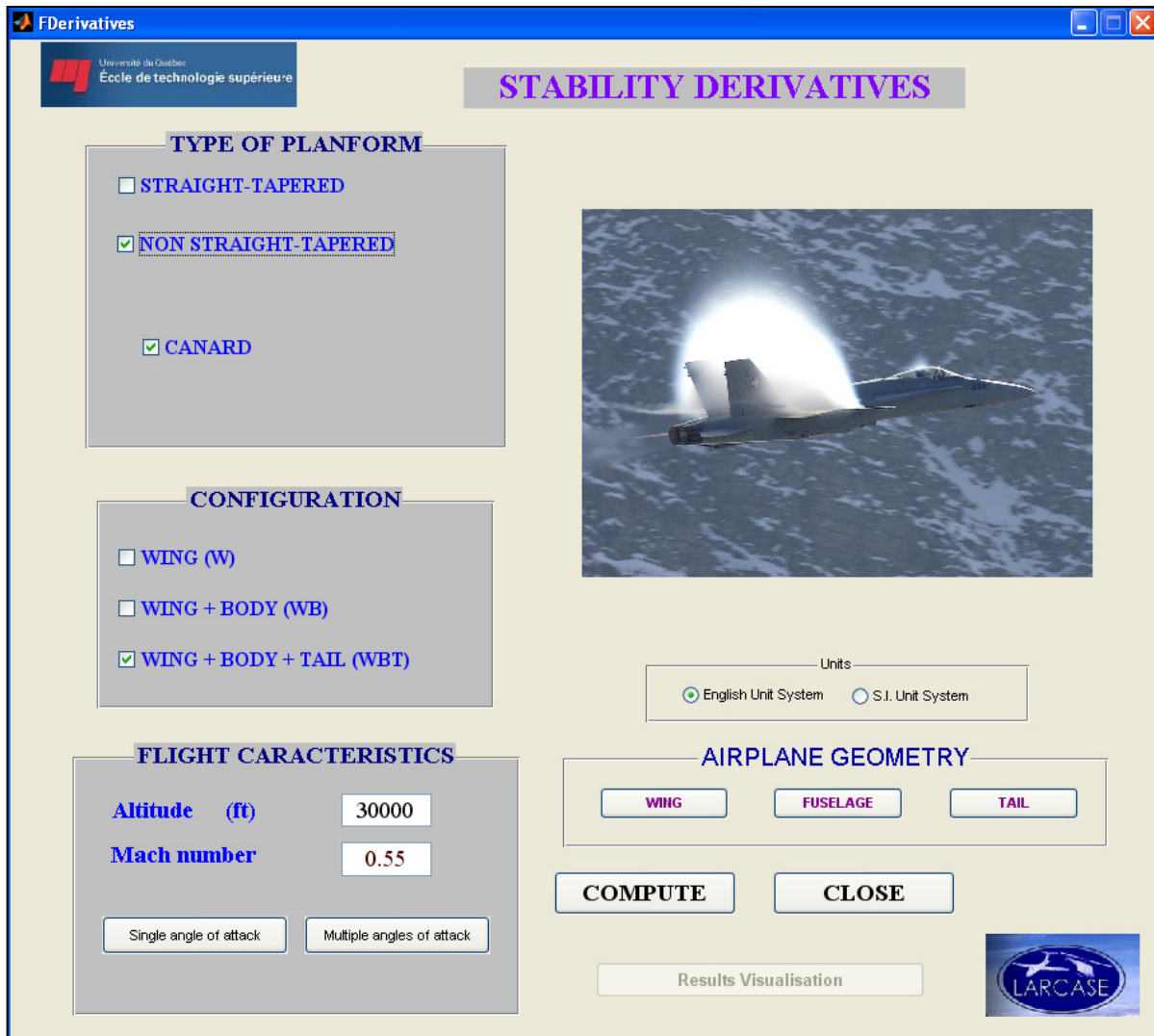


Figure 0.6 Main window of the graphical interface for the FDerivatives code

Two types of input data are needed for the program. The first set are the geometrical parameters defining the various components of an aircraft's wing, fuselage and nacelles, horizontal and vertical tails. The number of parameters is dictated by the geometry of each element, and the input done manually, through the « Airplane Geometry » graphic of the Stability Derivatives' main window software. The second set of data is composed of the coordinates of contour points, taken at representative locations on the surfaces, as well as contact points of the contour of the fuselage and nacelles. A function is responsible for their automatic import from Excel spreadsheets. The input parameters needed to calculate the aerodynamic coefficients and their stability derivatives are described in Tables 0.6 and 0.7.

The input data for the fuselage and nacelles are coordinates taken as contour points in two perpendicular planes: the horizontal plane parallel to the axis of reference of the aircraft and the vertical plane containing the axis of symmetry. These data are used for calculating the geometrical parameters required for asymmetric fuselage modeling.

Table 0.6 Inputs for Wing/Canard and Horizontal/Vertical Tail's geometry

Aspect ratio – $A_W = b^2/S_W$
Taper ratio – λ_W
Reference area [ft ²] – S_W
Quarter chord sweep angle [°] – $(A_{c/4})_W$
Dihedral angle [°] – Γ_W
Airfoils given for Root, MAC and Tip section in 3D coordinates
Parameters to estimate the Wing/Canard and Horizontal/Vertical Tail's geometry
Span [ft] – b_W
Root chord [ft] – c_{rW}
Tip chord [ft] – c_{tW}
Mean Aerodynamic Chord [ft] – \bar{c}
Lateral position of the MAC [ft]
Sweepback angle at leading edge [°] – A_{LE}
Sweepback angle at 25% chord line [°] – $A_{c/4}$
Sweepback angle at 50% chord line [°] – $A_{c/2}$
Sweepback angle at trailing edge [°] – A_{TE}
Twist of tip respect to root, negative for washout [°] – θ
Span of the exposed surface [ft] – b_{eW}
Root chord of exposed surface [ft] – c_{Re}
Tip chord of exposed surface [ft] – c_{Te}
Area of exposed surface [ft ²] – $(S_e)_W$
Sweepback angle of the exposed surface [°] – $A_{(LE)We}$
Aspect ratio of exposed surface – A_{We}

<p>Mean Aerodynamic Chord of the exposed surface [ft] – \bar{c}_{We}</p> <p>Lateral position of the MAC for exposed surface [ft]</p> <p>Twist of tip respect to root, for exposed surface $[\text{°}] - \theta_{We}$</p> <p>Sweepback angle at leading edge for exposed surface $[\text{°}] - A_{(LE)We}$</p> <p>Sweepback angle at 25% chord line for exposed surface $[\text{°}] - A_{(c/4)We}$</p> <p>Sweepback angle at 50% chord line for exposed surface $[\text{°}] - A_{(c/2)We}$</p> <p>Sweepback angle at trailing edge for exposed surface $[\text{°}] - A_{(TE)We}$</p>

Table 0.7 Inputs for fuselage parameters

<p>Body section – circular or elliptical</p> <p>Nose type – cone or ogive</p> <p>Forebody – conical or parabolic profile</p> <p>After body – conical or parabolic profile</p> <p>Body length [ft]</p> <p>Position of the gravity centre on x-axis [ft]</p> <p>Position of the gravity centre on z-axis [ft]</p> <p>Body coordinates in XOY plane and XOZ plane</p> <p>Number of nacelles</p> <p>Position Xo of the nacelle on x-axis [ft]</p> <p>Nacelle length [ft] -</p> <p>Nacelle coordinates in XOY plane and XOZ plane</p>
<p>Other usefully dimensions</p>
<p>Exposed wetted area of body (isolated body minus surface area covered by the wing at wing-body junction) $[\text{ft}^2] - (S_s)_e$</p> <p>Maximum fuselage diameter [ft] – d</p> <p>Maximum cross-section area – S_B</p> <p>Lateral fuselage area – S_{Se}</p> <p>Body base area – S_{base}</p> <p>Body side area – S_{bS}</p>

Total body volume – V_B

Wetted or surface body area excluding base area of wing at root – S_s

The new code is organized into several sub-directories, all grouped in a root directory called FDerivatives_Matlab. Figure 0.7 shows the subdirectories and part of the contents of the root directory of the code. Apart from sub-directories, this directory contains all the main MATLAB functions: the **FDerivatives.m** function which manages the main graphics window and the rest of the functions for calculating the aerodynamic coefficients and their stability derivatives.

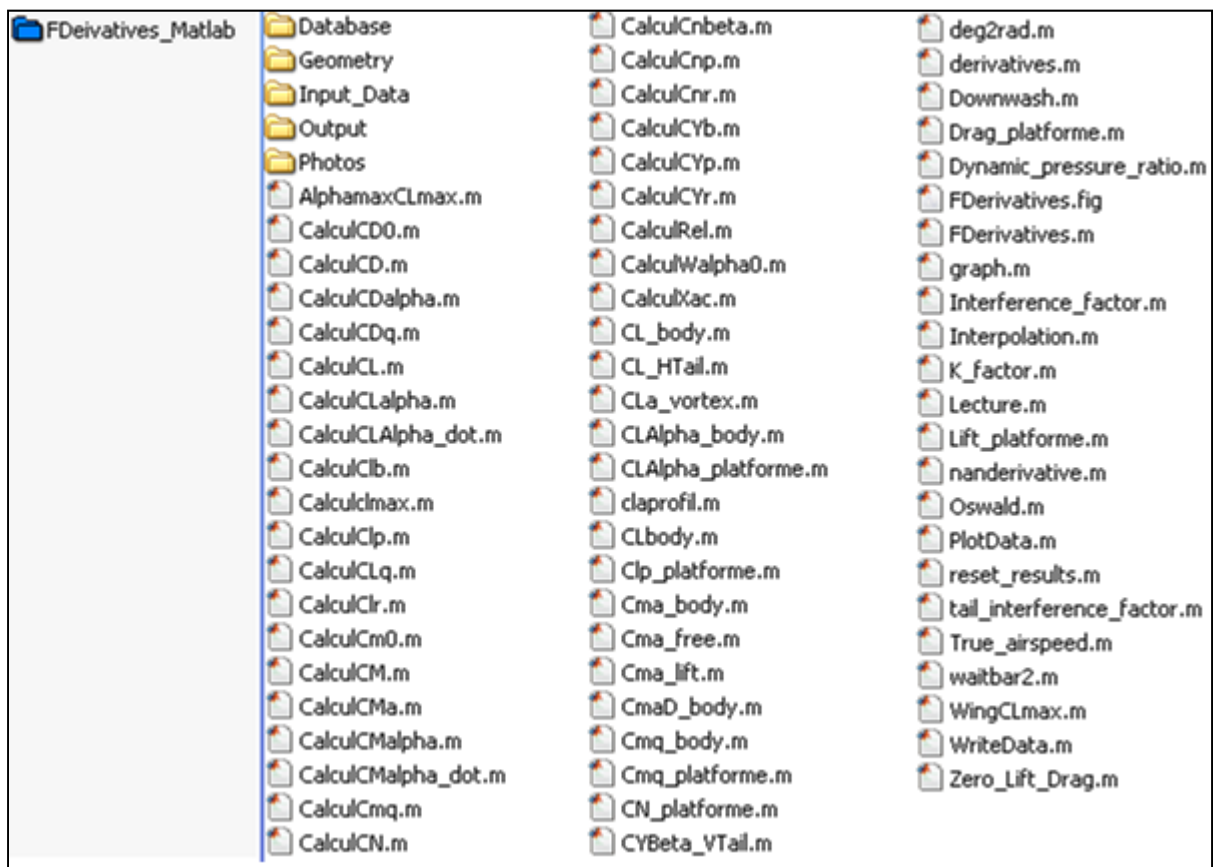


Figure 0.7 Root directory of the FDerivatives code

The subdirectories and their destinations are described below:

- **Database** folder contains all the text files containing the data obtained from the chart scanning;
- **Geometry** folder keeps all the functions, is of secondary in importance in the algorithm's operation;
- **Input_Data** folder is reserved for the parameters from the Excel data files required for the derivative calculation;
- **Output** folder represents the destination of the results at the end of program; and
- **Photos** folder stores the pictures, logos and designs used by the graphical interface.

In addition to the inputs of the Digital DATCOM code, FDerivatives code takes into account the aerodynamic contributions of nacelles, without any restrictions on their position relative to the fuselage or wing. However, for a given aircraft, the code considers only an even number of nacelles, attached either to the fuselage or to the wings, with no possibility of a combined arrangement (as in the Lockheed L1011 aircraft, for example, where the contribution of the third engine's nacelle, located on the dorsal part of the fuselage, is neglected).

For canard configuration, the wing is treated as the horizontal tail, while the canard is treated as the main wing. Neither the FDerivatives nor the Digital DATCOM code treat aircraft with three lifting surfaces, as DATCOM's methods lack that capability. By three lifting surfaces, we refer here to airplanes equipped with two main wings, one above the other (the biplane model), and aircraft with a main conventional wing, horizontal tail located at the rear and a canard in addition. The codes do not treat the winglets or vertical stabilizers with more than two lifting surfaces.

D. Improvements of the FDerivatives code to Digital DATCOM

From a methodological point of view, the new methods implemented in FDerivatives code and presented in this thesis discuss a qualitative approach. These methods promote the

approaches that we have used to produce a modern, user-friendly tool for calculating aerodynamic coefficients and stability derivatives.

For the main functions, a general model to implement all the calculation methods was developed and used in the new code. This model allows for easy replacement of the methodologies implemented, including adding new methods, and simplifies the debugging process.

Compared to Digital DATCOM's applicability limits, the FDerivatives code adds several enhancements. The possibilities of calculating have been extended to wings with variable airfoils along the span and negative sweepback. Different approaches to calculate the drag and pitching moment of the aircraft allow the results for the drag coefficient to be refined, and significantly improve the coefficient of pitching moment results. The improvements added to FDerivatives code versus Digital DATCOM code are detailed in the paragraphs that follow.

D.1. Pitching moment estimation for Wing-Body configuration in Digital DATCOM code

The solution presented and used in Digital DATCOM code for the calculus of the pitching moment estimated as a function of the angle of attack for the *WB* configuration is presented in this section. The equation implemented in the code is:

$$C_m = (C_{m0})_{WB} + (C_m)_L + (C_m)_D \quad (0.5)$$

where

$(C_{m0})_{WB}$ is the zero lift pitching moment coefficient for the *WB* configuration

$(C_m)_L$ is the moment coefficient given by the lift force as a function of the angle of attack

$(C_m)_D$ is the moment coefficient given by the drag force as a function of the angle of attack

In Digital DATCOM code, for WB configuration the terms $(C_{m0})_{WB}$ and $(C_m)_L$ are estimated verifying if the applicability criteria of two methods, where the zero lift pitching moment is estimated with eq.(0.6).

$$(C_{m0})_{WB} = \left[(C_{m0})_W + (C_{m0})_{B(W)} \right] \frac{(C_{m0})_M}{(C_{m0})_{M=0}} \quad (0.6)$$

where

$(C_{m0})_W$ is the zero lift pitching moment for the wing alone

$(C_{m0})_{B(W)}$ is the zero lift pitching moment coefficient given by the fuselage in the presence of the wing

$(C_{m0})_M / (C_{m0})_{M=0}$ is a correction factor, estimated as a function of Mach number

The zero lift pitching moment coefficient given by the fuselage in the presence of the wing presents an interesting concept. This coefficient is related to the wing position reported to the fuselage (Multhopp, 1942). Wind tunnel tests prove that $(C_{m0})_{B(W)}$ has a linear variation with the slip angle of the wing and changes significantly with the fuselage volume, while the longitudinal position of the wing and its height relative to the reference axis of the fuselage has less influence (Anscombe et al., 1950). The wing position is totally neglected in the DATCOM method, which causes a relatively large error in estimating the $(C_{m0})_{B(W)}$ coefficient, which in turn may influence the longitudinal stability derivatives calculations, including the pitching moment slope (C_{ma}) for the WB configuration.

Method given in DATCOM shows an empiric correlation obtained by a linear regression between 18 aerodynamics and geometrical parameters, appropriated to the WB configuration. To apply this method, the DATCOM procedure gives the correlation coefficients for 14 Mach number values, between $M = 0.4$ and $M = 2.5$. The Digital DATCOM code applies this method, making an extrapolation for Mach numbers up to 0.4. The DATCOM procedure specifies the reduced precision for this method, but does not specify the errors.

D.2. Zero lift pitching moment coefficient estimated in FDerivatives code

Given the arguments presented above, the linear regression method is abandoned. Instead, calculating the pitching moment coefficient given by the fuselage in the presence of the wing $(C_{m0})_{B(W)}$ is replaced with a semi-empirical method developed by the Royal Aeronautical Society and presented in reference (Etkin et al., 1998). In the FDerivatives code, this coefficient is calculated for the individual contributions of the wing, and then the fuselage contribution is added, considering (of course) the interference effects. Its calculation is given by eq.(0.7):

$$(C_{m0})_{WB} = \left[(C_{m0})_W + (C_{m0})_{B(W)} + \Delta C_{m0} \right] \frac{(C_{m0})_M}{(C_{m0})_{M=0}} \quad (0.7)$$

The first term, the zero lift pitching moment coefficient given only by the wing, $(C_{m0})_W$, is calculated based on method 1 described by the DATCOM procedure; this method is valid for all types of wings that have a the sweepback angle of equal to 45 degrees. The second term, $(C_{m0})_{B(W)}$ (eq.(0.8)), is calculated following analysis of the wind tunnel experimental data, obtained as a linear function of the angle $(i_w)_0$ between the direction of zero lift of the wing and the reference axis of the fuselage.

$$(C_{m0})_{B(W)} = \underbrace{\left[\frac{\bar{c} S_{ref} (C_{m0})_F}{(i_w)_0 S_F l_F} \right]}_{\text{term obtained by interpolation}} \frac{(i_w)_0 S_F l_F}{\bar{c} S_{ref}} \quad (0.8)$$

The term in brackets is obtained by interpolation between the curves shown in Figure 0.8, and is based on the geometric parameters related to the geometry of the *WB* configuration, namely:

- \bar{c} Mean Aerodynamic Chord of the wing;
- S_{ref} wing area;
- S_F surface of the fuselage projection in the horizontal plane;
- l_F fuselage length;
- w fuselage diameter, measured in the horizontal plane at the first quarter of the

MAC of the wing;

\bar{S}_F front surface of the fuselage projection in the horizontal plane, measured up the first quarter of the wing MAC; and

\bar{l}_F front length of the fuselage, measured in the longitudinal axis between the nose and the first quarter of the wing MAC.

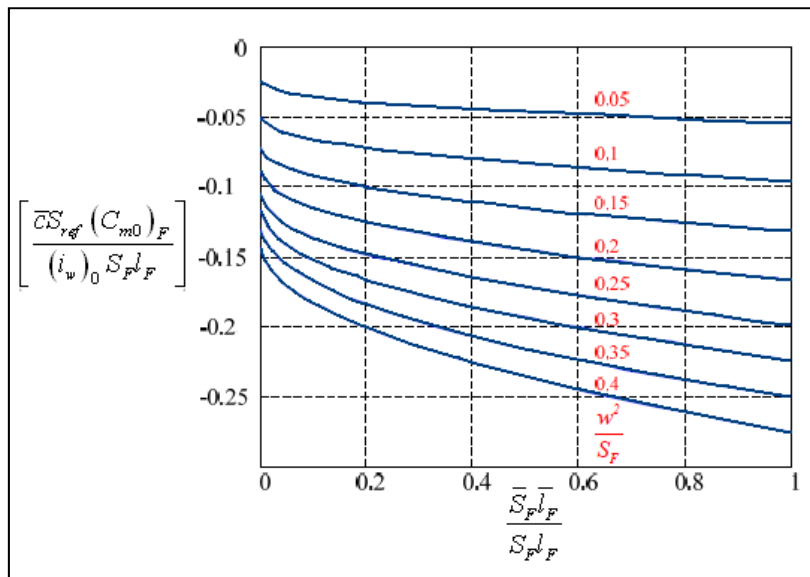


Figure 0.8 Fuselage effect on the zero lift pitching moment coefficient for the wing-body configuration (median position of the wing)

Source: This figure is a reproduction in MATLAB obtained by digitizing the curves of Figure B.8,2 (Etkin et al., 1998)

In the additional term ΔC_{m0} of eq.(0.9), the influence of the height position of the fuselage to the longitudinal axis is included and its values are next given.

$$\Delta C_{m0} = \begin{cases} +0.04 & \text{high wing} \\ 0 & \text{median wing} \\ -0.04 & \text{low wing} \end{cases} \quad (0.9)$$

The correction of the compressibility effect is given by the ratio $(C_{m0})_M / (C_{m0})_{M=0}$ and the value is obtained by interpolation as a function of Mach number, estimated starting at the curve presented in Figure 0.9.

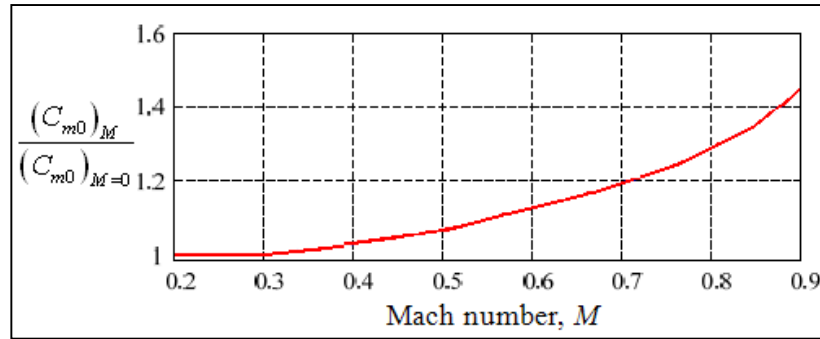


Figure 0.9 Effect of compressibility on the wing or wing-body zero lift pitching moment coefficient

Source: This figure is a MATLAB reproduction obtained by digitizing the curves of Figure 4.1.4.1–6 presented in (Williams et al., 1979a)

D.3. Pitching moment coefficient versus angle of attack for the wing-body configuration

In a rigorous formulation, the integral equation (eq.(0.10)) represents the pitching moment reported to the gravity centre of the fuselage in the wing presence.

$$(C_{m0})_{WB}(\alpha) = \int_0^{C_L(\alpha)} \left(\frac{dC_m}{dC_L} \right) d(C_L)_{WB} + (C_{m0})_{WB} \quad (0.10)$$

Under these conditions, the static margin dC_m / dC_L is estimated using eq. (0.11)

$$\left(\frac{dC_m}{dC_L} \right) = \frac{x_{CG}}{\bar{c}} + \frac{\sum(C_{m\alpha})}{\sum(C_{L\alpha})} \quad (0.11)$$

The presence of the wing changes the flow around the fuselage so that the airflow undergoes a deviation ahead of the wing, followed by a downward deflection downstream.

The result is given as a pair of destabilizing forces, proportional to the angle of attack, that reduce the slope of the moment coefficient given by the wing-body configuration (Multhopp, 1950). The contribution to the pitching moment due to the induced drag of the fuselage and the nacelles can be considered negligible by Multhopp (1950). By bringing together all the contributions to the slope of the pitching moment, we obtain (eq.(0.12)):

$$\sum(C_{m\alpha}) = (C_{m\alpha})_{BN} + (C_{m\alpha})_{W(D)} + (C_{m\alpha})_{W(B)+B(W)} + (C_{m\alpha})_{B(\varepsilon)+N(\varepsilon)} \quad (0.12)$$

The sum of the lift contributions generated by the fuselage and the nacelles are given by the term $(C_{m\alpha})_{BN}$. For a body of revolution, the slope of the pitching moment coefficient is given by eq.(0.13), and can be applied to the fuselage as well as to the nacelles.

$$C_{m\alpha} = \frac{2(k_2 - k_1)}{V_F} \int_0^{x_0} \frac{dS}{dx} (x_m - x) dx + \frac{4\alpha}{V_F} \int_{x_0}^{l_f} \eta r c_{d_c} (x_m - x) dx \quad [rad^{-1}] \quad (0.13)$$

The contribution due to the wing's drag is given by eq.(0.14):

$$(C_{m\alpha})_{W(D)} = -(C_L)_W \left(\frac{2}{\pi e A} \right) \frac{z_A}{\bar{c}} \quad (0.14)$$

where:

$(C_L)_W$ is the lift coefficient of the wing;

e is Oswald efficiency factor;

A is the wing aspect ratio; and

z_A is the vertical distance between the first quarter of wing's MAC and the aircraft gravity centre.

The contribution of the lift for the exposed wing in the presence of the fuselage to the slope of the pitching moment curve with respect to the center of gravity is given by the following (eq.(0.15)):

$$(C_{m\alpha})_{W(B)+B(W)} = \left(n - \frac{x_{ac}}{c_r} \right) \frac{c_r}{\bar{c}} \frac{S_{exposed}}{S_{ref}} (C_{L\alpha})_e \quad (0.15)$$

where:

n is the distance between the wing leading edge at the root and at the gravity centre, estimated as a function of the root chord (c_r);

$S_{exposed}$ is the exposed area of the wing; and

$(C_{L\alpha})_e$ is the lift curve slope of the exposed wing.

$$\frac{x_{ac}}{c_r} = \left(\frac{x'_{ac}}{c_{r_e}} \right) \frac{c_{r_e}}{c_r} + \frac{d}{2c_r} \tan \Lambda_{LE} \quad (0.16)$$

The last term of eq.(0.12) represents the contribution of the free moments due to the fuselage and the nacelles. For an N numbers of nacelles, this value is given as:

$$(C_{m\alpha})_{B(\varepsilon)+N(\varepsilon)} = (C_{m\alpha})_{B(\varepsilon)} + N(C_{m\alpha})_{N(\varepsilon)} \quad (0.17)$$

The calculus method for the individual contributions of the fuselage and nacelles is detailed in the DATCOM procedure.

The presence of nacelles generally has the effect of moving the aerodynamic centre forward and providing a negative contribution to the pitching moment coefficient through the lift. As we have seen, the contribution of the lift of the fuselage to the slope of pitching coefficient is expressed using eq.(0.13), which can also be applied to the nacelles. As for their effect on the position of the aerodynamic centre, the implemented method is based on the equation suggested by Torenbeek (1976), in which the individual contribution of a platform is given by eq.(0.18).

$$\Delta \left(\frac{x_{ac}}{c_r} \right) = k_n \frac{d_N^2 l_N}{c_r S_{ref} (C_{L\alpha})_{WB}} \quad (0.18)$$

where the proportionality coefficient as a function of the nacelle position by ratio of the wing or fuselage is:

$$k_n = \begin{cases} -4 & \text{nacelle placed on the wing} \\ -2.5 & \text{nacelle placed on the fuselage} \end{cases} \quad (0.19)$$

l_N = nacelle length;

d_N = maximal diameter of nacelle; and

$(C_{L\alpha})_{WB}$ = lift curve slope for the WB configuration.

The expression (0.18), multiplied by the number N of the nacelles, is added to eq.(0.16) to obtain the position of the aerodynamic center x_{ac} of the WB configuration.

D.4. Pitching moment coefficient for the wing-body-tail configuration

The total pitching moment coefficient for an aircraft is calculated as the sum of two major contributions (see eq.(0.20)): wing-body-nacelles $(C_m)_{WBN}$ and the horizontal tail contribution $(C_m)_H$, considering the effects of interferences between the horizontal tail and the fuselage, given by eq.(0.21) .

$$C_m = (C_m)_{WBN} + (C_m)_H \quad (0.20)$$

where:

$$(C_m)_H = \left[\frac{x_{CG}}{\bar{c}} + \frac{x_H}{\bar{c}} \right] (C_L)_H \quad (0.21)$$

x_{CG} is the longitudinal distance between the centre of gravity and the wing leading edge at the root;

x_H is the longitudinal distance between the first quarter of the horizontal tail's root chord and the wing leading edge at the root; and

$(C_L)_H$ is the horizontal tail lift coefficient calculated in the wing-body presence.

Supplementary results are presented in this section for a simple configuration presented by Thomas et al., (1957). Because the purpose of this work is to present the improvements added to FDerivatives code versus the DATCOM method, and implicitly versus the Digital DATCOM code, the moment coefficient for a third aircraft configuration was tested. The geometrical data are given in APPENDIX A. The results are presented for Mach number 0.13, Reynolds number of $0.71 \cdot 10^6$ and aspect ratio $AR = 4$.

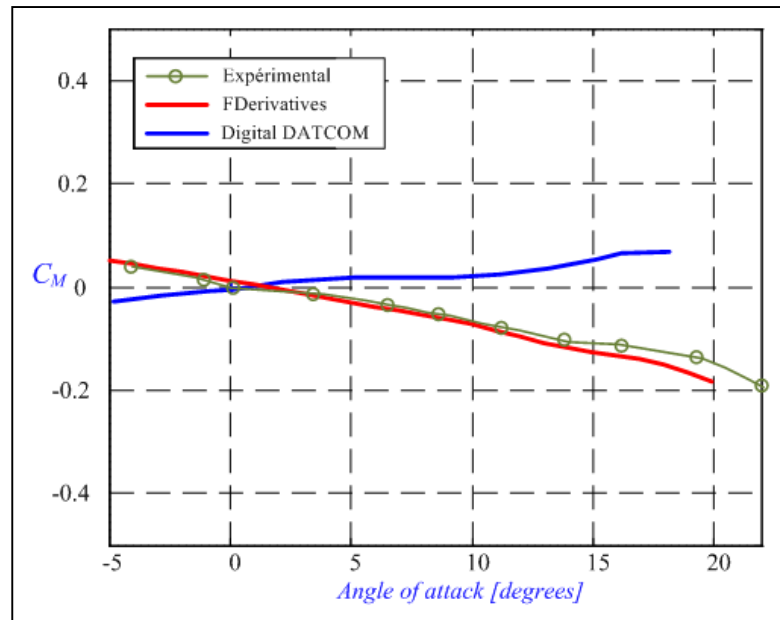


Figure 0.10 Pitching moment coefficient versus angle of attack estimated with FDerivatives and Digital DATCOM codes, compared with the experimental results provided by Thomas et al. (1957)

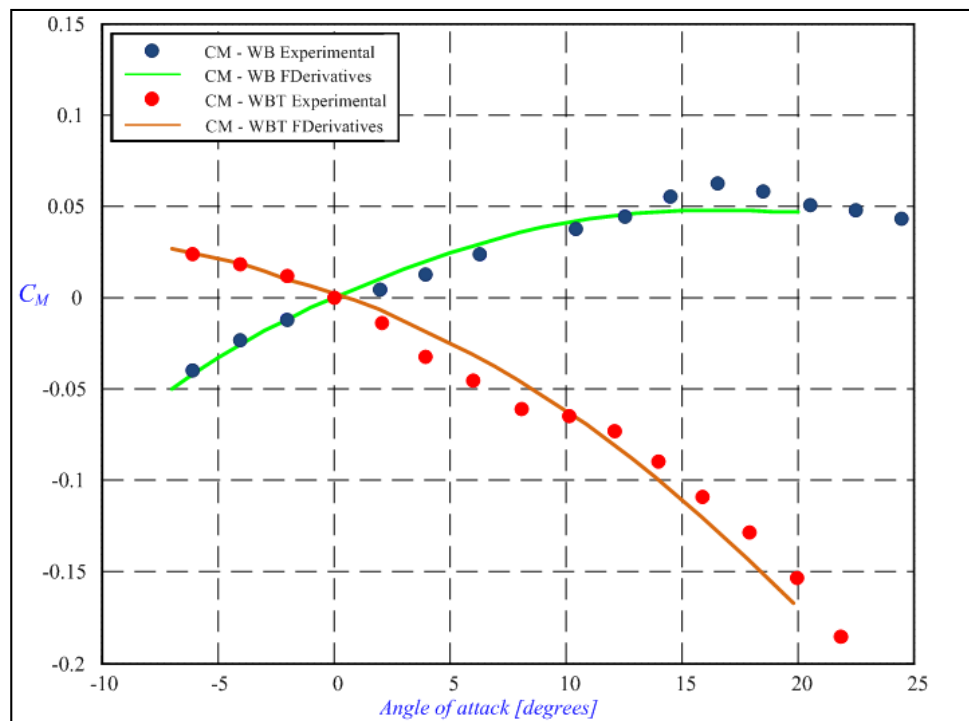


Figure 0.11 Pitching moment coefficient versus angles of attack for WB and WBT configurations estimated with the FDerivatives code and compared with experimental results provided by Thomas et al. (1957)

For all of the angles of attack presented in Figure 0.10 the pitching moment coefficient provided by the FDerivatives code is closer to the experimental results. It can be seen that the Digital DATCOM results are far from the experimental results. Therefore, in Figure 0.11 the only the FDerivatives code results versus the experimental results are presented, for two configurations: wing-body and wing-body-tail. It is obvious that the improvements to the FDerivatives code are found in the accuracy of the results.

E. Estimation of geometrical parameters in FDerivatives code versus Digital DATCOM code

Some of the most important inputs in any code that depends on aircraft geometry are the airfoil coordinates. The accuracy of their definition may change the results. Because the DATCOM method has its limitations, the next two sections present the improvements implemented in FDerivatives code for the airfoil coordinates and the calculus of the airfoil radius at the leading edge.

E.1. Airfoil coordinates implementation

In Digital DATCOM code, there are three methods to define an airfoil. The first method is the simplest: a NACA airfoil is defined by giving its standard name.

The second method is to provide an array of values, using the average curvature (the skeleton of the profile) and the thickness. If this method is selected, then inputs to introduce are the coordinates of a number of points, up to 50, situated on the curve of the average steepness of the profile and expressed in an orthonormal frame, with its origin as the leading edge of the profile. This distance, by definition, is the reference chord of the profile and of the x -axis. The user must also enter the values of the thickness of the profile corresponding to the abscissas of the points.

The third method consists of providing an array of values: the ordinates of the upper and lower surfaces in an orthonormal system with its origin as the leading edge of the profile and

the string equal to unity as the axis abscissa. The user must provide the ordinates of a number of points, up to 100, distributed evenly over the upper and lower profile (50 points for each surface). In addition, the values of the corresponding abscissa of the upper points should coincide with the abscissa values of the items on the lower surface.

E.2. Calculus of airfoil radius at the leading edge

The aerodynamic parameters, such as the ideal angle of attack, pitching moment and zero lift angle of attack, are obtained using the thin airfoils theory. The airfoil lift curve slope $c_{l\alpha}$ is calculated using the method developed by Weber (1955). The next step consists of correcting the compressibility and viscosity effects.

Weber's method requires the explicit equation of the camber's curve, the thickness distribution around the camber and the radius of the leading edge (r_{LE}) of the airfoil as input data. It is impossible to obtain the analytical equation of the camber curve from the coordinates of points of the airfoil contour. The Digital DATCOM code approximates it with a function defined by fragments using a smoothing method. The quality of the smoothing depends mainly on the optimal choice of contour points.

In the geometric sense, the radius of the leading edge is the radius of the minimum circle closest to the curve of the airfoil at the leading edge. Called the circle of camber or the osculating circle, it is located inside the concavity of the profile curve, tangent to the point defining the curve. In other words, the osculating circle is the best approximation of the curve in one point, a priori better than the tangent at this point. For a given function $y(x)$, twice differentiable, the radius of camber R (or the radius of the osculating circle) at any point is given by eq.(0.22).

$$R = \frac{\left[1 + \left(\frac{dy}{dx} \right)^2 \right]^{\frac{3}{2}}}{\frac{d^2 y}{dx^2}} \quad (0.22)$$

The calculation of the radius of the leading edge using eq.(0.22) requires explicit knowledge of the analytical expression of the function $y(x)$. We suggest replacing this function $y(x)$ by the equation of the ellipse that approximates, as closely as possible, the leading edge of the airfoil. The algorithm implemented in FDerivatives code is based on a non-iterative method (Fitzgibbon et al., 1996) and perfected by Halliř et al. (1998) to identify the equation of the ellipse, which is a special conic case with the general equation written as:

$$F(x, y) = AX = a_1x^2 + a_2xy + a_3y^2 + a_4x + a_5y + a_6 = 0 \quad (0.23)$$

By adding the condition $4a_1a_3 - a_2^2 > 0$, eq. (0.23) becomes the ellipse equation. Suppose that around the leading edge of the airfoil we have N points on its contour. Consider a point P_i on the airfoil contour and replace the (x_i, y_i) coordinates in the equation of the ellipse, eq.(0.23). Since the point P_i is not necessarily on the ellipse, its coordinates satisfy eq.(0.23) to a residue such that $F(x_i, y_i) = r_i$, $r_i \in R$, where r_i is the absolute error.

Over one contour point of the airfoil is close to the ellipse, plus the value of error r_i approaches zero. Because the error r_i can take negative values, it is more convenient to use the positive value obtained by the error square. By calculating the residue r_i for each point N on the contour of the profile and making the sum of their squares, an expression g dependent on the ellipse's parameters a_i , with $i = 1 \div 6$, is obtained in the form of eq. (0.24):

$$g(a_1, \dots, a_6) = \sum_{i=1}^N F(x_i, y_i)^2 = \|\mathbf{DA}\|^2 = \sum_{i=1}^N r_i^2 \quad (0.24)$$

where \mathbf{D} is the matrix of order $(N, 6)$ constructed with the coordinates of N points situated on the airfoil's contour:

$$\mathbf{D} = \begin{bmatrix} x_1^2 & x_1y_1 & y_1^2 & x_1 & y_1 & 1 \\ \cdot & \cdot & \cdot & \cdot & \cdot & \cdot \\ x_i^2 & x_iy_i & y_i^2 & x_i & y_i & 1 \\ \cdot & \cdot & \cdot & \cdot & \cdot & \cdot \\ x_N^2 & x_Ny_N & y_N^2 & x_N & y_N & 1 \end{bmatrix}$$

The approximation problem at the leading edge of an ellipse is reduced by minimizing the total squared errors (0.24) under the constraint of inequality. The values of the variables a_i , i

$= 1 \div 6$ bring the function $g(a_1, \dots, a_6)$ to a minimum. They are the parameters of the ellipse that best match the airfoil contour. In ideal circumstances, when the points N of the profile simultaneously belong to the ellipse, the total square errors approaches zero. The classical approach to solving an optimization with nonlinear constrained inequality is the application of Lagrange's multipliers method under the conditions of Karush-Kuhn-Tucker. In practice, taking these conditions into account is complicated, as several possible aspects must be considered without guaranteeing an optimal solution (Rao, 1996). Rao (1996) used the invariance property of a conic with respect to multiplication with a scalar, which offers a simplistic approach that reduces the optimization problem with inequality constraint to an optimization problem with an equality constraint. According to Rao (1996), multiplying the expression (0.23) by a real number of a particular value can make the inequality constraint $4a_1a_3 - a_2^2 > 0$ an equality constraint:

$$4a_1a_3 - a_2^2 = 1. \quad (0.25)$$

Using the matrix form, the identity defined by eq.(0.25) can be written in the following form

$$\mathbf{A}^T \mathbf{C} \mathbf{A} = 1 \quad (0.26)$$

where \mathbf{C} is the square matrix with constant coefficients of order 6 defined by eq. (0.27).

$$\mathbf{C} = \begin{bmatrix} 0 & 0 & 2 & 0 & 0 & 0 \\ 0 & -1 & 0 & 0 & 0 & 0 \\ 2 & 0 & 0 & 0 & 0 & 0 \\ 0 & 0 & 0 & 0 & 0 & 0 \\ 0 & 0 & 0 & 0 & 0 & 0 \\ 0 & 0 & 0 & 0 & 0 & 0 \end{bmatrix} \quad (0.27)$$

Using Lagrange's multipliers method to minimize the function given by eq.(0.24) under its constraint the function $\mathbf{L}(\lambda, \mathbf{A})$ defined by eq.(0.28) is given, where the parameter λ is a real number, known as the Lagrange parameter.

$$\mathbf{L}(\mathbf{A}, \lambda) = \|\mathbf{D}\mathbf{A}\|^2 + \lambda(\mathbf{A}^T \mathbf{C} \mathbf{A} - 1) \quad (0.28)$$

The equivalent matrix system of equations obtained by applying the gradient operator is written as:

$$\begin{cases} \mathbf{D}^T \mathbf{D} \mathbf{A} = \lambda \mathbf{C} \mathbf{A} \\ \mathbf{A}^T \mathbf{C} \mathbf{A} = 1 \end{cases} \quad (0.29)$$

To approach an ellipse, for a minimum number of points $N = 5$, the system (0.29) admits a solution set consisting of six pairs $(\lambda_j, \mathbf{A}_j)$, of which only one minimizes the total squared error. What can be remarked? The first observation is that the total square error $\|\mathbf{D}\mathbf{A}\|^2$, which can be written using the properties of matrices as eq.(0.30), establishes the equivalence between the total squared error and the variable λ of the system (eq.(0.29)):

$$\|\mathbf{D}\mathbf{A}\|^2 = \mathbf{A}^T \mathbf{D}^T \mathbf{D} \mathbf{A} = \lambda \underbrace{\mathbf{A}^T \mathbf{C} \mathbf{A}}_1 = \lambda \quad (0.30)$$

The second remark relates to the shape of the first equation of system (0.29), which is actually an equation for eigenvalues λ and eigenvectors $(\mathbf{C}\mathbf{A})$. Among the solutions of the system (0.29), of the six eigenvalues λ_i , only one is positive and corresponds to the minimal value of the total squared error expressed by eq.(0.30). This reduces the minimization problem in searching for the positive eigenvalue whose corresponding eigenvector is composed by the ellipse's coefficients that best approximate the curve of the airfoil.

In summary, the smallest positive eigenvalues λ of the matrix $\mathbf{M} = (\mathbf{D}^T \mathbf{D} \mathbf{C}^{-1})$ represent the minimum total square error given by eq.(0.30). Matrix \mathbf{C} is a singular matrix because of its particular shape.

$$\mathbf{C}(\mathbf{D}^T \mathbf{D})^{-1} \mathbf{C} \mathbf{A} = \frac{1}{\lambda} \mathbf{C} \mathbf{A} \quad (0.31)$$

Using eq.(0.31) avoids the singularity problem of matrix \mathbf{C} , but introduces a new problem with a possible singularity of the matrix $\mathbf{S} = \mathbf{D}^T \mathbf{D}$. Theoretically, matrix \mathbf{S} is singular if all N points satisfy the equation for the same ellipse (Rao, 1996).

In practice, because of the inaccuracy of the rounding errors for a large number of points belonging to an ellipse, matrix \mathbf{S} is singular and Fitzgibbon's algorithm can be applied without problems. This probability rapidly becomes significant for a small number of points, as in the case of the FDerivatives code, which only uses the coordinates of 11 points from the

leading edge of the airfoil. To avoid these singularity problems, we use an approach proposed by Hallíř et al. (1998) that divides the matrix \mathbf{S} into three sub-matrices of order 3 by the process:

$$\mathbf{S} = \begin{bmatrix} \mathbf{S}_1 & \mathbf{S}_2 \\ \mathbf{S}_2^T & \mathbf{S}_3 \end{bmatrix}$$

$$\mathbf{S}_1 = \begin{bmatrix} \mathbf{S}_{x^4} & \mathbf{S}_{x^3y} & \mathbf{S}_{x^2y^2} \\ \mathbf{S}_{x^3y} & \mathbf{S}_{x^2y^2} & \mathbf{S}_{xy^3} \\ \mathbf{S}_{x^2y^2} & \mathbf{S}_{xy^3} & \mathbf{S}_{y^4} \end{bmatrix}, \mathbf{S}_2 = \begin{bmatrix} \mathbf{S}_{x^3} & \mathbf{S}_{x^2y} & \mathbf{S}_{x^2} \\ \mathbf{S}_{x^2y} & \mathbf{S}_{xy^2} & \mathbf{S}_{xy} \\ \mathbf{S}_{xy^2} & \mathbf{S}_{y^3} & \mathbf{S}_{y^2} \end{bmatrix}, \mathbf{S}_3 = \begin{bmatrix} \mathbf{S}_{x^2} & \mathbf{S}_{xy} & \mathbf{S}_x \\ \mathbf{S}_{xy} & \mathbf{S}_{y^2} & \mathbf{S}_y \\ \mathbf{S}_x & \mathbf{S}_y & 1 \end{bmatrix} \quad (0.32)$$

The elements of these matrices are given by:

$$S_{x^m y^m} = \sum_{i=1}^N x_i^m y_i^m \quad (0.33)$$

Next, the authors replace the singular matrix \mathbf{C} , associated with condition (0.26), with the regular matrix \mathbf{C}_1 (eq.(0.34)), and reduce the matrix \mathbf{M} at a 3-dimensional square matrix \mathbf{M}_1 given by eq.(0.34) (Hallíř et al., 1998):

$$\mathbf{M}_1 = \mathbf{C}_1^{-1} [\mathbf{S}_1 - \mathbf{S}_2 \mathbf{S}_3^{-1} \mathbf{S}_2^T], \quad \mathbf{C}_1 = \begin{bmatrix} 0 & 0 & 2 \\ 0 & -1 & 0 \\ 2 & 0 & 0 \end{bmatrix} \quad (0.34)$$

The matrix \mathbf{M}_1 has two negative eigenvalues and one positive (or zero if all points belong to an ellipse) which coincide with the only positive eigenvalue of matrix \mathbf{M} . It should be noted that the matrix \mathbf{S}_3 can be singular only if the N chosen points are collinear.

FDerivatives uses a code, apart from the leading edge, composed of the coordinates of 5 points situated on the upper surface and of 5 points that belong to the lower surface. Initially the code built the matrix \mathbf{D} using the coordinates of 11 points situated at the leading edge. Next, the code constructs matrices \mathbf{S}_1 , \mathbf{S}_2 , \mathbf{S}_3 and matrix \mathbf{M}_1 . Finally, the code calculates the matrix \mathbf{M}_1 and retains the positive eigenvalues with which the code constructs the correspondent eigenvector. Once the ellipse equation has been determined, the FDerivatives code calculates the camber radius at the airfoil's leading edge, using eq.(0.22). The results for

the NACA 65A008 airfoil (Thomas et al., 1957) are presented in Figure 0.12 to verify the FDerivatives calculations.

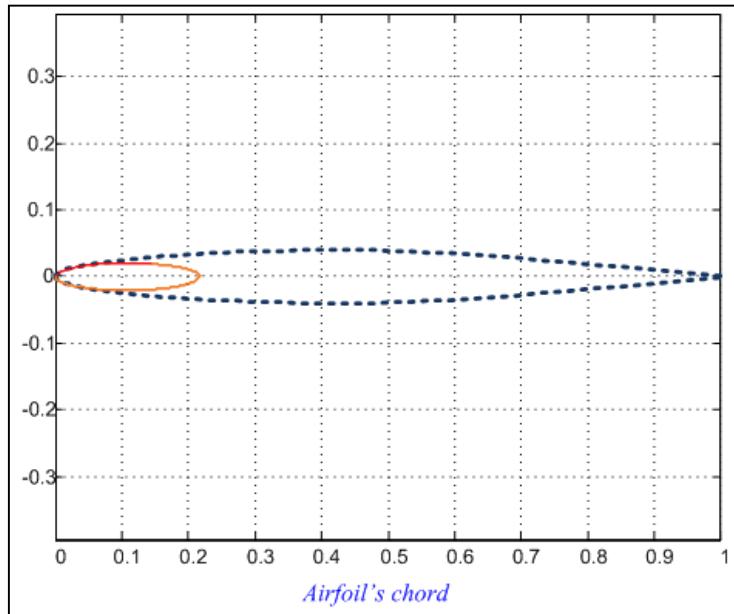


Figure 0.12 The ellipse that approximates the leading edge radius for the NACA 65A008 airfoil

Relative error of this method versus the experimental results is given in Table 0.8 for the NACA 65A008.

Table 0.8 Leading edge radius calculated versus experimental

	<i>NACA-TN-4077</i> (Thomas et al., 1957)	<i>FDerivatives</i> code	<i>Digital DATCOM</i> code
Leading edge radius	0.00408	0.0038	0.00293
Relative error		6.86%	28.18%

Ten other airfoils were tested and the relative errors have been estimated for experimental versus FDerivatives and Digital DATCOM codes (see Table 0.8). It can be seen that the method used in our code is better than the method implemented in Digital DATCOM, because in Digital DATCOM code the results are similar for the 4-digit or 6-series of NACA

airfoils with the same maximum thickness as chord percentages. The maximum camber, the camber position and the location of the minimum pressure coefficient are not considered in the calculus of the radius airfoil at the leading edge.

Table 0.9 Validation of the method presented above for the leading edge radius estimation

Airfoil	Test value	<i>FDerivatives</i> code	<i>Digital DATCOM</i> code	Relative error (vs. <i>FDerivatives</i>)	Relative error (vs. <i>Digital DATCOM</i>)
NACA 1410	0.0110	0.01101	0.01102	-0.09%	-0.18%
NACA 2410	0.0110	0.01101	0.01102	-0.09%	-0.18%
NACA 63210	0.0770	0.07680	0.01102	0.26%	85.68%
NACA 65210	0.0687	0.06850	0.01102	0.29%	83.95%
NACA 2415	0.0248	0.02480	0.02479	0.0%	0.04%
NACA 4415	0.0248	0.02480	0.02479	0.0%	0.04%
NACA 23015	0.0248	0.02481	0.02479	-0.04%	0.04%
NACA 63 ₂ 615	0.01594	0.01601	0.02546	-0.044%	-59.72%
NACA 2418	0.0356	0.03562	0.03570	-0.056%	-0.28%
NACA 66206	0.00223	0.00225	0.00397	-0.89%	-79.02%

0.5 Stability analysis method

This section provides theoretical descriptions of the methods used in the stability analysis: the Weight Functions Method (WFM), the Handling Qualities Method (HQM) and the continuity algorithm. The stability analysis results are presented for X-31 aircraft (Chapter 3), for the Hawker 800XP (Chapter 4) and for the HIRM aircraft (Chapter 5). The continuity algorithm is applied to the HIRM in section 0.4.4, along with the new flight envelope based on the model with control law. The mathematical formulas for stability derivative calculations are given in APPENDIX B.

F. Weight functions method (WFM)

In most practical problems, the differential equations that model the behavior of a dynamic system often depend on one or more parameters. The WFM is more efficient than the classical Lyapunov function method, since only one function has to be found at a time. The Lyapunov stability criteria are based on finding a Lyapunov function, which is not simple and is not always guaranteed. The Lyapunov method is very useful, however, when the linearization around the point of equilibrium leads to a matrix of evolution with eigenvalues having zero real parts.

The WFM replaces the classical Lyapunov function-finding problem with a method that finds a number of weight functions equal to the number of first-order differential equations that model the system (Stroe, 2008), (Stroe et al., 2008).

Theorem (Stroe, 2008): Let the autonomous system be $\dot{x} = f(x)$, $x \in \mathbb{R}^n$ and consider the existence of n positive functions $w_k(x_1, x_2, \dots, x_n)$ of the class C^1 in the neighborhood $|x| \leq \delta_0$

of the origin. The function $W = \sum_{k=1}^n x_k w_k f_k$ is formed so that the differentials form

$dV = \sum_{k=1}^n x_k w_k dx_k$ to be a total exact differential. The stability of the null solution of the

system is given by the following conditions:

- If W is a negative-defined function for any solution $x(t)$ of the given system, with $|x(0)| < \delta_0$, then the null solution is an asymptotic stable one;
- If W is a null function for any solution $x(t)$ of the given system, with $|x(0)| < \delta_0$, then the null solution is a simple stable one; and
- If W is a positive-defined function for any solution $x(t)$ of the given system, with $|x(0)| < \delta_0$, then the null solution is unstable.

The difference between the two methods is that the Lyapunov method finds all the functions simultaneously, while the WFM finds one function at a time, with their total number equal to the number of first-order differential equations.

To better visualize this method, a logical diagram is presented in Figure 0.13 with its basic principle defined by the following system equation (eq.(0.35)). The coefficients a_{1i} , b_{1i} , c_{1i} , and d_{1i} , with $i = 1 \div 4$ contain the stability derivatives terms. The x_1 , x_2 , x_3 , and x_4 coefficients represent the system unknowns.

$$\begin{cases} f_1 = a_{11}x_1 + a_{12}x_2 + a_{13}x_3 + a_{14}x_4 \\ f_2 = b_{11}x_1 + b_{12}x_2 + b_{13}x_3 + b_{14}x_4 \\ f_3 = c_{11}x_1 + c_{12}x_2 + c_{13}x_3 + c_{14}x_4 \\ f_4 = d_{11}x_1 + d_{12}x_2 + d_{13}x_3 + d_{14}x_4 \end{cases} \quad (0.35)$$

For a definition of this system, a function $W = \sum_{k=1}^4 w_k x_k f_k$ is found, whose signs will be studied. In the generic model, w_1 , w_2 , w_3 and w_4 are the weight functions that compose the total function W given by eq.(0.36) :

$$\begin{aligned} W = & w_1 x_1 (a_{11}x_1 + a_{12}x_2 + a_{13}x_3 + a_{14}x_4) + w_2 x_2 (b_{11}x_1 + b_{12}x_2 + b_{13}x_3 + b_{14}x_4) + \\ & + w_3 x_3 (c_{11}x_1 + c_{12}x_2 + c_{13}x_3 + c_{14}x_4) + w_4 x_4 (d_{11}x_1 + d_{12}x_2 + d_{13}x_3 + d_{14}x_4) \end{aligned} \quad (0.36)$$

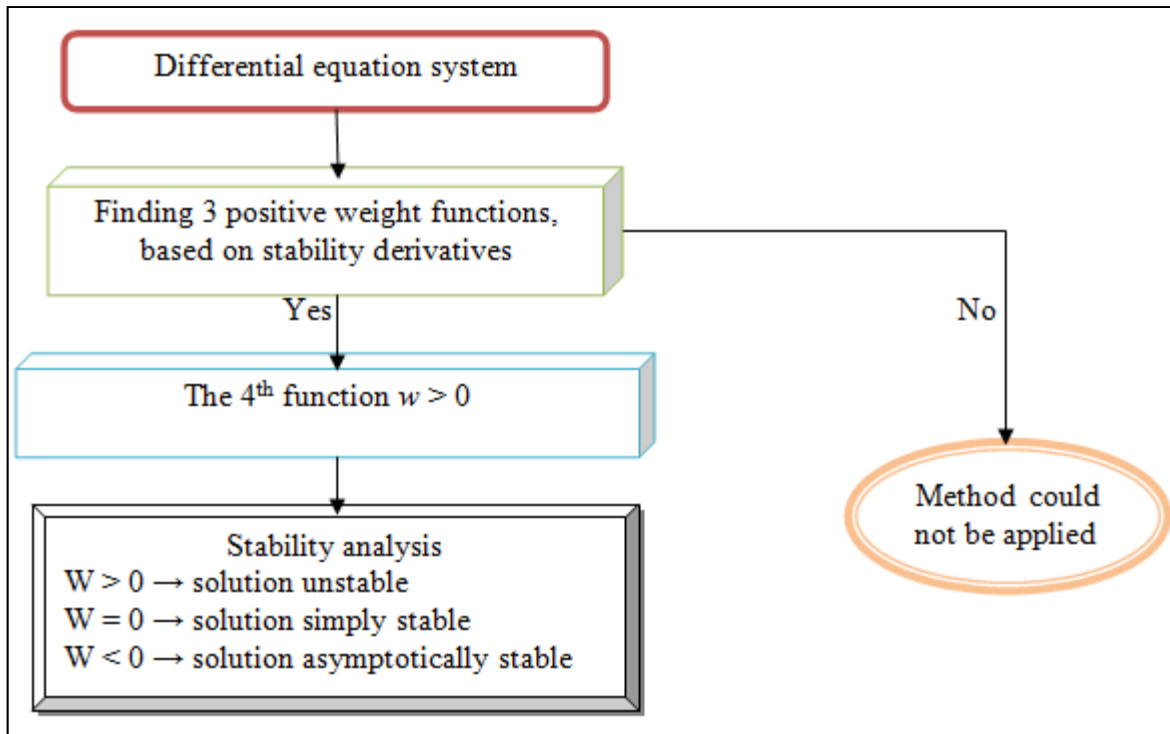


Figure 0.13 Logical diagram for the weight functions method

Three of the four functions, w_i , will be positively defined based on the sign of the coefficients a_{1i} , b_{1i} , c_{1i} , and d_{1i} with $i = 1 \div 4$. The last function will be constant and imposed by the author, $w_4 > 0$. If the positive weight functions can be well defined, then the sign of the total function W will be analyzed in order to identify the stability or instability areas of the system.

G. Handling Qualities Method

The handling and flying qualities are described qualitatively and formulated in terms of pilot opinions by Cooper et al. (1969). These descriptions reveal the properties that describe the easiness and effectiveness with which an aircraft responds to pilot commands in the execution of a flight or of mission tasks. Consequently, they tend to be subjective. The definition for the handling qualities for an aircraft can be paraphrased as: « Handling qualities are those qualities or characteristics which govern the ease and precision with which

an operator is able to perform the tasks required in support of the vehicle role. » (Cooper et al., 1969)

A distinction between the handling and flying qualities is shown in Figure 0.14, where it can be seen that they are interdependent and in practice are probably inseparable. The flying qualities are related to the mission task, while the handling qualities are related to the description of the short term dynamic response to controls in the execution of flight tasks.

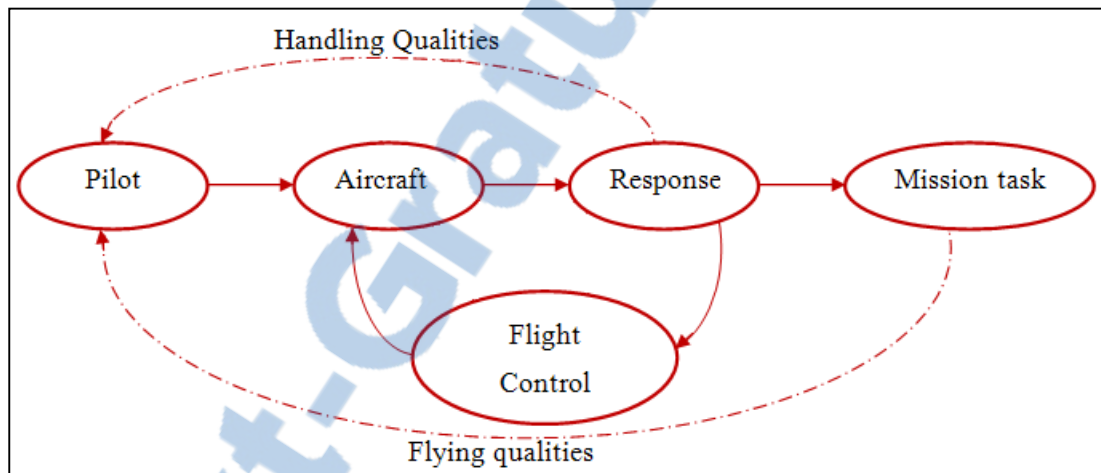


Figure 0.14 Difference between Handling Qualities and Flying Qualities

The handling qualities exact method was used in this thesis to validate the WFM results obtained for the aircraft stability analysis. Handling qualities involve the study and evaluation of the aircraft stability and control characteristics for all five of the dynamic modes of motion that describe the aircraft's response to an initial condition of any origin (turbulence, control input, etc.).

« Handling qualities criteria typically define a set of dynamic response characteristics of the vehicle that influence the operator-mission performance. Examples of criteria for aircraft include defined handling quality levels for the response rise time resulting from a step input, the control system bandwidth, and modal frequencies and damping. Traditionally, these response characteristics are necessary but not sufficient to attain satisfactory handling qualities. That is, if the vehicle violates one of these dynamic requirements, the handling qualities of the vehicle will be degraded. On the other hand, the

vehicle may meet all the formal dynamic requirements and still not possess satisfactory handling qualities due to some other phenomena for which there are no criteria. » (RTO Technical Report 61, 2002)

A diagram for the qualitative and quantitative analysis of an aircraft is presented in Fig. 0.15. The Handling Qualities (HQ's) specified by the MIL-F-8785C document (MIL-F-8785C, 1996) are those defined in our method. This document is the most current military reference for defining the HQ specifications for military aircraft, and is widely used as a standard for civilian aircraft. The airplanes are divided by size and weight into four classes, as seen in Table 0.10. The flying quality levels are shown in Table 0.11 and the flight phases in Table 0.12 (MIL-F-8785C, 1996).

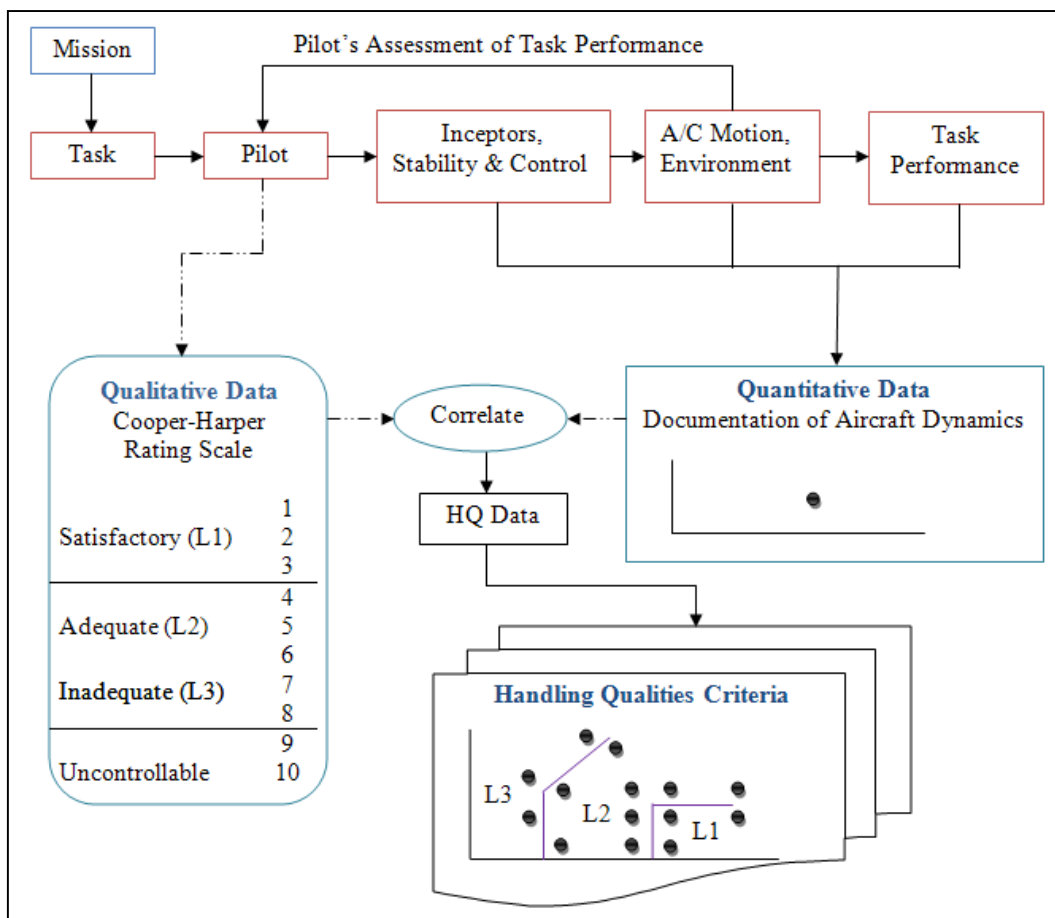


Figure 0.15 Diagram for developing Handling Qualities criteria
 Source: Reproduction of Figure presented in RTO Technical Report 61 (2002, p.95)

Table 0.10 Airplanes classification
Source: Reproduction of Table presented in (MIL-F-8785C, 1996)

Class I	Small, light airplanes <ul style="list-style-type: none"> • Light utility, Primary trainer, Light observation
Class II	Medium weight, low-to-medium maneuverability airplanes <ul style="list-style-type: none"> • Heavy utility/search and rescue • Light or medium transport/cargo/tanker • Early warning/electronic countermeasures/airborne command, control, or communication relay • Antisubmarine, Assault transport, Reconnaissance, Tactical bomber, Heavy attack, Trainer for Class II
Class III	Large, heavy, low-to-medium maneuverability airplanes <ul style="list-style-type: none"> • Heavy transport/cargo/tanker, Heavy bomber • Patrol/early warning/electronic airborne command, control, or communication relay • Trainer for Class III
Class IV	High maneuverability airplanes <ul style="list-style-type: none"> • Fighter/interceptor, Attack, Tactical reconnaissance, Observation, Trainer for Class IV

Table 0.11 Levels of flying qualities
Source: Reproduction of Table presented in (MIL-F-8785C, 1996)

Level I (Satisfactory)	Flying qualities clearly adequate for the mission Flight Phase
Level II (Acceptable)	Flying qualities adequate to accomplish the mission Flight Phase, but some increase in pilot workload or degradation in mission effectiveness, or both, exists
Level III (Controllable)	Flying qualities such that the airplane can be controlled safely, but pilot workload is excessive or mission effectiveness is inadequate, or both. Category A Flight Phases can be terminated safely, and Category B and C Flight Phases can be completed.

Table 0.12 Flight phase categories
 Source: Reproduction of Table presented in (MIL-F-8785C, 1996)

Non-terminal Flight Phase	
Category A	Require rapid maneuvering, precision tracking, or precise flight path control <ul style="list-style-type: none"> ▪ Air-to-air combat (CO) ▪ Ground attack (GA) ▪ Weapon delivery/launch (WD) ▪ Aerial recovery (AR) ▪ Reconnaissance (RC) ▪ In-flight refuelling (receiver) (RR) ▪ Terrain following (TF) ▪ Antisubmarine search (AS) ▪ Close formation flying (FF)
Category B	Normally accomplished using gradual maneuvers and without precision tracking, although accurate flight path control may be required <ul style="list-style-type: none"> ▪ Climb (CL) ▪ Cruise (CR) ▪ Loiter (LO) ▪ In-flight refuelling (tanker) (RT) ▪ Descent (D) ▪ Emergency descent (ED) ▪ Emergency deceleration (DE) ▪ Aerial delivery (AD)
Terminal Flight Phase	
Category C	Normally accomplished using gradual maneuvers and usually requires accurate flight path control <ul style="list-style-type: none"> ▪ Take-off (TO) ▪ Catapult take-off (CT) ▪ Approach (PA) ▪ Wave-off/go-around (WO) ▪ Landing (L)

The decision route used by flight-tests engineers and pilots to turn qualitative opinions of aircraft performance into a quantitative rating is provided by the Cooper-Harper rating scale, as illustrated in Figure 0.16 (Botez, 2004), (Hodgkinson, 1999), (Hahn et al., 1981).

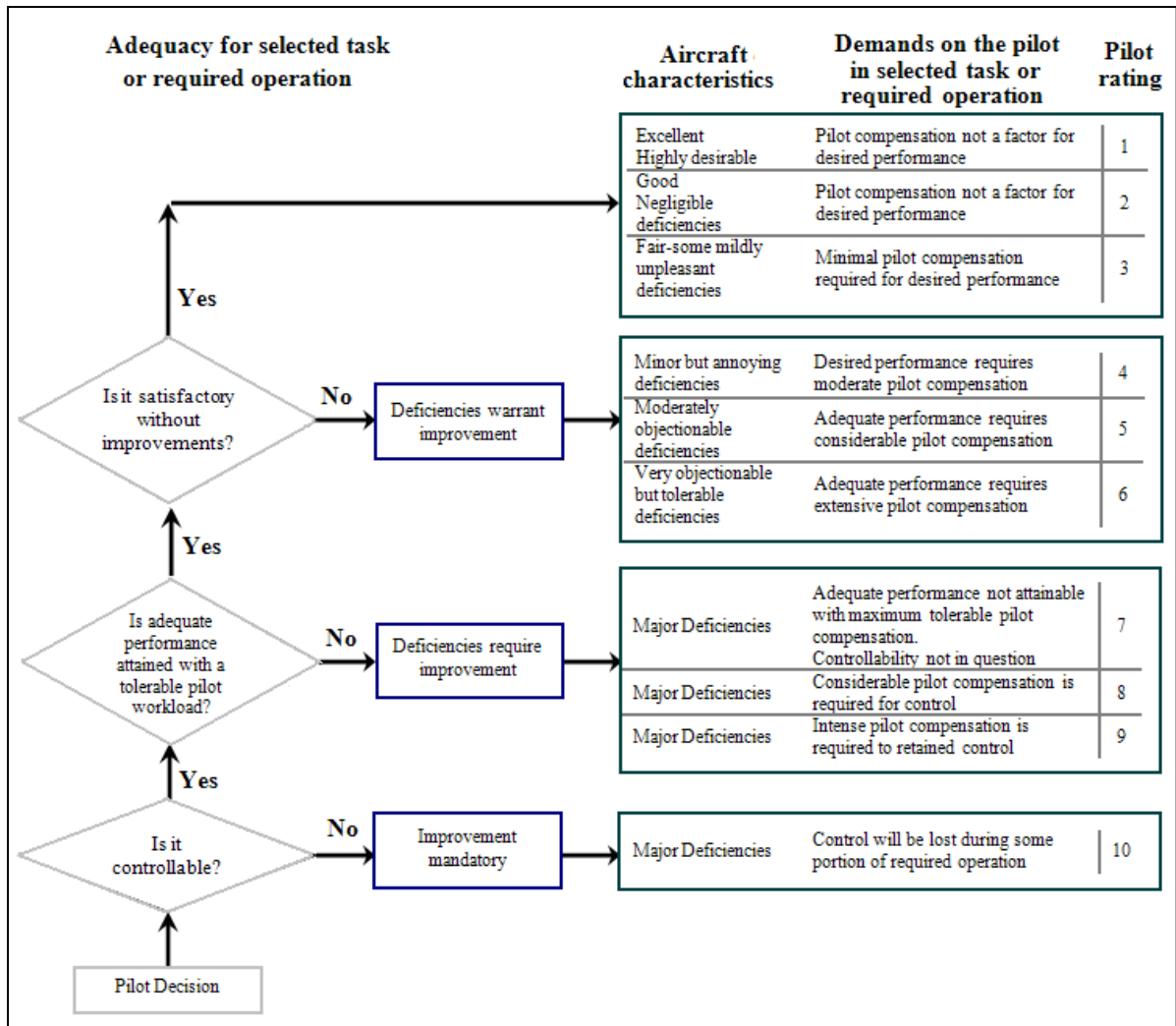


Figure 0.16 Cooper-Harper rating scale

H. Root Locus method

The Root Locus method developed by Walter R. Evans to determine the stability of a system is in fact a graphical method which examines how the roots of a system change with the variation of certain system parameters. This method was applied here for longitudinal and lateral dynamic analysis of the three types of aircraft.

The five modes of an aircraft are: the short period and the long period for longitudinal motion and the roll, Dutch roll and spiral for lateral motion. The natural frequency (ω_n) and the

damping ratio (ζ) are defined for each mode from the eigenvalues. For the longitudinal stability analysis, two modes are studied: the short period and the phugoid. The short-term pitch is a second order response. The phugoid mode is the long-term motion of an aircraft after a disturbance.

The mathematical model of longitudinal dynamics is given in eq.(0.37) (Botez, 2004):

$$\mathbf{A}_{long} = \begin{bmatrix} X_u & \frac{X_\alpha}{V} & 0 & -\frac{g}{V} \\ \frac{VZ_u}{V-Z_{\dot{\alpha}}} & \frac{Z_\alpha}{V-Z_{\dot{\alpha}}} & \frac{V+Z_q}{V-Z_{\dot{\alpha}}} & 0 \\ VM_u + \frac{VZ_uM_{\dot{\alpha}}}{V-Z_{\dot{\alpha}}} & M_\alpha + \frac{Z_\alpha M_{\dot{\alpha}}}{V-Z_{\dot{\alpha}}} & M_q + M_{\dot{\alpha}} \frac{V+Z_q}{V-Z_{\dot{\alpha}}} & 0 \\ 0 & 0 & 1 & 0 \end{bmatrix}, \quad (0.37)$$

$$\mathbf{x}_{long} = \begin{bmatrix} \Delta u \\ \Delta \alpha \\ \Delta q \\ \Delta \theta \end{bmatrix}, \quad \mathbf{B}_{long} = \begin{bmatrix} \frac{X_\delta}{V} \\ \frac{Z_\delta}{V-Z_{\dot{\alpha}}} \\ M_\delta + \frac{Z_\delta M_{\dot{\alpha}}}{V-Z_{\dot{\alpha}}} \\ 0 \end{bmatrix}, \quad u_{long} = \Delta \delta_e$$

The roots of the characteristic equation $\det(\lambda \mathbf{I} - \mathbf{A}_{long}) = 0$ are used to determine the eigenvalues λ_1 to λ_4 . For both longitudinal modes, the natural frequency ω_n and the damping ratio ζ are estimated directly from the characteristic equation $|\lambda \mathbf{I} - \mathbf{A}_{long}| = 0$, as a function of the longitudinal eigenvalues (eq.(0.38)); the eigenvalues $\lambda_{1,2}$ correspond to short-period and $\lambda_{3,4}$ to phugoid modes.

$$\begin{cases} \zeta \omega_n = |\operatorname{Re}(\lambda_{1,2})| \\ \omega_n \sqrt{1-\zeta^2} = |\operatorname{Im}(\lambda_{1,2})| \end{cases}, \quad \begin{cases} \zeta \omega_n = |\operatorname{Re}(\lambda_{3,4})| \\ \omega_n \sqrt{1-\zeta^2} = |\operatorname{Im}(\lambda_{3,4})| \end{cases} \quad (0.38)$$

The matrices of the aircraft lateral model are defined in eq.(0.39) (Botez, 2004).

$$\mathbf{A}_{lat} = \begin{bmatrix} \frac{Y_\beta}{V} & \frac{Y_p}{V} & \frac{Y_r - V}{V} & \frac{g}{u_0} \cos \theta_0 \\ G\left(L_\beta + N_\beta \frac{I_{xz}}{I_x}\right) & G\left(L_p + N_p \frac{I_{xz}}{I_x}\right) & G\left(L_r + N_r \frac{I_{xz}}{I_x}\right) & 0 \\ G\left(N_\beta + L_\beta \frac{I_{xz}}{I_z}\right) & G\left(N_p + L_p \frac{I_{xz}}{I_z}\right) & G\left(N_r + L_r \frac{I_{xz}}{I_z}\right) & 0 \\ 0 & 1 & 0 & 0 \end{bmatrix},$$

$$\mathbf{x}_{lat} = \begin{bmatrix} \Delta\beta \\ \Delta p \\ \Delta r \\ \Delta\phi \end{bmatrix}, \quad \mathbf{B}_{lat} = \begin{bmatrix} \frac{Y_\delta}{V} \\ G\left(L_\delta + N_\delta \frac{I_{xz}}{I_x}\right) \\ G\left(N_\delta + L_\delta \frac{I_{xz}}{I_z}\right) \\ 0 \end{bmatrix}, \quad u_{lat} = \Delta\delta_a$$
(0.39)

Three modes are considered in the aircraft lateral motion modelling:

- Spiral mode, representing a convergent or a divergent motion;
- Roll mode, representing a fast convergent motion, and
- Dutch roll mode, representing a lightly-damped oscillatory motion with a low frequency.

These modes are significant factors, mainly in the uniform cruise flight. For the lateral aircraft motion modeling, two real roots correspond to the roll and spiral modes, and a pair of complex roots correspond to the Dutch roll mode, obtained from the characteristic equation $|\lambda\mathbf{I} - \mathbf{A}_{lat}| = 0$.

The rolling motion is generally quite damped, and reaches the steady state in a very short time. An unstable spiral mode results in a turning flight path. The Dutch roll is a nuisance mode that appears in the basic roll response to lateral control that can induce uncontrolled and undesired motions in roll and yaw modes. These motions have a serious impact on the ability of the pilot to control lateral-directional motions with precision.

0.6 Continuity algorithm: application on High Incidence Research Model aircraft

This section presents the continuity algorithm (Hacker, 1992) and its application on the HIRM aircraft for longitudinal motion. For a better grasp of this procedure, a graphical scheme is very helpful; Fig. 0.17 shows the continuity algorithm broken into steps .

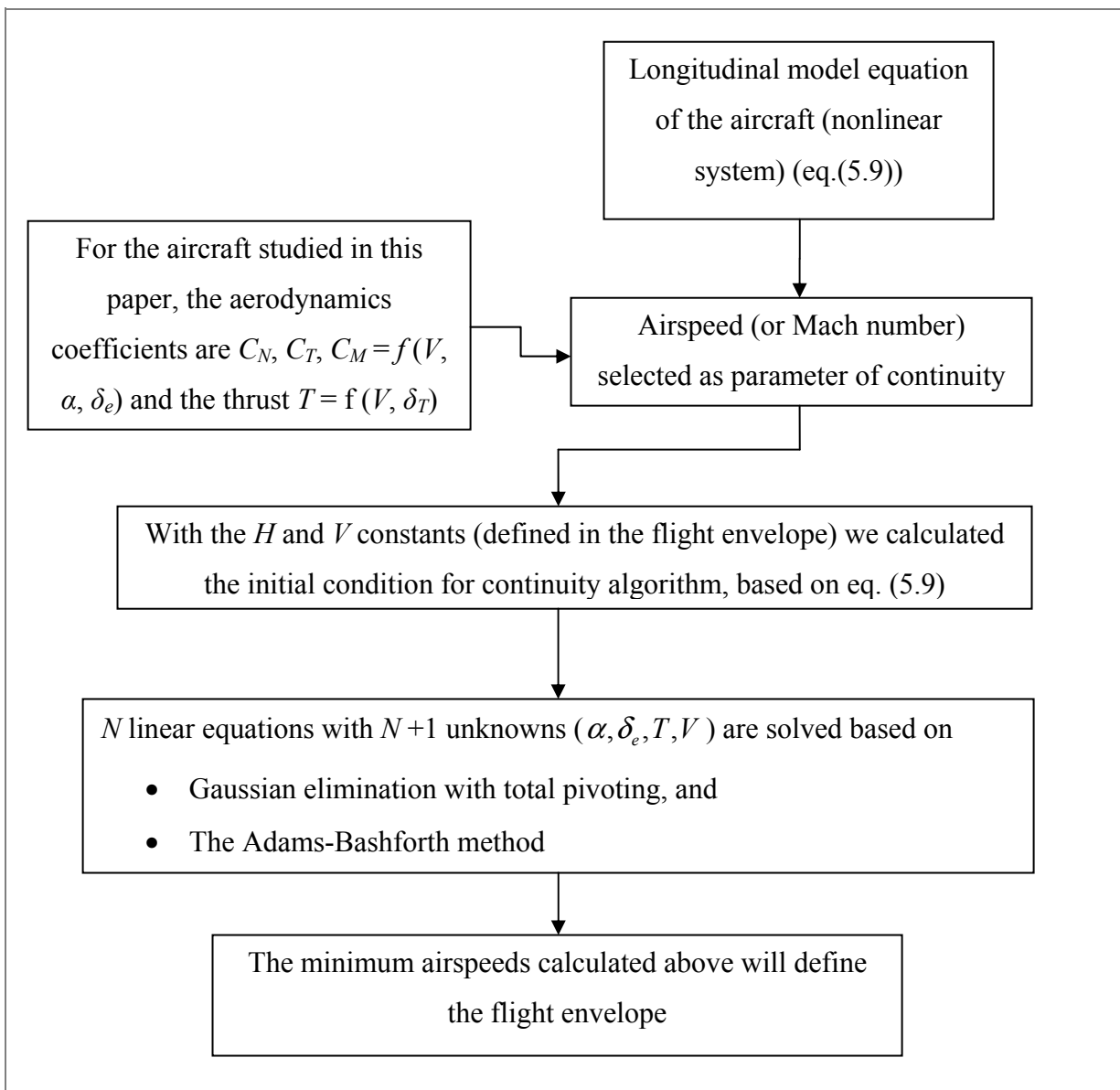


Figure 0.17 Steps of the continuity algorithm

The continuity algorithm is applied in this thesis for longitudinal dynamics modeling of a High Incidence Research Model (HIRM) aircraft implemented on the Aero-Data Model In Research Environment (ADMIRE) model developed by the Swedish Defense Research Agency FOI (Sweden), based on the Generic Aerodata Model (GAM) developed by SAAB AB in the framework of the GARTEUR Group: « The ADMIRE describes a generic small-single seated, single-engine fighter aircraft with a delta-canard configuration, implemented in MATLAB/SIMULINK Release 13 » (Lars et al., 2005, p iii].

The HIRM of a generic fighter aircraft was used in this study ((Admirer4p1), (Lars et al., 2005), (Terlouw et al., 1996)). Its flight envelope is presented in Figure 0.18 and its shape shows how this model was chosen for the continuity algorithm. In the minimum airspeeds range this envelope can be improved, stabilized with control laws.

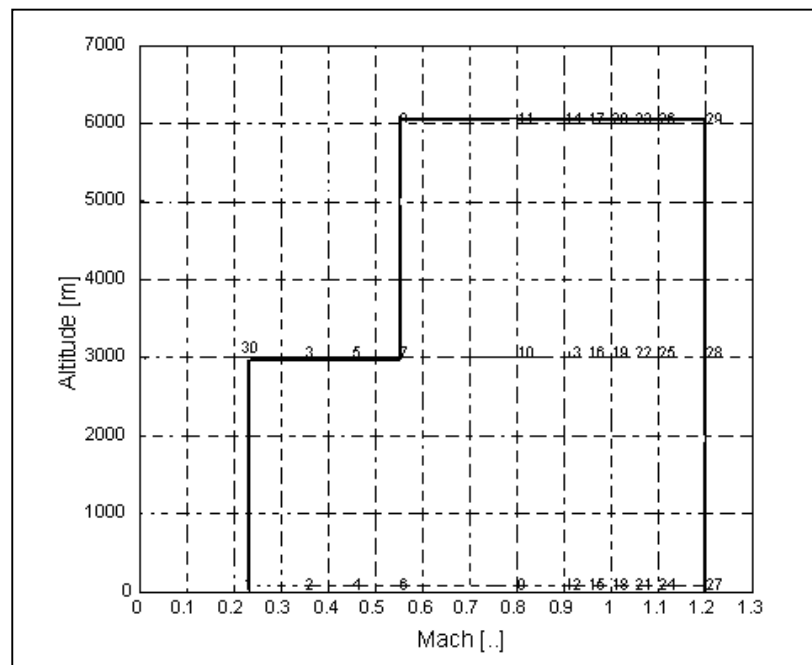


Figure 0.18 Flight envelope of the HIRM aircraft
Source: Reproduction of Figure presented by Lars et al., (2005)

The aerodynamics coefficients were obtained based on wind tunnel and flight tests (Admirer4p1) for a model « ... originally designed to investigate flight at high angles of

attack ... but [that] does not include compressibility effects resulting from high subsonic speeds. » (Terlouw et al., 1996, p 21). These coefficients were further implemented in the ADMIRE model using the main graphical window simulation presented in Figure 0.19, which also shows the response of the aircraft model. The tests and analyses provided in the GARTEUR program were focused on PIO detection, while this paper evaluates a new method to investigate the model's stability.

« The ADMIRE contains twelve states ($V_T, \alpha, \beta, p_b, q_b, r_b, \psi, \theta, \varphi, x_v, y_v, z_v$) plus additional states due to actuators and [the] Flight Control System (FCS). Available control effectors are left- and right canard, leading edge flap, four elevons, rudder and throttle setting. The model is also equipped with thrust vectoring capability and an extendable landing gear. The model is prepared for the use of atmospheric turbulence as external disturbance. The ADMIRE is augmented with an FCS in order to provide stability and sufficient handling qualities within the operational envelope (altitude <6 km, Mach < 1.2). The FCS contains a longitudinal and a lateral part. (...) The lateral controller enables the pilot to perform roll control where the roll motion is initiated around the velocity vector of the a/c, and [at the] angle of sideslip control. Sensor models are incorporated. The 20 ms flight computer delay on the actuator inputs that is implemented in other versions of ADMIRE was not used here. The model has the facility to define model uncertainties, but this was not used. ADMIRE is implemented in MATLAB and SIMULINK using a combination of standard SIMULINK blocks and S-functions written in C. » (GARTEUR FM(AG12), 2001, p 36).

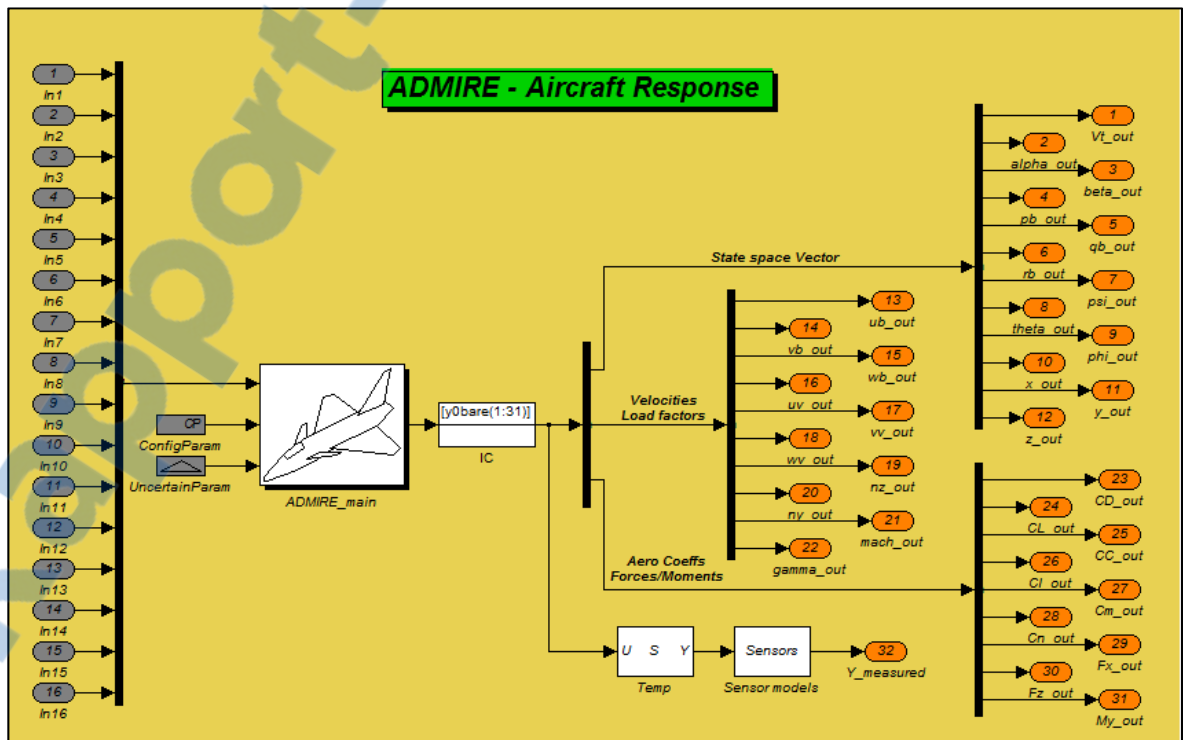
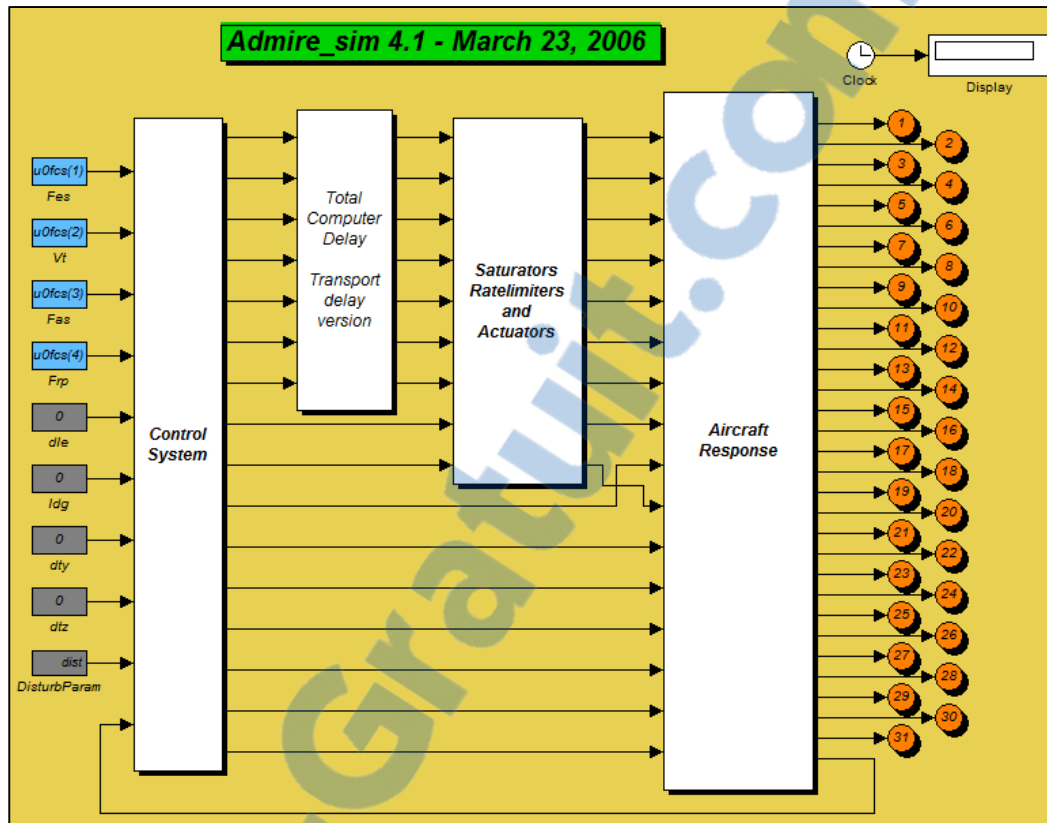


Figure 0.19 ADMIRE: Main graphical window simulation and the aircraft response
 Source: Screenshot from Admirer4p1 interface

I. Mathematical model of the continuity algorithm

Let us consider that the system dynamics is expressed by the following autonomous non-linear equation (Hacker, 1992):

$$\dot{x} = f(x, u) \quad (0.40)$$

with the output $y = g(x, u)$. We assume that $\dim y = \dim u$. When a transition from one regime to another is performed, the constant command value \hat{u} must be determined. This command corresponds to a steady state; its attraction area contains the initial state and the output has the required steady state \hat{y} , with the condition that the permanent regime is located in an allowed given area. A continuous motion, given by a constant command u , described by a stationary solution of the studied system, satisfies the nonlinear system of eq.(0.41)

$$f(x, u) = 0 \quad (0.41)$$

If required output value is defined as $y = \hat{y} = \text{constant}$, a corresponding command will be given by one of the values of u that satisfies the system equations with $(n+p)$ unknowns (x and u).

$$F(x, u, \hat{y}) = 0 \quad (0.42)$$

If the matrix $\frac{\partial f}{\partial x}(\hat{x}, \hat{u})$ is a Hurwitz matrix (i.e., all eigenvalues have negative real parts), the asymptotic stability of the point \hat{x} is ensured. Obtaining the desired regime depends, in general, on the initial regime; it does not depend on the starting point from where the command \hat{u} is applied.

Assume that the airplane is in its flight mode corresponding to the stationary point x_0 , the command u_0 and the output y_0 , so that $f(x_0, u_0) = 0$. x_0 is stable and $\frac{\partial f}{\partial x}(x_0, u_0)$ is a

Hurwitz matrix, with $\det \frac{\partial f}{\partial x}(x_0, u_0) \neq 0$. Then, the implicit function theorem can be applied; in this theorem a function \tilde{x} is defined in the neighborhood of u_0 , with values in the vicinity of x_0 , with $\tilde{x}_0(u_0) = x_0$ and $f[\tilde{x}(u), u] \equiv 0$ through (x_0, u_0) .

A path is considered, which connects u_0 to \hat{u} without leaving the area where $\frac{\partial f}{\partial x}[\tilde{x}(u), u]$ remains a Hurwitz matrix; the command changes the value u_0 into a value u_1 that corresponds to the regime $\tilde{x}(u_1)$, neighbor to x_0 . That point x_0 is close to $\tilde{x}(u_1)$ and is within its attraction field after a short phase, so that we can consider that the state $\tilde{x}(u_1)$ is reached. The command then changes to the neighbor value u_2 to reach the state $\tilde{x}(u_2)$ and the process continues in the same manner until a stable, steady branch of the stationary regime past state \hat{x} is reached.

Any asymptotically stable steady state \hat{x} can be achieved based on other stable steady state x_0 values, if there is at least one branch of a stable stationary regime with acceptable values (« allowed ») which link them together.

The equilibrium points defined as pairs of (α, δ_e, T) at a constant Mach number and altitude for the HIRM model stabilized with control laws are defined based on system eq.(0.43). They are subsequently used in the continuity algorithm by integration of the same system equations.

J. Application on the longitudinal motion of the HIRM aircraft

The longitudinal system of equations (Lars et al., 2005) is given by eq.(0.43)

$$\begin{cases} \dot{V} = -\frac{1}{m}(\tilde{q}SC_D - T \cos \alpha) - g \sin \gamma \\ \dot{\gamma} = \frac{1}{mV}(\tilde{q}SC_L + T \sin \alpha) - \frac{1}{V}g \cos \gamma \\ \dot{q} = \frac{1}{I_y}[\tilde{q}S\bar{c}C_m + x_{CG}\tilde{q}SC_T + z_e T] \\ \dot{\alpha} = q \end{cases} \quad (0.43)$$

for which the altitude H is constant and the output is defined in the range of $[V_{min}, V_{max}]$. The system variables are $(V, \gamma, q$ and $\alpha)$ with a command defined by (δ_e, δ_T) . The aim is to find the values of $(\alpha, \delta_e$ and $T)$ of the nonlinear system's solutions found by using

$$\begin{cases} \tilde{q}SC_D - T \cos \alpha + mg \sin \gamma = 0 \\ \tilde{q}SC_L + T \sin \alpha - mg \cos \gamma = 0 \\ \tilde{q}S\bar{c}C_m + x_{CG}\tilde{q}SC_T + z_e T = 0 \end{cases} \quad (0.44)$$

based on the equilibrium points.

If conditions such as $\gamma = \text{const.}$ and $\delta_c = 0$ are imposed, the equation system of eq.(0.44) can also be written as:

$$\begin{cases} \tilde{q}SC_D - T \cos \alpha = 0 \\ \tilde{q}SC_L + T \sin \alpha - mg = 0 \\ \tilde{q}S\bar{c}C_m + x_{CG}\tilde{q}SC_T + z_e T = 0 \end{cases}, \text{ where } \begin{cases} C_D = C_N \sin \alpha + C_T \cos \alpha \\ C_L = C_N \cos \alpha - C_T \sin \alpha \end{cases} \quad (0.45)$$

The thrust is calculated using eq. (0.46).

$$T = \frac{\tilde{q}SC_D}{\cos \alpha} \quad (0.46)$$

The following combinations of altitude and Mach number were chosen from the flight envelope: case 1 (20 m, 0.22), case 2 (3,000 m, 0.22) and case 3 (6,000 m, 0.55). The control law is defined as $\delta_e = \delta_{e0} + k_\alpha \alpha + k_q q$, where the regulator gains are known from the model implemented in ADMIRE simulation (Admirer4p1). Based on the system of eq.(0.45), for all three study cases the points of equilibrium (or the critical points) and the gain values are

presented in Table 0.15. For each combination of altitude and airspeed the aerodynamic coefficients are known.

Table 0.13 Points of equilibrium; initial conditions of continuity algorithm

	<i>Case 1</i>	<i>Case 2</i>	<i>Case 3</i>
Altitude	H = 20 m	H = 3000 m	H = 6000 m
Mach number (M)	0.22	0.22	0.55
Angle of attack (α_0)	9.5537 deg	13.0627 deg	3.5522 deg
Elevon angle (δ_{e0})	3 deg	5 deg	0 deg
Thrust (T)	13683.47 N	18654.87 N	8481.61 N
k_α	0.4321	0.4630	0.4574
k_q	1.5729	0.8810	0.4693

Based on the differentiation method with respect to a parameter $z(\alpha)$ proposed by Davidenko (1953), the following eq.(0.47) is considered:

$$F(z(\alpha), \alpha) = 0 \quad (0.47)$$

where the solution is given as $z(\alpha_0) = z_0$.

Because the aerodynamic coefficients C_N , C_T and C_M depend on (V , α and δ_e) and the thrust T is a function of (V and δ_T), the airspeed (or Mach number) was chosen to be a parameter of the continuity algorithm.

We can now define all of the functions of the continuity algorithm for $\gamma = 0$ (see eq.(0.48))

$$\begin{aligned} F(1) &= \tilde{q}SC_D - T \cos \alpha \\ F(2) &= \tilde{q}SC_L + T \sin \alpha - mg \\ F(3) &= \tilde{q}S\bar{c}C_m + x_{CG}\tilde{q}SC_T + z_e T \end{aligned} \quad (0.48)$$

To find a solution for the case $V = V_{min}$, which is considered as the initial system condition (0.45), the system will be integrated over the interval $[0.1 \div V_{min}]$. In this way, the initial values of α, δ_e will be added to the third unknown which is the thrust T .

The system defined by eq.(0.45) could be written in the following form (Hacker, 1992):

$$\left\{ \begin{aligned}
 & \left\{ \frac{1}{2} \rho M^2 a^2 S \left[\frac{\partial C_N}{\partial \alpha} \sin \alpha + C_N \cos \alpha + \frac{\partial C_T}{\partial \alpha} \cos \alpha - C_T \sin \alpha \right] + T \sin \alpha \right\} \frac{d\alpha}{dM} + \\
 & + \left[\frac{1}{2} \rho M^2 a^2 S \left(\frac{\partial C_N}{\partial \delta_e} \sin \alpha + \frac{\partial C_T}{\partial \delta_e} \cos \alpha \right) \right] \frac{d\delta_e}{dM} - \cos \alpha \frac{dT}{dM} = \cos \alpha \frac{\partial T}{\partial M} - \\
 & - \rho M a^2 S (C_N \sin \alpha + C_T \cos \alpha) - \frac{1}{2} \rho M^2 a^2 S \left(\frac{\partial C_N}{\partial M} \sin \alpha + \frac{\partial C_T}{\partial M} \cos \alpha \right) \\
 & \left\{ \frac{1}{2} \rho M^2 a^2 S \left[\frac{\partial C_N}{\partial \alpha} \cos \alpha - C_N \sin \alpha - \frac{\partial C_T}{\partial \alpha} \sin \alpha - C_T \cos \alpha \right] + T \cos \alpha \right\} \frac{d\alpha}{dM} + \\
 & + \left[\frac{1}{2} \rho M^2 a^2 S \left(\frac{\partial C_N}{\partial \delta_e} \cos \alpha - \frac{\partial C_T}{\partial \delta_e} \sin \alpha \right) \right] \frac{d\delta_e}{dM} + \sin \alpha \frac{dT}{dM} = -\sin \alpha \frac{\partial T}{\partial M} - \\
 & - \rho M a^2 S (C_N \cos \alpha - C_T \sin \alpha) - \frac{1}{2} \rho M^2 a^2 S \left(\frac{\partial C_N}{\partial M} \cos \alpha - \frac{\partial C_T}{\partial M} \sin \alpha \right) \\
 & \frac{1}{2} \rho M^2 a^2 S \left[\bar{c} \frac{\partial C_M}{\partial \alpha} + x_{cg} \frac{\partial C_T}{\partial \alpha} \right] \frac{d\alpha}{dM} + \frac{1}{2} \rho M^2 a^2 S \left[\bar{c} \frac{\partial C_M}{\partial \delta_e} + x_{cg} \frac{\partial C_T}{\partial \delta_e} \right] \frac{d\delta_e}{dM} = \\
 & = -\rho M a^2 S (\bar{c} C_M + x_{cg} C_T) - \frac{1}{2} \rho M^2 a^2 S \left(\bar{c} \frac{\partial C_N}{\partial M} + x_{cg} \frac{\partial C_T}{\partial M} \right) - z_{eng} \frac{\partial T}{\partial M}
 \end{aligned} \right. \quad (0.49)$$

The notations are defined below to simplify eq.(0.49) as:

$$G_{11} = \bar{q} S \left(\frac{\partial C_N}{\partial \alpha} \sin \alpha + \frac{\partial C_T}{\partial \alpha} \cos \alpha + C_N \cos \alpha - C_T \sin \alpha \right) + T \sin \alpha$$

$$G_{12} = \bar{q} S \left(\frac{\partial C_N}{\partial \delta_e} \sin \alpha + \frac{\partial C_T}{\partial \delta_e} \cos \alpha \right)$$

$$G_{13} = -\cos \alpha$$

$$G_{14} = \rho M a^2 S (C_N \sin \alpha + C_T \cos \alpha) + \bar{q} S \left(\frac{\partial C_N}{\partial M} \sin \alpha + \frac{\partial C_T}{\partial M} \cos \alpha \right) - \cos \alpha \frac{\partial T}{\partial M}$$

$$\begin{aligned}
G_{21} &= \bar{q}S \left(\frac{\partial C_N}{\partial \alpha} \cos \alpha - \frac{\partial C_T}{\partial \alpha} \sin \alpha - C_N \sin \alpha - C_T \cos \alpha \right) + T \cos \alpha \\
G_{22} &= \bar{q}S \left(\frac{\partial C_N}{\partial \delta_e} \cos \alpha - \frac{\partial C_T}{\partial \delta_e} \sin \alpha \right) \\
G_{23} &= \sin \alpha \\
G_{24} &= \rho Ma^2 S (C_N \cos \alpha - C_T \sin \alpha) + \bar{q}S \left(\frac{\partial C_N}{\partial M} \cos \alpha - \frac{\partial C_T}{\partial M} \sin \alpha \right) + \sin \alpha \frac{\partial T}{\partial M} \\
G_{31} &= \bar{q}S \left(\bar{c} \frac{\partial C_M}{\partial \alpha} \cos \alpha + x_{cg} \frac{\partial C_T}{\partial \alpha} \right) \\
G_{32} &= \bar{q}S \left(\bar{c} \frac{\partial C_M}{\partial \delta_e} \cos \alpha + x_{cg} \frac{\partial C_T}{\partial \delta_e} \right) \\
G_{33} &= z_{eng} \\
G_{34} &= \rho Ma^2 S (\bar{c} C_M + x_{cg} C_T) + \bar{q}S \left(\bar{c} \frac{\partial C_M}{\partial M} + x_{cg} \frac{\partial C_T}{\partial M} \right) + z_{eng} \frac{\partial T}{\partial M}
\end{aligned} \tag{0.50}$$

The following eq.(0.51) is equivalent with eq.(0.49) and (0.50):

$$\begin{cases}
G_{11} \frac{d\alpha}{dM} + G_{12} \frac{d\delta_e}{dM} + G_{13} \frac{dT}{dM} = G_{14} \\
G_{21} \frac{d\alpha}{dM} + G_{22} \frac{d\delta_e}{dM} + G_{23} \frac{dT}{dM} = G_{24} \\
G_{31} \frac{d\alpha}{dM} + G_{32} \frac{d\delta_e}{dM} + G_{33} \frac{dT}{dM} = -G_{34}
\end{cases} \tag{0.51}$$

The following algorithm allows N linear equations with $N + 1$ unknowns (α, δ_e, T, V) to be solved, based on Gaussian elimination with total pivoting (Olson, 2006)] and the Adams-Bashforth method (Hoffman, 2001). The Gaussian algorithm with total pivoting is performed in two steps:

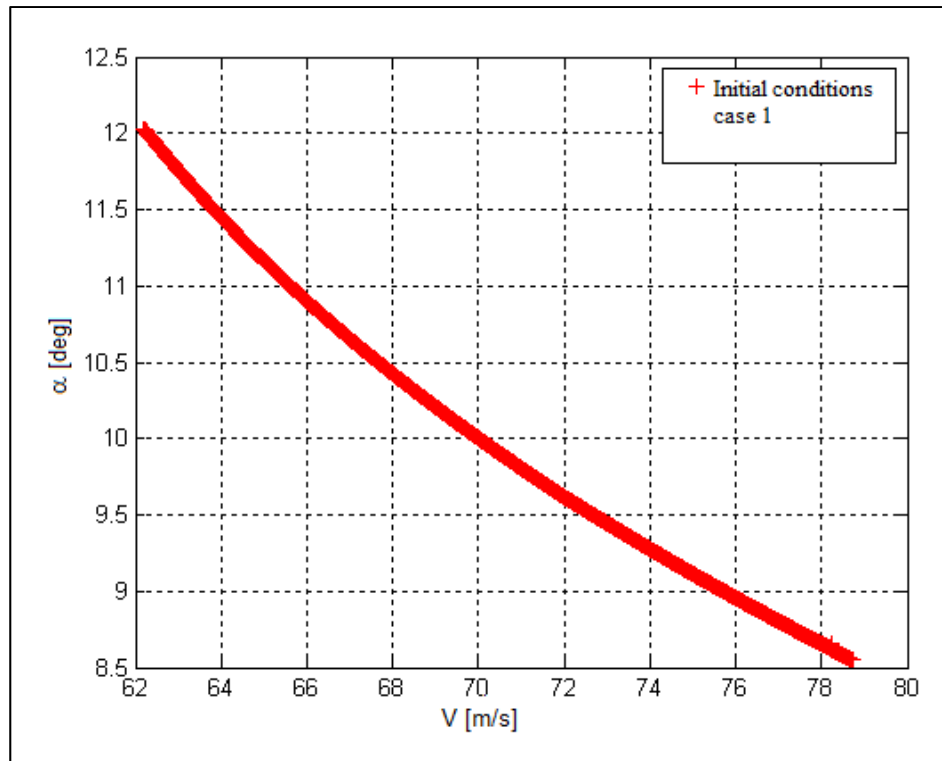
- *forward elimination* when a matrix is transformed into an upper triangular equivalent matrix; and
- *backward substitution*.

The pivot element is chosen as the greatest element, in absolute value, between the elements that are found in the upper triangular equivalent matrix; once the greatest element is identified, an interchange is performed between the rows and columns.

The Adams-Bashforth method is an explicit linear multistep method that depends on multiple previous solution points for solving initial value problems for ordinary differential equations. It is a numerical method to solve an ordinary differential equation (ODE) to obtain an approximate solution, step-by-step in discrete increments across the interval of integration.

The system of eq.(0.51) is integrated with initial conditions defined as points of equilibrium, and the minimum airspeed is calculated using the principle presented before. Starting from the initial pair of equilibrium points, a new asymptotically stable steady state is found at each integration step and a branch of the stable stationary regime is defined.

The range variation of Mach number is $M = [M_{min} \div 0.22]$, for $H = 20$ m, 3,000 m $M = [M_{min} \div 0.55]$ for $H = 6,000$ m with angle of attack $\alpha = [-10 \div 30]^\circ$ and elevon angle $\delta_e = [-30 \div 30]^\circ$. The results are presented in Figures 0.20 to 0.22 for each case studied, for angle of attack α , elevon angle δ_e and thrust T versus airspeed V .



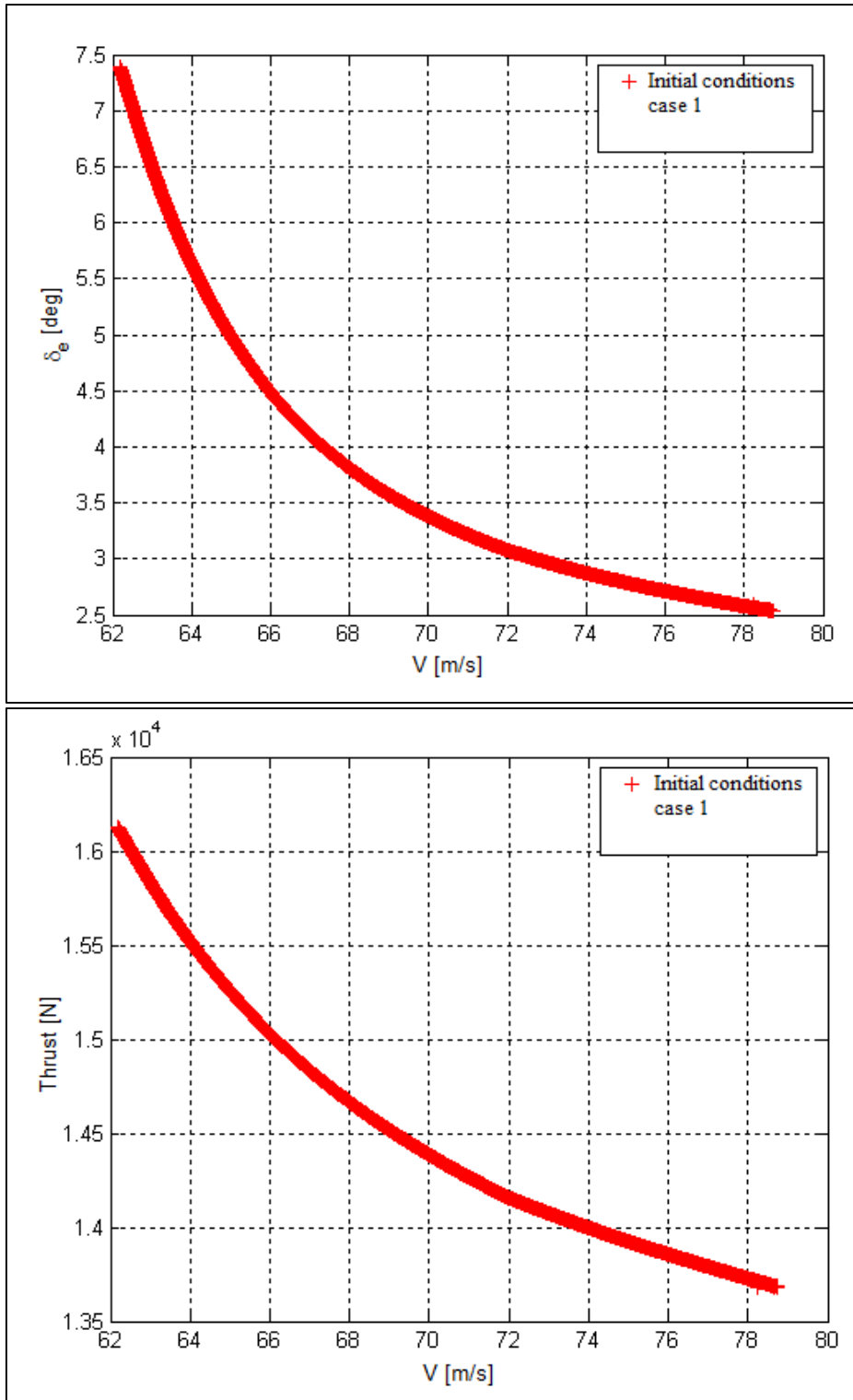
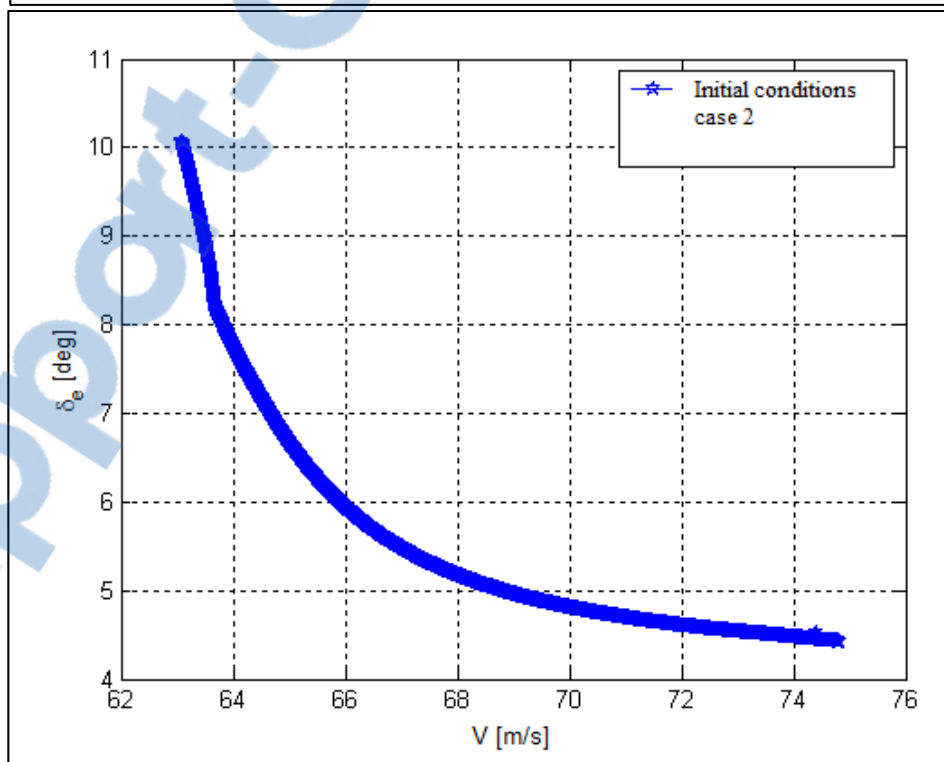
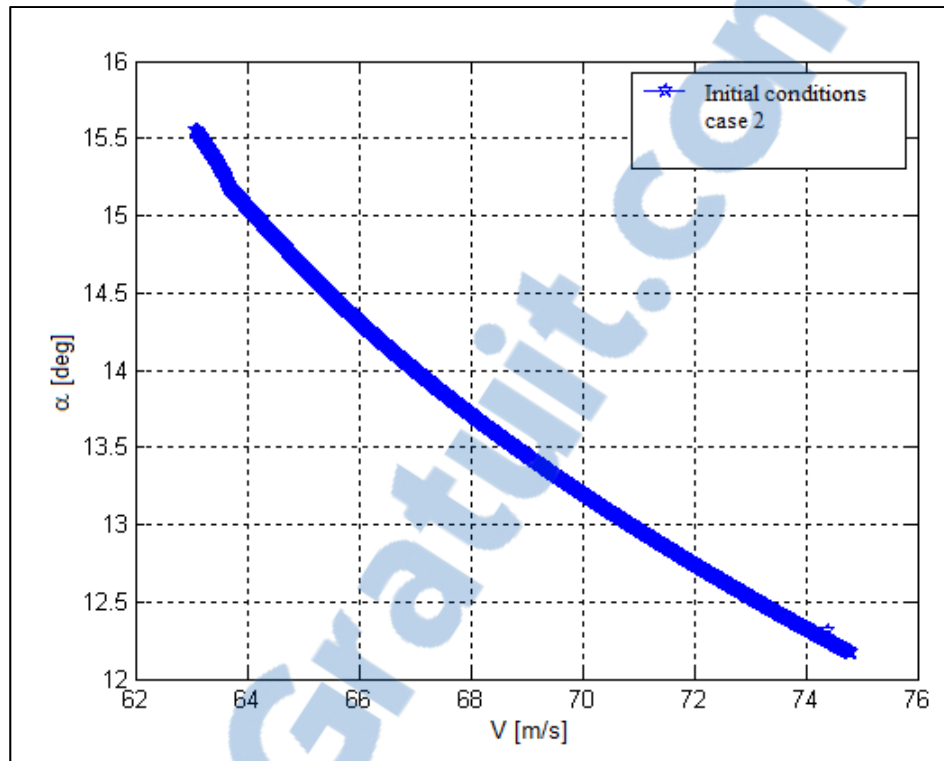


Figure 0.20 Angle of attack, elevon angle and thrust variation versus airspeed V , starting at the initial conditions presented in Table 5.4 for $H = 20$ m and $M = 0.22$



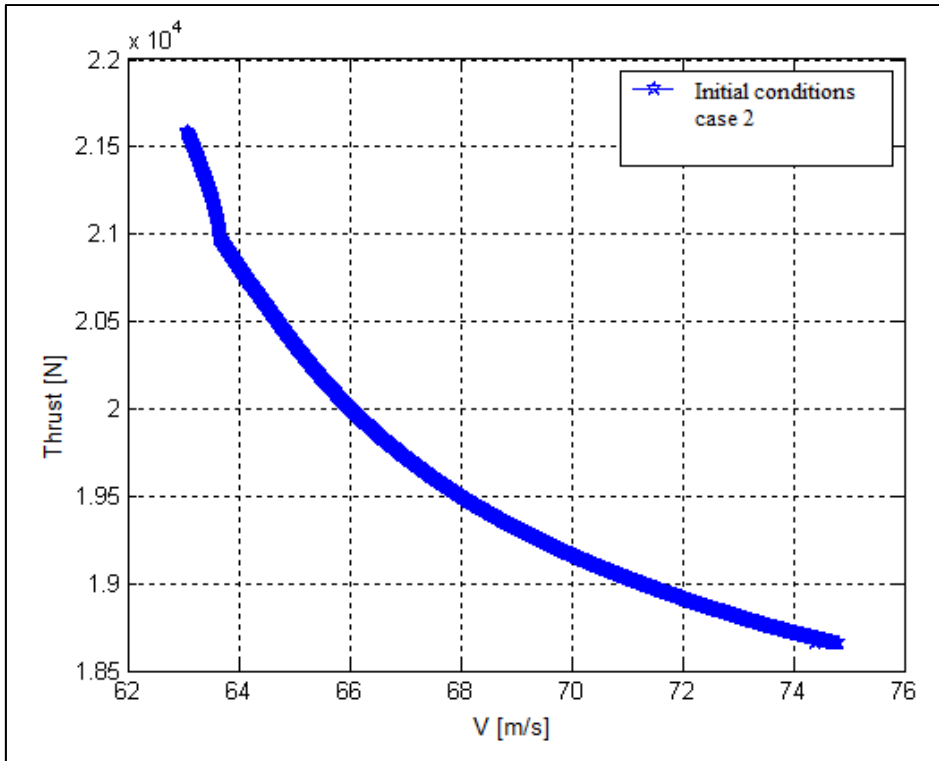
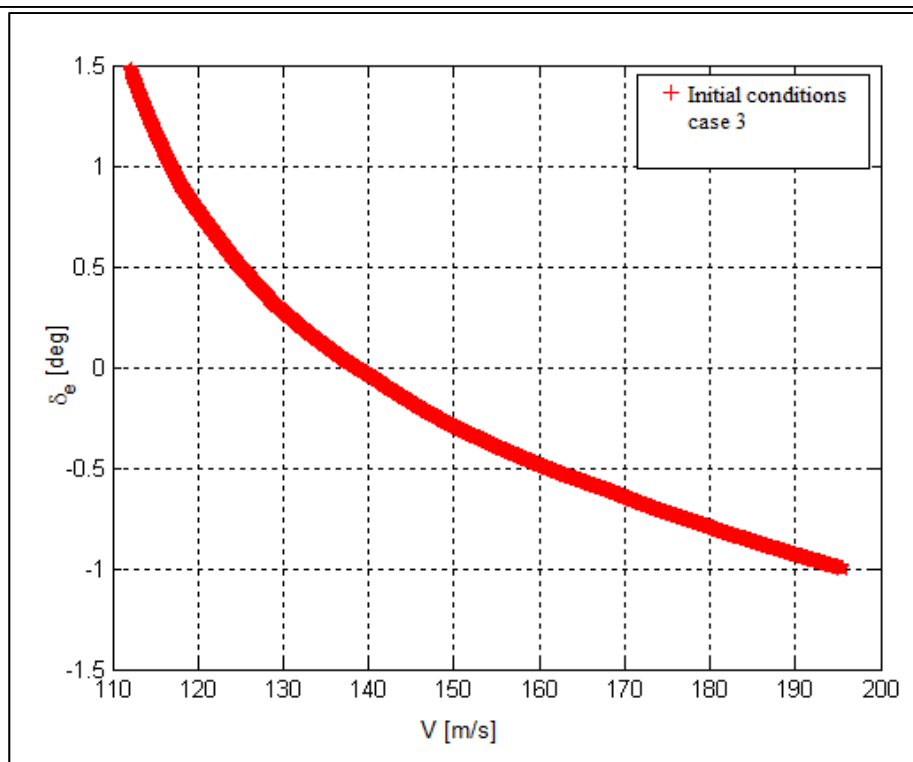
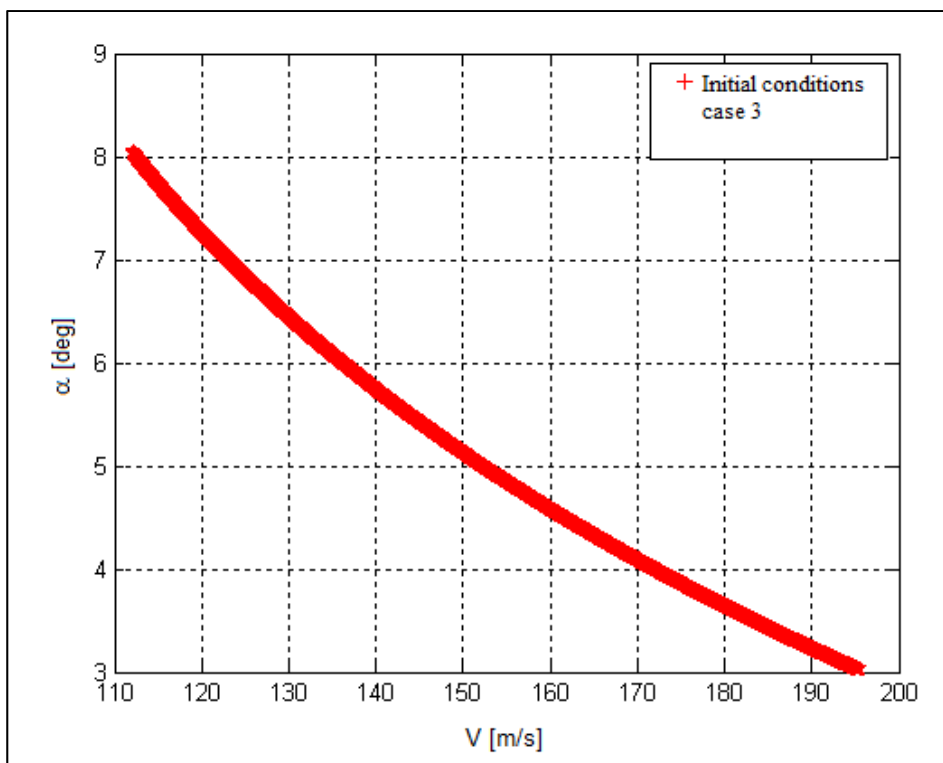


Figure 0.21 Angle of attack, elevon angle and thrust variation versus airspeed V , starting at the initial conditions presented in Table 5.4 for $H = 3000$ m and $M = 0.22$



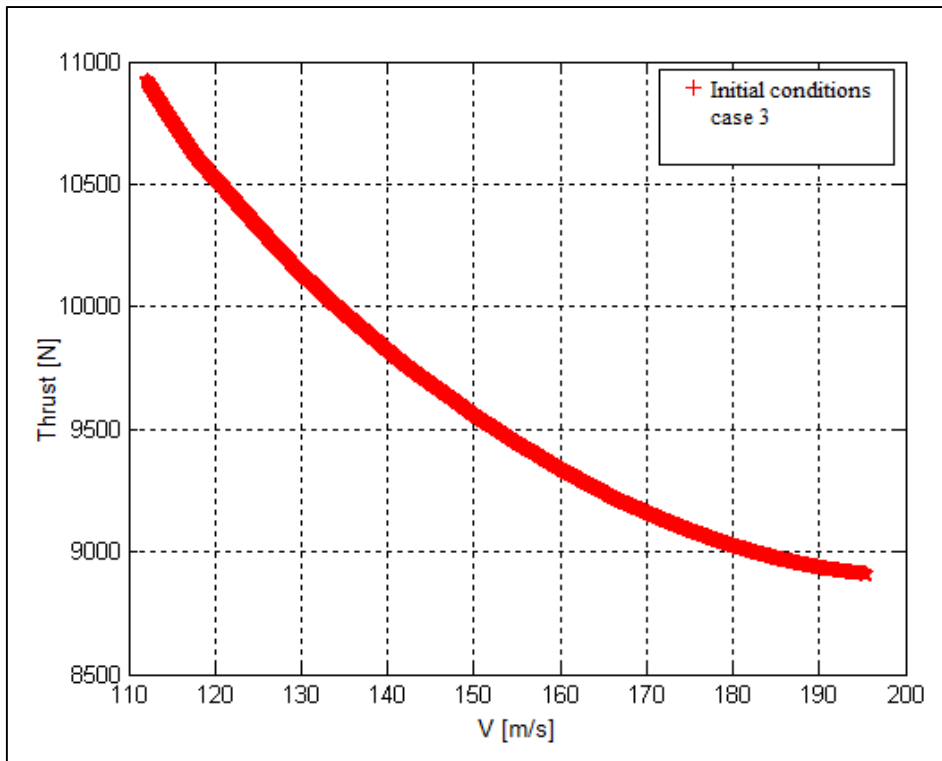


Figure 0.22 Angle of attack, elevon angle and thrust variation versus airspeed V , starting at the initial conditions presented in Table 5.4 for $H = 6000$ m and $M = 0.55$

All three minimum airspeeds for the initial conditions (α , δ_e and T) presented in Table 0.13 have been determined, such as $V_{case1} = 62.09$ m/s, $V_{case2} = 63.15$ m/s, and $V_{case3} = 111.8$ m/s. The new flight envelope for HIRM aircraft stabilized with control laws is presented in Figure 0.23.

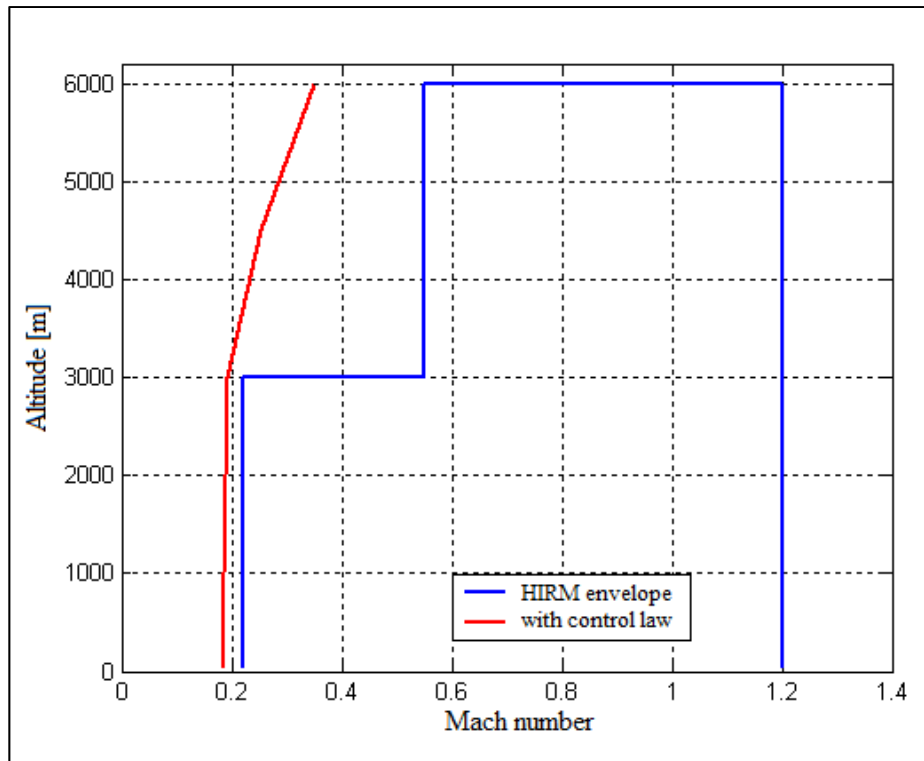


Figure 0.23 The flight envelope for HIRM aircraft stabilized with control laws

For a smaller Mach number and altitude less than or equal to 3,000 m, the flight envelope was improved, up to Mach number $M = 0.182$ from $M = 0.22$, but for altitude between 3,000 m and 6,000 m this improvement is more considerable from $M = 0.55$ to $M = 0.35$.

CHAPTER 1

LITERATURE REVIEW

The literature review is explained in different sections. The first section presents the bibliographical research on the semi-analytical techniques needed to calculate stability derivatives from aircraft geometry using parameter estimation methods. The theory of the Computational Fluid Dynamics method required for the calculation of aerodynamics coefficients and their derivatives is presented in the second section, and the weight functions method review is in the third. Independent codes have been developed based on the DATCOM or vortex methods.

1.1 Methods used by semi-empirical codes to calculate the aerodynamics coefficients and their stability derivatives

The aerodynamic coefficients and their stability derivatives based on the DATCOM method have been estimated in the literature. Some methods were adapted directly from the original method and others combined DATCOM with the vortex-lattice method. Grasmeyer (1998) has estimated the stability and control derivatives of Boeing 747-100 aircraft using a method adapted from the USAF Stability and Control DATCOM (Williams et al., 1979a).

MacMillin (1996) has used a similar approach for the High-Speed Civil Transport (HSCT). The baseline stability and control derivatives were estimated using the vortex-lattice method, and then the DATCOM method was used to increase these baseline values with the effects due to vertical tail geometry changes.

A computer code for calculating the dynamic stability derivatives of an airplane from static wind tunnel tests was developed by Chang et al. (2004). This methodology was mainly based on the DATCOM method, but the wing and tail static coefficients were obtained from breakdowns of body, wing-body, and tail-body tests instead of from direct tests of each

component. Evaluation of the code was carried out for a Standard Dynamic Model of a twin prop airplane. The results of this code were better than results achieved with DATCOM.

1.1.A Digital DATCOM (DATCOM+) code description

Digital DATCOM code (Galbraith), also known as DATCOM+, is the first implementation of the DATCOM procedures in an automatic calculation code. The software is a portable application, directly executable. Input data, consisting of geometric and aerodynamic parameters of the aircraft and flight conditions, are introduced through a text file called « *aircraft_name.dcm* » whose format is specific to the software. The input format of Digital DATCOM is a series of NAMELIST statements. The data entry file can contain more than 300 variables for a complete aircraft configuration.

The DATCOM+ program calculates the static stability, the high lift and control, and the dynamic derivative characteristics. This program applies to aircraft flying in the subsonic, transonic and supersonic regimes, more precisely to traditional wing-body-tail and canard-equipped aircraft. DATCOM+ offers a trim option that computes the control deflections and aerodynamic data needed to trim the aircraft in the subsonic Mach regimes. The program has a modular basis with 3 master routines:

Main programs	Perform the executive functions of organizing and directing the operations performed by other program components.
Executive subroutines	Perform user-oriented non-method operations such as ordering input data, switching logic, input error analysis, and output format selection.
Utility subroutines	Perform mathematical tasks repetitively, using subroutines.
Module 1/ Module 3 / Module 5	Contain the coefficients at the angle of attack for the subsonic, transonic, and supersonic regime (C_D , C_L , C_m ,

	$C_N, C_{L\alpha},$ and C_{ma}).
Module 2 / Module 4 / Module 6	Contain the coefficients at the sideslip angle for the subsonic, transonic, supersonic regime ($C_{y\beta}, C_{n\beta},$ and $C_{l\beta}$).
Module 7	Gives the low-aspect wing-body ratio at subsonic speeds for different configurations, with a trim option.
Module 8	Provides aerodynamic control effectiveness at hypersonic speeds for special configurations. A special configuration means the low aspect ratio wing or wing-body configurations (lifting bodies) are treated in subsonic regimes, and the two-dimensional flap and transverse jet effects are treated in hypersonic regimes.
Module 9	Provides traverse-jet control effectiveness at hypersonic speeds for special configurations.
Module 10	Gives the dynamic derivatives at the subsonic, transonic, and supersonic regimes ($C_{Lq}, C_{mq}, C_{L\dot{\alpha}}, C_{m\dot{\alpha}}, C_{lp}, C_{yp}, C_{np}, C_{nr}, C_{lr}$).
Module 11	Acts as a high lift and control device for subsonic, transonic, supersonic regimes.

Once the airplane's geometry is defined, the outputs can be obtained rapidly; their accuracy depends mainly on the accuracy of the inputs. Despite its drawbacks, there remains significant interest in the Digital DATCOM code in the aviation field.

For an input file called *aircraft_name.dcm*, the outputs of DATCOM+ are given in the following formats:

- *aircraft_name.out* – contains values of the inputs defined in *aircraft_name.dcm*. For each section of wing, horizontal tail, vertical tail and canard (if it exists), the following 11 parameters are estimated.

Ideal angle of attack	=	value (deg)
Zero lift angle of attack	=	value (deg)
Ideal lift coefficient	=	value
Zero lift pitching moment coefficient	=	value
Mach zero lift-curve-slope	=	Value (1/deg)
Leading Edge radius	=	value (Chord fraction)
Maximum airfoil thickness	=	value (Chord fraction)
Delta-y	=	value (Percent chord)
Mach	=	value
Lift-curve-slope	=	value (1/deg)
x_{AC}	=	value

Complete aircraft configuration results are presented in Table 1.1, as functions of the flight conditions and reference dimensions.

Table 1.1 Outputs of Digital DATCOM code

----- FLIGHT CONDITIONS -----											
MACH_NUMBER	ALTITUDE	VELOCITY	PRESSURE	TEMPERATURE	REYNOLD_NUMBER						
	FT	FT/SEC	LB/FT ²	DEG R	1/FT						
----- REFERENCE DIMENSIONS -----											
REF_AREA	REFERENCE_LONG.	LENGTH_LAT.	MOMENT_REF.	HORIZ.	CENTER_VERT						
FT ²	FT	FT	FT	FT	FT						
----- DERIVATIVE (PER RADIAN) -----											
ALPHA	CD	CL	CM	CN	CA	XCP	CLA	CMA	CYB	CNB	CLB
	ALPHA	Q/QINF	EPSLON	D(EPSLON)/D(ALPHA)							
----- DYNAMIC DERIVATIVES (PER RADIAN) -----											
----PITCHING----			---ACCELERATION---			-----ROLLING-----			----YAWING----		
ALPHA	CLQ	CMQ	CLAD	CMAD	CLP	CYP	CNP	CNR	CLR		
BASIC BODY PROPERTIES											
WETTED	XCG	ZCG	BASE	ZERO LIFT	BASE	FRICITION	PRESSURE				
AREA			AREA	DRAG	DRAG	DRAG	DRAG				
XCG RELATIVE TO THEORETICAL LEADING EDGE MAC											

BASIC PLANFORM PROPERTIES								
AREA	TAPER	ASPECT	QUARTER	MAC	QUARTER	Y(MAC)	ZERO	FRICITION
	RATIO	RATIO	CHORD		CHORD		LIFT	COEFFICIENT
			SWEEP		X(MAC)		DRAG	
Estimated for:								
<ul style="list-style-type: none"> • Wing - total theoretical and total exposed • Horizontal Tail - total theoretical and total exposed • Vertical Tail - total theoretical and total exposed 								
CHARACTERISTICS OF HIGH LIFT AND CONTROL DEVICES TAIL PLAIN TRAILING-EDGE FLAP CONFIGURATION								
-----INCREMENTS DUE TO DEFLECTION-----			---DERIVATIVES (PER DEGREE)---					
DELTA	D(CL)	D(CM)	D(CL MAX)	D(CD MIN)	(CLA)D	(CH)A	(CH)D	
----- INDUCED DRAG COEFFICIENT INCREMENT , D(CDI) , DUE TO DEFLECTION -----								
For each delta(trailing-edge flap, in this case) as function of angle of attack α								
CHARACTERISTICS OF HIGH LIFT AND CONTROL DEVICES WING-BODY-TAIL TRIM WITH CONTROL DEVICE ON TAIL								
---UNTRIMMED---			-----AT TRIM DEFLECTION-----					
ALPHA	CL	CD	CM	DELTAT	D(CL)	D(CL MAX)	D(CDI)	D(CD MIN) CH(A) CH(D)

- [aircraft_name.ac](#) – shows the 3D aircraft visualization

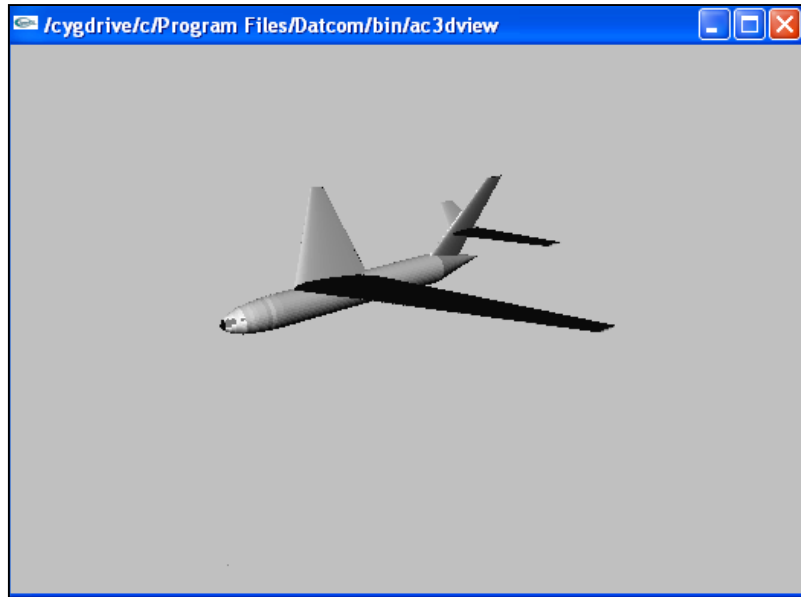


Figure 1.1 3D aircraft's visualization in Digital DATCOM code

- *aircraft_name.xml* – generates a folder called *aircraft_name.jiff* which contains images with extension .png for all outputs computed with Digital DATCOM code.

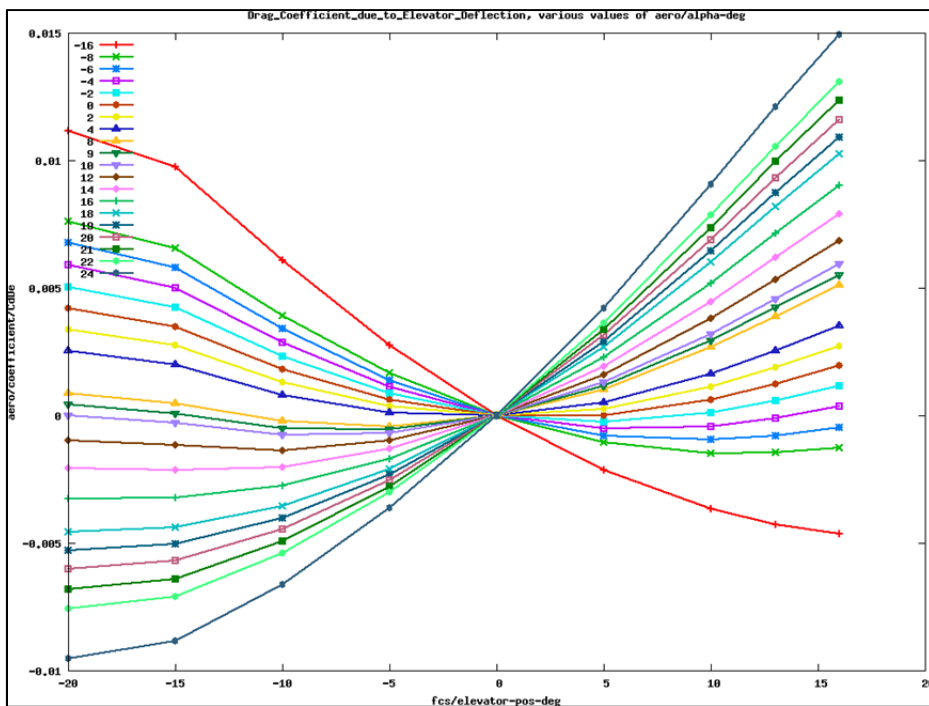


Figure 1.2 Drag coefficient due to elevator deflection results obtained with *aircraft_name.xml* command for A-380 aircraft, presented in the example given by Digital DATCOM code

- *aircraft_name.lfi* – generates the results obtained for each coefficient.

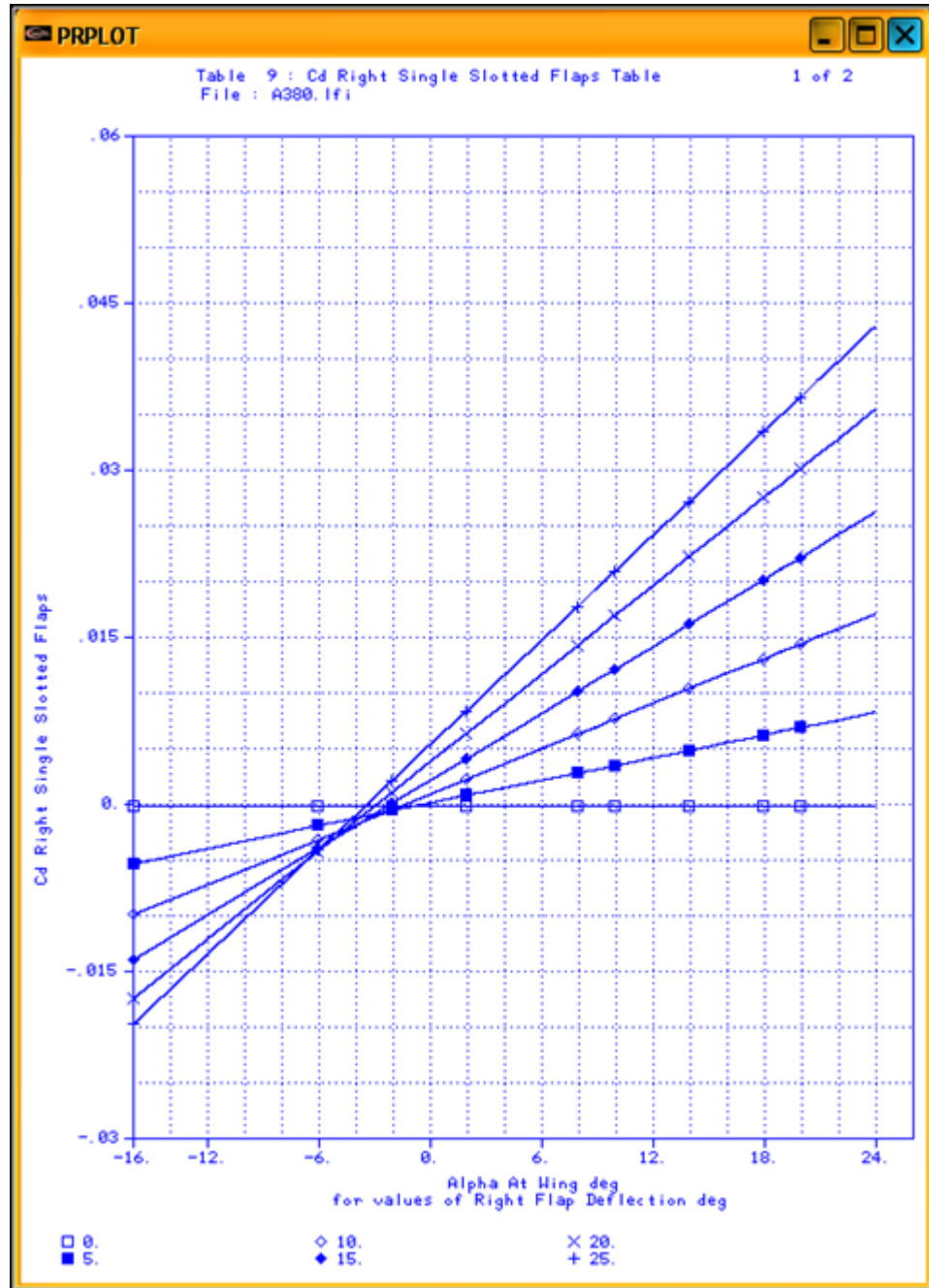


Figure 1.3 Other modality to view the results for each coefficient in Digital DATCOM code



1.1.B Advanced Aircraft Analysis (AAA) code

ADVANCED AIRCRAFT ANALYSIS (AAA) (Advanced Aircraft Analysis 3.3 code) is a code created by the Design, Analysis and Research Corporation (DARcorporation), an American company. This code is a computational tool utilized in an iterative process for preliminary aircraft design. AAA uses methodologies, statistical databases, formulas and drawings described in the following books: Airplane Design (Roskam, 2000), Airplane Flight Dynamics and Automatic Flight Controls (Roskam, 1995) and Airplane Aerodynamics and Performance (Lan *et al.*, 1981), . AAA is the industry standard aircraft design, stability and control analysis code; it can be used for small civil, military and transport aircrafts. The software has 10 independent modules, including one that estimates the aerodynamic coefficients and stability derivatives for the subsonic regime. Other modules estimate the weight, aerodynamics, performance, geometry, propulsion, stability and control, dynamics, loads, structures, cost analysis, atmosphere and flight conditions.

1.1.C MISSILE code

The MISSILE code (Champigny et al., 2004) was developed by the National Office for Studies and Research Aerospace (ONERA) in France to provide rapid estimations of aerodynamic missiles' characteristics, for Mach numbers up to 10, angles of attack up to 40° , angles of control surfaces of maximum $\pm 30^{\circ}$ and different roll angles. The methodology used in this code is based on the concept that the angle of incidence is equivalent to the integration of vortex effects. It relies on semi-empirical theoretical methods and database correlations. The MISSILE code uses DATCOM's methods.

1.2 Computational Fluid Dynamics (CFD) methods

Another, more expensive method in terms of computational resources, and therefore in calculation time, is the use of CFD methods, fundamentally based on the Navier–Stokes equations. The steady (time-invariant) aerodynamic forces and moments are defined at

different flight conditions expressed in terms of Mach numbers and angles of attack (Limache, 2000). This model required the extension of standard (inertial) CFD formulations to non-inertial reference coordinates systems, in which the aerodynamic forces corresponding to the steady flows around the moving aircraft are numerically calculated. The advantage of a CFD method lies in the way in which the aerodynamic forces are defined as functions of motion variables.

A low-order panel method code on a simplified F-16XL fighter configuration was presented in Green et al., 2004, where the twist effects on the performance of a finite wing of arbitrary shape were also determined. This approach was based on Prandtl's classical lifting-line theory, where the Fourier coefficients depended only on the wing geometry.

In (Phillips et al., 2006), the predicted results obtained with the new lifting-line method were compared with the results predicted from computational fluid dynamics (CFD) solutions. In every case, the CFD solutions showed that the drag reduction achieved with optimum twist was equal to or greater than that predicted by the lifting-line method.

The CFD method predicted the maximum lift coefficient for a finite wing from knowledge of the wing geometry and maximum lift coefficient for an airfoil section (Alley et al., 2007). The method used a correlation obtained from grid-resolved CFD solutions for 25 different wing geometries. These wings had aspect ratios ranging from 4 to 20, taper ratios from 0.5 to 1.0, quarter-chord sweep angles from 0 to 30 degrees, and linear geometric washout ranging from 0 to 8 degrees. For these ranges of parameters, the ratio of maximum wing lift to maximum airfoil section lift coefficients varied from about 0.70 to 0.98, with high aspect ratio tapered wings producing the highest lift coefficient values and low aspect ratio wings with washout and sweep producing the lowest lift coefficient values.

A novel CFD method of calculating dynamic stability derivatives was presented in Murman, (2005). This method used a non-linear reduced-frequency approach to simulate the response to a forced oscillation using a single frequency component at the forcing frequency. The

reduced–frequency approach was implemented using an automated Cartesian mesh scheme. This combination of Cartesian meshing and a reduced–frequency solver enables damping derivatives for arbitrary flight condition and geometric complexity to be efficiently and accurately calculated. The method was validated for 3D reference missile and aircraft dynamic test configurations during transonic and high–alpha flight regimes.

Babcock and Arena (2004) developed a CFD method for the determination of rate dependent aerospace vehicle stability derivatives based on finite element analysis. This method implemented an Euler routine capable of solving flow equations in a non–inertial reference frame. The non–inertial boundary condition equation of the flow solver was modified in order to decouple the position and velocity boundary conditions. The decoupled boundary condition method gave reliable results comparable to the results obtained by theoretical equations, empirical methods, and experimental data over a range of Mach numbers and geometric complexities, including results for the F–18 aircraft in the transonic regime.

1.3 Weight Functions Method

The Weight Functions Method (WFM) has been applied in various engineering fields. For example, it has been used to determine stress factors for crack problems. The WFM was applied by Yoichi et al. (2003) to solve two- and three-dimensional crack problems and to calculate stress intensity factors for arbitrary loading conditions. Their application has been generalized to calculate the response analysis of structures and to solve two-dimensional elasticity and plate bending problems. The weight functions method was found to be useful for analyzing structures subjected to a variety of loading conditions, since the responses expressed in terms of displacements and stresses may be calculated by integrating the inner product of a universal weight function and a load vector. The stress intensity factor for a patched crack within an infinite plate was successfully numerically validated using the WFM (Kim et al., 2000).

Paris et al. (1976) presented a method that is an alternate use of Bueckner and Rice's proposal (Rice, 1972) for the deviation of a two-dimensional weight function to eliminate crack tip stress intensity factors. A generalized weight functions method was developed by Wu et al. (1983) based on applying Maxwell-Betti's reciprocal theorem to the equivalent cracks problem involving mixed boundary conditions. Fett (1991) contributed an analytical solution for determining stress distribution using a weight function based on the Boundary Collocation Method. Schneider et al. (1989) used a closed-form weight function formula to calculate the stress intensity factor of an edge crack for an elastic disc. A three-dimensional linear elastic fracture mechanics (LEFM) problem was also solved using the WFM (Vainshtok et al., 1987).

Stroe (2008) solved the Lurie-Postnikov problem using general vibration equations involving linear transformations. Stroe also analyzed a holonomic system with dependent variable equations, where the WFM was applied to vibration and stability studies in cases of damped holonomic systems (Stroe et al., 2008).

The selections of H_∞ weighting functions were presented for practical applications by Jiankun et al. (2000), where the authors showed that an H_∞ weighting function for a single-input single-output system could be obtained by considering it as a series of connections of elementary low-order systems. For a constrained control effort, an explicit weighting function was obtained. They proposed a novel method for the selection of weighting functions in an H_∞ mixed sensitivity design to directly control the percentage overshoot. Real-time experimental results were presented for the roll-angle control of a laboratory scale model of a vertical take-off aircraft (Jiankun et al., 2000).

1.4 Other methods in the literature

Bryson developed a technique to determine static and dynamic stability derivatives of in slender bodies. The technique was based on the transformation of three-dimensional flow problems into two-dimensional, incompressible flow problems applied on the cross section

perpendicular to the long axis of the body, and used the concept of apparent-mass coefficients (Bryson, 1953).

An adaptive estimation method for determining unknown parameters in linear time invariant state equations was presented (Nakamura et al., 2002). The system was described using multiple observers for virtual systems with linear combinations. This method was applied to estimate the stability derivatives for an aircraft and proved its usefulness. It utilizes the subspace method with the coefficient matrices derived from input and output data to identify the state space models.

A new parameter identification algorithm called the Modified-Gain Extended Kalman Filter (MGEKF) was applied of an F-111 aircraft to solve the on-line state estimation and identification of the stability derivatives (Speyer et al., 1987). The filter formulation included a simplified Dryden wind gust model. The inclusion of the wind gust model resulted mainly in a slow response in the estimation of the stability derivatives associated with the acceleration state; estimates of the stability derivatives with the pitch rate were also calculated.

Using the concepts of aerodynamic and structural influence coefficients, Roskam (1973) has presented a method for estimating longitudinal stability derivatives for rigid and elastic airplanes. The structure of the airplane was divided into a large number of surface panels. The elastic properties of the airplane were represented by a flexibility influence coefficient matrix. Matrix algebra was used to obtain explicit expressions for longitudinal stability derivatives, with angles of attack α , speeds on the x -axis u , and pitch rates q . To validate this method, comparisons were performed with wind tunnel data for angles of attack α and speeds on the z -axis w ; derivatives obtained with a Boeing 707 model and with rigid and elastic models of a variable sweep supersonic transport configuration. There was very good agreement between the theory and tunnel data.

Vorstab95 (online source) is a computer program developed at Kansas University for aircraft aerodynamic coefficients and stability derivatives predictions for any aircraft configuration. This code uses the vortex method to predict stability derivatives at high angles of attack.

Vorstab95 calculates the lift, drag, side force, pitching moment, rolling moment, yawing moment, hinge moment, torsional moment, bending moment, longitudinal stability derivatives and lateral directional stability derivatives.

CHAPTER 2

ARTICLE 1: NEW METHODOLOGY AND CODE FOR HAWKER 800XP AIRCRAFT STABILITY DERIVATIVES CALCULATIONS FROM GEOMETRICAL DATA

Nicoleta Anton, Ruxandra Mihaela Botez and Dumitru Popescu
École de Technologie Supérieure, Montréal, Canada
Laboratory of Research in Active Controls, Aeroservoelasticity and Avionics
This article was published in The Aeronautical Journal, Vol. 114, No. 1156,
June 2010, Paper No. 3454

Résumé

Le nouveau programme FDerivatives a été conçu et développé pour calculer des dérivées de stabilité statiques et dynamiques d'un aéronef en régime subsonique, en se basant sur ses données géométriques. Le code est robuste et utilise les données géométriques et les conditions du vol pour calculer les dérivées de stabilité de l'avion. Le programme FDerivatives contient des nouveaux algorithmes et des nouvelles méthodes qui ont été ajoutés à la méthode classique DATCOM, présentée dans la référence « USAF Stability and Control DATCOM ». Le nouveau code a été écrit en utilisant MATLAB et il possède une structure complexe, qui contient une interface graphique pour faciliter le travail des potentiels utilisateurs. Les résultats obtenus avec le nouveau code ont été évalués et validés avec des données d'essais en vol prévus par CAE Inc. pour l'avion d'affaires Hawker 800XP.

Abstract

The new FDerivatives code was conceived and developed for calculating static and dynamic stability derivatives of an aircraft in the subsonic regime, based on its geometrical data. The code is robust and it uses geometries and flight conditions to calculate the aircraft's stability derivatives. FDerivatives contains new algorithms and methods that have been added to DATCOM's classical method, presented in a USAF Stability and Control DATCOM reference. The new code was written using MATLAB and has a complex structure which

contains a graphical interface to facilitate the work of potential users. Results obtained with the new code were evaluated and validated with flight test data provided by CAE Inc. for the Hawker 800XP business aircraft.

2.1 Introduction

In this paper, we describe how we used and improved DATCOM procedures (Finck et al., 1978) for the estimation of the semi-empirical aerodynamic coefficients and stability derivatives, based on geometrical aircraft data. The main advantage of these procedures is their collection of non-iterative faster methods – in terms of execution time – compared with the numerical aerodynamic computational fluid dynamics methods used within the aeronautical field.

Digital DATCOM (Galbraith) is the first implementation of the DATCOM procedures in an automatic calculations code. Better estimation has been presented by Blake et al. (2005) for the cambered fuselage pitching moment, compared to the one given in the DATCOM procedures. In this new estimation, the equations using the thin airfoil theories for the calculation were modified ((Williams et al., 1979a), (Williams et al., 1979b)). The results obtained with this new estimation, expressed in terms of the cambered fuselage pitching moment, were different for an asymmetric fuselage with respect to the DATCOM procedure, but remained the same for the symmetric fuselage.

The ADVANCED AIRCRAFT ANALYSIS (AAA) is a code, created by the American company Design, Analysis and Research Corporation (DARcorporation). This code is a computational tool used in the iterative process for preliminary aircraft design, and uses methodologies described in the Roskam (1973, 1995) and Roskam et al. (1997) books. This code has 10 independent modules, including one which provides the estimation of aerodynamic coefficients and stability derivatives for the subsonic regime (Advanced Aircraft Analysis 3.3 code).

The MISSILE code (Champigny et al., 2004) was developed by ONERA, in France, for the aerodynamic characteristics estimation of missiles at angles of attack up to 40° , for control surfaces angles of $\pm 30^\circ$ and at different rolling angles. The MISSILE and AAA codes use the DATCOM methods.

The DATCOM procedures review allowed us to discover its lack of methods for the calculation of the angle of attack at zero lift (α_0) and the pitching moment coefficient at zero lift (C_{m0}). Furthermore, the available methods in the procedures for the wing lift–curve slope calculations have not taken into account the aerodynamic twist, the stall angle (α_{CLmax}) and the maximum lift–coefficient estimations. Almost all methods of DATCOM procedure, concerning the fuselage aerodynamic, are applied to bodies of revolution.

Stability derivatives are considered to be part of an aircraft's intrinsic parameters, as they are dependent on its geometry and flight condition. A cost–effective way to reduce the necessary amount of flight test data is to estimate the aircraft's stability derivatives from its geometrical data, by use of efficient numerical prediction methods.

In Section 2.2 a brief description of the classical DATCOM method is presented, followed by the Hawker 800XP aircraft presentation given in Section 2.3.

The new FDerivatives code and its graphical interface (Section 2.4) does not only allow designers to evaluate derivatives, but also to evaluate new aircraft design concepts, to predict their performance, and to make modifications before performing more detailed design evaluations.

This section also contains a logical description of the code. All of the parameters involved in the stability derivatives estimation procedure are calculated with the new code for the following three configurations: Wing alone (W), Wing – Body (WB), and Wing – Body – Tail (WBT), from the essential geometrical data.

All improvements that were added to the DATCOM method (Popescu, 2009) are covered in Section 2.5. For example, the wing lift–distribution method is improved, the drag coefficient for *WB* configuration is calculated using a new nonlinear regression analysis, the longitudinal dynamic stability coefficients C_{Lq} and C_{mq} are estimated by considering their dependence on the dynamic–pressure ratio, and new functions are implemented for rolling–moment, side–force and yawing–moment coefficients due to the time variation in the sideslip angle, for the WBT configuration.

In Section 2.6, the stability derivatives obtained with *FDerivatives* are validated and presented for various flight cases, expressed in terms of Mach numbers and altitudes, for which experimental and geometrical Hawker 800XP aircraft data is available.

The aircraft data (geometrical and experimental) available in the literature is used for validation of the *FDerivatives* code and methodologies for the *W* and *WB* configurations. The flight test and geometrical data for the Hawker 800 XP were provided by CAE Inc. at subsonic speeds and since their numerical values are confidential, they are not presented. Results obtained with the *FDerivatives* code were validated at an altitude of 30 ft and a Mach number between 0.2 and 0.6 for the WBT configuration of the Hawker 800 XP. For future work, we are considering the validation of the stability derivatives obtained with *FDerivatives* code for the WBT configuration of the Hawker 800 XP aircraft on a Cessna Citation X research aircraft simulator at the LARCASE laboratory.

2.2 Brief description of the DATCOM method

The static and dynamic derivatives may be estimated from a knowledge of aircraft geometry alone (Finck et al., 1979a), using the DATCOM method. The traditional WBT geometries, including the control effectiveness for a variety of high–lift/control devices, are treated in the USAF’s Stability and Control DATCOM program. The Digital DATCOM program written in FORTRAN (Galbraith) is used to validate a number of stability derivatives obtained with *FDerivatives* code, which are the ones described in the next two paragraphs.

- All of the static stability derivatives (longitudinal and the lateral–directional) are expressed in the stability–axis system. The body–axis normal force and the axial–force coefficients are also estimated. For various flight conditions, i.e. Mach numbers (speeds) and angles of attack, and for all three configurations, the longitudinal drag, lift, moment, normal and axial coefficients C_D , C_L , C_m , C_N and C_A and their corresponding lift, moment, side–force, normal and roll derivatives with respect to the angle of attack and sideslip angle $C_{L\alpha}$, $C_{m\alpha}$, $C_{y\beta}$, $C_{n\beta}$ and $C_{l\beta}$ are obtained.
- The lift, moment, roll, side–force, and normal dynamic derivatives with respect to the pitch, angle of attack, roll and yaw rates C_{Lq} , C_{mq} , $C_{L\dot{\alpha}}$, $C_{m\dot{\alpha}}$, C_{lp} , C_{np} , C_{nr} and C_{lr} are also obtained. In the *FDerivatives* code, other functions available within the DATCOM method are implemented for the calculation of drag, side force, normal and roll derivatives with respect to the sideslip angle rate $\dot{\beta}$ such as $C_{D\dot{\alpha}}$, $C_{y\dot{\beta}}$, $C_{n\dot{\beta}}$ and $C_{l\dot{\beta}}$.

2.3 Aircraft model

The Hawker 800XP is a midsize twin–engine corporate aircraft with low swept–back one–piece wings, a high tailplane and rear–mounted engines, for which the maximum Mach number is equal to 0.9. This aircraft operates in the subsonic and transonic regimes. Three views of the Hawker 800XP aircraft are represented in the OXYZ reference system (Figure 2.1).

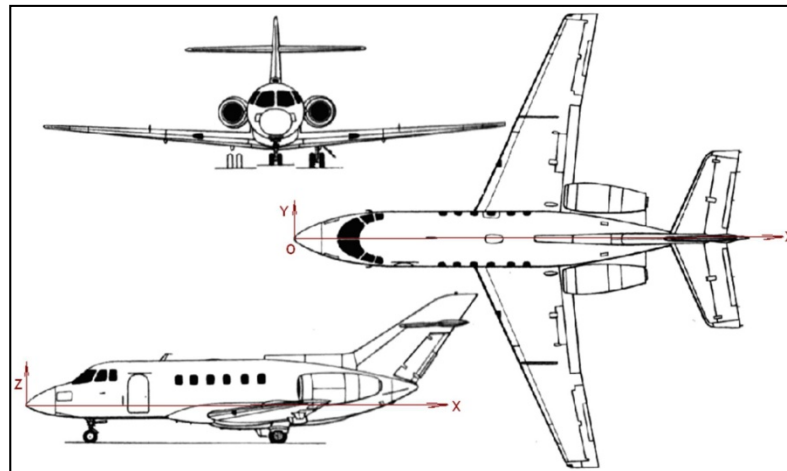


Figure 2.1 Three views of the Hawker 800XP aircraft

The most important geometrical characteristics of the Hawker aircraft, estimated from its geometrical drawings and verified with other methods available in the literature, are found for two different surfaces – fuselage and lift surfaces such as wing, horizontal tail and vertical tail:

- The length and the position of the gravity centre for the body;
- The reference area, span, aspect ratio, Mean Aerodynamic Chord (MAC), thickness ratio, leading–edge sweep (inboard/outboard), semi–span of exposed surface, root chord, tip chord and MAC for the wing, horizontal tail and vertical tail surfaces.

2.4 FDerivatives' new code

The new features (i.e. advantages) of the FDerivatives code, developed at the LARCASE laboratory with respect to the Digital DATCOM code, are described next.

The principal main advantage of this new code is the estimation of the lift, drag and moment coefficients and their corresponding stability derivatives by use of a select few aircraft geometrical data: area, aspect ratio, taper ratio and sweepback angle for the wing and the horizontal and vertical tails. In addition, the airfoils for wing, horizontal and vertical tail, as well as the fuselage and nacelle parameters, are introduced in a three–dimensional plane.

The FDerivatives code was written on MATLAB and has a complex structure which contains a graphical interface to facilitate the work of potential users. The code uses a total of **82** MATLAB functions; the aerodynamic coefficients and their stability derivatives are calculated with **24** of these:

- **3** functions for estimation of the lift, drag and moment coefficients C_L , C_D and C_m ;
- **6** functions for estimation of the static derivatives $C_{L\alpha}$, $C_{D\alpha}$, $C_{m\alpha}$, $C_{y\beta}$, $C_{n\beta}$ and $C_{l\beta}$;
- **15** functions for estimation of the dynamic derivatives:
 - i. **3** pitch rate (q) derivatives C_{Lq} , C_{mq} and C_{Dq} ;
 - ii. **3** angle of attack rate ($\dot{\alpha}$) derivatives $C_{L\dot{\alpha}}$, $C_{m\dot{\alpha}}$ and $C_{D\dot{\alpha}}$;
 - iii. **3** roll rate (p) derivatives C_{lp} , C_{np} and C_{yp} ;

- iv. 3 yaw rate (r) derivatives C_{nr} , C_{yr} and C_{lr} ;
- v. 3 sideslip angle rate ($\dot{\beta}$) derivatives $C_{Y\dot{\beta}}$, $C_{n\dot{\beta}}$ and $C_{n\dot{\beta}}$.

The 58 other functions are needed to define necessary geometric factors (two- or three-dimensional) and for proper definition of certain aerodynamic functions.

Figure 2.2 shows the logical scheme of the code, in which the inputs are the geometrical parameters for the three configuration types, and for the flight conditions characterized by Mach numbers and altitudes. The outputs are the stability derivatives for all three configurations, having already taken into account the values for Mach number and altitude. This code will be improved by calculation of the control surface (elevator, aileron and rudder) derivatives (Roskam, 2000).

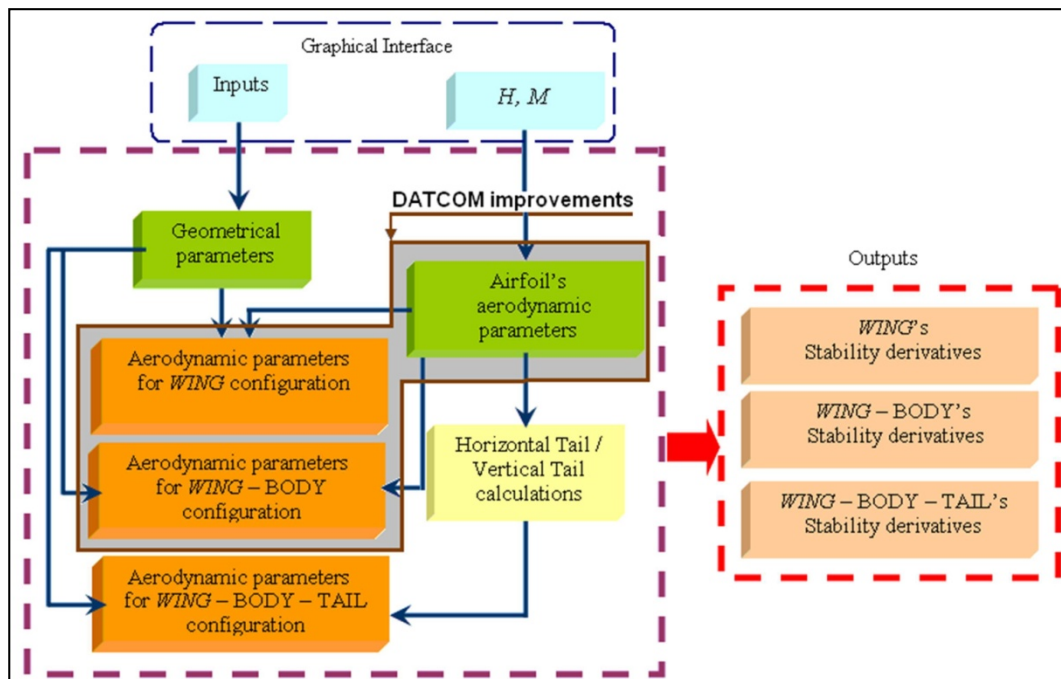


Figure 2.2 Logical scheme of FDerivatives code

The main function of the FDerivatives code is located in the MATLAB file DATCOM.m, which calls the other MATLAB functions and the text files. Modifications were made in the aerodynamics and derivatives functions. For example:

- The wing lift–distribution is calculated using the method presented by Sivells et al. (1947) and Phillips et al. (2007). In this paper it is assumed that airfoil section characteristics are not constant across the airfoil span;
- For *WB* configuration, the drag coefficient is calculated using a new nonlinear regression analysis and the pitching moment was improved ((Multhopp, 1942), (Etkin et al., 1996));
- The longitudinal dynamic stability coefficients C_{Lq} and C_{mq} are estimated by considering their dependence on the dynamic–pressure ratio;
- The new functions were implemented for rolling–moment, side–force and yawing–moment coefficients due to a time variation in the sideslip angle, for *WBT* configuration.

The primary functions for the aircraft and airfoils' geometry estimation are `aircraft_geometry.m`, which has the global aim to determine the Wing, Horizontal/Vertical Tail, Body and Nacelles geometries, while the function `airfoil_properties.m` is used to define the geometrical and aerodynamic characteristics of different airfoils (two–/three–dimensional).

The zero–lift angle and pitching moment for a wing section are calculated using the thin wing section theory (Abbot et al., 1959). The details are presented in the section 0.4.

The graphical interface for the stability derivatives calculations (Figure 2.3) allows users to make changes easily and rapidly in the aircraft geometrical data, and to choose different flight conditions. For the same aircraft configuration, it will be possible to change only the airfoil's geometries.

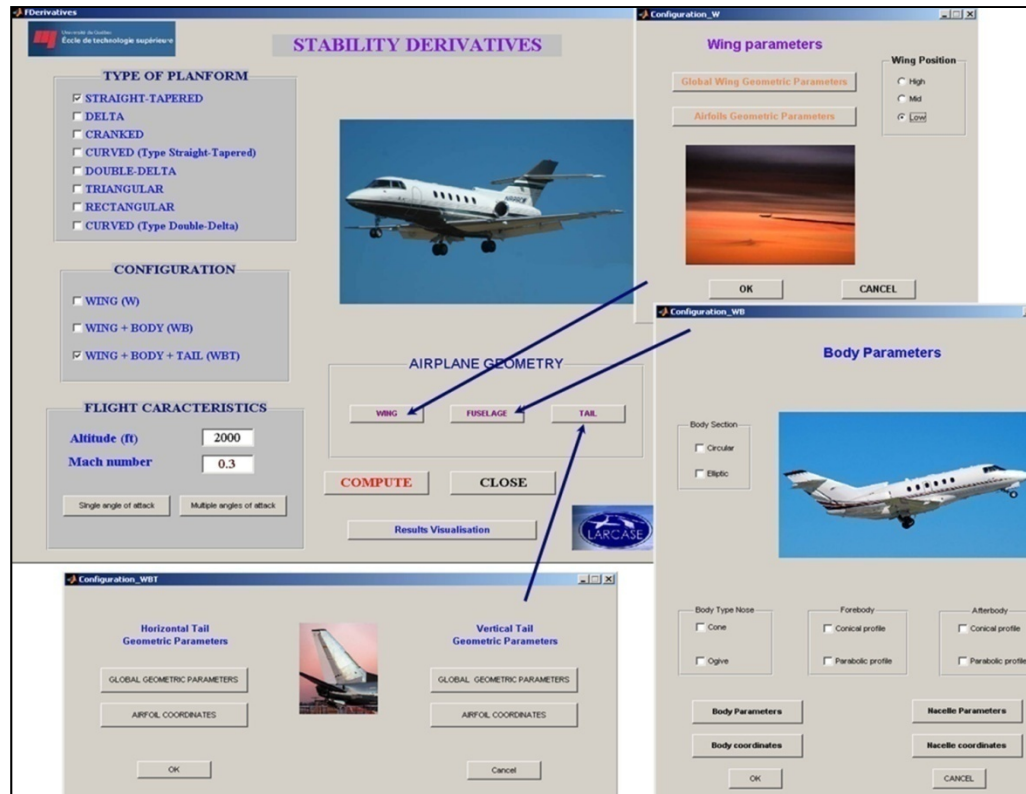


Figure 2.3 Graphical interface of the FDerivatives code

In the main window, called Stability Derivatives, the platform's (wing) type, configuration, flight conditions (Mach numbers, altitudes and angles of attack ranges) are defined. It is possible to fix the wing position and its roughness. For each of the three major components (Wing, Horizontal/Vertical Tail), global parameters and airfoil coordinates situated at the root, MAC and tip sections are considered. The Horizontal stabilizer may be positioned on the fuselage or on the Vertical stabilizer. The inputs to the body configuration are the three global parameters: body length, position of the gravitational centre and the fuselage coordinates (in three dimensions) relative to the reference system (Figure 2.4). The positions of the nacelles are described by their number, axial positions, lengths and coordinates relative to the reference system.

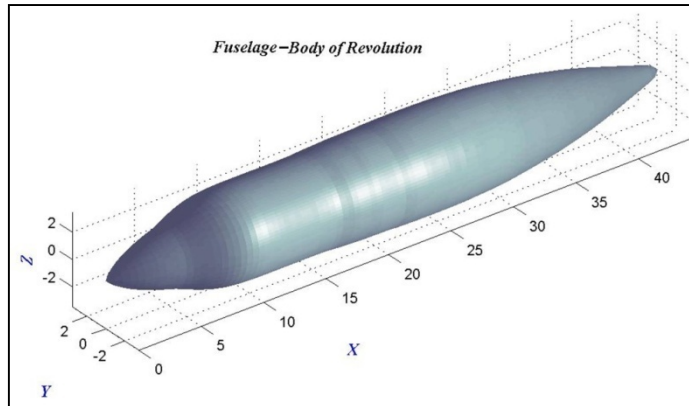


Figure 2.4 Fuselage represented as a body of revolution

The outputs of the FDerivatives code are saved in three formats: jpeg, MATLAB figures, and text files, which contain all of the numerical data.

2.5 DATCOM improvements for stability derivatives calculations

In the new FDerivatives code, it has implemented an additional number of derivatives, calculated with DATCOM methods, which are not implemented in the Digital DATCOM code. In addition, the method for lift-coefficient estimation has also been improved, and lift-coefficient values were found that are closer to the experimental values than are Digital DATCOM values. Table 2.1 shows all of the improvements associated with the FDerivatives code.

Table 2.1 Outputs for Wing – Body – Tail configuration

Static derivatives								
C_L	C_D	C_m	C_{La}	C_{Da}	C_{ma}	$C_{l\beta}$	$C_{n\beta}$	$C_{y\beta}$
◆	●	●	●	■	●	●	●	●
Dynamic derivatives								
C_{Lq}	C_{Dq}	C_{mq}	C_{Ladot}	C_{Dadot}	C_{madot}	C_{lp}	C_{np}	C_{yp}
●	●	●	●	■	●	●	●	●

C_{lr}	C_{nr}	C_{yr}	$C_{y\beta\dot{}}$	$C_{n\beta\dot{}}$	$C_{l\beta\dot{}}$			
●	●	■	■	■	■			
<ul style="list-style-type: none"> ● DATCOM method ■ DATCOM method implemented in the FDerivatives code ◆ C_L estimation method improved in the FDerivatives code 								

- A. The lift, drag and moment coefficients as well as their static and dynamic derivatives were calculated for a three-dimensional flow around the aircraft.
- B. The DATCOM method assumes that airfoil section characteristics are constant across the airfoil span, and so keeps only the root section for the entire wing (or the horizontal and vertical tails). With these conditions, it cannot obtain a good aircraft configuration using Digital DATCOM code – a better estimation is needed for the lift-coefficient. The FDerivatives code achieves this by considering several sections across the wing span, taking ten sections into consideration.

With the FDerivatives code:

- The total twist (aerodynamic plus geometrical) is estimated, compared with only the geometrical twist estimated in the DATCOM method;
- Several sections are considered across the wing span and are estimated with good precision by taking into account the wing root, the MAC and the tip airfoils.

To obtain the global lift coefficient for a wing with a nonlinear twist, a lift-line type method is used (Sivells et al., 1947).

The wing lift-distribution is calculated using the induced angle of attack for a finite wing span and the airfoil lift data are then calculated at ten wing sections along its span. These ten wing airfoils are situated at the root, MAC, tip and seven other intermediate bi-dimensional sections. If the airfoil coordinates are not all given as inputs, FDerivatives code has a function that can reconstruct them for any intermediate airfoils.

The determining lift–distribution method used in this code uses successive approximations. For each airfoil section, a section lift–coefficient distribution is assumed, and then the bi–dimensional lift coefficients are calculated. Equation (2.1) developed by Phillips et al. (2007) is used here to estimate the maximum lift coefficient C_{Lmax}

$$C_{Lmax} = \left(\frac{c_L}{c_{Lmax}} \right)_{\substack{\theta=0 \\ \Lambda=0}} \kappa_{Ls} \kappa_{L\Lambda} (c_{Lmax} - \kappa_{L\theta} C_{L\alpha} \theta) \quad (2.1)$$

This method applies to any wing geometry, including a twisted wing, and is intended to replace the old algorithm used in the DATCOM method for a linear twisted wing.

The original formula contained a stall correction factor κ_{Ls} which was eliminated in FDerivatives code. The maximum lift coefficient for the entire wing is then calculated for various flight conditions with the following equation:

$$C_{Lmax} = \left(\frac{c_L}{c_{Lmax}} \right)_{\substack{\theta=0 \\ \Lambda=0}} \kappa_{L\Lambda} (c_{Lmax} - \kappa_{L\theta} C_{L\alpha} \theta) \quad (2.2)$$

The sweep correction factor depends on the aspect and taper ratios, as shown in eq.(2.3)

$$\kappa_{L\Lambda} \cong 1 + \kappa_{\Lambda 1} \Lambda - \kappa_{\Lambda 2} \Lambda^{1.2} \quad (2.3)$$

The maximum lift coefficient of the section c_{Lmax} used in eq.(2.2) is calculated in the section for which the lift coefficient has the highest value. After obtaining the lift distribution along the wing span, the stall coefficient (corresponding to the maximum lift coefficient) of the entire wing is obtained using eq.(2.2).

Because the experimental data for W and WB configurations for the Hawker 800XP are unavailable (are provided by CAE Inc. just for WBT configuration), we need to validate the results obtained with the FDerivatives code by using other aircraft models founded in the literature for which experimental data are available for complete aircraft configurations.

The first set of results expressed in terms of lift–coefficient versus the angle of attack is shown in Figure 2.4 for the wing characteristics (Table 2.2) at Mach number 0.35 and

altitude $H = 4500\text{ft}$ (Nelly et al., 1947). The maximum lift-coefficient C_{Lmax} obtained with and without corrections (see eq.(2.1) and (2.2)) are compared with the experimental C_{Lmax} shown in the lower part of the Table 2.2 (Nelly et al., 1947). The relative error between the experimental and calculated values without the stall correction factor is 0.22%, and with the stall correction factor is 8.7%. The formula necessary to estimate the maximum lift coefficient is the same with eq.(2.2).

Table 2.2 Wing characteristics

Airfoils	Root section	NACA 4420
	Tip section	NACA 4412
Taper ratio		2.5
Aspect ratio		10.05
Span		15 [ft]
Area		22.39 [ft ²]
Root chord		2.143 [ft]
MAC		1.592 [ft]
Tip chord		0.8572 [ft]
Geometrical twist		-3.5 ⁰
Aerodynamical twist		-3.4 ⁰
Sweepback angle of leading edge		12 ⁰
Dihedral angle		2 ⁰
Reynolds number		3490000
Results		
C_{Lmax} experimental	C_{Lmax} with correction eq.(2.1)	C_{Lmax} without correction eq.(2.2)
1.37	1.2510	1.3730

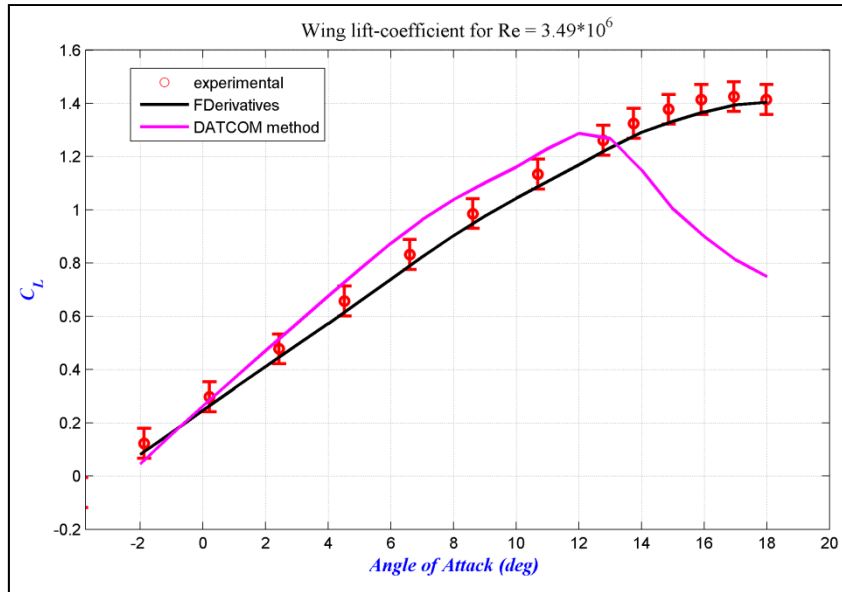


Figure 2.5 Lift coefficient distribution for the W configuration at $Re = 3.49 \cdot 10^6$

The lift-coefficient's curve (Figure 2.5) estimated with the method implemented in FDerivatives code is contained in the marginal error calculated for the experimental data. This error represents 3.5% of maximum lift-coefficient provided by the experimental. On the other hand, the results provided by DATCOM method are quite far from experimental, where the slope of the lift-coefficient is different and the maximum lift-coefficient appears for a lower stall angle.

The WB model configuration is presented by Letko et al. (1950), in which the lift and drag coefficients obtained experimentally for a Mach number of 0.166 and an altitude of 2,075 ft are also given. The geometrical characteristics for the wing and fuselage are given in Table 2.3.

Table 2.3 Basic model geometrical characteristics

Fuselage	
Length	40.0 [in]
Fineness ratio	6.67
Wing	
Span	36 [in]
Area	324 [in ²]

Aspect ratio	4.0
Taper ratio	0.6
MAC	9.19 [in]
Quarter-chord sweepback angle	0 ⁰
Twist	0 ⁰
Dihedral angle	0 ⁰
Airfoil section	NACA 65A008

Figure 2.6 shows the very good validation (near-overlap) of calculated with experimental lift-coefficient, both versus angle of attack data, using the new FDerivatives code.

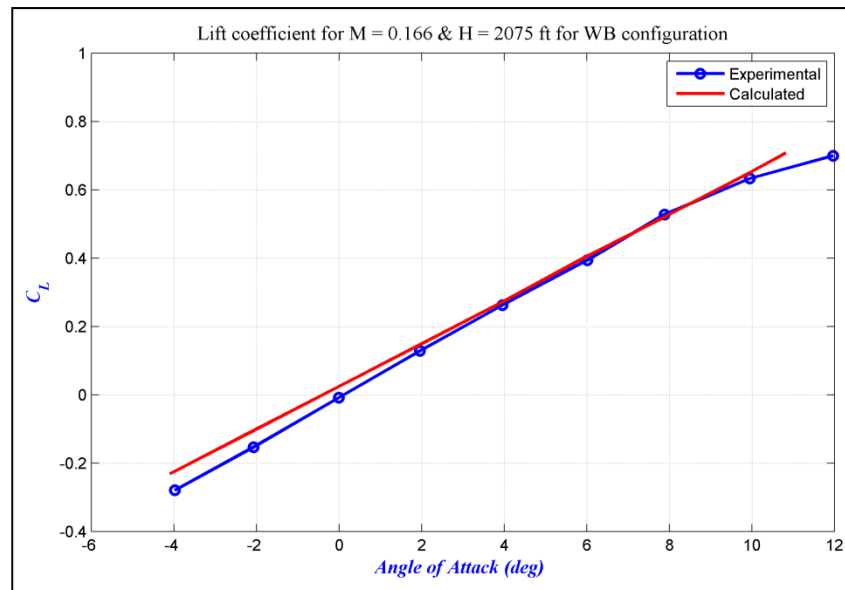


Figure 2.6 C_L versus α (experimental versus calculated) for *WB* configuration

C. Better estimation of drag for the *WB* configuration by using a new nonlinear regression analysis. Better estimation of pitching moments for the *WB* configuration.

This method evaluates and combines the isolated moment due to lift of the wing and of the body, with allowance for their effect on each other. The wing pitching moments due to effective wing lift includes the effects of body up-wash on the wing and wing carryover onto the fuselage. These are accounted for on the basis of relations already in the DATCOM method. Fuselage and nacelles' free moments due to induced flow from the wing can be estimated by the technique developed by Multhopp (1942). The sum of these two

contributions added to the wing pitching moment due to wing drag gives a better estimation of the pitching moment than the linear regression analysis method in DATCOM for a WB configuration.

The new FDerivatives code has changed the way the total moment coefficient is computed. The nacelles' contribution is included and the total moment is presented as a sum of the moment given by the Wing–Body–Nacelles (WBN) and the Horizontal Tail (HT) contributions:

$$(C_{m0})_{total} = (C_m)_{WBN} + (C_m)_{HT} \quad (2.4)$$

$$(C_m)_{WBN} = \int_0^{C_L(\alpha)} \left(\frac{dC_m}{dC_L} \right)_{CG} d(C_L)_{WBN} + (C_{m0})_{WBN} \quad (2.5)$$

where $\left(\frac{dC_m}{dC_L} \right)_{CG} = \frac{x_{CG}}{\bar{c}} + \frac{\sum(C_{m\alpha})}{\sum(C_{L\alpha})}$ is estimated as a function of gravitational centre position

and

$$\sum(C_{m\alpha}) = (C_{m\alpha})_{free} + (C_{m\alpha})_{drag} + (C_{m\alpha})_{BN} + (C_{m\alpha})_{W(B)+B(W)}$$

$$(C_{m0})_{WBN} = \left[(C_{m0})_W + (C_{m0})_{BN} + \Delta C_{m0} \right] \frac{(C_{m0})_M}{(C_{m0})_{M=0}} .$$

The moment coefficient's contribution to the body $(C_{m0})_B$ is defined by Etkin et al. (1996), where the fuselage's zero pitching moment coefficients and the two–times–zero pitching moment coefficients provided by the nacelles are also given. Figure 2.7 shows the moment coefficients (experimental and calculated) versus the angle of attack.

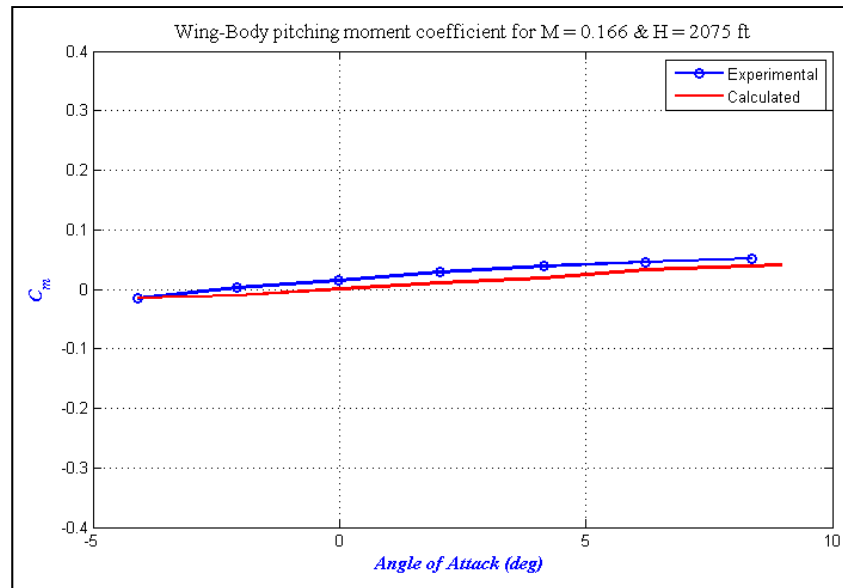


Figure 2.7 C_m versus α (experimental and calculated), *WB* configuration

- D.** The longitudinal dynamic stability coefficients C_{Lq} and C_{mq} computed in Digital DATCOM are assumed to be linear. In the *FDerivatives* code, these derivatives are estimated by considering their dependence on the dynamic-pressure ratio (q/q_∞). These two derivatives are represented for different Mach numbers versus the angle of attack at the altitude of 30 ft in Figure 2.8. The linearity appears only if the ratio $q/q_\infty = 1$.

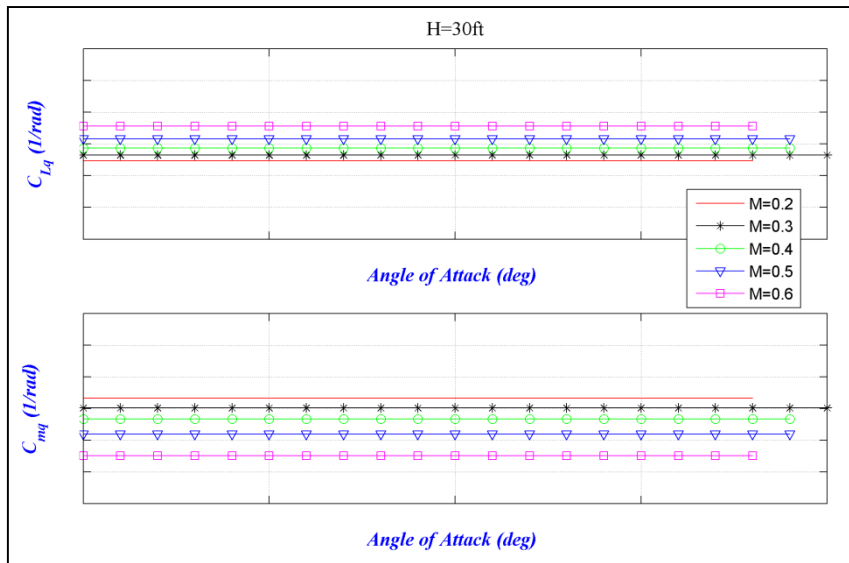


Figure 2.8 C_{Lq} and C_{mq} versus α , Hawker 800XP, WBT configuration

In addition, C_{Dq} is computed in the new code using the method described in DATCOM, and depends on the pitching rate q , which is defined in the interval [0 to 10] deg/s. The variation of C_{Dq} with the angle of attack for different Mach numbers is presented in Figure 2.9 for $M = 0.2$ to 0.6 and altitude $H = 30$ ft in the WBT configuration, where the pitch rate $q = 5$ deg/s.

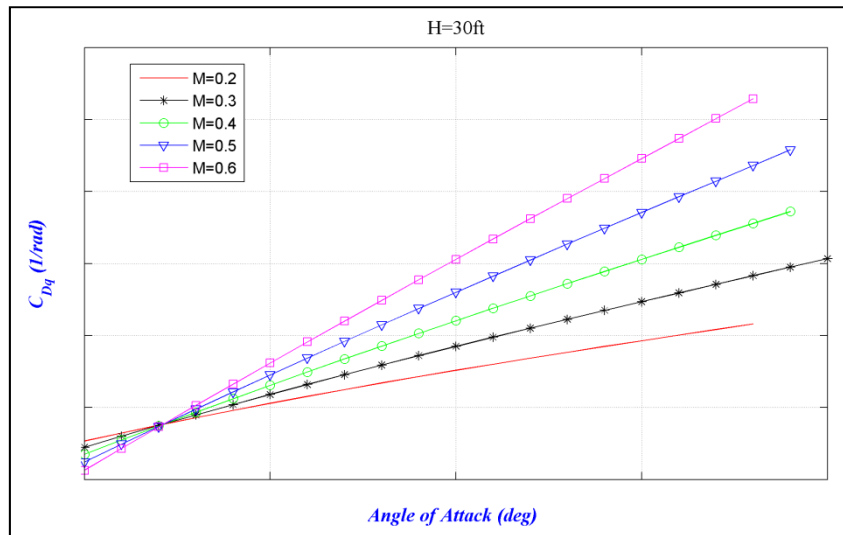


Figure 2.9 C_{Dq} versus α at the altitude $H = 30$ ft and $q = 5$ deg/s

- E. The zero-lift angle and pitching moment for a wing section are also calculated in the FDerivatives code, using the thin wing section theory (Abbot, 1959) and a Fourier method. Very good approximations for the zero-lift coefficients and pitching moments are obtained using the Pankhurst method (Abbot, 1959).
- F. In the subsonic regime, the new FDerivatives code was improved by taking into account equations for the following dynamic stability derivatives (with the results presented in Figures 2.10 to 2.12):
- Rolling moment coefficient due to a time variation in the sideslip angle $C_{l\dot{\beta}}$ for the WBT configuration,

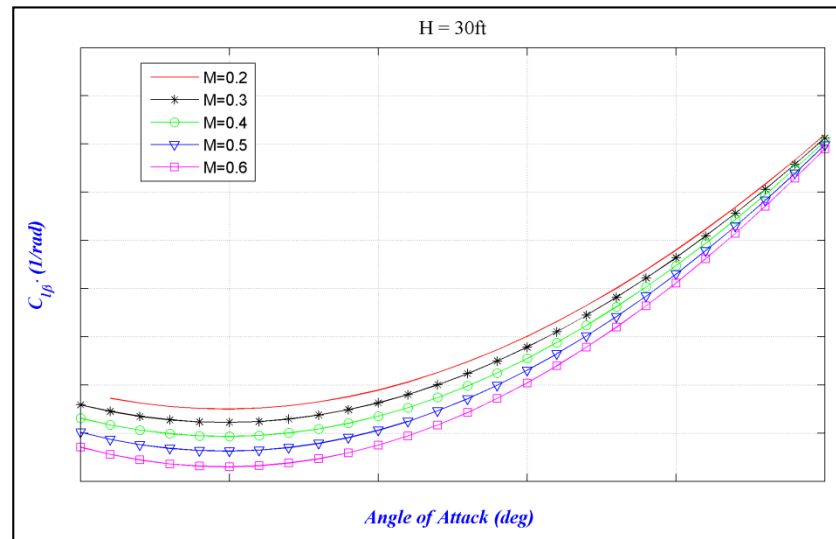


Figure 2.10 $C_{l\dot{\beta}}$ versus α at the altitude $H = 30$ ft

- Side-force coefficient due to a time variation in the sideslip angle $C_{y\dot{\beta}}$ for the WBT configuration,

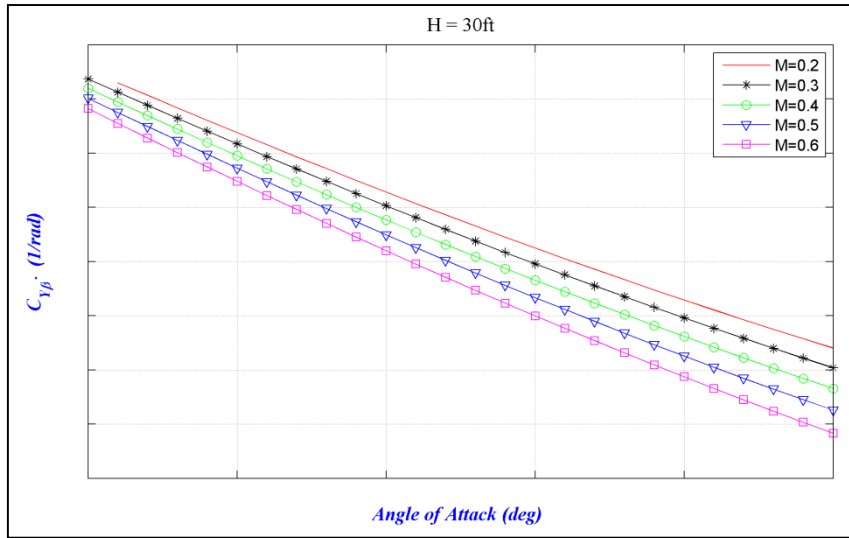


Figure 2.11 $C_{y\beta}$ versus α at the altitude H = 30 ft

- The yawing-moment coefficient due to a time variation in the sideslip angle $C_{n\dot{\beta}}$ for the WBT configuration.

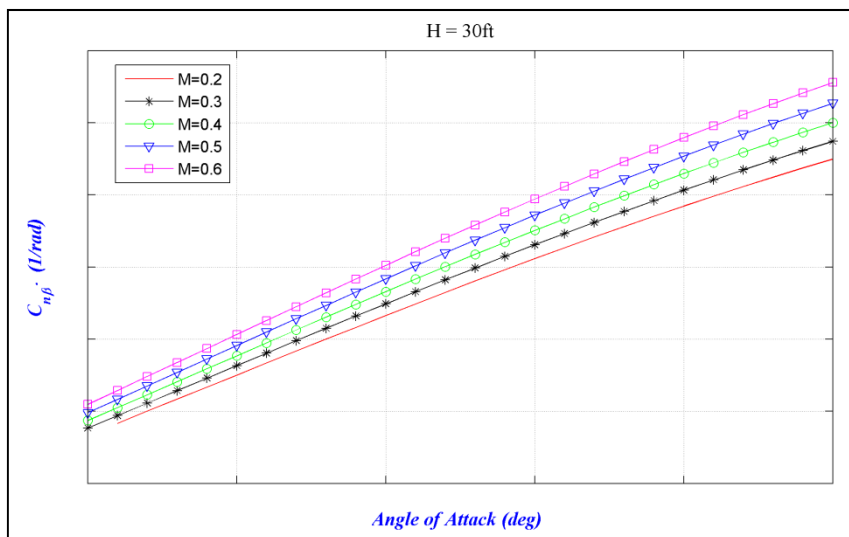


Figure 2.12 $C_{n\dot{\beta}}$ versus α at the altitude H = 30 ft

2.6 Validation results obtained for the entire Hawker 800XP aircraft

Results are presented in terms of stability derivatives for the flight cases expressed by the following air conditions:

- Altitude = 30.0 ft;
- Mach numbers = 0.2, 0.3, 0.4, 0.5 and 0.6;
- Angle of attack = -5 to 20 deg.

To validate the results, expressed in terms of lift and drag coefficients obtained with the FDerivatives code, these types of results are compared with the numerical results obtained from the Digital DATCOM code and experimental Hawker 800XP results (that means the flight tests), as shown in Figures 2.13 to 2.16, for Mach number $M = 0.4, 0.5$. The FDerivatives curves are closer for the experimental data, then the Digital DATCOM code are. The flight test and geometrical data were provided by CAE Inc for the Hawker 800 XP, and for this reason, the results are confidential and no numbers are shown on the graphs.

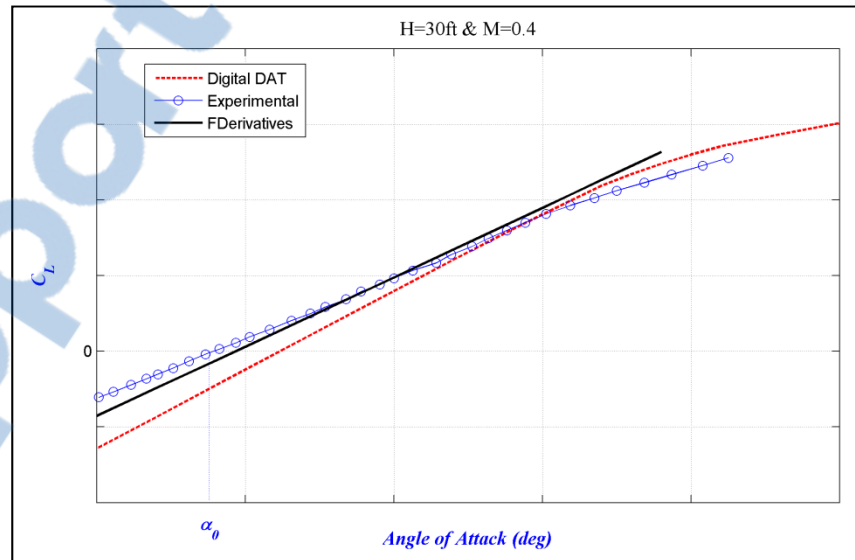


Figure 2.13 C_L versus α at $M = 0.4$

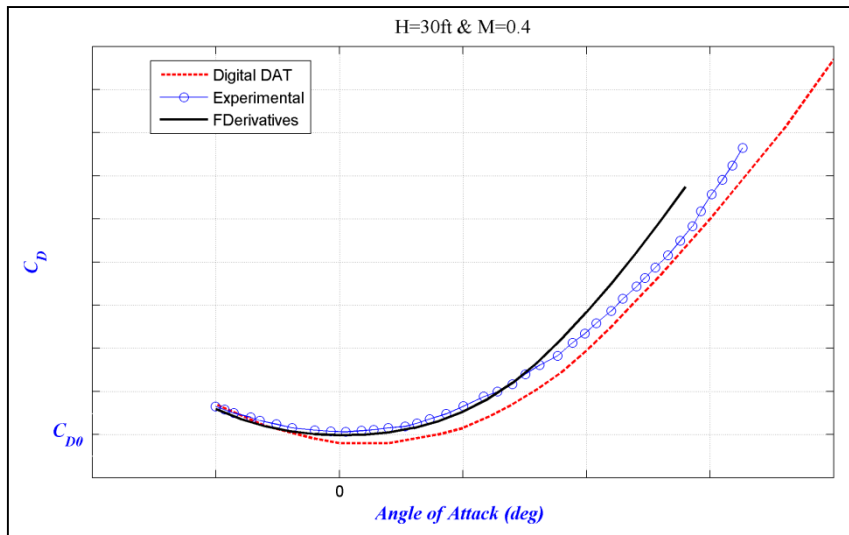


Figure 2.14 C_D versus α at $M = 0.4$

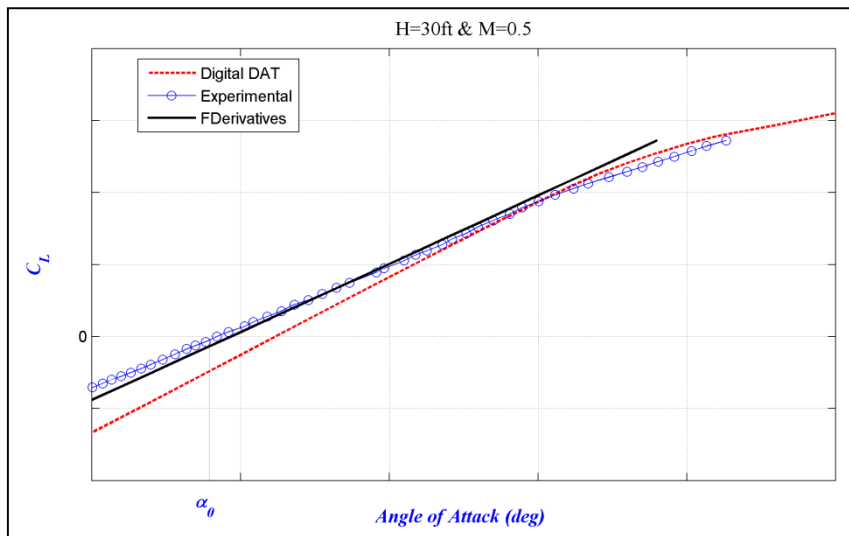


Figure 2.15 C_L versus α at $M = 0.5$

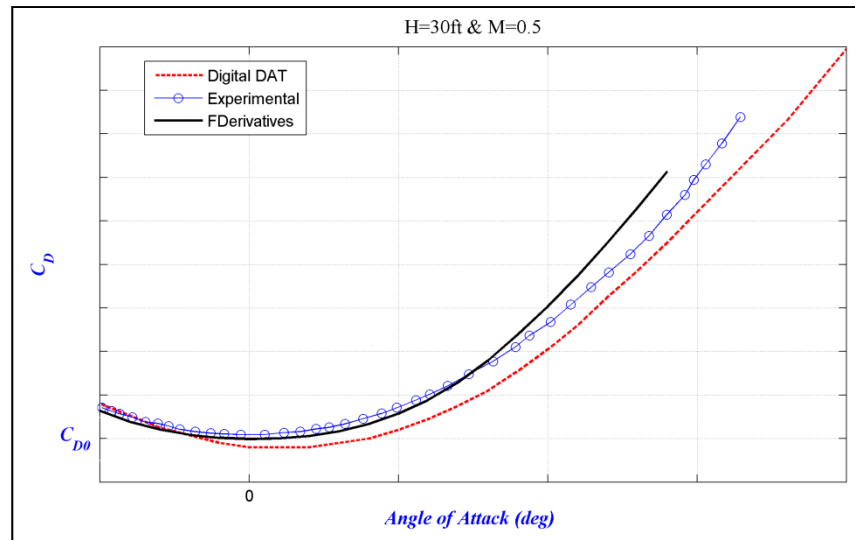


Figure 2.16 C_D versus α at $M = 0.5$

From the above figures, we can see that differences appear for angles of attack greater than 10 degrees.

Results expressed in terms of derivatives with the exception of the three results presented in part **F** (Figures 2.10 to 2.12) obtained with the new FDerivatives code are slightly different from those obtained with the Digital DATCOM program (Figures 2.17 to 2.24), due to the fact that FDerivatives code is improved with respect to the DATCOM method implemented in Digital DATCOM code.

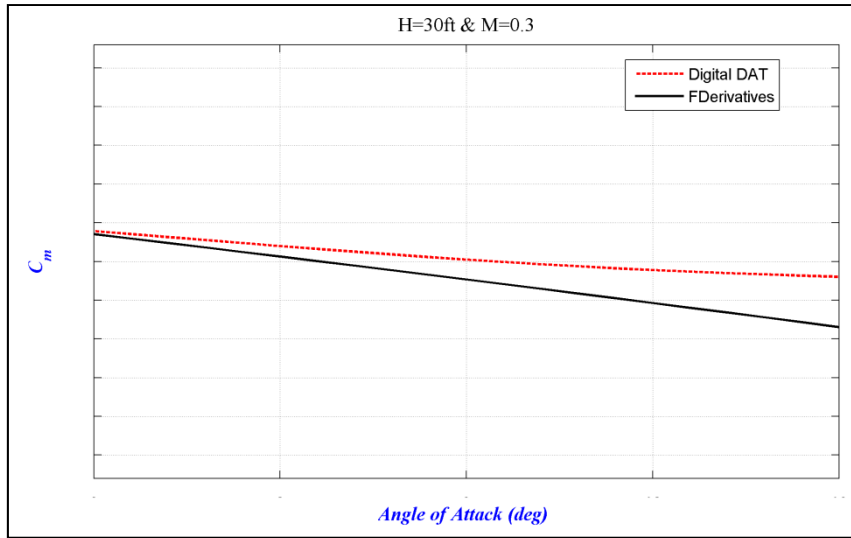


Figure 2.17 C_m versus α at Mach number = 0.3

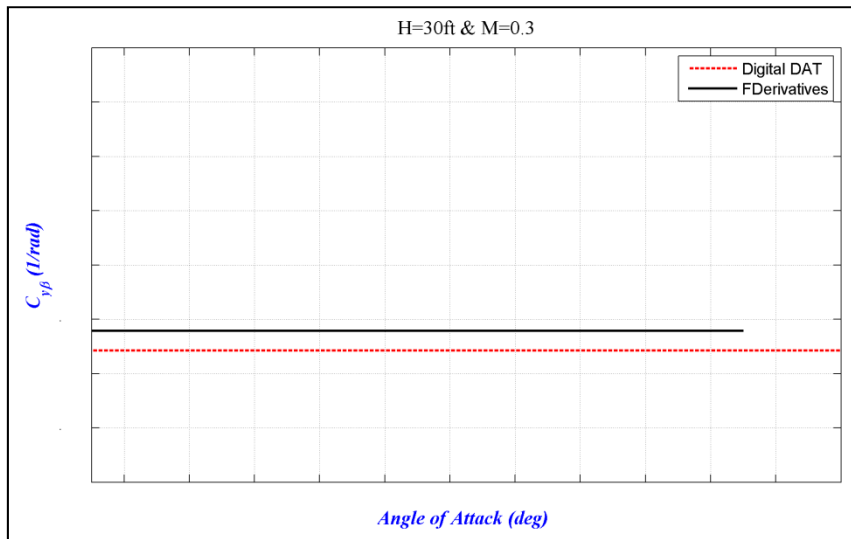


Figure 2.18 $C_{y\beta}$ versus α at Mach number = 0.3

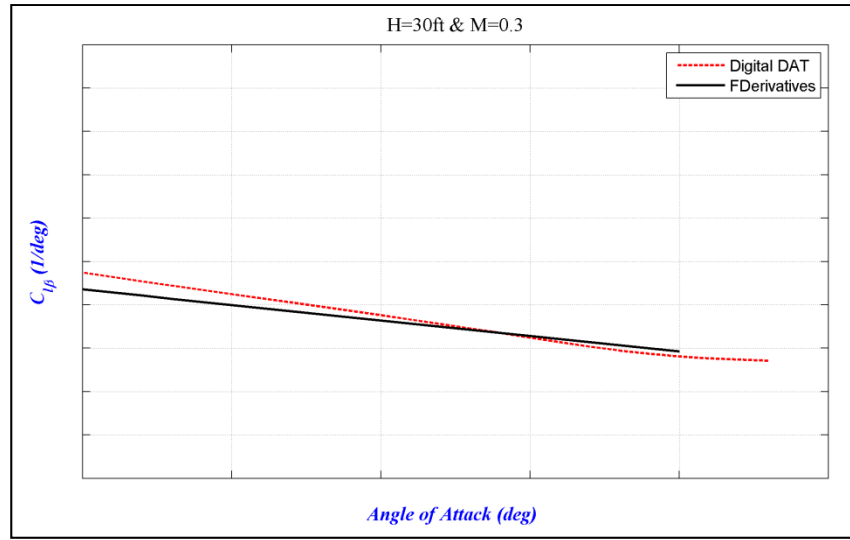


Figure 2.19 $C_{l\beta}$ versus α at Mach number $M = 0.3$

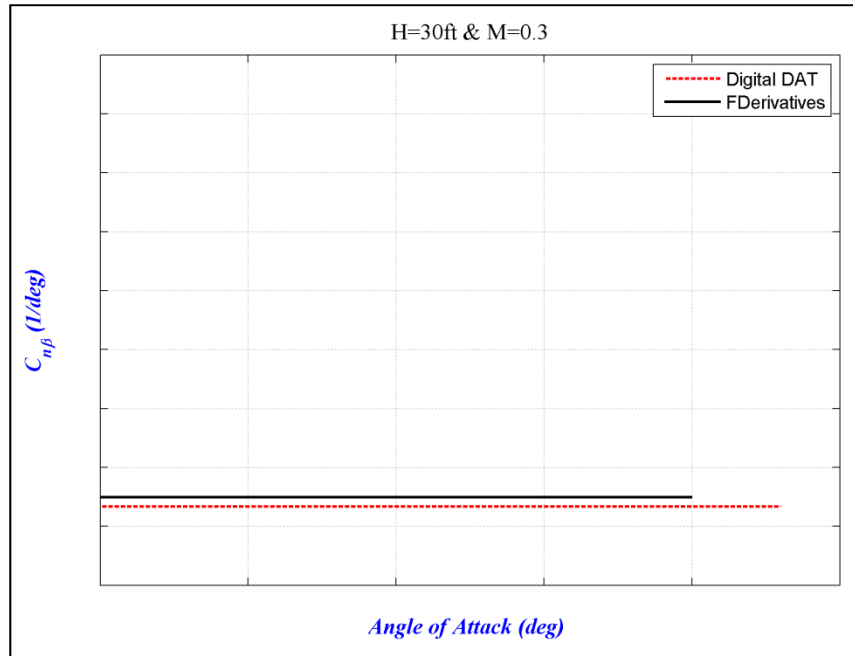


Figure 2.20 $C_{n\beta}$ versus α at Mach number $M = 0.3$

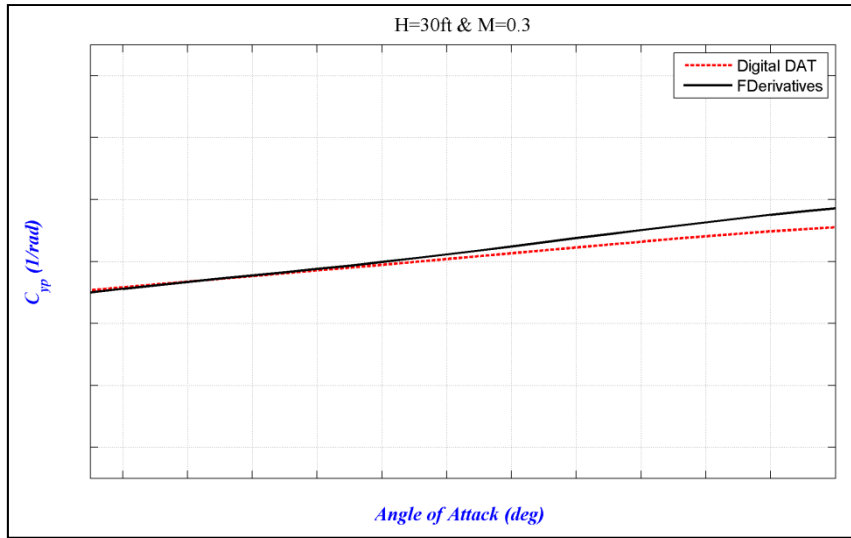


Figure 2.21 C_{yp} versus α at Mach number $M = 0.3$

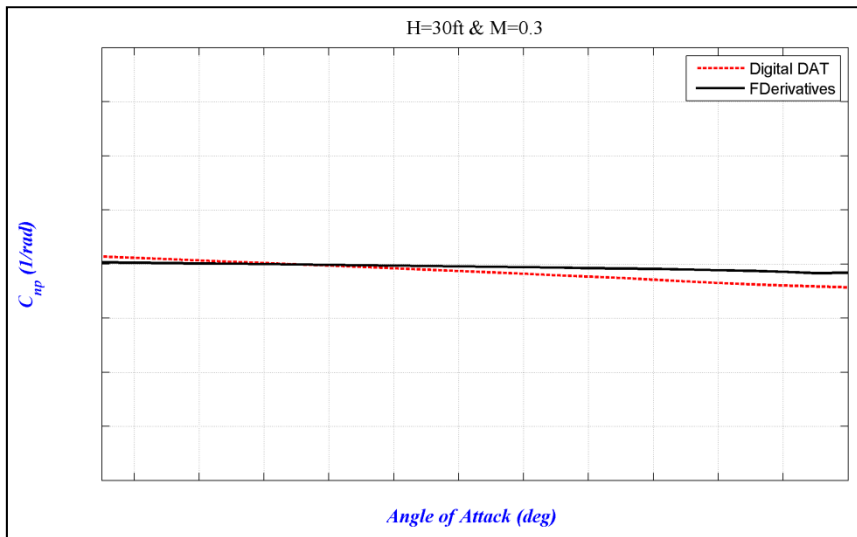


Figure 2.22 C_{np} versus α at Mach number $M = 0.3$

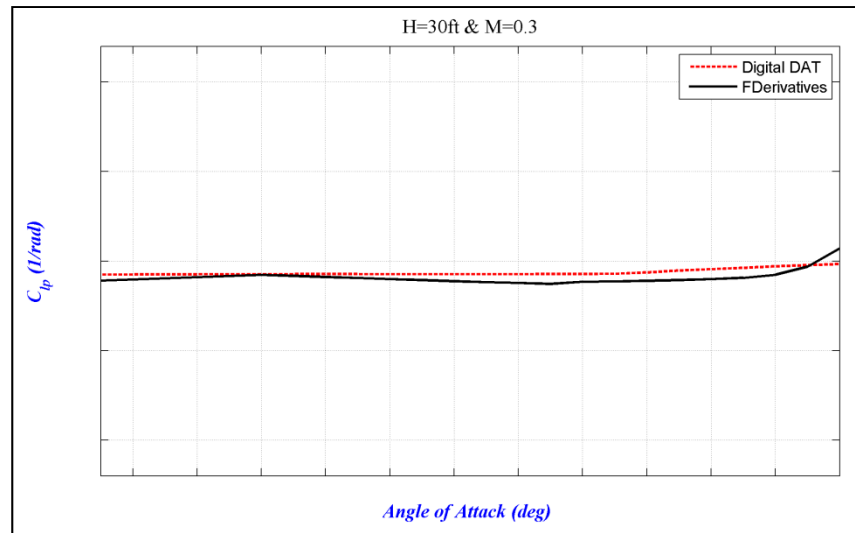


Figure 2.23 C_{lp} versus α at Mach number $M = 0.3$

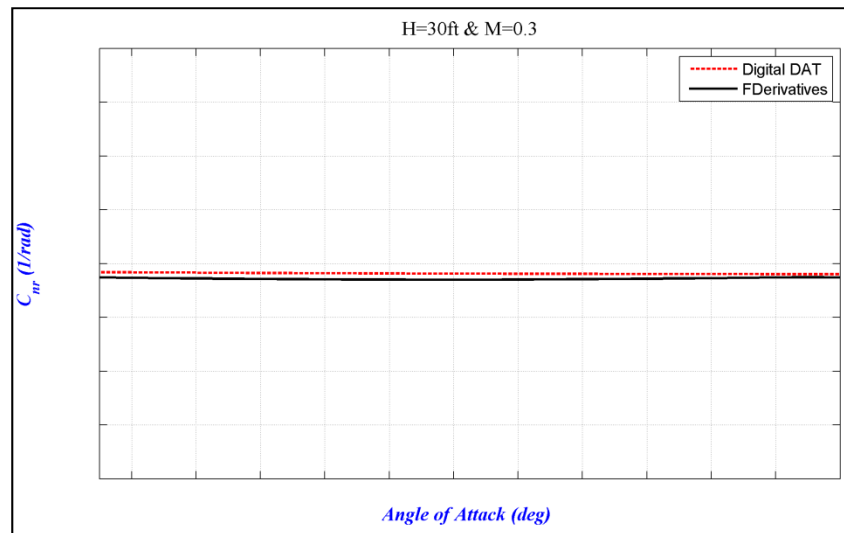


Figure 2.24 C_{nr} versus α at Mach number $M = 0.3$

2.7 Conclusions

The new FDerivatives code was conceived by using different methods found in the literature, along with the main method presented in DATCOM. This new code was designed to obtain all of the aircraft stability derivatives by considering only a small amount of geometrical data as inputs. The code is very easy to modify, as it gives the user the possibility to choose the

number of derivatives, the aircraft configuration and the flight cases. All the outputs become inputs for a model that will be implemented in an aircraft simulator at LARCASE laboratory.

The lift-coefficient method implemented in the presented code is better than the lift calculated with the DATCOM method due to better evaluation of the wing geometry – much closer to a real wing with changes in geometry and airfoil characteristics, and with a nonlinear twist. Other derivatives, which are not calculated in the Digital DATCOM code, are implemented in this new FDerivatives code.

To estimate the aerodynamic characteristics and stability derivatives for a single aircraft configuration, FDerivatives provides the best results. The user needs only to employ the proper dimensions for the desired configuration. This code represents a significant amount of work – it contains over 10,000 lines of MATLAB and 226 text files. Its methodology and a part of results are validated using the Hawker 800XP aircraft flight tests and the rest of them are verified with the Digital DATCOM results.

CHAPTER 3

ARTICLE 2: STABILITY DERIVATIVES FOR X-31 DELTA-WING AIRCRAFT VALIDATED USING WIND TUNNEL TEST DATA

Nicoleta Anton, Ruxandra Mihaela Botez and Dumitru Popescu
École de Technologie Supérieure, Montréal, Canada

Laboratory of Research in Active Controls, Aeroservoelasticity and Avionics

This article was published in Proceeding of the Institution of Mechanical Engineers, Vol.225,
Part G, Journal of Aerospace Engineering, pp. 403-416, April 2011

DOI: 10.1243/09544100JAERO799

Résumé

Le calcul et la validation des coefficients aérodynamiques et des dérivées de la stabilité de l'avion X-31 font l'objet de cette étude. Afin d'améliorer les calculs des dérivées de stabilité d'un avion à aile delta en régime subsonique, un recueil de nouvelles méthodes est programmé dans un nouveau code, FDerivatives, et ajouté à la méthode classique DATCOM. Le code FDerivatives est décrit, de même que les améliorations obtenues pour la configuration de l'avion avec le canard. Toutes les données géométriques requises pour l'estimation des coefficients aérodynamiques de l'avion X-31 sont calculées pour la configuration totale de l'avion (aile – fuselage – empennage). Le code Digital DATCOM a été utilisé pour valider la géométrie et les coefficients aérodynamiques, ainsi que la méthode implicite et la méthode de Jorgensen. Les résultats expérimentaux sont fournis pour le modèle X-31 dans la soufflerie à basse vitesse allemande – hollandais (DNW-NWB). Le code FDerivatives donne de très bons résultats en comparaison avec ces résultats expérimentaux obtenus en soufflerie. Une analyse du mouvement longitudinal de l'avion X-31 basée sur des résultats obtenus avec le code FDerivatives, est présentée à la fin de l'article.

Abstract

The calculation and validation of the aerodynamic coefficients and stability derivatives for the X-31 model aircraft are the focus of this study. To improve the stability derivative calculations for a delta-wing aircraft in the subsonic regime, a compendium of new methods is programmed into a new code, *FDerivatives*, and added to the classical DATCOM method. The *FDerivatives* code is described, as are the improvements achieved in the aircraft canard configuration. All of the required geometrical data relative to the aerodynamic coefficient estimation of the X-31 aircraft are calculated for the Wing-Body-Tail configuration. Digital DATCOM code was used to validate the geometry and the aerodynamic coefficients, as well as the implicit method and the Jorgensen method. Experimental results are provided for the X-31 model in the Low-Speed Wind Tunnel of the German-Dutch Wind Tunnels (DNW-NWB). The *FDerivatives* code gives very good results in comparison with experimental results. An analysis of longitudinal motion, based on *FDerivatives* results, is presented at the end.

3.1 Introduction

From a methodological perspective, this paper discusses a qualitative approach and presents the approaches we used to produce a tool for calculating the aerodynamic coefficients and derivatives of stability in an open and cooperative fashion. One of the most difficult aspects of aircraft development is defining the stability and control characteristics. To predict these characteristics, some tools can be used – wind tunnel tests and flight tests. Flight testing is more accurate, but it is very expensive. Other methods work with models that have different levels of fidelity, such as Computational Fluid Dynamics (CFD) for a nonlinear aircraft model.

Several studies have been conducted on the X-31 aircraft. Yeh et al. (1991) performed numerical calculations for pre-stall and post-stall flight regimes, including variable canard

deflection settings, and the numerical results were compared with wind tunnel and flight test data.

Phenomena such as wing rock, spins, and departures, which can dominate the high-alpha behavior of the X-31 configuration and restrict its usable flight envelope, were identified (Croom et al., 1993) by using dynamic model testing techniques for high angle-of-attack. The results of these tests have been used to design flight control concepts and configuration modifications to minimize the adverse effects of these phenomena.

The self-induced roll characteristics of a 2% subscale X-31 aircraft model were investigated by Williams et al. (1994). Some unusual aerodynamic phenomena have emerged during X-31 model testing, namely wing rock, HIKR departure, and autorotation.

A method for determining the yawing moment asymmetry from flight data was developed along with an analysis of the various configuration changes (Cobleigh, 1994). Several aerodynamic modifications were made to the X-31 forebody with the goal of minimizing the asymmetry. Applying symmetrical boundary-layer transition strips along the forebody sides increased the magnitude of the asymmetry and widened the angle-of-attack range over which the largest asymmetry acted.

For the model at scale 1:5.6 tested in the German-Dutch Wind Tunnels (DNW-NWB), very few stability derivatives results have been published. Boelens (2009) presents the results from lift, drag and pitching-moment coefficients and pressure coefficients using the Computational Fluid Dynamics method employing three leading-edge configurations: all leading edge flap gaps, only the longitudinal flap gaps, and with no leading edge flap gaps.

In this context, we chose to use the new code, FDerivatives ((Anton et al., 2009), (Popescu, 2009)), developed at the LARCASE laboratory, to estimate the aerodynamic coefficients and their corresponding stability derivatives. This code was written in MATLAB language and has a complex structure which contains a graphical interface to facilitate the work of

potential users. The static and dynamic derivatives may be estimated based only on knowledge of the aircraft geometry, using the DATCOM method (Williams et al., 1979a). The DATCOM procedure is one of the best compilations of knowledge in the field of analytical calculation of aircraft aerodynamic coefficients and stability derivatives. Designed as a tool for the evaluation of aerodynamic coefficients and stability derivatives for preliminary aircraft design, DATCOM provides methods for making these calculations for various aircraft configurations and different flight regimes, based on the wing geometry. For the main functions of calculation, the implementation of the general model has been developed and applied to all the calculation methods used in the code. This facilitates the replacement of calculation methods, including adding new methods, and simplifies troubleshooting throughout the code. Also, we have developed a process for the systematic utilization of various monograms in the DATCOM procedure, incorporating MATLAB's interpolation tools.

After these stability derivatives have been calculated, an aircraft's stability can be determined for longitudinal and lateral motions. This paper considers only an aircraft's longitudinal behavior about the pitch-axis reference frame, presented in the last section. The set of the first-order linear differential equations was solved for short-period and phugoid motions. Numerical results are given as eigenvalues, modal damping, natural frequency, magnitude and phasing, magnitude scaling and phase angle difference. Time-history traces of the short-period and phugoid responses due to an initial condition of the eigenvector are also presented. The system's control response has been investigated using a step control input for the short-period approximation.

3.2 FDerivatives' code description

The first main advantage of the FDerivatives code (Anton et al., 2009, Popescu, 2009) developed at the LARCASE laboratory (www.larcase.etsmtl.ca) with respect to Digital DATCOM code (Galbraith) is the estimation of the lift, drag and moment coefficients and their corresponding stability derivatives by use of a minimum of aircraft geometrical data.

This data are the area, aspect ratio, taper ratio, sweepback angle and dihedral angle for the wing, canard and vertical tail. In addition, their coordinates and body parameters are also determined in the three-dimensional planes.

The FDerivatives program was written based on MATLAB, and has a complex structure which contains a graphical interface to facilitate the work of potential users.

3.2.1 FDerivatives: Logical scheme and graphical interface

Figure 3.1 shows a brief logical scheme of this code, which works in two steps. The first step is the pre-processing level, in which the geometry is completely calculated based on initial characteristics such as the length and the gravity centre position for the fuselage and the reference area, and on the span, aspect ratio, Mean Aerodynamic Chord (MAC), thickness ratio, leading-edge sweep (inboard/outboard), semi-span of exposed surface, root chord, tip chord and MAC for the wing, canard and vertical tail. During the second step, the aerodynamic coefficients (lift, drag, normal and pitching moment coefficient) for different flight conditions are calculated. The accuracy of these four aerodynamic coefficients directly influences the calculation of stability derivatives.

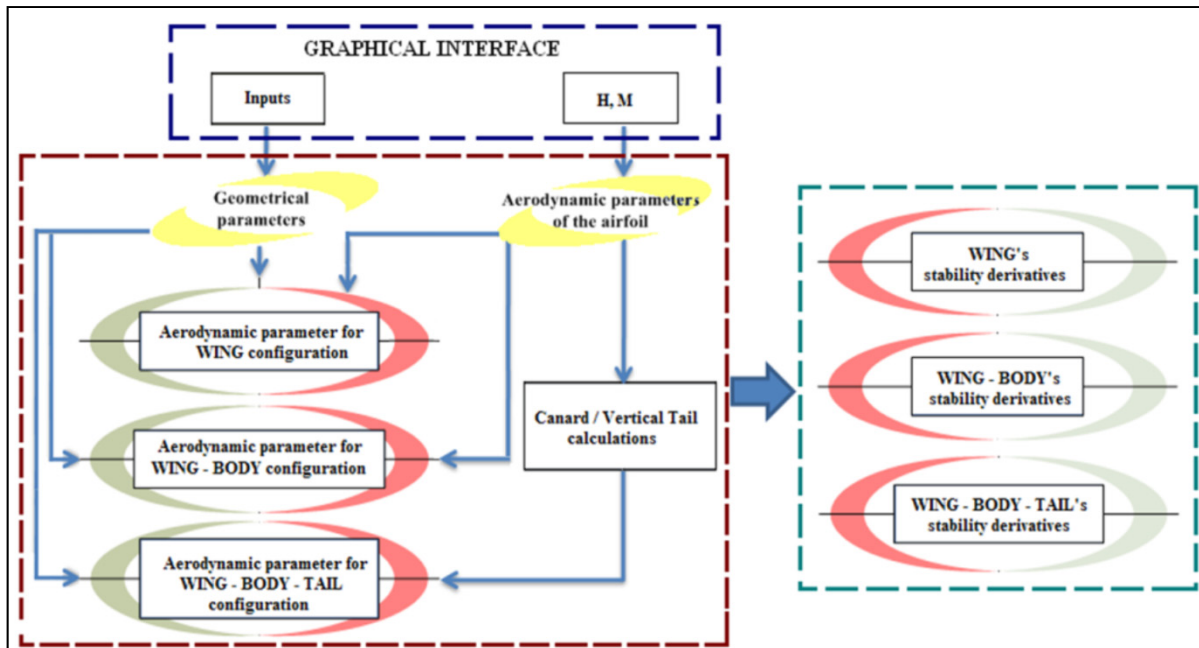


Figure 3.1 FDerivatives' logical scheme

The graphical interface (Figures 3.2 to 3.5) allows users to easily and rapidly change the aircraft geometrical data for different flight conditions (for the same aircraft configuration, it will be possible to change only the geometry).

The principle images of the graphical interface are shown for the main window (Figure 3.2), Wing and Canard parameters (Figure 3.3), Fuselage parameters (Figure 3.4) and Vertical Tail parameters (Figure 3.5). The results obtained for the Hawker 800XP aircraft, and thus for a classical Wing–Body–Tail aircraft, were presented by Anton et al. (2009). To obtain the results presented in this paper for the X–31 aircraft, the code and graphical interface for the Hawker 800XP were changed, due to the canard configuration, and therefore new functions were added. FDerivatives code can also be used for a non straight–tapered (double trapezoidal) wing, and not just for a straight–tapered wing configuration (see Figure 3.3).

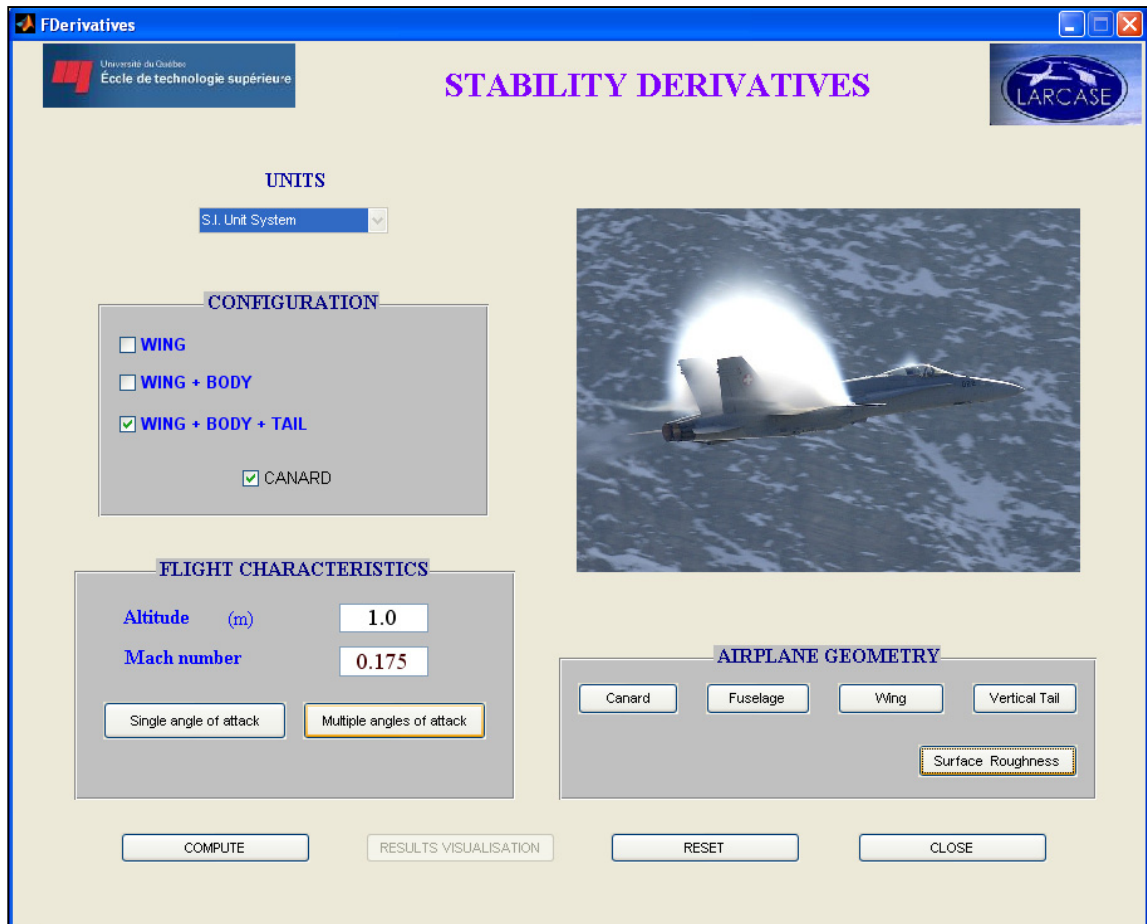


Figure 3.2 Main window

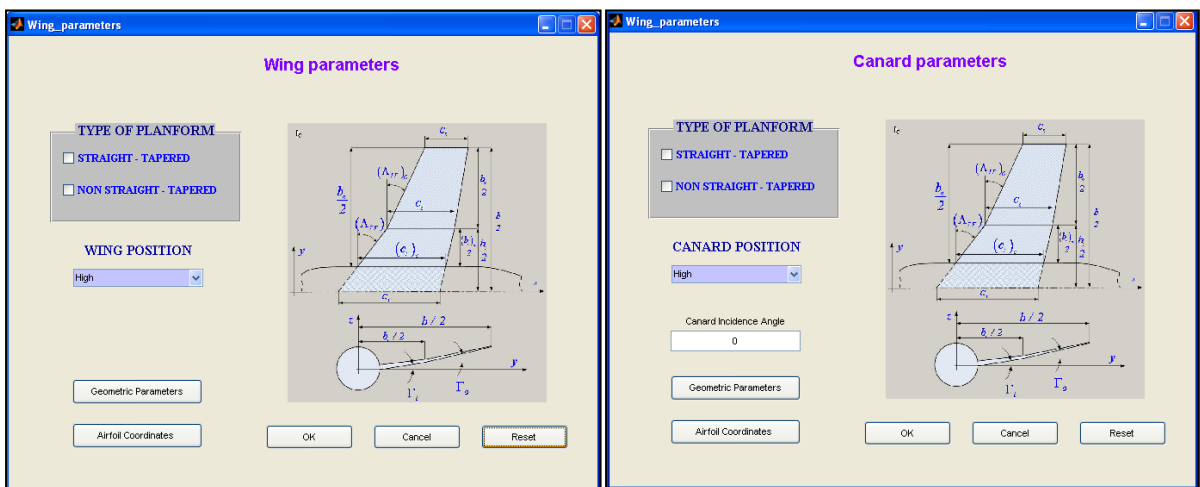


Figure 3.3 Wing and Canard parameters

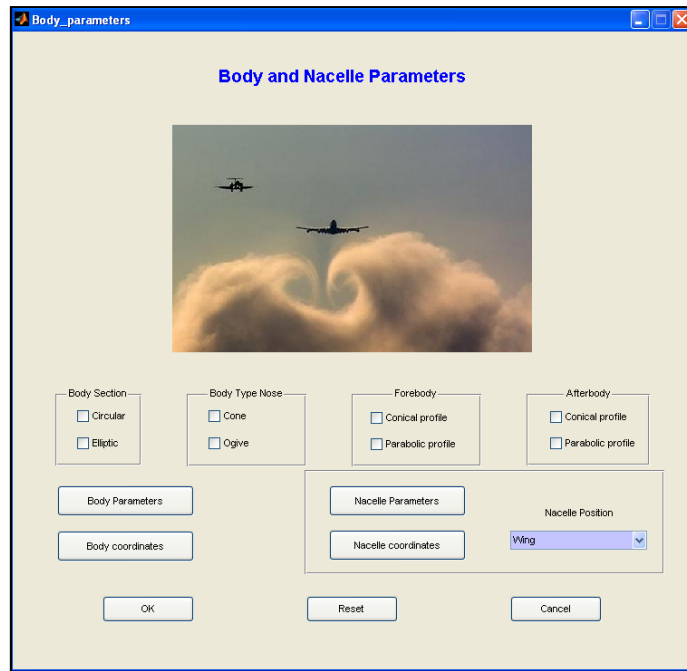


Figure 3.4 Fuselage parameters

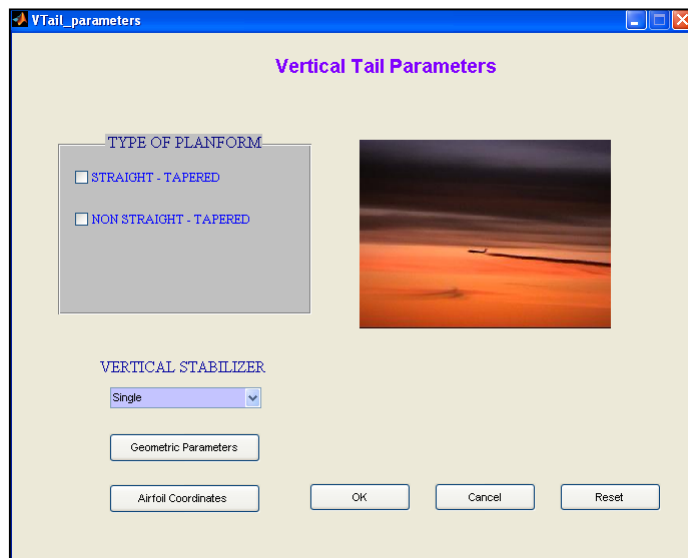


Figure 3.5 Vertical Tail parameters

In the main window, entitled Stability Derivatives (Figure 3.2), the configuration type and the flight conditions (Mach numbers, altitudes and angles of attack ranges) are defined. It is possible to fix the wing position and its roughness. For each of the three major surfaces (Wing, Canard and Vertical Tail), the global parameters and the airfoil coordinates situated at

the root, MAC and tip sections are considered. The inputs to the body configuration are the three parameters: fuselage length, position of the gravitational centre, and fuselage coordinates (in three dimensions), measured with respect to the reference system.

3.2.2 FDerivatives: functions' description

FDerivatives code uses a total of **82** MATLAB functions; the aerodynamic coefficients and their stability derivatives are calculated with **24** of these functions, which are the following:

- **3** functions for lift, drag and moment coefficient estimation (C_L , C_D and C_m);
- **6** functions for the static derivatives estimation: lift, drag and pitching moment derivatives due to the angle of attack ($C_{L\alpha}$, $C_{D\alpha}$, $C_{m\alpha}$); side-force, yawing, and rolling moments due to the sideslip angle ($C_{Y\beta}$, $C_{n\beta}$, $C_{l\beta}$); and
- **15** functions for the estimation of the following dynamic derivatives: lift, drag and pitching moments due to pitch rate derivatives (C_{Lq} , C_{Dq} , C_{mq}); lift, drag and pitching moments due to angle of attack rate derivatives ($C_{L\dot{\alpha}}$, $C_{m\dot{\alpha}}$, $C_{D\dot{\alpha}}$); side-force, rolling and yawing moments due to roll rate derivatives (C_{yp} , C_{lp} , C_{np}); side-force, rolling and yawing moment due to yaw rate derivatives (C_{yr} , C_{lr} , C_{nr}); and side-force, rolling and yawing moments due to sideslip angle rate derivatives ($C_{Y\dot{\beta}}$, $C_{l\dot{\beta}}$, $C_{n\dot{\beta}}$).

The **58** other functions are needed to calculate the geometrical factors (two- or three-dimensional) and the aerodynamic functions. The main function of the FDerivatives code is found in the MATLAB file **DATCOM.m**, which calls the rest of the MATLAB functions and text files. The main functions for the aircraft and airfoils' geometry estimation are **aircraft_geometry.m**, to determine the Wing, Canard, Vertical Tail and Body geometries, and the function **airfoil_properties.m** which is used to define the geometrical and aerodynamic characteristics of different airfoils (two- and three- dimensional). The zero-lift angle and the pitching moment for a wing section are calculated using thin wing section theory.

The inputs to the body configuration are three global parameters: body length, centre of gravity position at the fuselage station and at the wing level and the fuselage coordinates (in three–dimensions). The final numerical results are saved in three formats: jpeg, MATLAB figures and text files.

3.2.3 FDerivatives: Improvements of DATCOM method

All of the improvements have been given in detail ((Anton et al., 2009), (Popescu, 2009)). Only the improvements that are proposed in the FDerivatives code with respect to the classical DATCOM method are summarized in this paper. These improvements are:

- ✓ The lift, drag and moment coefficients as well as their static and dynamic derivatives calculations for the three- dimensional flow around the aircraft.
- ✓ The consideration of several sections across the wing span and their estimations with good precision, found by taking into account the wing root, the MAC and the tip airfoils (Figure 3.6).

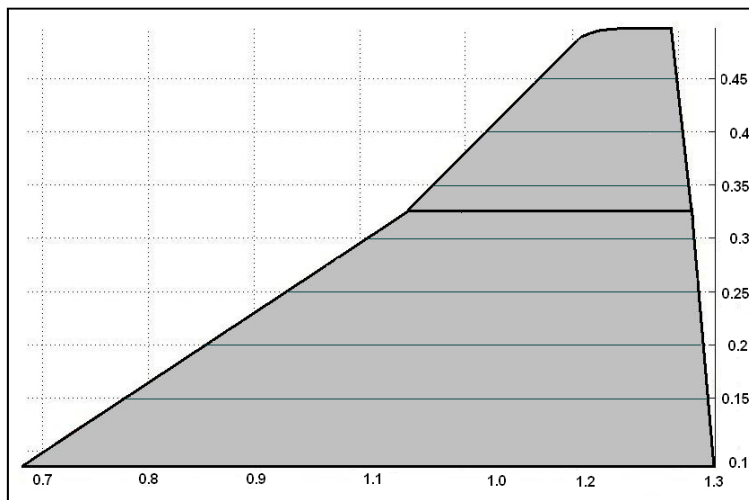


Figure 3.6 Wing geometry for X-31 model aircraft

- The obtaining of the lift coefficient C_L for a nonlinear twist wing (Figure 3.7).

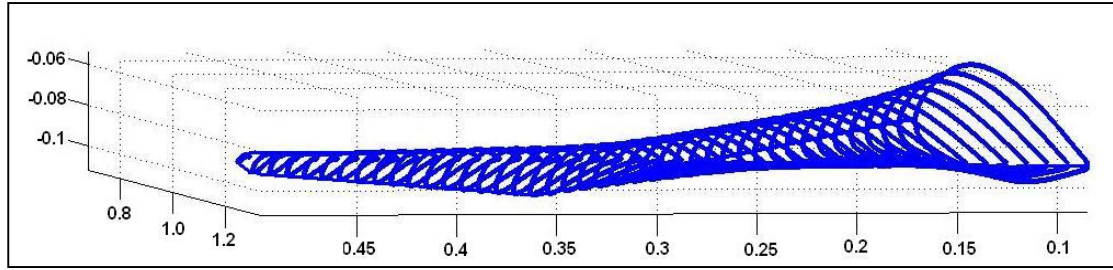


Figure 3.7 Twisted nonlinear wing for the X-31 aircraft

- The lift–line type method is used to obtain the global lift coefficient for a nonlinear twist wing (Sivells et al., 1947).

The wing lift–distribution is calculated using the induced angle of attack for a finite wing span, while the airfoil lift data are calculated at ten wing sections along its span. These ten wing airfoils are found at the root, the MAC, the tip and seven other intermediate sections. If the airfoil coordinates are not all given as inputs, the FDerivatives code has a function that could reconstruct them for any intermediate airfoils.

A lift-distribution method, using successive approximations, is used in the FDerivatives code. For each airfoil section, a section lift–coefficient distribution is assumed, for which the two–dimensional lift coefficients are calculated. Equation (3.1) developed by Phillips et al. (2007) is used to estimate the maximum lift coefficient C_{Lmax} .

$$C_{Lmax} = \left(\frac{c_L}{C_{Lmax}} \right)_{\substack{\theta=0 \\ \Lambda=0}} \kappa_{L\Lambda} (c_{Lmax} - \kappa_{L\theta} C_{L\alpha} \theta) \quad (3.1)$$

This method applies to any wing geometry, including to a nonlinear twisted wing, and replaces the old algorithm used in the DATCOM method for a linear twisted wing.

The sweep correction factor depends on the aspect and taper ratios, as shown in eq.(3.2)

$$\kappa_{L\Lambda} \cong 1 + \kappa_{\Lambda 1} \Lambda - \kappa_{\Lambda 2} \Lambda^{1.2} \quad (3.2)$$

The section maximum lift coefficient used in eq.(3.1) is calculated in the section where the lift coefficient has the highest value. After obtaining the lift distribution along the wing span,

the stall coefficient (corresponding to the maximum lift coefficient) is obtained for the entire wing.

- With respect to Digital DATCOM code, the new FDerivatives code, for WB configuration, gives better estimation of drag using a nonlinear regression analysis and better estimation of pitching moments.

This method evaluates and combines the isolated moment due to the lift for the WB configuration, with allowance for their effect on each other. The wing pitching moments due to the effective wing lift include the effects of body up-wash on the wing and of the wing carryover onto the fuselage. Fuselage and nacelles' free moments due to wing-induced flow can be estimated by the technique developed by Multhopp (1942). The sum of these two contributions added to the wing pitching moment due to its drag gives a better estimation of the pitching moment than the linear regression analysis method in the Digital DATCOM code for a WB configuration.

- The zero-lift angle and the pitching moment for a wing section are also calculated with FDerivatives code using the thin wing section theory (Abbot, 1959) and the Fourier method. Very good approximations for the zero lift coefficients and pitching moments are obtained using the Pankhurst method (Abbot, 1959).

3.3 Testing with the X-31 aircraft model

The X-31 aircraft was designed to break the « stall barrier », allowing it to fly at angles of attack which would typically cause an aircraft to stall resulting in loss of control. The X-31 employs thrust vectoring paddles which are placed in the jet exhaust, allowing the aircraft's aerodynamic surfaces to maintain their control at very high angles. For its control, the aircraft has a small canard, a single vertical tail with a conventional rudder, and wing Leading-Edge and Trailing-Edge flaps.

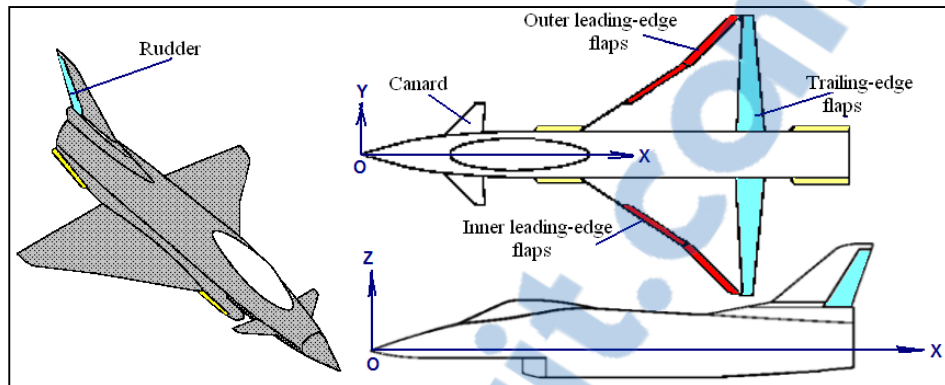


Figure 3.8 Three-views of the X-31 model

The X-31 aircraft also uses computer controlled canard wings to stabilize the aircraft at high angles of attack. The stall angle at low Mach numbers is $\alpha = 30^\circ$. The X-31 model geometry was given by the DLR, at the scale 1:5.6 (Table 3.1) in the AVT-161 meeting. The geometrical parameters are detailed (Henne et al., 2005).

Table 3.1 Geometrical parameters

Fuselage length	1.725 m
Wing span	1.0 m
Wing Mean Aerodynamic Chord (MAC)	0.51818 m
Wing reference area	0.3984 m ²
Wing sweep angle, inboard	57 deg
Wing sweep angle, outboard	45 deg
Canard span	0.36342 m
Canard reference area	0.04155 m ²
Canard sweep angle	45 deg
Vertical Tail reference area	0.0666 m ²
Vertical Tail sweep angle	58 deg

The main part of the X-31 model (Figure 3.8) is a wing-fuselage section with eight servomotors for changing the angles of the canard (δ_c), the wing Leading-Edge inner/outer flaps

(δ_{LEi} / δ_{LEo}), wing Trailing-Edge flaps (δ_{TE}) and the rudder (δ_r) (Rein et al., 2008). The variation of these angles, for each control surface, is given as:

- Canard: $-700 \leq \delta_c \leq 200$,
- Wing inner Leading-Edge flaps: $-700 \leq \delta_{LEi} \leq 00$,
- Wing outer Leading-Edge flaps: $-400 \leq \delta_{LEo} \leq 00$,
- Wing Trailing-Edge flaps: $-300 \leq \delta_{TE} \leq 300$,
- Rudder: $-300 \leq \delta_r \leq 300$.

The Wing parameters were introduced in Digital DATCOM for the Horizontal Tail and the Canard as a Wing.

3.4 Validation of the results obtained with the X-31 aircraft

The VN01004 test run was selected from the wind tunnel test data (Henne et al., 2005). This test took place for angles of attack $\alpha = -6^\circ$ to 55° . The wind tunnel speed was 60 m/s, which corresponds to Mach number 0.18. The Reynolds number based on the MAC value was $Re = 2.07 \cdot 10^6$, the pressure $P = 101045 \text{ N/m}^2$ at temperature $T = 293.7\text{K}$, and the altitude was $H = \text{Sea Level}$. Results are presented in this paper for $\alpha = -2^\circ$ to 20° .

To validate the lift, drag and moment coefficients obtained with both codes, as shown in Figures 3.9, 3.10 and 3.12, the wind tunnel tests presented in ((Boelens, 2009), (Henne et al., 2005), (Schütte, 2009)) were chosen. The default method and the Jorgensen method were both used for this validation. Jorgensen (1978) generated a semi-empirical method to predict the normal and pitching-moment coefficients, as well as the aerodynamic centre position for circular and elliptical bodies with and without wings. Method validity is in the range for an angle of attack of between 0 to 90 degrees.

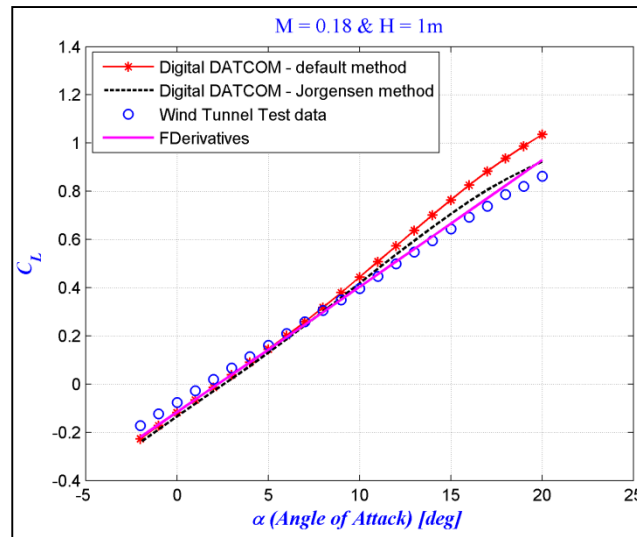


Figure 3.9 Lift coefficient variations with angle of attack

Following the results analysis, shown in Figures 3.9, 3.10 and 3.12, one can say that very good approximations were obtained with all methods for the range of angle of attack in the linear zone. Because two codes were used in the paper to generate the results, their interpretations are made for two zones: the linear zone and the close-to-stall angle zone.

- The slopes of the lift coefficient versus the angle of attack are similar, but the closest curve to the experimental results is obtained with the FDerivatives code.

Table 3.2 Relative errors of lift coefficient variation with angle of attack

Alpha [deg]	Digital DATCOM default method [%]	Digital DATCOM Jorgenson method [%]	FDerivatives code [%]
-2	23.930	31.458	20.735
0	19.134	27.578	18.156
2	16.601	23.205	15.012
4	12.838	19.896	14.012
6	4.647	4.441	7.957
8	4.088	4.262	2.075
10	10.674	11.949	1.885
12	12.931	14.852	1.820
14	15.258	18.005	3.079
16	16.128	19.229	3.722

18	16.051	19.120	4.553
20	16.650	19.976	7.197

Relative errors were calculated with the classical formula $e = \frac{|x_{WTT} - x_{calc}|}{x_{WTT}} \times 100$, where e is the relative error and x_{WTT} is the value obtained in the wind tunnel. The FDerivatives code results are the closest to the WTT results, with a relative error smaller than 18% (see Table 3.2).

The fuselage was modeled as a body of revolution using the DLR Wind Tunnel model (see Figure 3.11).

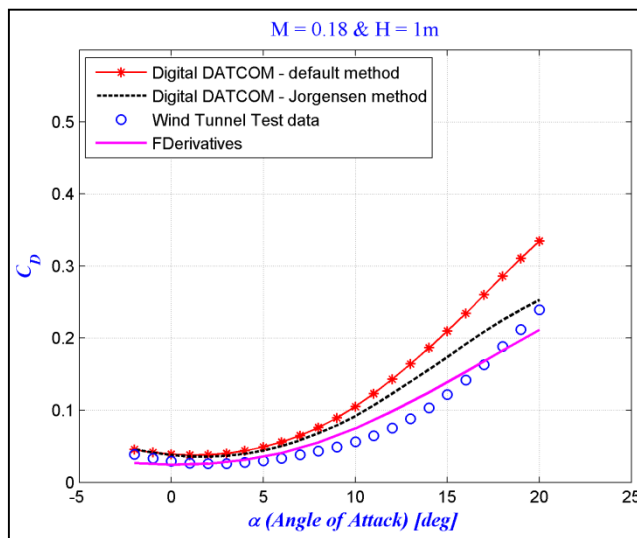


Figure 3.10 Drag coefficient variations with angle of attack

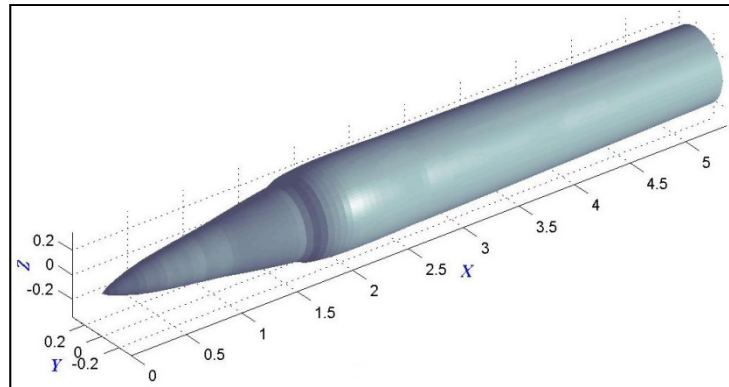


Figure 3.11 X-31 aircraft fuselage, modeled as a revolution body

For angles of attack between 0 and 20 degrees, the best drag coefficient values are obtained with FDerivatives (see Figure 3.10 and Table 3.3).

Table 3.3 Relative errors of drag coefficient variation with angle of attack.

Alpha [deg]	Digital DATCOM default method [%]	Digital DATCOM Jorgenson method [%]	FDerivatives code[%]
-2	11.679	9.938	28.286
0	22.071	16.581	12.216
2	32.280	21.749	0.449
4	39.047	24.624	7.670
6	44.470	26.676	11.739
8	50.077	28.596	14.236
10	57.856	30.975	16.498
12	59.603	31.469	15.478
14	53.499	29.681	11.398
16	43.270	26.239	4.901
18	34.429	22.704	2.094
20	26.598	19.012	8.861

The pitching moment coefficient is very sensitive to geometrical changes and to the aircraft's centre of gravity position. Because all the coefficients presented in this paper were calculated from the aircraft's geometry, by considering only a small amount of geometrical data as inputs, the final results were not the best when extended for moment coefficients. The curve shapes are similar for the moment coefficient (Figure 3.12), but the maximum and minimum values obtained by the default method of Digital DATCOM are higher than the wind tunnel test data. The FDerivatives C_m values are good compared with the wind tunnel tests. The main structure of the aircraft, without any approximation (the fuselage is not considered as a revolution body), is modeled using CFD (Boelens, 2009). Differences in results are mainly seen for angles of attack between 10 to 20 degrees.

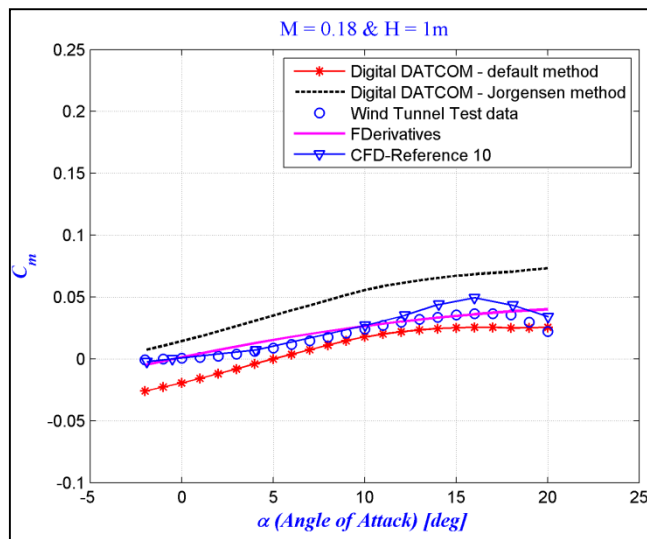


Figure 3.12 Pitching moment coefficient variations with angles of attack

Figures 3.13 to 3.15 show the comparison between the stability derivative values obtained with FDerivatives versus those obtained with Digital DATCOM codes (default & Jorgensen method).

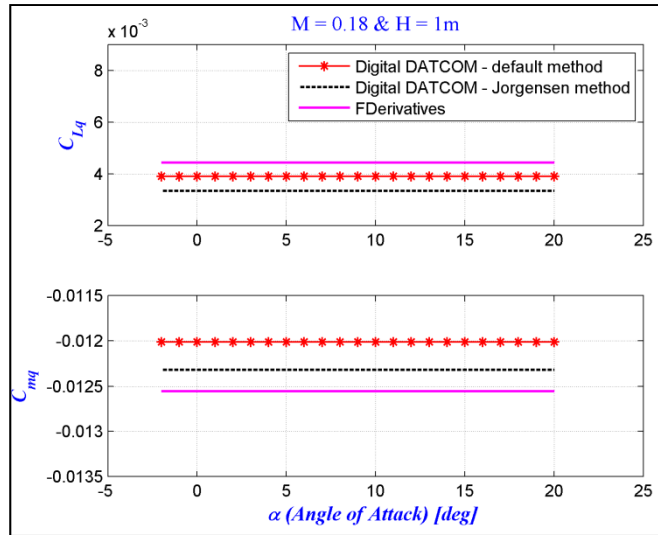
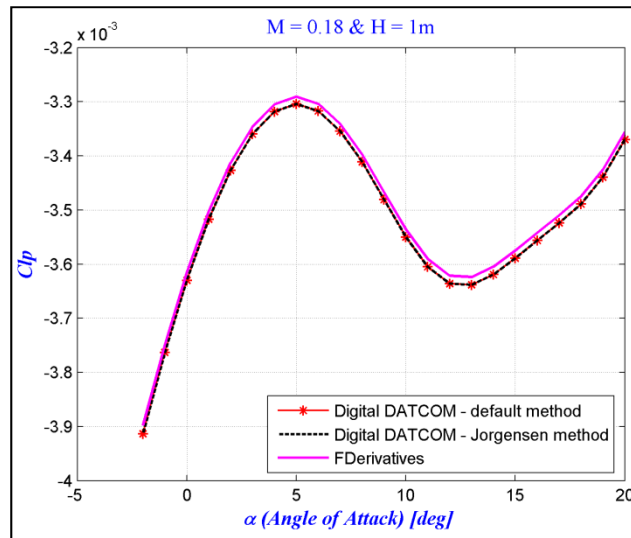


Figure 3.13 Lift and pitch moment coefficients due to the pitch rate (C_{Lq}, C_{mq}) versus the angle of attack

A very small difference can be seen in Figure 3.14 for lift and pitching moment coefficients due to the pitch rate calculated with the FDerivatives & Digital DATCOM codes. Very good results are obtained for yawing and rolling moments and side forces due to roll-rate derivatives (Figure 3.15).



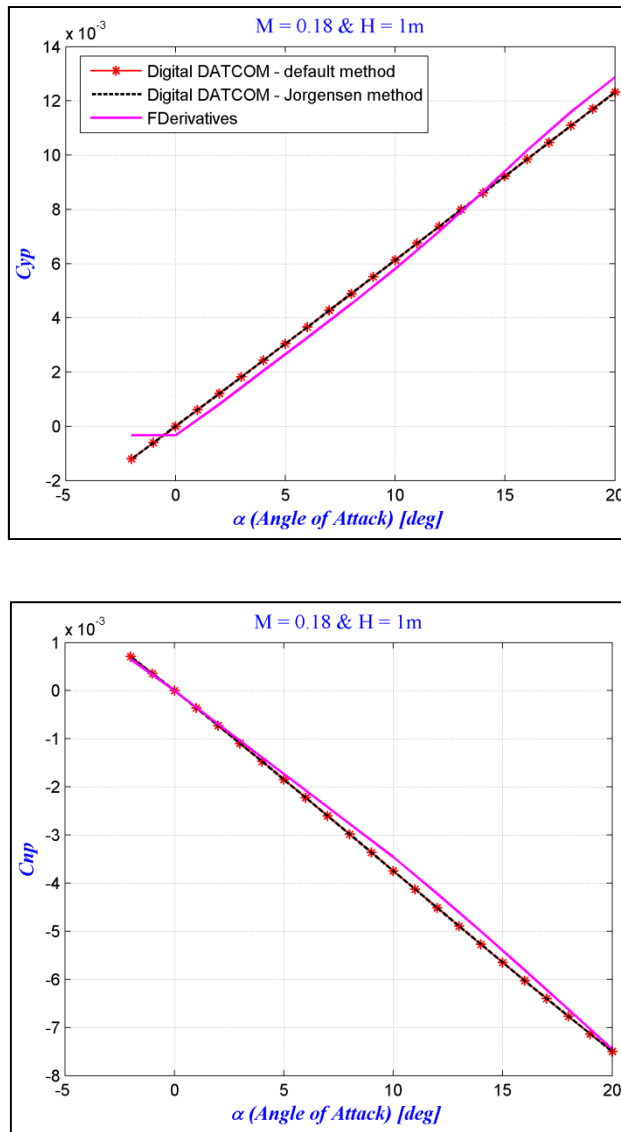


Figure 3.14 Yawing, side force and rolling moments due to the roll-rate derivatives' variations with the angle of attack

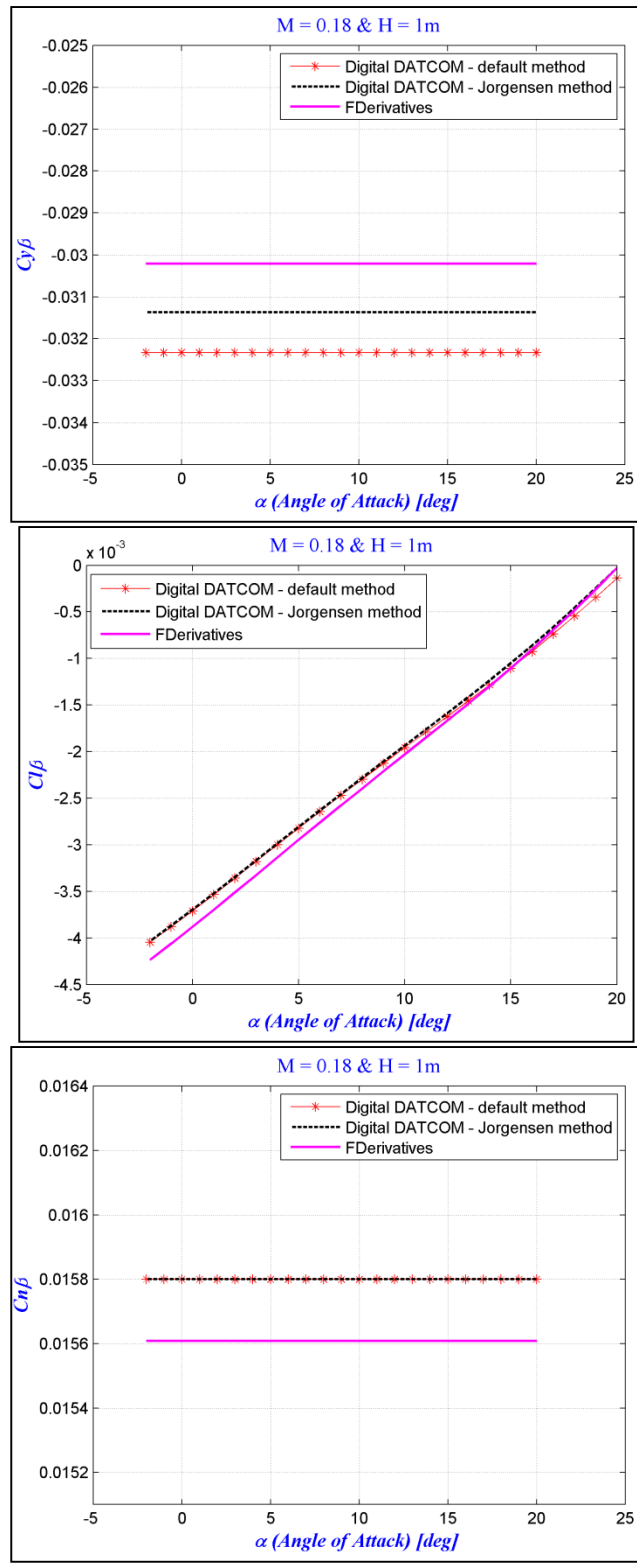
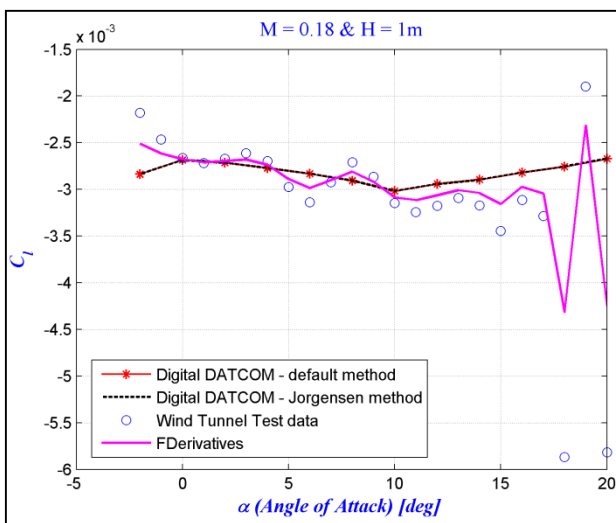
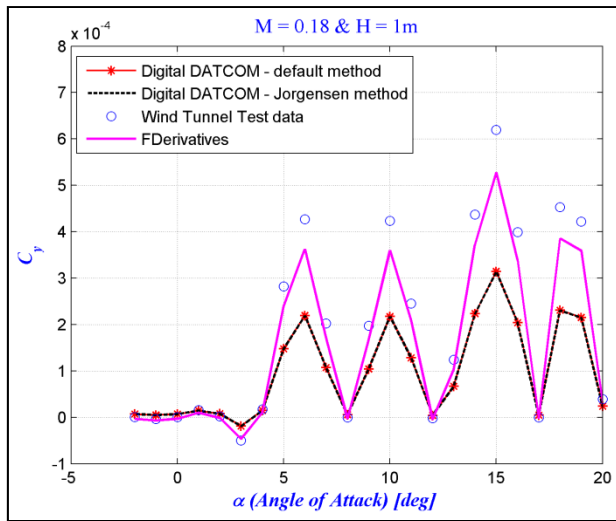


Figure 3.15 Side force, yawing and rolling moments due to the sideslip angle derivatives' variations with the angle of attack



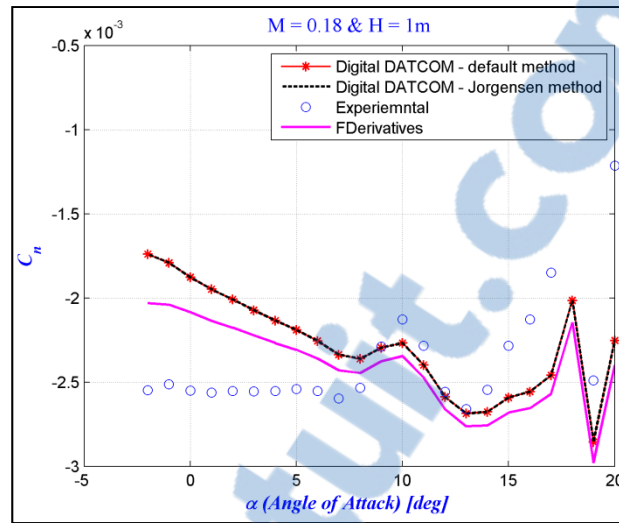


Figure 3.16 Side force, rolling and yawing moment coefficients variation with angle of attack

Side force, rolling, and yawing moment coefficients are shown in Figure 3.16 with wind tunnel test data (Schütte, 2009). These derivatives were calculated based on the aircraft's geometrical data, which implies the occurrence of small errors, and one can see, in Figure 3.16, the small side force coefficient variation with angle of attack with FDerivatives code, as well as with the Digital DATCOM code. Very good results were obtained using the FDerivatives codes for rolling and yawing moment coefficients variation with angle of attack, and the wind tunnel tests results (see Figure 3.16).

3.5 Longitudinal motion analysis

This paper considers only the aircraft's longitudinal behavior about the pitch-axis reference frame. The numerical cases are presented here for three high angles of attack, $\alpha = 20^\circ$, 28° , 38° , based on the previous results.

We start from the decoupled equations for longitudinal motion with commands fixed. An aircraft's mathematical model for longitudinal motion can be represented by a differential equations system of the form (Schmidt, 1998).

$$\begin{cases} \dot{u}/V = X_u \left(\frac{u}{V} \right) + \frac{X_\alpha}{V} - g \cos \Theta_0 \theta + X_\delta \delta \\ \dot{\alpha} = \frac{VZ_u}{V-Z_{\dot{\alpha}}} \left(\frac{u}{V} \right) + \frac{Z_\alpha}{V-Z_{\dot{\alpha}}} \alpha + \frac{V+Z_q}{V-Z_{\dot{\alpha}}} q - \frac{q}{V-Z_{\dot{\alpha}}} \sin \Theta_0 \theta + Z_\delta \delta \\ \dot{q} = \left(VM_u + \frac{VZ_u M_{\dot{\alpha}}}{V-Z_{\dot{\alpha}}} \right) \left(\frac{u}{V} \right) + \left(M_\alpha + \frac{Z_\alpha M_{\dot{\alpha}}}{V-Z_{\dot{\alpha}}} \right) \alpha + \left(M_q + M_{\dot{\alpha}} \frac{V+Z_q}{V-Z_{\dot{\alpha}}} \right) q + M_\delta \delta \\ \dot{\theta} = q \end{cases} \quad (3.3)$$

If a longitudinal state vector is defined by $\mathbf{x} = [u/V \ \alpha \ q \ \theta]^T$ along with a single control term (δ), then the linearized airframe longitudinal dynamics becomes

$$\dot{\mathbf{x}} = \mathbf{A}\mathbf{x} + \mathbf{B}\delta \quad (3.4)$$

where \mathbf{A} is the longitudinal air-frame plant matrix and \mathbf{B} is the control matrix.

The two pairs of complex conjugate roots of the linearized longitudinal dynamics correspond to short-period (fast mode) and phugoid motions (slow mode). The homogeneous form of eq.(3.4) is given by

$$\dot{\mathbf{x}} = \mathbf{A}\mathbf{x} \quad (3.5)$$

The following assumptions are done $H = \text{const}$, $V = \text{const}$ ($M = \text{const}$), $\gamma = 0$ and the calculation conditions are at $H = \text{Sea Level}$ and $M = 0.18 \rightarrow a = 430.2885 \text{ m/s}$, $\rho = 1.2249 \text{ kg/m}^3$.

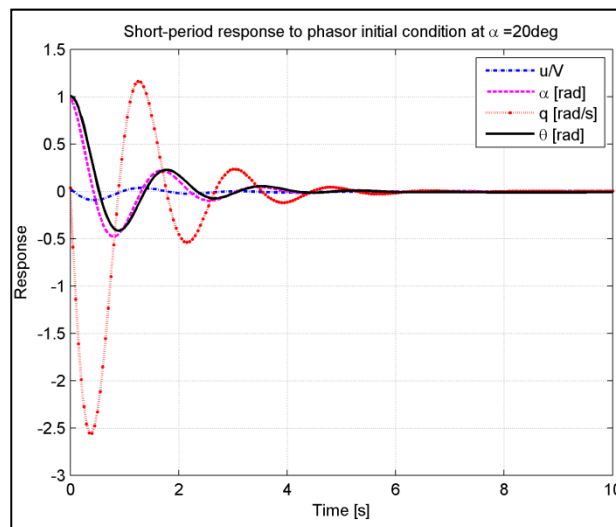
The set of the first-order linear differential order was solved for short-period and phugoid motions. The short-period motion involves rapid changes to the angle of attack and pitch attitude at roughly constant airspeed. This mode is usually highly damped. Its frequency and damping are very important in the assessment of aircraft handling. In Table 3.4 numerical results of the short-period are given as eigenvalues, modal damping, natural frequency, magnitude and phasing, magnitude scaling and phase angle difference.

Table 3.4 Short-period motion

	$\alpha = 20^\circ$	$\alpha = 28^\circ$	$\alpha = 38^\circ$
$\lambda_{sp} [\text{rad/s}]$	$-0.8866 \pm 3.5461i$	$-0.4732 \pm 4.3106i$	$-0.7337 \pm 3.6971i$

$\omega_{nsp} [rad/s]$	3.6553	4.3365	3.7692
ζ_{sp}	0.2425	0.1091	0.1947
$\begin{Bmatrix} u/V \\ \alpha \\ q \\ \theta \end{Bmatrix}$	$\begin{Bmatrix} 0.1386 \angle 74.0162^\circ \\ 1 \angle 0^\circ \\ 3.6832 \angle 85.2549^\circ \\ 1.0076 \angle -18.7821^\circ \end{Bmatrix}$	$\begin{Bmatrix} 0.1640 \angle 89.6792^\circ \\ 1 \angle 0^\circ \\ 4.5056 \angle 92.7223^\circ \\ 1.0390 \angle -3.5417^\circ \end{Bmatrix}$	$\begin{Bmatrix} 0.1635 \angle 87.1089^\circ \\ 1 \angle 0^\circ \\ 3.8826 \angle 87.2358^\circ \\ 1.0301 \angle -13.989^\circ \end{Bmatrix}$
$ q $	3.6831	4.5056	3.8827
$\Delta\phi_{sp}$	104.0371°	96.2641°	101.2250°

The pitch attitude appears smaller in magnitude as the angle of attack. A time–history trace of the short–period response due to an initial condition of the eigenvector is shown in Figure 3.17. The angle of attack and pitch attitude responses are nearly the same for all three angles of attack. For angles of attack equal to 20 and 38 degrees the response becomes stable at 7 seconds, but for a value of angle of attack close to the stall angle the stabilization time is more than 10 seconds.



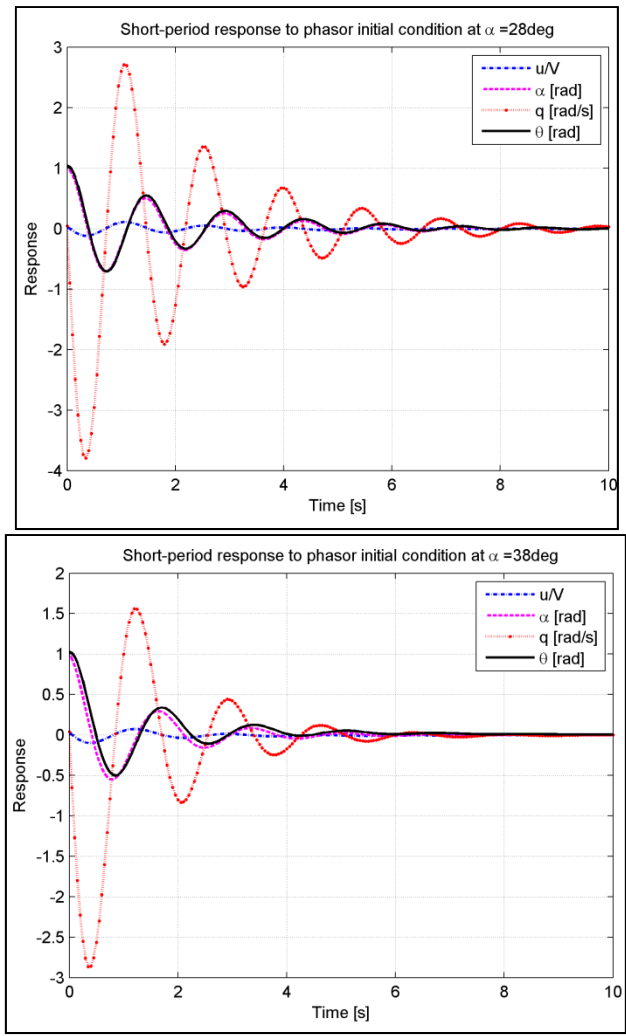


Figure 3.17 Short-period response to phasor initial condition

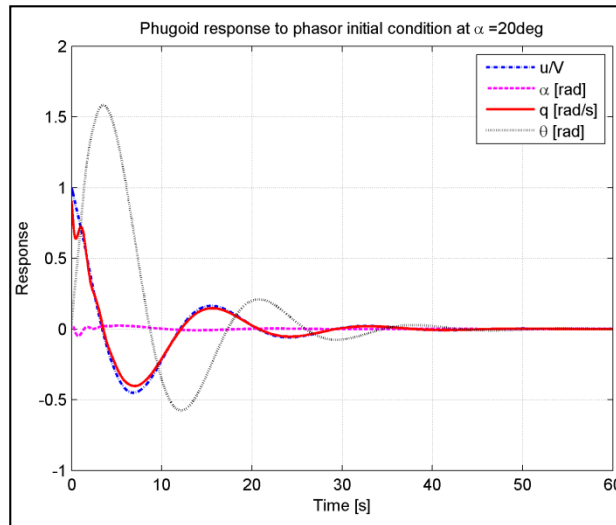
The phugoid mode involves a trade-off between kinetic and potential energy. In this mode, the aircraft, at nearly constant angle of attack, climbs and slows, then dives, losing altitude while picking up speed.

Table 3.5 Phugoid motion

	$\alpha = 20^0$	$\alpha = 28^0$	$\alpha = 38^0$
λ_p [rad/s]	$-0.1171 \pm 0.3643i$	$-0.2521 \pm 0.3491i$	$-0.3936 \pm 0.1624i$
ω_{np} [rad/s]	0.3826	0.4306	0.4258
ζ_p	0.3060	0.5854	0.9244

$\begin{Bmatrix} u/V \\ \alpha \\ q \\ \theta \end{Bmatrix}$	$\begin{Bmatrix} 1\angle 0^\circ \\ 0.0434\angle -146.717^\circ \\ 0.9069\angle -2.3979^\circ \\ 2.3701\angle -110.2176^\circ \end{Bmatrix}$	$\begin{Bmatrix} 1\angle 0^\circ \\ 0.0296\angle -137.3727^\circ \\ 1.1276\angle -0.3939^\circ \\ 2.6188\angle -126.2279^\circ \end{Bmatrix}$	$\begin{Bmatrix} 1\angle 0^\circ \\ 0.0221\angle -145.4172^\circ \\ 1.1167\angle -0.4837^\circ \\ 2.6225\angle -158.062^\circ \end{Bmatrix}$
$ q $	0.9068	1.1277	1.1167
$T_p [s]$	17.2489	17.9992	38.6864

The angle of attack component is smaller than the u/V component. For this reason, a modal approximation would typically be based on the assumption that the oscillation occurs with the aircraft remaining at a constant lift coefficient. The time–history response is shown in Figure 3.18.



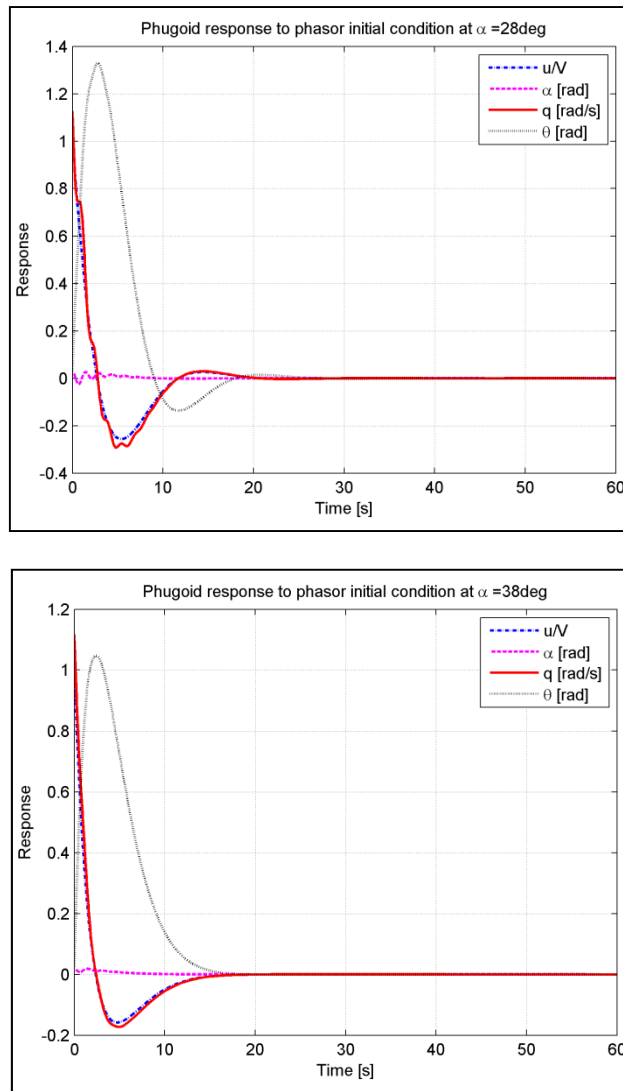


Figure 3.18 Phugoid response to phasor initial condition

The stabilization time differs for the three cases. The longest time is for $\alpha = 20^\circ$, up to 50 seconds, after that it diminishes until the 20 seconds for $\alpha = 38^\circ$, and between them the time of 30 seconds corresponds to $\alpha = 28^\circ$.

The system's control response has been investigated using a step control input. The mathematical model which describes the short-period approximation is given by eq.(3.6).

$$\begin{cases} \dot{\alpha} = \frac{Z_{\alpha}}{V} \alpha + q + \frac{Z_{\delta}}{V} \delta \\ \dot{q} = \left(M_{\alpha} + \frac{Z_{\alpha} M_{\dot{\alpha}}}{V} \right) \alpha + (M_q + M_{\dot{\alpha}}) q + \left(M_{\delta} + \frac{Z_{\delta} M_{\dot{\alpha}}}{V} \right) \delta \end{cases} \quad (3.6)$$

The control input is a step elevator input with the form given by eq. (2.7)

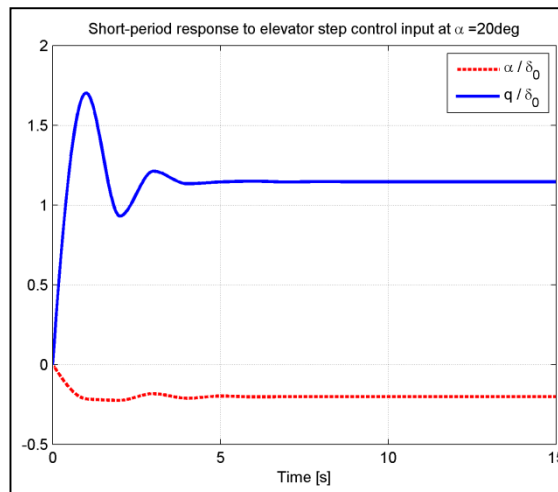
$$\delta_e(t) = \delta_0(t) = \begin{cases} 0, & \text{for } t < 0 \\ \delta_0, & \text{for } t > 0 \end{cases} \quad (3.7)$$

The time–history plots of α/δ_0 and q/δ_0 are shown in Figure 3.19, for time varying from $t = 0$ to 10 seconds for $\alpha = 20^\circ$ and 38° , and from $t = 0$ to 15 seconds for $\alpha = 28^\circ$. The stabilized values are shown in Table 3.6.

Table 3.6 Static values for short-period approximation

	$\alpha = 20^\circ$	$\alpha = 28^\circ$	$\alpha = 38^\circ$
α/δ_0 [rad/rad]	-0.2018	2.3857	1.0657
q/δ_0 [rad/rad-s]	1.1459	1.3313	1.0308

The positive elevator deflection corresponds to the trailing–edge moving down, which normally results in negative values for both parameters (α and q) when the aircraft is stable. Based on the short–period approximation results, the conclusion is that the X–31 aircraft is not stable for these three angles of attack.



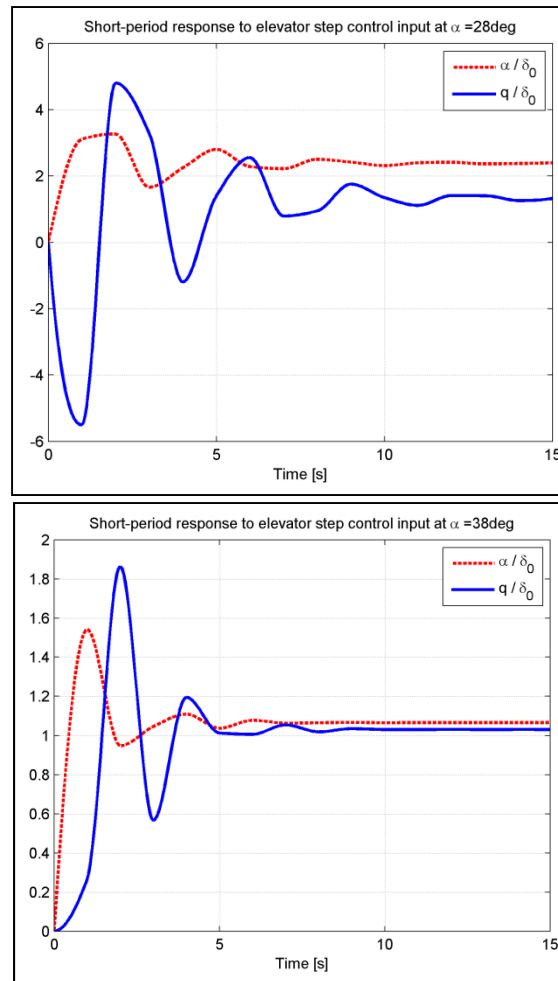


Figure 3.19 Short-period response to elevator step input

3.6 Conclusions

The aerodynamic coefficients of the X-31 model aircraft and their stability derivatives were calculated based on its geometrical data. The codes used to analyze the model were the classical Digital DATCOM and the FDerivatives code developed at LARCASE laboratory. Following the AVT-168 meeting, the run test VN01004 ($M = 0.18$, $Re = 2.07 \cdot 10^6$, $P = 101045 \text{ N/m}^2$, $T = 293.7\text{K}$) performed in the Low Speed Wind Tunnel of the German-Dutch Wind Tunnels (DNW-NWB) was used.

By taking into account the small number of geometrical parameters, the remaining geometrical data were calculated to complete the aircraft's geometry knowledge. The fuselage was modeled as a body of revolution and the wing was considered as an equivalent straight tapered platform.

Proper geometry modelling is essential to obtain correct aerodynamic coefficients and their derivatives. Pitching moment coefficient analysis demonstrates how a correct approximation of the aircraft's geometry could be obtained. Lift, drag and pitching moment coefficients, for angles of attack between -2 and 20 degrees, were calculated with very good accuracy by the FDerivatives code. In addition, rolling and yawing moment coefficients and side force coefficients were well-estimated.

For short-period motion the pitch attitude appears smaller in magnitude than the angle of attack. The angle of attack and pitch attitude responses are nearly the same for all three angles of attack. For angles of attack of 20 and 38 degrees the response becomes stable at 7 seconds, but for a value of angle of attack close to stall angle the stabilization time is more than 10 seconds. A modal approximation would typically be based on the assumption that the oscillation occurs with the aircraft remaining at a constant lift coefficient. Based on the short-period approximation results, the conclusion is that the X-31 aircraft is not stable for these three angles of attack.

CHAPTER 4

ARTICLE 3: THE WEIGHT FUNCTIONS METHOD APPLICATION ON A DELTA-WING X-31 CONFIGURATION

Nicoleta Anton and Ruxandra Mihaela Botez
École de Technologie Supérieure, Montréal, Canada
Laboratory of Research in Active Controls, Aeroservoelasticity and Avionics
This article was published in INCAS Bulletin, Vol. 3, Issue 4/2011,
pp. 3-16, ISSN 2066-8201

Résumé

L'analyse de la stabilité d'une configuration de l'avion est étudiée en utilisant une nouvelle méthode appelée la méthode de la fonctions du poids. Cette nouvelle méthode trouve un certain nombre de fonctions du poids qui sont égales au nombre d'équations différentielles du premier ordre. Cette méthode est appliquée sur un avion à aile delta, le X-31, pour les mouvements longitudinaux et latéraux. Les coefficients aérodynamiques et les dérivés de stabilité obtenues en utilisant le code numérique Digital DATCOM ont été validés avec les expériences à basse vitesse en soufflerie données obtenues à l'aide de la soufflerie germano-néerlandaise (DNW-NWB). La méthode du lieu des racines est utilisée pour valider la méthode proposée dans cet article.

Abstract

The stability analysis of an aircraft configuration is studied using a new system stability method called the weight functions method. This new method finds a number of weight functions that are equal to the number of first-order differential equations. This method is applied for longitudinal and lateral motions on a delta-wing aircraft, the X-31, designed to break the « stall barrier ». Aerodynamic coefficients and stability derivatives obtained using the Digital DATCOM code have been validated with the experimental Low-Speed Wind

tunnel data obtained using the German–Dutch Wind Tunnel (DNW–NWB). Root Locus Method is used to validate the method proposed in this paper.

4.1 Introduction

Modern fighter aircraft are designed with an unstable configuration or a marginal stability, and control laws are needed to stabilize the aircraft. A new method for systems stability analysis, called the Weight Functions Method, is used to analyze the longitudinal and lateral motions of the X-31.

The X-31 aircraft was designed to achieve its best performance, flexibility and effectiveness in air combat, due to its canard configuration that provided a better longitudinal maneuverability. Its aerodynamics contains degrees of non linearity's that are representative for a modern fighter aircraft, that was designed to investigate its behavior at high angles of attack (-5 to 56) degrees.

The mathematical model uses aerodynamic data obtained from wind tunnel tests and the results provided by Digital DATCOM code, for subsonic speeds. Digital DATCOM code (Galbraith), known also as DATCOM+, is the first implementation of the DATCOM procedures in an automatic calculations code. The software is a directly executable portable application.

Input data, consisting of geometric and aerodynamic parameters of the aircraft, and flight conditions, are introduced through a text file called « aircraft_name.dcm » whose format is specific to the software.

The DATCOM+ program calculates the static stability, the high lift and control, and the dynamic derivative characteristics. This program applies to aircraft flying in the subsonic, transonic and supersonic regimes, more precisely to traditional wing–body–tail and canard–equipped aircraft.

The computer program offers a trim option that computes control deflections and aerodynamic data needed to trim the aircraft in the subsonic Mach regimes.

4.2 Weight Functions Method description

In most practical problems, differential equations that model the behaviour of a dynamical system often depend on more than one parameter. The Lyapunov stability criterion is based on finding a Lyapunov function. It is not simple and is not always guaranteed to find a Lyapunov function. The Lyapunov method is very useful, however, when the linearization around the point of equilibrium leads to a matrix of evolution with eigenvalues having zero real parts (Stroe, 2008).

The Weight Functions Method (WFM) replaces the classical Lyapunov function finding problem with a method that finds a number of weight functions equal to the number of the first order differential equations modeling the system ((Stroe, 2008), (Stroe et al., 2008)).

The difference between the two methods is that the Lyapunov method finds all functions simultaneously, while the weight functions method finds one function at a time, with their total number equal to the number of the first order differential equations. For this reason WFM is found to be more efficient than the Lyapunov method.

For a better understanding of this method, its basic principle is defined in the next system of eq.(4.1). The coefficients a_{1i} , b_{1i} , c_{1i} , d_{1i} , $i = 1 \div 4$ contain the stability derivatives terms. The x_1 , x_2 , x_3 , x_4 represent the unknowns of the system of equations:

$$\begin{cases} f_1 = a_{11} x_1 + a_{12} x_2 + a_{13} x_3 + a_{14} x_4 \\ f_2 = b_{11} x_1 + b_{12} x_2 + b_{13} x_3 + b_{14} x_4 \\ f_3 = c_{11} x_1 + c_{12} x_2 + c_{13} x_3 + c_{14} x_4 \\ f_4 = d_{11} x_1 + d_{12} x_2 + d_{13} x_3 + d_{14} x_4 \end{cases} \quad (4.1)$$

The total weight function W is defined, in which w_1, w_2, w_3 and w_4 are the weight functions whose sign should be negative to ensure the aircraft stability. In the aircraft model, the sign of the total function W given by eq.(4.2) should be negative to ensure the aircraft stability.

$$W = w_1 x_1 (a_{11} x_1 + a_{12} x_2 + a_{13} x_3 + a_{14} x_4) + w_2 x_2 (b_{11} x_1 + b_{12} x_2 + b_{13} x_3 + b_{14} x_4) + w_3 x_3 (c_{11} x_1 + c_{12} x_2 + c_{13} x_3 + c_{14} x_4) + w_4 x_4 (d_{11} x_1 + d_{12} x_2 + d_{13} x_3 + d_{14} x_4) \quad (4.2)$$

In our paper, three of the four functions $w_i : w_1, w_2$ and w_3 will be positively defined based on the sign of the coefficients $a_{1i}, b_{1i}, c_{1i}, d_{1i}$ with $i = 1 \div 4$. The last one will be constant and imposed by the author, $w_4 > 0$. If the positive weight functions will be well defined, then the sign of total function W will be analyzed in order to identify the stability or instability areas of the system.

4.3 Application on X-31 aircraft

The X-31 aircraft was designed to break the « stall barrier », allowing the aircraft to remain under control at very high angles of attack. The X-31 aircraft employs thrust vectoring paddles which are placed in the jet exhaust, allowing its aerodynamic surfaces to maintain their control at very high angles.

For its control, the aircraft has a canard, a vertical tail with a conventional rudder, and wing Leading-Edge and Trailing-Edge flaps.

The main part of the X-31 aircraft model is a wing-fuselage section with eight servo-motors for changing the canard angles ($-70^0 \leq \delta_c \leq 20^0$), the wing Leading-Edge inner/outer flaps ($-70^0 \leq \delta_{LEi} \leq 0^0$) / ($-40^0 \leq \delta_{LEo} \leq 0^0$), the wing Trailing-Edge flaps ($-30^0 \leq \delta_{TE} \leq 30^0$) and the rudder ($-30^0 \leq \delta_r \leq 30^0$) angles (Williams et al., 1994). The X-31 aircraft is capable of flying at high angles of attack [-5^0 to 56^0] and at sideslip angles [-20^0 to 20^0].

The aircraft geometrical data are: reference wing area of 0.3984 m^2 , MAC of 0.51818 m , reference wing span of 1.0 m . In addition, its mass is 120 kg at Mach number of 0.18 and sea

level. The variations of aerodynamic coefficients with angle of attack used in this analysis have been estimated using the Digital DATCOM code ((Anton et al., 2011), (Anton et al., 2010)).

4.3.1 Aircraft longitudinal motion analysis

If a longitudinal state vector $\mathbf{x} = [u/V \ \alpha \ q \ \theta]^T = [x_1 \ x_2 \ x_3 \ x_4]^T$ is defined along with a single control term δ (elevator), then the aircraft's linearized longitudinal dynamics becomes (Schmidt, 1999)

$$\dot{\mathbf{x}} = \mathbf{A}_{long} \mathbf{x} + \mathbf{B}_{long} \delta \quad (4.3)$$

where \mathbf{A} is the system matrix and \mathbf{B} is the control matrix.

The two pairs of complex conjugate roots of the linearized longitudinal dynamics correspond to short-period (fast mode) and phugoid (slow mode).

The non dimensional longitudinal equations of motion (4.1) are written, with $x_1 = u/V$, $x_2 = \alpha$, $x_3 = q$ and $x_4 = \theta$ as follows:

$$\begin{cases} f_1 = a_1 (u/V) + a_2 \alpha + a_3 \theta + d_1 \delta \\ f_2 = a_4 (u/V) + a_5 \alpha + a_6 q + a_7 \theta + d_2 \delta \\ f_3 = a_8 (u/V) + a_9 \alpha + a_{10} q + d_3 \delta \\ f_4 = a_{11} q \end{cases} \quad (4.4)$$

where the coefficients a_1 to a_{11} are determined with eq.(4.5):

$$\begin{cases} a_1 = X_u, a_2 = \frac{X_\alpha}{V}, a_3 = -\frac{g}{V} \cos \Theta_0, a_4 = \frac{V Z_u}{V - Z_\alpha}, a_5 = \frac{Z_\alpha}{V - Z_\alpha}, a_6 = \frac{V + Z_q}{V - Z_\alpha}, \\ a_7 = -\frac{g}{V - Z_\alpha} \sin \Theta_0, a_8 = \left(V M_u + \frac{V Z_u M_\alpha}{V - Z_\alpha} \right), a_9 = \left(M_\alpha + \frac{Z_\alpha M_\alpha}{V - Z_\alpha} \right), \\ a_{10} = \left(M_q + M_\alpha \frac{V + Z_q}{V - Z_\alpha} \right), a_{11} = 1, d_1 = \frac{X_\delta}{V}, d_2 = \frac{Z_\delta}{V - Z_\alpha}, d_3 = \left(M_\delta + \frac{Z_\delta M_\alpha}{V - Z_\alpha} \right) \end{cases} \quad (4.5)$$

The term (u/V) is then replaced with \tilde{u} . By taking into account eq.(4.4) and (4.5), knowing the term $a_7 = 0$ (because $\theta = 0$), the final total weight function W becomes:

$$W = \sum_{k=1}^4 w_k x_k f_k = (w_1 a_1 \tilde{u}^2 + w_2 a_5 \alpha^2 + w_3 a_{10} q^2) + \alpha \tilde{u} (w_1 a_2 + w_2 a_4) + \alpha q (w_2 a_6 + w_3 a_9) + \tilde{u} (w_3 a_8 q + w_1 a_3 \theta) + w_4 a_{11} q \theta + \delta (w_1 d_1 \tilde{u} + w_2 d_2 \alpha + w_3 d_3 q) \tag{4.6}$$

In order to analyze the sign of the total weight function W , it is needed to analyze the signs of all terms $a_i, i = 1 \div 11$ and $d_j, j = 1 \div 3$.

For this reason, the graphs of the variations of coefficients a_1 to a_{11} and d_1 to d_3 with angle of attack are shown in Figure 4.1, where it can be seen that the coefficients $a_1 < 0, a_3 < 0, a_6 > 0, a_{11} > 0$ as well as other coefficients have fluctuant behavior.

All three terms d_j have a oscillating behavior.

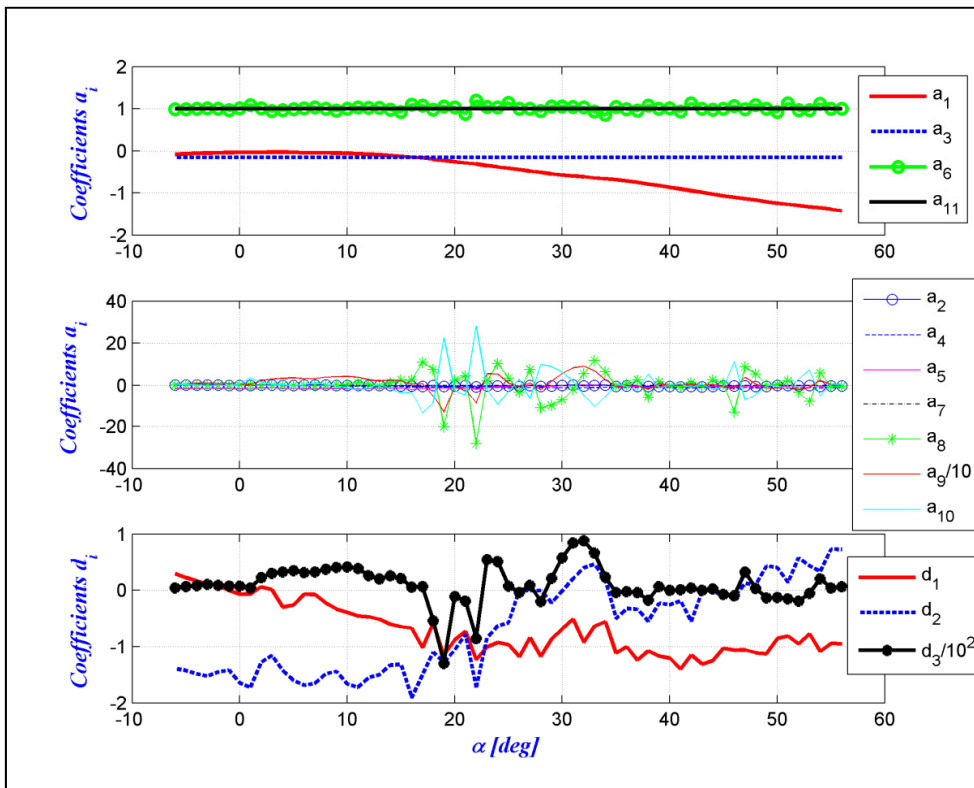


Figure 4.1 Coefficients a_i and d_j variation with the angle of attack

The weight functions are chosen considering the signs of the coefficients a_i , d_j and the tested cases for the pitch angles $\theta = [-20 \text{ to } 20]^\circ$ and pitch rates $q = [-10 \text{ to } 10]^\circ/\text{s}$. The aim of the *WFM* is to find 3 positive weighting functions w_1 , w_2 and w_3 presented in Figure 4.2, based on the coefficients variations presented in Figure 4.1.

For the flight case configuration presented in this paper, it is considered that the canard angle $\delta_c = 0^\circ$ and the flap angle $\delta = 5^\circ$. The positive weight functions are defined as:

$$\begin{aligned} w_1 &= \tilde{u}(a_1 \tilde{u} + a_2 \alpha + a_3 \theta + d_1 \delta)^2 \\ w_2 &= \alpha^2 (a_4 \tilde{u} + a_5 \alpha + a_6 q + d_2 \delta)^2 \\ w_3 &= q^2 (a_8 \tilde{u} + a_9 \alpha + a_{10} q + d_3 \delta)^2 \\ w_3 &= 1,100 \end{aligned} \quad (4.7)$$

and the corresponding final form of the total weight function W is given by eq.(4.8).

$$\begin{aligned} W &= \sum_{k=1}^4 w_k x_k f_k = w_1 f_1 \tilde{u} + w_2 f_2 \alpha + w_3 f_3 q + w_4 f_4 \theta = \tilde{u}^2 (a_1 \tilde{u} + a_2 \alpha + a_3 \theta + d_1 \delta)^3 \\ &+ \alpha^3 (a_4 \tilde{u} + a_5 \alpha + a_6 \theta + d_2 \delta)^3 + q^3 (a_6 \tilde{u} + a_9 \alpha + a_{10} q + d_3 \delta)^3 + w_4 q \theta a_{11} \end{aligned} \quad (4.8)$$

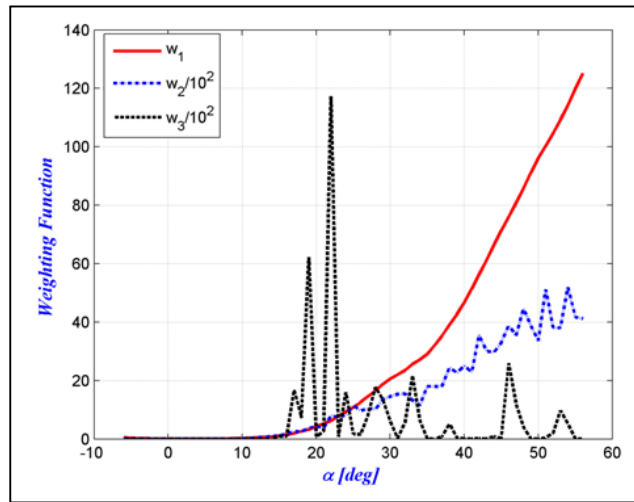


Figure 4.2 Weight functions chosen for longitudinal dynamics

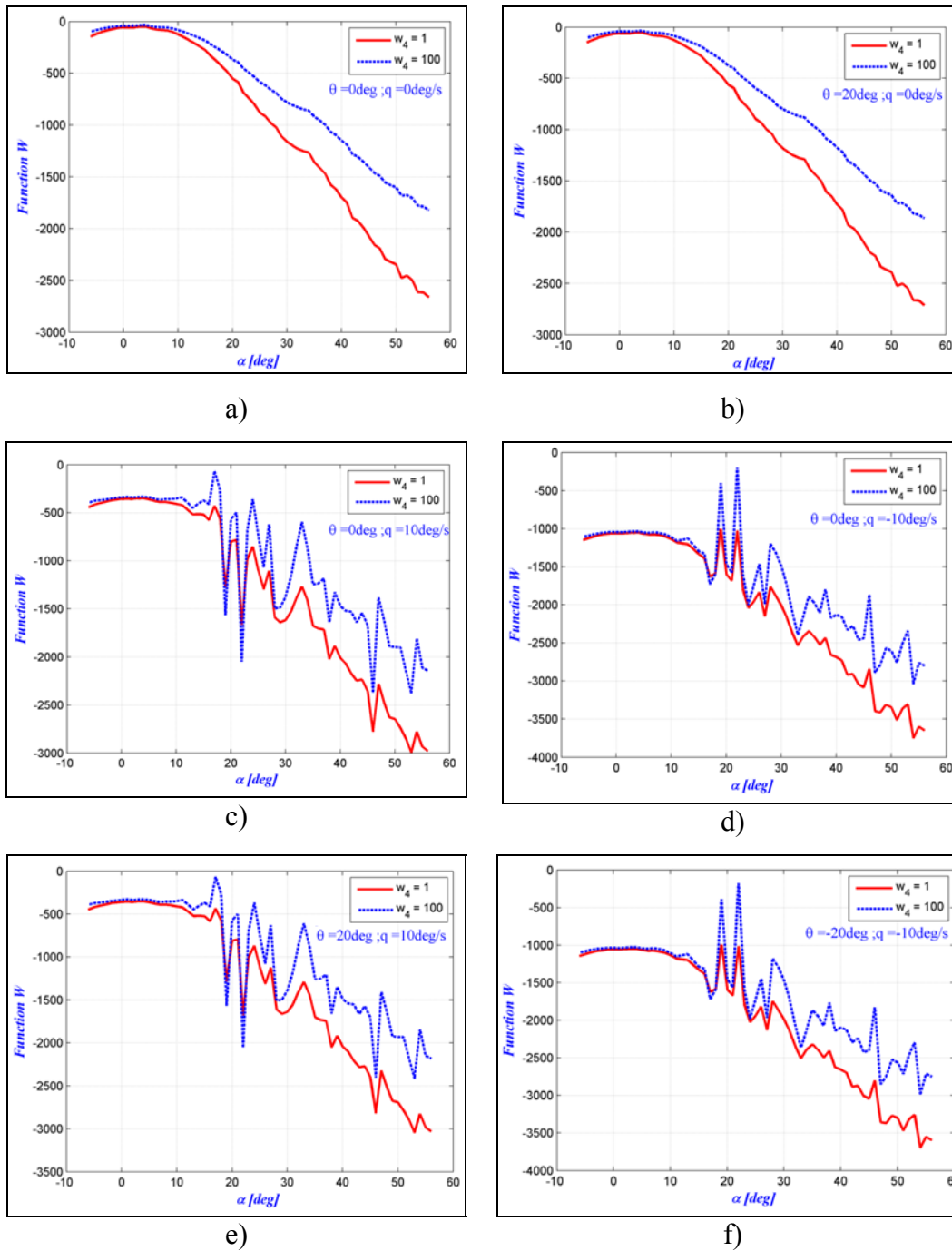


Figure 4.3 Stability analyses with the weight functions method for different values of constant w_4 as a function of angle of attack

Two positive values for w_4 are chosen: 1 and 100. It can be observed in Figure 4.3 that the shape of the stability curve does not change with the values of pitch angle θ and pitch rate q ,

probably because the terms multiplying the pitch angle are small and constant ($a_3 = 0.1601$ and $a_{11} = 1$) as seen also on Figure 4.1; for this reason, their contributions are quite insignificant in comparison with the rest of the coefficients. Under these circumstances, for any considered range of pitch rates q and pitch angles θ the system remains always stable.

4.3.2 Aircraft lateral analysis motion

Next, the non-dimensional lateral–directional equations of motion are given in eq.(4.9).

$$\begin{cases} \dot{\beta} = c_1 \beta + c_2 p + c_3 \varphi + c_4 r + b_1 \delta \\ \dot{p} = c_5 \beta + c_6 p + c_7 r + b_2 \delta \\ \dot{r} = c_8 \beta + c_9 p + c_{10} r + b_3 \delta \\ \dot{\phi} = c_{11} p \end{cases} \quad (4.9)$$

where

$$\begin{cases} c_1 = \frac{Y_\beta}{V}, c_2 = \frac{Y_p}{V}, c_3 = \frac{g}{V} \cos \Theta_0, c_4 = \frac{Y_r - V}{V}, b_1 = \frac{Y_\delta}{V} \\ c_5 = G \left(L_\beta + N_\beta \frac{I_{xz}}{I_x} \right), c_6 = G \left(L_p + N_p \frac{I_{xz}}{I_x} \right), c_7 = G \left(L_r + N_r \frac{I_{xz}}{I_x} \right), \\ b_2 = G \left(L_\delta + N_\delta \frac{I_{xz}}{I_x} \right), c_8 = G \left(N_\beta + L_\beta \frac{I_{xz}}{I_z} \right), c_9 = G \left(N_p + L_p \frac{I_{xz}}{I_z} \right), \\ c_{10} = G \left(N_r + L_r \frac{I_{xz}}{I_z} \right), b_3 = G \left(N_\delta + L_\delta \frac{I_{xz}}{I_z} \right), c_{11} = 1 \end{cases} \quad (4.10)$$

The weighting function W can be thus written under the following form, where $x_1 = \beta$ (sideslip rate), $x_2 = p$ (roll rate), $x_3 = r$ (yaw rate), $x_4 = \phi$ (bank angle), $x_5 = \delta$:

$$\begin{aligned} W = \sum_{k=1}^4 w_k x_k f_k = w_1 \beta (c_1 \beta + c_2 p + c_4 r + c_3 \varphi + \delta b_1) + \\ w_2 p (c_6 p + c_5 \beta + c_7 r + \delta b_2) + w_3 r (c_{10} r + c_8 \beta + c_9 p + \delta b_3) + w_4 c_{11} p \varphi \end{aligned} \quad (4.11)$$

All possible positive and negative values of sideslip rate, roll rate, yaw rate and bank angle were considered. To analyze the sign of the weight function W , the sign of terms c_i , $i = 1 \div 11$ and b_j , $j = 1 \div 3$ where analyzed. In Figure 4.4, it can be observed that $b_1, b_2, b_3 < 0$, $c_1,$

$c_2, c_4, c_5, c_9 < 0$ and $c_3, c_{11} > 0$, while a non linear behavior can be seen for the other four coefficients c_6, c_7, c_8 and c_{10} presented.

In eq.(4.11), the parenthesis which multiplies the first term is negative $(c_1\beta + c_2p + c_4r + c_3\phi + \delta b_1)$. For positive values of β , this term is always negative. We know that $c_1 < 0$, and for this reason the first weighting function $w_1 = c_1^2/\beta^2$. Equation (4.11) becomes:

$$W = \frac{c_1^2}{\beta^2} \beta(c_1\beta + c_2p + c_4r + c_3\phi + \delta b_1) + w_2p(c_6p + c_5\beta + c_7r + \delta b_2) + w_3r(c_{10}r + c_8\beta + c_9p + \delta b_3) + w_4c_{11}p\phi \tag{4.12}$$

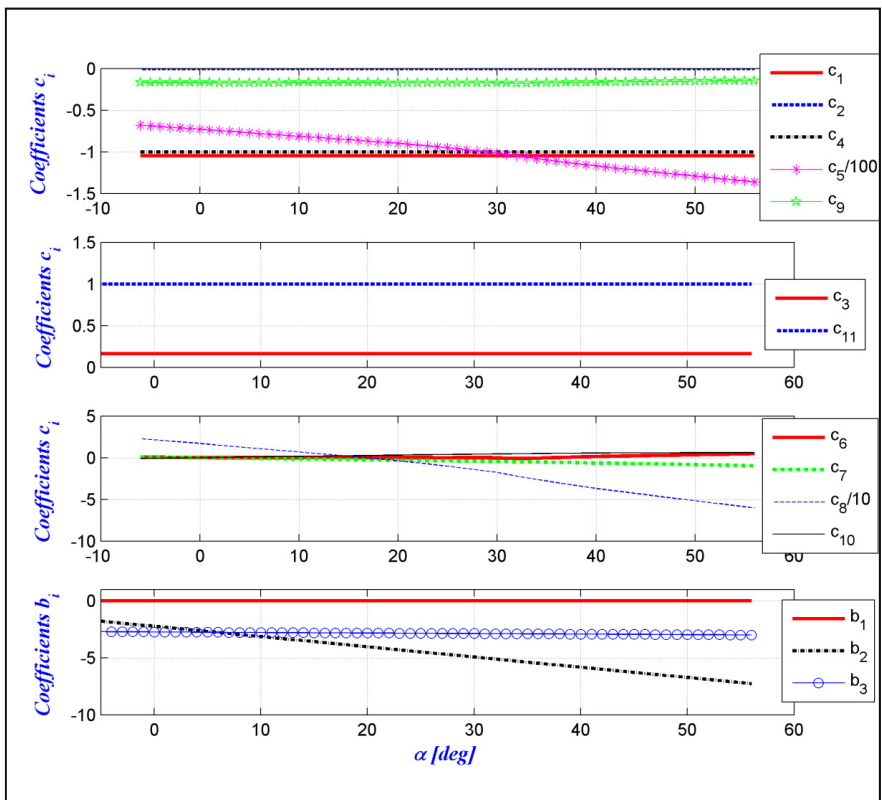


Figure 4.4 The c_i and b_j coefficients' variation with the angle of attack

The parenthesis which multiplies w_2p is also negative $(c_6p + c_5\beta + c_7r + \delta b_2) < 0$. Based on its sign the second function w_2 are defined as $w_2 = p^2(c_6p + c_5\beta + c_7r + \delta b_2)^2$.

The total function W is now given by eq.(4.13).

$$W = \frac{c_1^2}{\beta^2} \beta (c_1 \beta + c_2 p + c_4 r + c_3 \varphi + \delta b_1) + p^2 (c_6 p + c_5 \beta + c_7 r + \delta b_2)^2 \times$$

$$p (c_6 p + c_5 \beta + c_7 r + \delta b_2) + w_3 r (c_{10} r + c_8 \beta + c_9 p + \delta b_3) + w_4 c_{11} p \varphi \quad (4.13)$$

At this point it is possible to define w_3 or w_4 as a positive constant. Because $c_{11} > 0$, it was chosen $w_4 = c_{11} p \varphi$. The final form of function W is given by eq.(4.14).

$$W = \frac{c_1^2}{\beta} (c_1 \beta + c_2 p + c_4 r + c_3 \varphi + \delta b_1) + p^3 (c_6 p + c_5 \beta + c_7 r + \delta b_2)^3 +$$

$$+ w_3 r (c_{10} r + c_8 \beta + c_9 p + \delta b_3) + (c_{11} p \varphi)^2 =$$

$$= c_1^3 + (c_2 p + c_4 r + c_3 \varphi + \delta b_1) \frac{c_1^2}{\beta} + c_{11}^2 p^2 \varphi^2 + p^3 (c_6 p + c_5 \beta + c_7 r + \delta b_2)^3 +$$

$$+ w_3 r (c_{10} r + c_8 \beta + c_9 p + \delta b_3) \quad (4.14)$$

Two of the weighting functions chosen have a constant variation with angle of attack (w_1 and w_4); w_2 is variable and the last one is defined as $w_3 = 1$ and 100.

It was considered that the roll rate $p = [-6 \text{ to } 6]^0/\text{s}$, the yaw rate $r = [-2 \text{ to } 2]^0/\text{s}$, the sideslip rate $\beta = [-10 \text{ to } 10]^0$ and the bank angle $\Phi = [-30 \text{ to } 30]^0$.

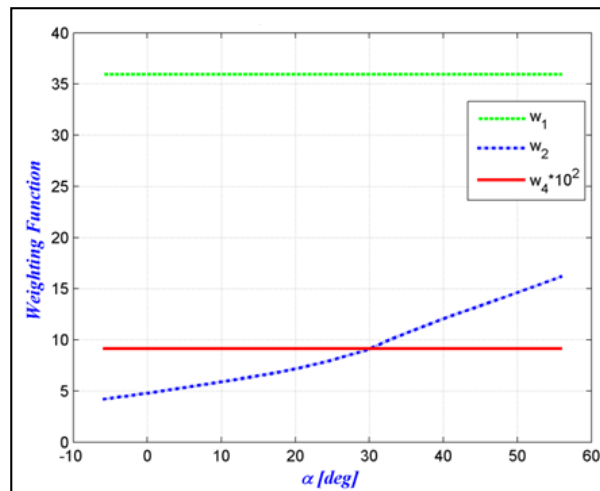


Figure 4.5 Weight functions chosen for the lateral dynamics

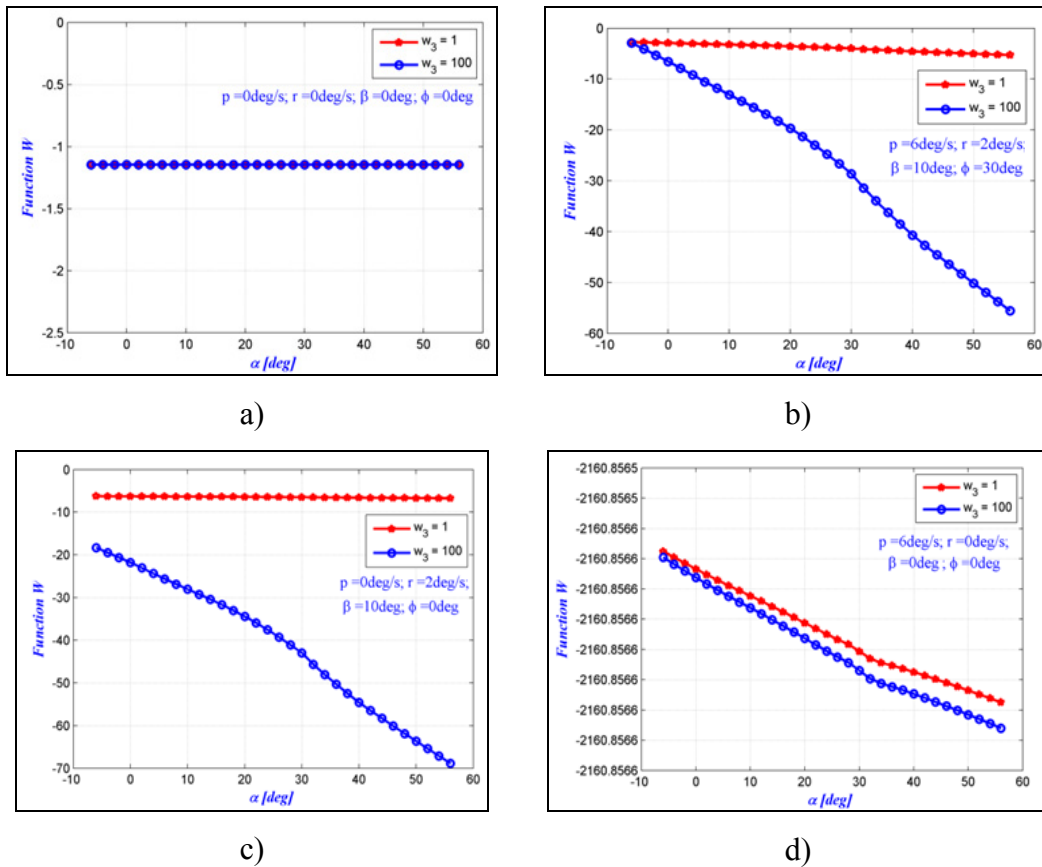


Figure 4.6 Lateral-Directional stability analysis with the weight functions method for different values of constant w_3 as a function of angle of attack

For the lateral motion, the weight functions are overlapped only if p , r , β and ϕ are zero; that means the value chosen for the weight function w_3 have no influence on the total weight function W . The system is stable for roll, spiral and Dutch roll modes as the total weight function W is negative as shown in Figure 4.6 for extreme values chosen for p , r , β and ϕ . For the studied case, the X-31 aircraft is stable for any type of motion within limits for p , r , β , ϕ (short-period, phugoid, roll, Dutch roll and spiral modes).

4.4 Root Locus Map

The five modes of motion for the X-31 aircraft are: the short period and the long period for longitudinal motion of the aircraft and the roll, Dutch roll and spiral for lateral motion. The

natural frequency (ω_n) and the damping ratio (ζ) are defined for each mode from the values of the eigenvalues. For the longitudinal stability analysis, two modes are studied: the short period and the phugoid. The short term pitch is a second order response. The phugoid mode is the long-term motion of an aircraft after a disturbance.

The matrices of eq.(4.3) are given in the next eq.(4.15), as described by Schmidt (1999):

$$\mathbf{A}_{long} = \begin{bmatrix} X_u & \frac{X_\alpha}{V} & 0 & -\frac{g}{V} \\ \frac{VZ_u}{V-Z_{\dot{\alpha}}} & \frac{Z_\alpha}{V-Z_{\dot{\alpha}}} & \frac{V+Z_q}{V-Z_{\dot{\alpha}}} & 0 \\ VM_u + \frac{VZ_uM_{\dot{\alpha}}}{V-Z_{\dot{\alpha}}} & M_\alpha + \frac{Z_\alpha M_{\dot{\alpha}}}{V-Z_{\dot{\alpha}}} & M_q + M_{\dot{\alpha}} \frac{V+Z_q}{V-Z_{\dot{\alpha}}} & 0 \\ 0 & 0 & 1 & 0 \end{bmatrix}, \quad (4.15)$$

$$\mathbf{x}_{long} = \begin{bmatrix} \Delta u \\ \Delta \alpha \\ \Delta q \\ \Delta \theta \end{bmatrix}, \quad \mathbf{B}_{long} = \begin{bmatrix} \frac{X_\delta}{V} \\ \frac{Z_\delta}{V-Z_{\dot{\alpha}}} \\ M_\delta + \frac{Z_\delta M_{\dot{\alpha}}}{V-Z_{\dot{\alpha}}} \\ 0 \end{bmatrix}, \quad u_{long} = \Delta \delta_e$$

The roots of the characteristic equation $\det(\lambda \mathbf{I} - \mathbf{A}_{long}) = 0$ gave these eigenvalues λ_1 to λ_4 .

For both longitudinal modes, the natural frequency ω_n and damping ratio ζ are estimated directly from the characteristic equation $|\lambda \mathbf{I} - \mathbf{A}_{long}| = 0$, as function of the longitudinal eigenvalues (eq.(4.16)); the eigenvalues $\lambda_{1,2}$ correspond to short-period and $\lambda_{3,4}$ to phugoid modes.

$$\begin{cases} \zeta \omega_n = |\operatorname{Re}(\lambda_{1,2})| \\ \omega_n \sqrt{1-\zeta^2} = |\operatorname{Im}(\lambda_{1,2})| \end{cases}, \quad \begin{cases} \zeta \omega_n = |\operatorname{Re}(\lambda_{3,4})| \\ \omega_n \sqrt{1-\zeta^2} = |\operatorname{Im}(\lambda_{3,4})| \end{cases} \quad (4.16)$$

A representation of the eigenvalues obtained for the longitudinal motion of an X-31 aircraft is shown in Figure 4.7. All real parts of eigenvalues are negative, which means that the X-31 aircraft is stable in its longitudinal motion.

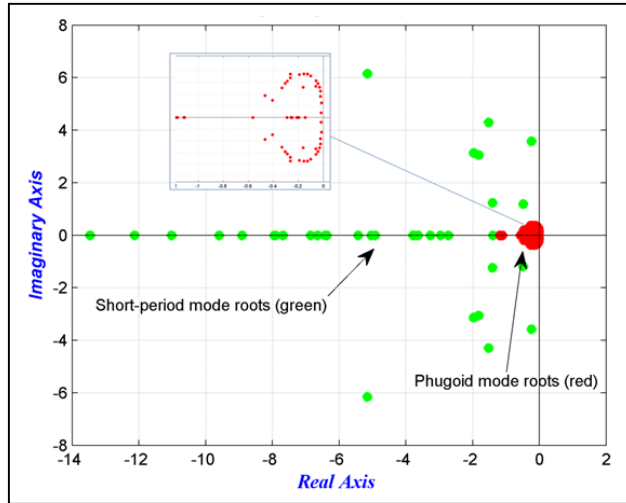


Figure 4.7 Root locus map longitudinal motion of the X-31 aircraft

The matrices of the aircraft lateral model are next defined in eq.(4.17), based on (Schmidt, 1998).

$$\mathbf{A}_{lat} = \begin{bmatrix} \frac{Y_\beta}{V} & \frac{Y_p}{V} & \frac{Y_r - V}{V} & \frac{g}{u_0} \cos \theta_0 \\ G\left(L_\beta + N_\beta \frac{I_{xz}}{I_x}\right) & G\left(L_p + N_p \frac{I_{xz}}{I_x}\right) & G\left(L_r + N_r \frac{I_{xz}}{I_x}\right) & 0 \\ G\left(N_\beta + L_\beta \frac{I_{xz}}{I_z}\right) & G\left(N_p + L_p \frac{I_{xz}}{I_z}\right) & G\left(N_r + L_r \frac{I_{xz}}{I_z}\right) & 0 \\ 0 & 1 & 0 & 0 \end{bmatrix},$$

$$\mathbf{x}_{lat} = \begin{bmatrix} \Delta\beta \\ \Delta p \\ \Delta r \\ \Delta\phi \end{bmatrix}, \quad \mathbf{B}_{lat} = \begin{bmatrix} \frac{Y_\delta}{V} \\ G\left(L_\delta + N_\delta \frac{I_{xz}}{I_x}\right) \\ G\left(N_\delta + L_\delta \frac{I_{xz}}{I_z}\right) \\ 0 \end{bmatrix}, \quad u_{lat} = \Delta\delta_a$$

(4.17)

Three modes are considered in the aircraft lateral motion modeling:

- Spiral mode representing, a convergent or a divergent motion;
- Roll mode representing a fast convergent motion, and
- Dutch roll mode representing a light damped oscillatory motion with a low frequency.

These modes are significant factors mainly in the uniform cruise flight. For the lateral aircraft motion modelling, two real roots correspond to roll and spiral modes, and a pair of complex roots correspond to Dutch roll mode obtained from the characteristic equation $|\lambda\mathbf{I} - \mathbf{A}_{lat}| = 0$.

The rolling motion is generally very much damped and reaches the steady state in a very short time. An unstable spiral mode results into a turning flight path. The Dutch roll is a nuisance mode that appears in the basic roll response to lateral control and can induce non-controlled and non-desired motions in roll and yaw modes. These motions can significantly influence the ability of the pilot to control the lateral-directional motions with precision.

The eigenvalues for all three motions described above for X-31 aircraft are represented in Figure 4.8: blue for Dutch Roll, red for spiral and green for roll mode.

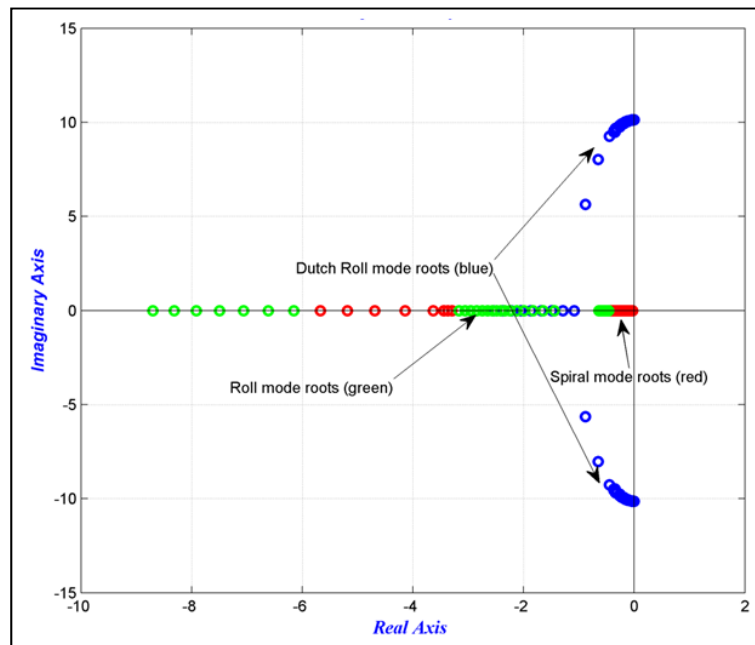


Figure 4.8 Root locus map for lateral motion

Results obtained with the weight functions method shown in Figure 4.6, have proven that the aircraft is stable in its lateral motion. Results presented with root locus map presented in Figure 4.8 show that the X-31 aircraft has a stable lateral motion, because all eigenvalues calculated with the root locus map are situated in the negative plane. The Handling Qualities Method could be used in further studies to determine the aircraft stability (Hodgkinson, 1999), (Bihrlé, 1965), (Cotting, 2010).

4.5 Conclusions

A stability analysis based on the null solutions stability studies for differential equation systems was presented in this paper. The main aim was to find the positive weight functions in order to analyze the X-31 aircraft stability. The aerodynamics coefficients and their stability derivatives were determined with Digital DATCOM code. Based on the aircraft's aerodynamic model in the WFM, 3 functions were defined as function of stability derivatives terms, and the last fourth function was considered positive and chosen to be 1 and 100. The WFM was applied for longitudinal and lateral motions. A discussion of results was done for each case, and the stability was defined and is summarized in the previous sections. HQM was also applied to validate the aircraft stability results found with WFM.

X-31 has a stable longitudinal and lateral dynamics. For the considered altitude and Mach number, the aircraft was found to be stable, regardless the angle of attack. Both modes tested here, the slow and the fast, did not induced any oscillations and/or instabilities.

CHAPTER 5

ARTICLE 4: WEIGHT FUNCTIONS METHOD FOR STABILITY ANALYSIS APPLICATIONS AND EXPERIMENTAL VALIDATION FOR HAWKER 800XP AIRCRAFT

Nicoleta Anton and Ruxandra Mihaela Botez

École de Technologie Supérieure, Montréal, Canada

Laboratory of Research in Active Controls, Aeroservoelasticity and Avionics

This article was presented at AIAA Modeling and Simulation Technologies Conference 13-16 August 2012, Minneapolis, Minnesota, DOI: 10.2514/6.2012-4718

Résumé

Les coefficients de portance, traînée et du moment ainsi que leurs dérivées de stabilité ont été obtenues en utilisant le code récent *FDerivatives* développé à LARCASE et le code *Digital DATCOM* écrit en Fortran. Les résultats obtenus par l'utilisation de ces codes ont été validés avec les données d'essais en vol fourni par CAE Inc., pour le Hawker 800XP, un avion d'affaires de taille moyenne, bimoteur avec les ailes d'une seule pièce. Ensuite, à l'aide de deux méthodes, ces résultats ont été utilisés pour analyser la stabilité de l'aéronef: 1) La méthode des fonctions du poids (*WFM*) et 2) La méthode des qualités de vol (HQM). La méthode *WFM* trouve un nombre de fonctions de poids qui sont égales au nombre d'équations différentielles nécessaires à la modélisation du système. La méthode HQM détermine la stabilité de l'avion à partir du signe de la partie réelle des valeurs propres. Le *WFM* détermine la stabilité de l'avion en fonction du signe de la fonction total du poids. Les signes devraient être négatifs dans les deux méthodes. Les cas de vol suivants sont considérés: le nombre de Mach = 0.4 et 0.5, altitude = 5000 m, 8000 m et 10000 m, et les angles d'attaque $\alpha = -5^0$ à 20^0 . Par conséquent, la stabilité des avions est validée en utilisant deux méthodes: le *WFM* et HQM. L'originalité du travail se trouve dans la validation de la *WFM* à une analyse de stabilité appliquée à un avion réel.

Abstract

A new method for system stability analysis, the weight functions method, is applied to estimate the longitudinal and lateral stability of a Hawker 800XP aircraft. This paper assesses the application of the weight functions method to a real aircraft and a method validation with an eigenvalues stability analysis of linear small-perturbation equations. The method consists of finding the weight functions that are equal to the number of differential equations required for system modelling. The aircraft's stability is determined from the sign of the total weight function - the sign should be negative for a stable model. Aerodynamic coefficients and stability derivatives of the mid-size twin-engine corporate aircraft Hawker 800XP are obtained using the in-house FDerivatives code, recently developed at our laboratory of applied research in active controls, avionics and aeroservoelasticity LARCASE, with the results validated with the flight test data supplied by CAE Inc. This aircraft model was selected because it was part of a research project for FDerivatives code; continued with the weight functions method for stability analysis in order to develop a design tool, based only on aircraft geometrical parameters for the subsonic regime. The following flight cases are considered: Mach numbers = 0.4 and 0.5, altitudes = 3000 m, 5000 m, 8000 m and 10000 m, and angles of attack $\alpha = -5^{\circ}$ to 20° .

5.1 Introduction

Modern fighter aircraft are designed with an unstable configuration which gives marginal stability. A control law is necessary to stabilize the aircraft. Aerodynamic models contain nonlinearities representative of a modern fighter. The stability analysis for a real aircraft was done in this paper using the longitudinal and the lateral-directional motion mathematical model. The mid-size Hawker 800XP is a twin-engine corporate aircraft with low swept-back one-piece wings, a high tailplane and rear-mounted engines, for which the maximum Mach number is 0.9. This aircraft operates in the subsonic and transonic regimes; the flight test data were provided by CAE Inc. A new method for systems stability analysis, the weight functions method, was used to replace the use of Lyapunov functions. This method can be

used as a design tool because it can be applied if an aircraft's geometrical parameters are known.

The Weight Functions Method (WFM) has been used mostly for crack problems, to determine stress factors. The method was applied by Yoichi et al. (2003) to solve two- and three-dimensional crack problems, to calculate stress intensity factors for arbitrary loading conditions. The stress intensity factor for a patched crack within an infinite plate was successfully numerically validated using the WFM (Kim et al., 2000). Different formula to calculate the stress intensity factor are presented by (Paris et al., 1976), (Wu et al., 1983), (Fett, 1991), (Schneider et al., 1989).

A different approach was presented by Stroe (2008), who solved the Lurie-Postnikov problem using general equations for linear or nonlinear vibrations by linear transformations. Stroe also analyzed a holonomic system with dependent variable equations where the weight functions method was applied for vibration and stability studies in the cases of linear and nonlinear damped holonomic systems (Stroe et al., 2008).

The WFM has been applied in the aerospace industry for the modelling of the longitudinal motion of a canard configuration generic fighter aircraft, called the High Incidence Research Model (HIRM) by the first author of this paper, Anton (2005). The HIRM, a non-linear aircraft model developed by FOI, the Swedish Defense Research Agency based on the Generic Aerodata Model (GAM) developed by SAAB AB, has been the subject of collaboration within the Group for Aeronautical Research and Technology in EUROpe (GARTEUR Action Group FM (AG08)). The results were presented for a complete range of angle of attack $[-10 \text{ to } 30]^\circ$ and elevon deflection angle $[-30 \text{ to } 30]^\circ$, constant value of Mach number of 0.25 and altitude 500 m. The WFM was applied in the case of short-period longitudinal approximations for the system of equations with unstable characteristics given by the pitching-moment coefficients, and the aircraft model was stabilized using control laws. The stability field was augmented from an angle of attack of 10.9 degrees up to 26

degrees. This model had increased complexity because the thrust component was included in the system equations.

In this paper, the WFM and the eigenvalues stability method are applied to study the Hawker 800XP aircraft's stability, based on aerodynamic coefficients and their derivatives provided by the FDerivatives code (Anton et al., 2010). This is the first time that the weight functions method is being used to analyze longitudinal and lateral aircraft model stability. The WFM is used here to model the stability of a mid-size business aircraft with a typical wing-body-tail configuration and three basic control surfaces: the ailerons, elevator and rudder, designed to change and control the moments about the reference axis. This airplane has swept-back wings that are used to delay the drag divergence.

The results, expressed in terms of weighting functions for the WFM, and in terms of damping and frequency for the eigenvalues method, are presented for the subsonic regime characterized by Mach numbers equal to 0.4 and 0.5, and four altitudes: 3,000 m, 5000 m, 8000 m and 10000 m. The pitch angles $\theta = [-20 \text{ to } 20]^\circ$ and pitch rates $q = [-3.5 \text{ to } 3.5]^\circ/\text{s}$ are the longitudinal motion variables, and the roll rate $p = [-6 \text{ to } 6]^\circ/\text{s}$, yaw rate $r = [-2 \text{ to } 2]^\circ/\text{s}$, sideslip angle $\beta = [-5 \text{ to } 5]^\circ$ and roll angle $\Phi = [-15 \text{ to } 15]^\circ$ are the variables for lateral motion. It was also considered that we have a value $\delta = 5^\circ$ for the control term. In the following sections, the WFM and root locus method are described and the related results using both methods are presented.

5.2 The Weight Functions Method

Quadratic forms have a matrix representation, and studying their representation can be reduced to a study of symmetric matrices. Consider the function $F: R^2 \rightarrow R$, where $F = a_{11}x_1^2 + a_{12}x_1x_2 + a_{22}x_2^2$ (Wilde, 2011). This quadratic form in R^n is $F(x) = \sum_{i,j=1}^n a_{ij}x_i x_j$, where $x = (x_1, \dots, x_n)$, and the matrix \mathbf{A} is a unique and $n \times n$ symmetric matrix. The matrix \mathbf{A} is:

- 1) positive definite if $F(x) > 0$, for $x \neq 0$ in R^n . $x = 0$ is a unique global minimum of the quadratic form given by \mathbf{A} .

- 2) positive semidefinite if $F(x) \geq 0$, for $x \neq 0$ in R^n . $x = 0$ is a global minimum, but not a unique global one, of the quadratic form given by \mathbf{A} .
- 3) negative definite if $F(x) < 0$, for $x \neq 0$ in R^n . $x = 0$ is a unique global maximum of the quadratic form given by \mathbf{A} .
- 4) negative semidefinite if $F(x) \leq 0$, for $x \neq 0$ in R^n . $x = 0$ is a global maximum, but not a unique global one, of the quadratic form given by \mathbf{A} .
- 5) indefinite if $F(x) > 0$, for some $x \in R^n$ and < 0 for some other $x \in R^n$. $x = 0$ is neither a maximum nor a minimum of the quadratic form given by \mathbf{A} .

In most practical problems, differential equations that model the behavior of a dynamic system often depend on more than one parameter. For example, the WFM is more efficient than the classical Lyapunov functions method since only one function has to be found at a time, while the Lyapunov method finds all the functions simultaneously. In fact, the Lyapunov stability criteria are based on finding only one Lyapunov function. Finding a Lyapunov function is not simple and is not guaranteed.

The WFM finds a number of weight functions that is equal to the number of the first-order differential equations modelling the system (Stroe, 2008), (Stroe et al., 2008).

Theorem (Stroe et al., 2008): Given the autonomous system $\dot{x} = f(x), x \in R^n$, if $w_k(x_1, x_2, \dots, x_n)$

exist such that $dV = \sum_{k=1}^n x_k w_k dx_k$ is a total exact differential, then the stability is given by

$W = \sum_{k=1}^n x_k w_k f_k$ as follows: W is negative-definite, the solution is asymptotic stable; W is the null function, the solution is simple stable; W is positive-definite, the solution is unstable.

w_k represents the weight functions, with $k =$ number of equations and unknowns, and f_k are the functions equivalent to the derivatives of x_k variables.

Four positive-defined weight functions are considered in this paper; three expressed as functions of the system's coefficients and determined gradually, and the last being positive-

constant defined. The fourth weight function, defined as 1 (the smaller positive integer) or 100 (a high positive integer) are utilized to analyze the longitudinal and lateral-directional stability of the Hawker 800XP aircraft. Both values of the last weight function have been considered in order to determine if the stability does (or does not) depend on its order of measure. The analysis of the WFM results was conducted based on the values of the aerodynamic coefficients and stability derivatives estimated from the aircraft geometry, and were validated with flight test data.

5.3 Description of the model

5.3.1 Longitudinal motion

Longitudinal dynamic stability is characterized by short-period and phugoid modes (Schmidt, 1998). If a longitudinal state vector $\mathbf{x} = [u/V \ \alpha \ q \ \theta]^T$ is defined along with a single control term δ , then the aircraft's equations of motion for the linearized longitudinal motion become:

$$\dot{\mathbf{x}} = \mathbf{A}\mathbf{x} + \mathbf{B}\delta \quad (5.1)$$

where \mathbf{A} is the plant matrix and \mathbf{B} is the control matrix. The two pairs of complex conjugate roots of the linearized longitudinal dynamics correspond to the short-period (fast) and phugoid (slow) modes. The homogeneous form of eq.(5.1) is given by

$$\dot{\mathbf{x}} = \mathbf{A}\mathbf{x} \quad (5.2)$$

Equation (5.1) can be further represented as eq.(5.3), using following notations:

$$\begin{cases} f_1 = a_1(u/V) + a_2\alpha + a_3\theta + d_1\delta \\ f_2 = a_4(u/V) + a_5\alpha + a_6q + a_7\theta + d_2\delta \\ f_3 = a_8(u/V) + a_9\alpha + a_{10}q + d_3\delta \\ f_4 = a_{11}q \end{cases} \quad (5.3)$$

where the functions f_1, f_2, f_3 and f_4 are equivalent to derivatives of x_1, x_2, x_3 and x_4 . The right hand coefficients of eq.(5.3) are the following:

$$\left\{ \begin{array}{l} x_{1long} = u/V \\ x_{2long} = \alpha \\ x_{3long} = q \\ x_{4long} = \theta \end{array} \right. , \left\{ \begin{array}{l} a_1 = X_u, a_2 = \frac{X_\alpha}{V}, a_3 = -\frac{g}{V} \cos \Theta_0, \\ a_4 = \frac{VZ_u}{V-Z_{\alpha\&}}, a_5 = \frac{Z_\alpha}{V-Z_{\alpha\&}}, \\ a_6 = \frac{V+Z_q}{V-Z_{\alpha\&}}, a_7 = -\frac{g}{V-Z_{\alpha\&}} \sin \Theta_0 \\ a_8 = \left(VM_u + \frac{VZ_u M_{\alpha\&}}{V-Z_{\alpha\&}} \right), a_9 = \left(M_\alpha + \frac{Z_\alpha M_{\alpha\&}}{V-Z_{\alpha\&}} \right), \\ a_{10} = \left(M_q + M_{\alpha\&} \frac{V+Z_q}{V-Z_{\alpha\&}} \right), a_{11} = 1 \\ d_1 = \frac{X_\delta}{V}, d_2 = \frac{Z_\delta}{V-Z_{\alpha\&}}, d_3 = M_\delta + \frac{Z_\delta M_{\alpha\&}}{V-Z_{\alpha\&}} \end{array} \right. \quad (5.4)$$

In the next equation, the term (u/V) is then replaced with \tilde{u} . By taking the above two equations into account and knowing that the term $a_7 = 0$, and that the unknowns x_{1long} , x_{2long} , x_{3long} and x_{4long} have been defined in eq.(5.4), the total weight function W_{long} is defined by:

$$W_{long} = \sum_{k=1}^4 w_k x_k f_k = w_{1long} \tilde{u} (a_1 \tilde{u} + a_2 \alpha + a_3 \theta + d_1 \delta) + w_{2long} \alpha (a_5 \alpha + a_4 \tilde{u} + a_6 q + d_2 \delta) + \\ + w_{3long} q (a_{10} q + a_9 \alpha + a_8 \tilde{u} + d_3 \delta) + w_{4long} a_{11} q \theta \quad (5.5)$$

5.3.2 Lateral motion

Lateral-directional motion equations are given in matrix form as eq.(5.1). Therefore, the initial system can be written as follows:

$$\begin{cases} f_1 = c_1 \beta + c_2 p + c_3 \phi + c_4 r + b_1 \delta \\ f_2 = c_5 \beta + c_6 p + c_7 r + b_2 \delta \\ f_3 = c_8 \beta + c_9 p + c_{10} r + b_3 \delta \\ f_4 = c_{11} p \end{cases} \quad (5.6)$$

where f_1 , f_2 , f_3 and f_4 are given by the left hand side of eq.(5.7) and the coefficients of eq.(5.6) are expressed as functions of the stability derivative values on the right hand side of eq.(5.7):

$$\begin{cases}
x_{1lat} = \beta \\
x_{2lat} = p \\
x_{3lat} = r \\
x_{4lat} = \phi
\end{cases}, \begin{cases}
c_1 = \frac{Y_\beta}{V}, c_2 = \frac{Y_p}{V}, c_3 = \frac{g}{V} \cos \Theta_0, c_4 = \frac{Y_r - V}{V}, b_1 = \frac{Y_\delta}{V} \\
c_5 = G \left(L_\beta + N_\beta \frac{I_{xz}}{I_x} \right), c_6 = G \left(L_p + N_p \frac{I_{xz}}{I_x} \right), \\
c_7 = G \left(L_r + N_r \frac{I_{xz}}{I_x} \right), b_2 = G \left(L_\delta + N_\delta \frac{I_{xz}}{I_x} \right) \\
c_8 = G \left(N_\beta + L_\beta \frac{I_{xz}}{I_z} \right), c_9 = G \left(N_p + L_p \frac{I_{xz}}{I_z} \right), \\
c_{10} = G \left(N_r + L_r \frac{I_{xz}}{I_z} \right), b_3 = G \left(N_\delta + L_\delta \frac{I_{xz}}{I_z} \right) \\
c_{11} = 1, b_1 = \frac{Y_\delta}{V}, b_2 = G \left(L_\delta + N_\delta \frac{I_{xz}}{I_x} \right), b_3 = G \left(N_\delta + L_\delta \frac{I_{xz}}{I_z} \right)
\end{cases} \quad (5.7)$$

The function W_{lat} can be written for aircraft lateral motion in the following general form, where $x_{1lat} = \beta$, $x_{2lat} = p$, $x_{3lat} = r$ and $x_{4lat} = \phi$:

$$\begin{aligned}
W_{lat} = \sum_{k=1}^4 w_k x_k f_k = w_{1lat} \beta (c_1 \beta + c_2 p + c_4 r + c_3 \phi + b_1 \delta) + \\
+ w_{2lat} p (c_6 p + c_5 \beta + c_7 r + b_2 \delta) + w_{3lat} r (c_{10} r + c_8 \beta + c_9 p + b_3 \delta) + w_{4lat} c_{11} p \phi
\end{aligned} \quad (5.8)$$

5.4 Results obtained using the weight functions method for the Hawker 800XP aircraft

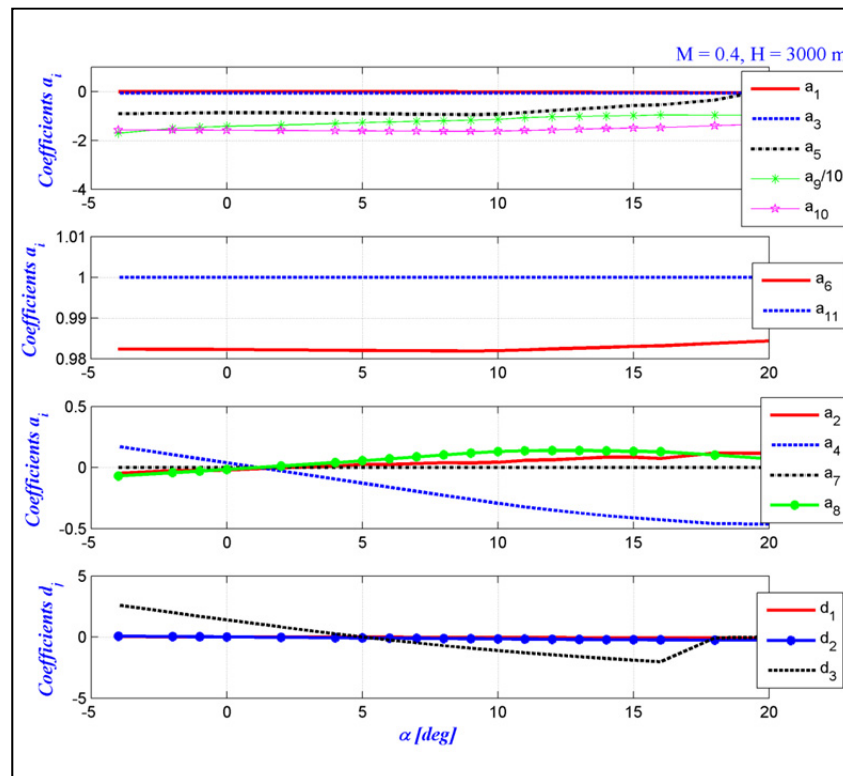
The Hawker 800 XP aircraft has the following main geometrical characteristics: reference wing area of 34.75 m², reference wing span of 15.66 m, mean aerodynamic chord of 2.44 m and a mass of 12,701 kg. The flight cases are characterized by two Mach numbers: 0.4 and 0.5, four altitudes of 3,000 m, 5,000 m, 8,000 m and 10,000 m, and various angles of attack between -4° and 20°.

Stability derivatives for the Hawker 800XP aircraft were determined using the new FDerivatives code (Anton et al., 2010), (Anton et al., 2011) dedicated to the analytical and numerical calculation of aerodynamic coefficients and their corresponding stability derivatives.

The main goal of the WFM is to find, one by one, the eight positive weight functions – four functions for longitudinal motion and four functions corresponding to lateral motion. To analyse the sign of a function W , it is necessary to analyze the signs of all coefficients a_i , $i = 1 \div 11$ and d_j , $j = 1 \div 3$ (longitudinal motion), and c_i , $i = 1 \div 11$ and b_j , $j = 1 \div 3$ (lateral motion). The positive and negative values of pitch rate (q), pitch angle (θ), sideslip rate (β), roll rate (p), yaw rate (r) and roll angle (Φ) were considered in the calculations, because the sign of each of these terms could have an influence on the sign of the total function W .

5.4.1 Results obtained for longitudinal motion using the weight functions method

For longitudinal motion studies, the expressions of the a_i and d_j coefficients are given in eq.(5.4) as functions of stability derivatives, and their variations with the angle of attack are shown in Figure 5.1 for two flight conditions expressed in terms of Mach numbers and altitude Mach number = 0.4 and altitude $H = 3,000$ m, and Mach number = 0.5 and altitude $H = 8,000$ m, where it is clear that the coefficients a_1 and a_3 are negative, and that a_2 and d_1 have a nonlinear behavior.



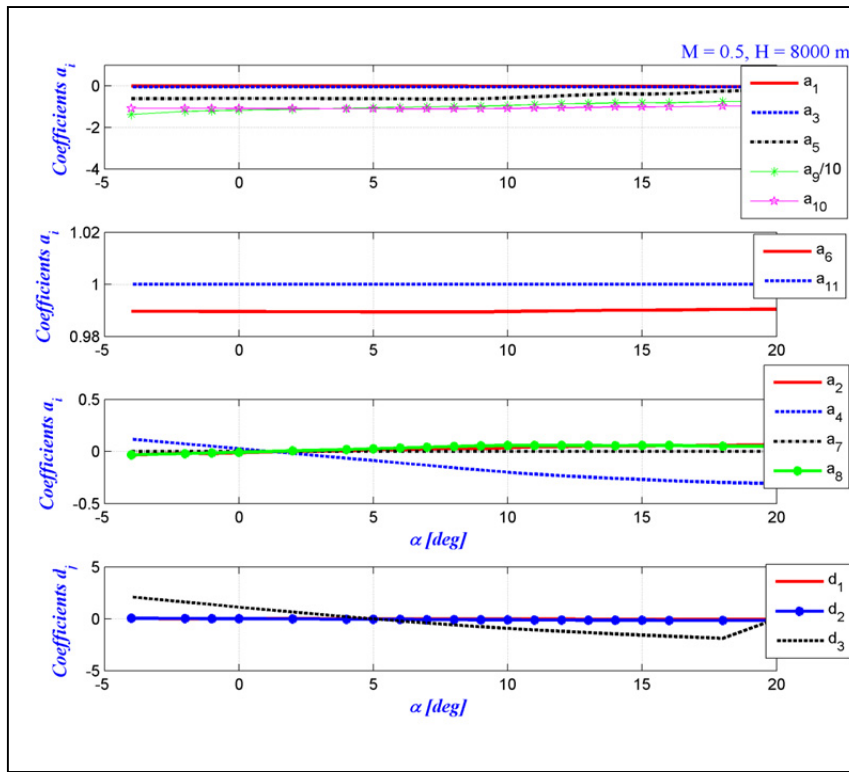


Figure 5.1 The a_i and d_j coefficients' variation with the angle of attack for Mach numbers $M = 0.4$ at altitude $H = 3,000$ m and $M = 0.5$ at $H = 8,000$ m

The first term of eq.(5.5), $w_{1long} \mathcal{L}(a_1\theta + a_2\alpha + a_3\theta + d_1\delta)$, is negative, since $w_{1long} = \mathcal{L}^2(a_2\alpha + a_3\theta + d_1\delta)^2$ is positive, and the quantity within the parenthesis multiplying w_{1long} should be negative to respect the stability requirements.

$$W_{long} = \mathcal{L}^3(a_1\theta + a_2\alpha + a_3\theta + d_1\delta)^3 + w_{2long} \alpha(a_5\alpha + a_4\theta + a_6q + d_2\delta) + w_{3long} q(a_{10}q + a_9\alpha + a_8\theta + d_3\delta) + w_{4long} a_{11}q\theta \tag{5.9}$$

In the second term of eq.(5.9), which should be negative to respect the stability requirements, the coefficient multiplying w_{2long} should also be negative, since $w_{2long} = \alpha^2 a_5^2 > 0$.

$$W_{long} = \mathcal{L}^3(a_1\theta + a_2\alpha + a_3\theta + d_1\delta)^3 + \alpha^2 a_5^2 (a_5\alpha + a_4\theta + a_6q + d_2\delta) + w_{3long} q(a_{10}q + a_9\alpha + a_8\theta + d_3\delta) + w_{4long} a_{11}q\theta \tag{5.10}$$

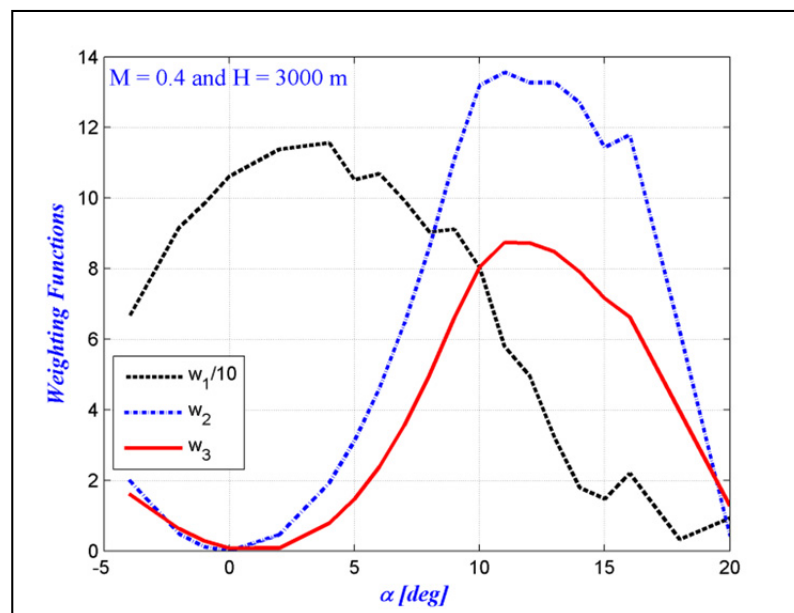
In the third term of eq.(5.10), the third weighting function is $w_{3long} = q^2 (a_8\theta + a_9\alpha + d_3\delta)^2 > 0$. The last positive function is defined as $w_{4long} = 1$ or 100.

$$W_{long} = \theta^3 (a_1\theta + a_2\alpha + a_3\theta + d_1\delta)^3 + \alpha^2 a_5^2 (a_5\alpha + a_4\theta + a_6q + d_2\delta) + q^3 (a_8\theta + a_9\alpha + d_3\delta)^2 (a_{10}q + a_9\alpha + a_8\theta + d_3\delta) + w_{4long} a_{11}q\theta \quad (5.11)$$

In the new w_i functions defined above (eq.(5.9) to (5.11)) we have obtained the final form of the W_{long} function for the aircraft longitudinal motion, expressed in the following equation:

$$W_{long} = \theta^3 (a_1\theta + a_2\alpha + a_3\theta + d_1\delta)(a_2\alpha + a_3\theta + d_1\delta)^2 + (a_5^3\alpha^4 + a_4a_5^2\alpha^3\theta + a_5^2a_6\alpha^3q + a_5^2d_2\delta\alpha^3) + q^3 (a_{10}q + a_9\alpha + a_8\theta + d_3\delta)(a_8\theta + a_9\alpha + d_3\delta)^2 + w_{4long} a_{11}q\theta \quad (5.12)$$

For two cases: Mach numbers 0.4 and 0.5 with corresponding altitudes of 3,000 m and 8,000 m, respectively, the variations of the positive weight functions w_{1long} , w_{2long} and w_{3long} are shown in Figure 5.2, while w_{4long} is constant and equal to 1 or 100.



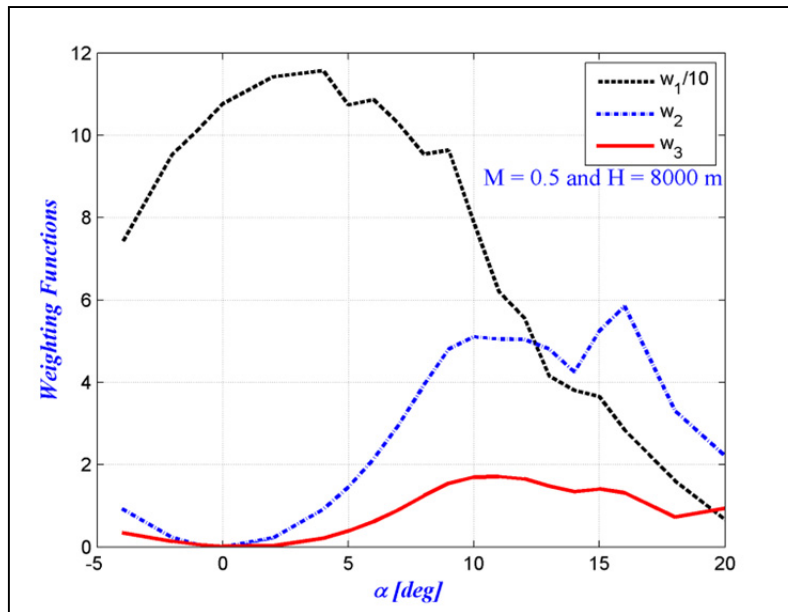


Figure 5.2 Weight functions w_{1long} , w_{2long} and w_{3long} chosen for longitudinal dynamics at Mach numbers $M = 0.4$ and 0.5 corresponding to altitudes $H = 3,000$ and $8,000$ m (left and right diagrams, respectively)

To demonstrate the validity range of the WFM, various combinations of pitch angle θ and pitch rate q are considered. Passenger's comfort limits were taken into account to define these two parameters. These combinations were taken between the null value $(\theta, q) = (0^0, 0^0/s)$ and the upper and lower limits $(\theta, q) = (\pm 20^0, \pm 3.5^0/s)$, $(\theta, q) = (0^0, \pm 3.5^0/s)$ and $(\theta, q) = (\pm 20^0, 0^0/s)$. The total weighting function W 's variation with angle of attack remains negative for the flight conditions expressed by Mach numbers $M = 0.4$ and 0.5 and four altitudes $H = 3,000$ m, $5,000$ m, $8,000$ m and $10,000$ m, and for the considered pairs of pitch angle/pitch rate θ/q , as shown in Figures 5.3 and 5.4.

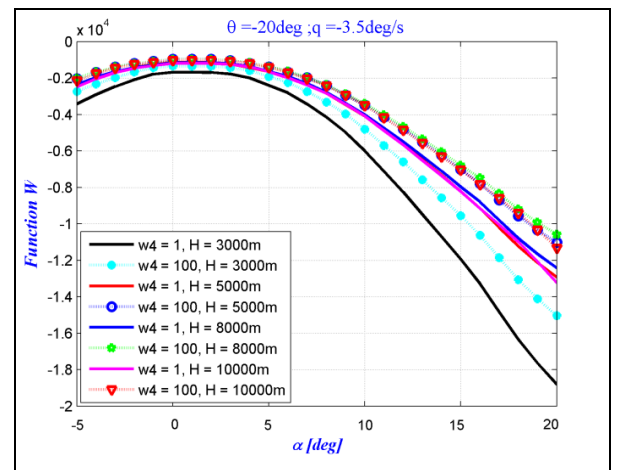
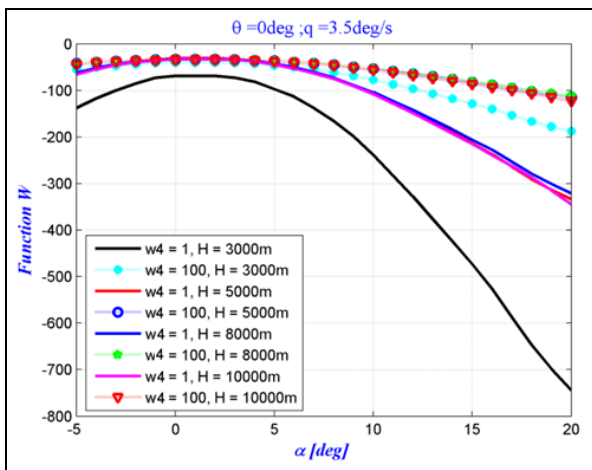
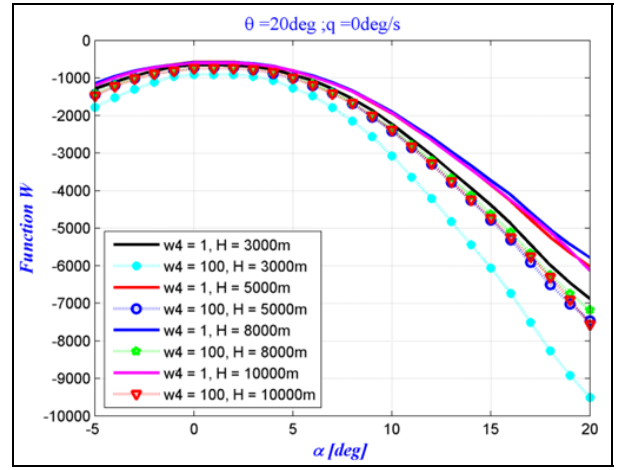
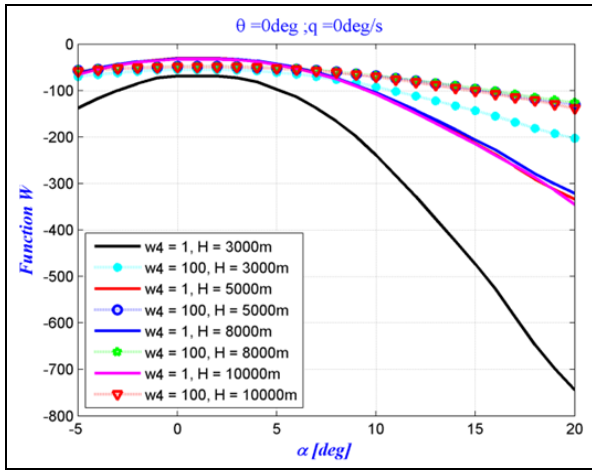


Figure 5.3 Stability analysis with the WFM for different values of constant $w_{4\text{long}}$ as a function of angle of attack for Mach number $M = 0.4$

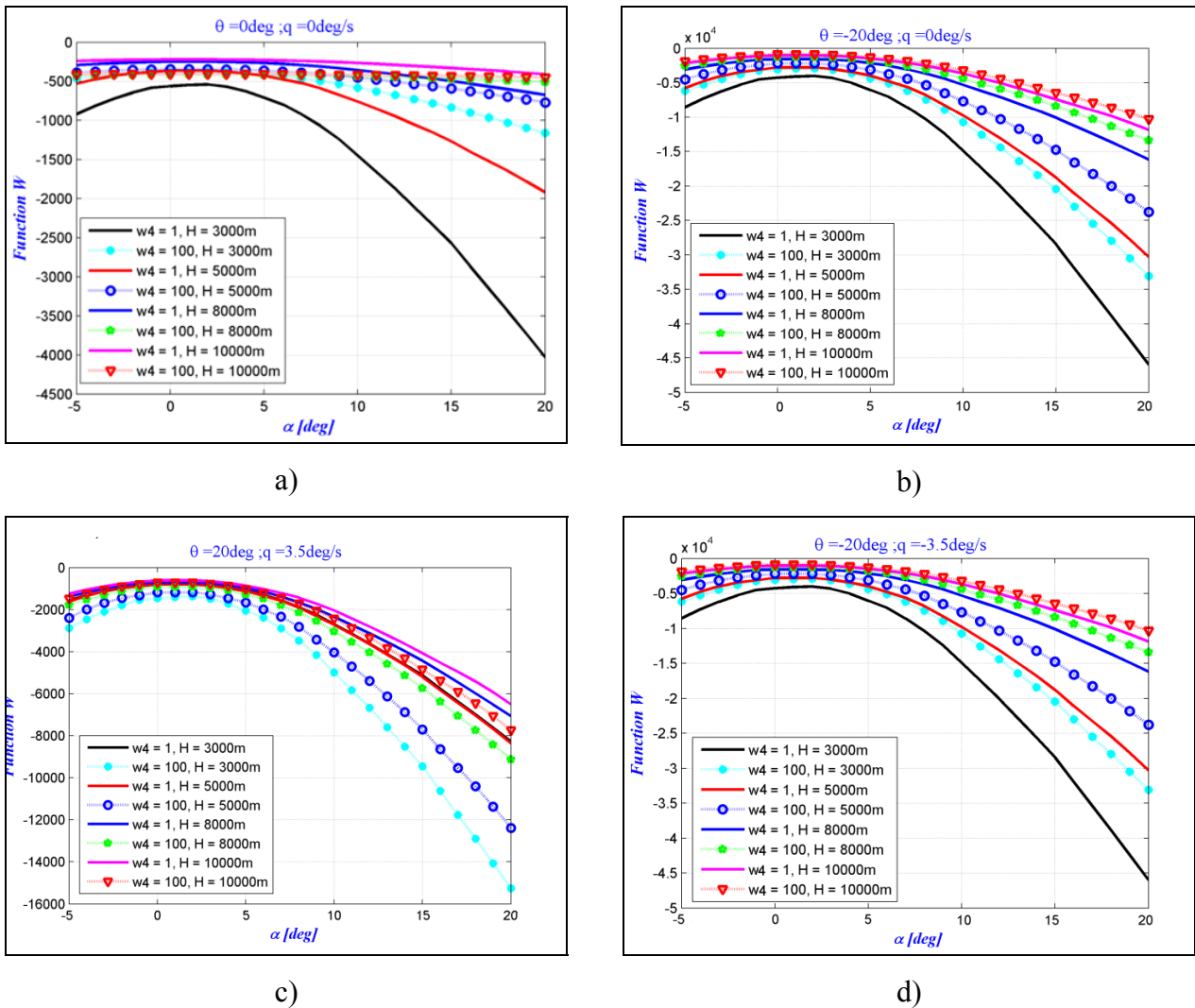


Figure 5.4 Stability analysis with the WFM for different values of constant $w_{4\text{long}}$ as a function of angle of attack for Mach number $M = 0.5$

It can be seen that for the selected $w_4 > 0$ (1 or 100), the W function is always negative, which allows us to conclude that the longitudinal dynamics of the Hawker 800XP remains stable for any combination of pitch angle/pitch rate θ/q . We then found the three positive weight functions for which the sign of the total function W can be analyzed. The most stable case was obtained for the combination of $\theta/q = (0^0, 0^0/\text{sec})$ (see Figures 5.3.a) and 5.4.a)), and for the cases where $\theta/q = (-20^0, 0^0/\text{sec})$ (Figure 5.4.b)) and $\theta/q = (-20^0, -3.5^0/\text{sec})$ (Figure 5.4.d)) the stability field becomes almost unstable. We can conclude that a stability limit should be defined for Mach number 0.5.

5.4.2 Results obtained for lateral motion using the weight functions method

To study the stability of the aircraft, the same type of analysis is done for the lateral motion as for the longitudinal motion. The first term of eq.(5.8), $w_{1lat}\beta(c_1\beta + c_2p + c_4r + c_3\phi + b_1\delta)$, is negative when $w_{1lat} = (c_2p + c_3\phi)^2 / \beta^2$ and the term multiplying w_{1lat} is negative,

$$W_{lat} = \beta^2 (c_1\beta + c_2p + c_4r + c_3\phi + b_1\delta)^2 + w_{2lat}p(c_6p + c_5\beta + c_7r + b_2\delta) + w_{3lat}r(c_{10}r + c_8\beta + c_9p + b_3\delta) + w_{4lat}c_{11}p\phi \quad (5.13)$$

while for the second term of eq.(5.13) c_5 , and c_6 are negative and w_{2lat} is defined as $w_{2lat} = (c_7^2r^2 + b_2\delta) / p^2 > 0$:

$$W_{lat} = \beta^2 (c_1\beta + c_2p + c_4r + c_3\phi + b_1\delta)^2 + (c_7^2r^2 + b_2\delta)(c_6p + c_5\beta + c_7r + b_2\delta) / p + w_{3lat}r(c_{10}r + c_8\beta + c_9p + b_3\delta) + w_{4lat}c_{11}p\phi \quad (5.14)$$

In the third term of eq.(5.14) the function w_{3lat} was chosen to be $w_{3lat} = r^2 (c_9p + b_3\delta)^2 > 0$, and so the term multiplying it will be negative, in order to ensure airplane stability.

$$W_{lat} = \beta^2 (c_1\beta + c_2p + c_4r + c_3\phi + b_1\delta)^2 + (c_7^2r^2 + b_2\delta)(c_6p + c_5\beta + c_7r + b_2\delta) / p + r^2 (c_9p + b_3\delta)^2 (c_{10}r + c_8\beta + c_9p + b_3\delta) + w_{4lat}c_{11}p\phi \quad (5.15)$$

In the fourth term of eq.(5.15), the last function is defined as $w_{4lat} = 1, 100$, and the variations of the other three functions, w_{1lat} , w_{2lat} and w_{3lat} (eq.(5.13), (5.14), (5.15)) are shown in Figure 5.5 with their angles of attack for Mach numbers 0.4 and 0.5 and altitudes 3,000 m and 8,000 m. It is assumed that their variations, based on the limits of passenger comfort, are thus obtained for roll rate $p = [-6 \text{ to } 6]^0/\text{s}$, yaw rate $r = [-2 \text{ to } 2]^0/\text{s}$, sideslip angle $\beta = [-5 \text{ to } 5]^0$ and roll angle $\Phi = [-15 \text{ to } 15]^0$.

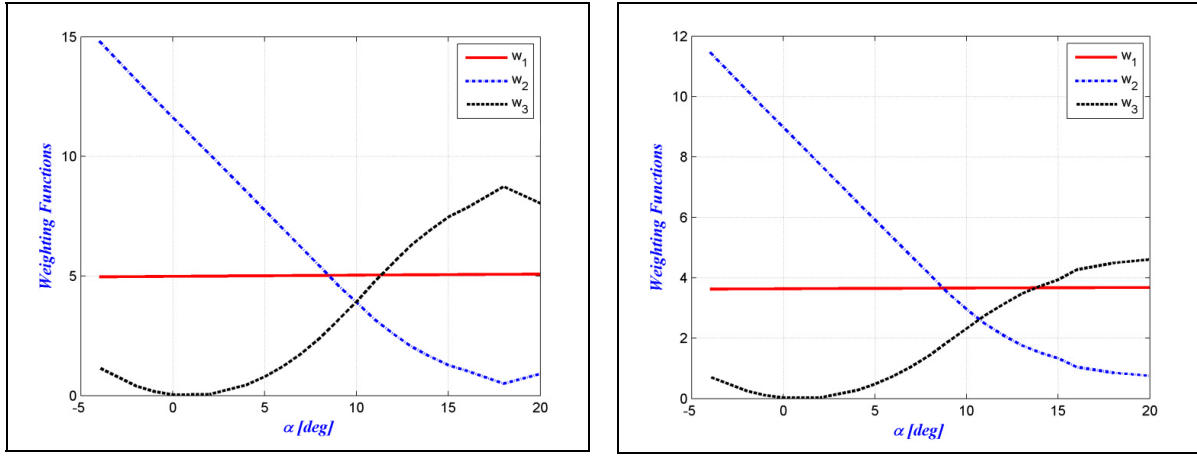


Figure 5.5 Weight functions variation with the angle of attack for lateral-directional motion for $M = 0.4$ and $H = 3,000$ m (left) and $M = 0.5$ and $H = 8,000$ m (right)

By replacing the values of w_{1lat} , w_{2lat} and w_{3lat} , the final form of the weight function W_{lat} for lateral motion can be written in the following form:

$$\begin{aligned}
 W_{lat} = & (c_2 p + c_3 \phi)^2 (c_1 \beta + c_2 p + c_4 r + c_3 \phi + b_1 \delta) \frac{1}{\beta} + \\
 & + (c_7^2 r^2 + b_2 \delta) (c_6 p + c_5 \beta + c_7 r + b_2 \delta) \frac{1}{p} + \\
 & + r^3 (c_9 p + b_3 \delta)^2 (c_{10} r + c_8 \beta + c_9 p + b_3 \delta) + w_{4lat} c_{11} p \phi
 \end{aligned} \tag{5.16}$$

Figures 5.6 and 5.7 show the variation of the weighting function W_{lat} with the angle of attack α for various values of w_{1lat} , w_{2lat} and w_{3lat} and for combinations between the extreme values of p , r , β and ϕ defined in the above paragraphs.

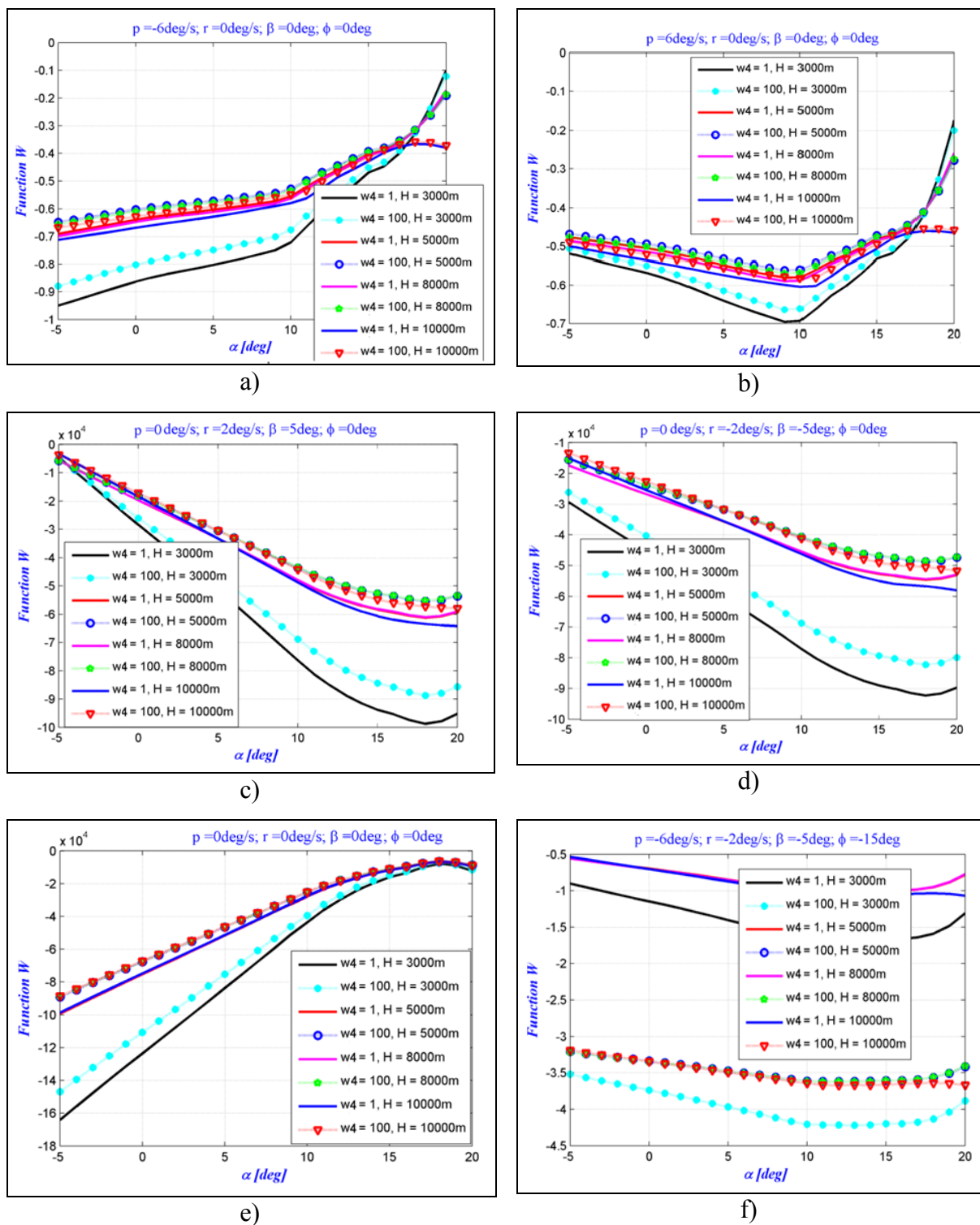
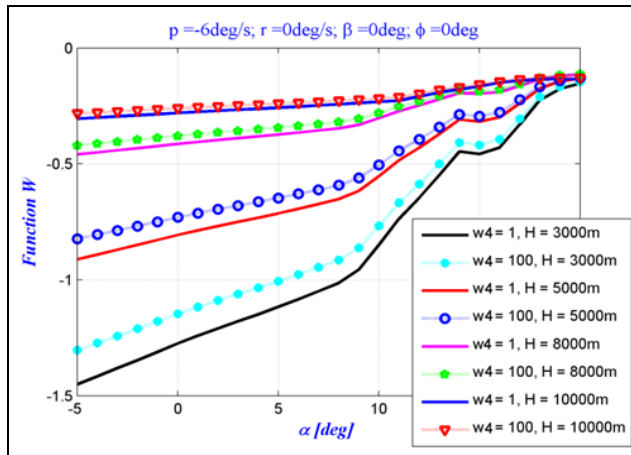
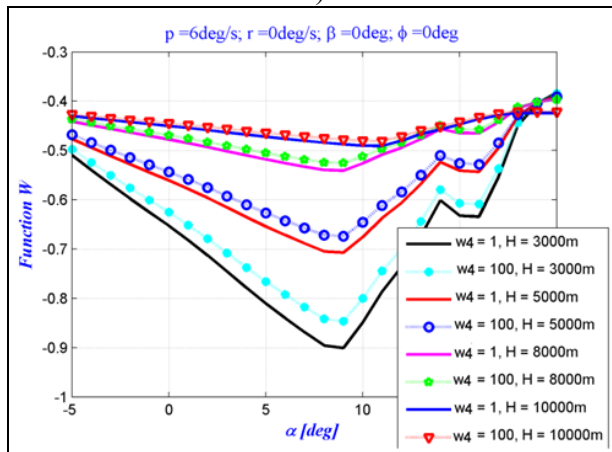


Figure 5.6 Lateral-directional stability analysis with the WFM for different values of constant w_4 as a function of the angle of attack for $M = 0.4$

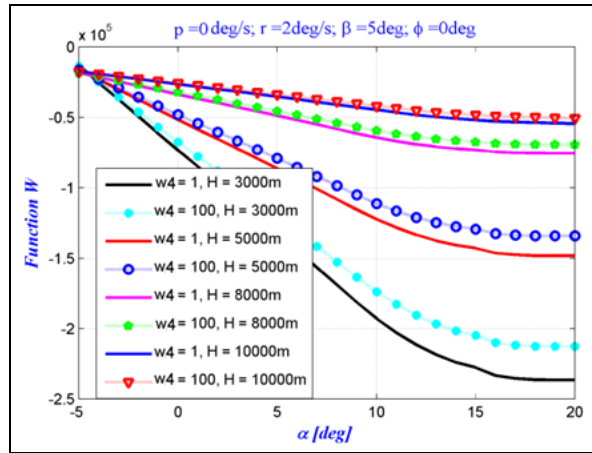
It has been found that the Hawker 800XP aircraft has stable lateral dynamics during climb or descent for roll, Dutch roll and spiral motions, since the total weight function W_{lat} 's variation with the angle of attack is negative, as seen in Figures 5.6 and 5.7 for the subsonic regime characterized by Mach numbers 0.4 and 0.5 for four altitudes and for various combinations of p , r , β and φ .



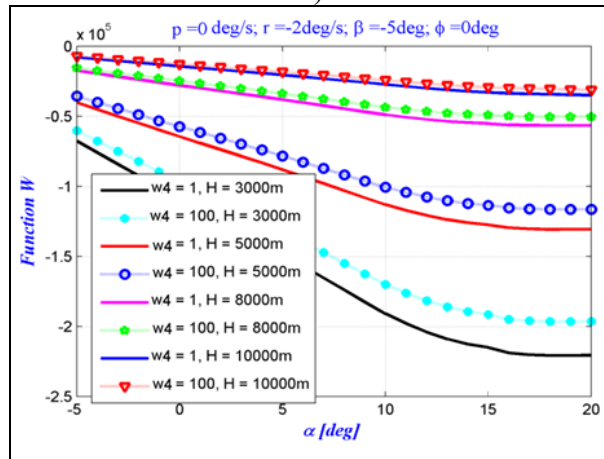
a)



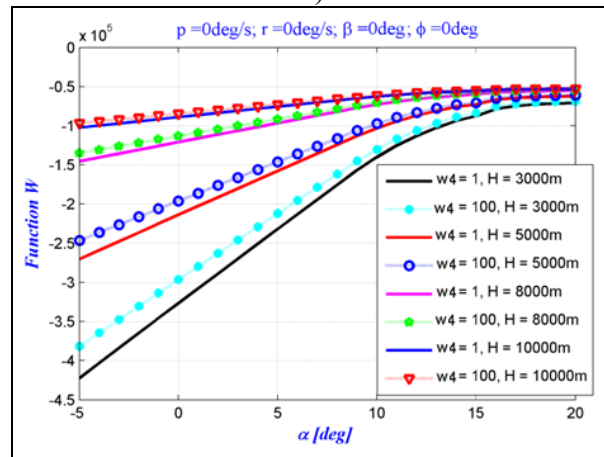
b)



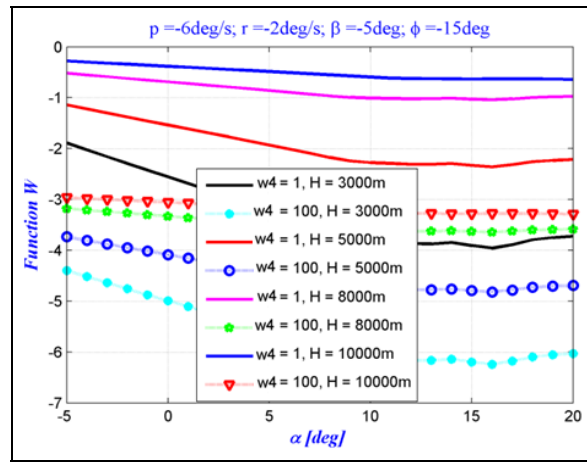
c)



d)



e)



f)

Figure 5.7 Lateral-directional stability analysis with the WFM for different values of constant w_{4lat} as a function of the angle of attack for $M = 0.5$

The stability fields for lateral motion are presented in Figures 5.6 and 5.7. We can see that instability can occur for $M = 0.4$ if the limits are increased, for high angles of attack in the cases presented in Figures 5.6a), b), and e), and for $M = 0.5$ for the cases presented in Figures 5.7a) and e). Meanwhile, for small angles of attack we can have stability fields if the limits presented in Figures 5.6c), d) and f), 5.7c) and d) are increased.

The Hawker 800XP is proven to be a stable aircraft in its longitudinal and lateral motions because the sign of the W function remains negative. The next section presents a stability analysis using the eigenvalues method to validate and compare the results obtained with the WFM.

5.5 Eigenvalues stability analysis of linear small-perturbation equations

The eigenvalues stability analysis was used to validate the results obtained with the Weight Functions Method, based on the aerodynamic coefficients and their derivatives obtained with FDerivatives code. Five dynamic modes of motion describe the aircraft's response to an initial condition of any origin (turbulence, control input, etc.). These five modes are: the short period and the long period for the longitudinal aircraft motion, and the roll, Dutch roll and spiral for the lateral motion. These modes are separated as they are defined by the equations

described in sections 5.5.1 and 5.5.2 for longitudinal and lateral motions, respectively. Their estimation is made in open-loop.

5.5.1 Longitudinal motion results

The longitudinal motion can be divided into two motions: short period and phugoid. The short period pitch response is the short answer (from 1 sec to 4 sec) of a longitudinal motion to a disturbance, and is extremely useful to investigate. The main variables are the angle of attack α , the load factor n and the pitch angle θ . It is interesting to find the relationships between the damping ratio of the short period oscillation (ζ_{sp}), the undamped natural frequency of the short period oscillation (ω_{sp}), and the change in steady state normal acceleration per unit change in angle of attack for incremental pitch control deflections at constant airspeeds and Mach numbers.

The mathematical model (Hodgkinson, 1999) describing this longitudinal motion can be represented in the form of the state space first equation (eq.(5.2)) :

$$A_{long} = \begin{bmatrix} X_u & \frac{X_\alpha}{V} & 0 & -\frac{g}{V} \\ \frac{VZ_u}{V-Z\dot{\alpha}} & \frac{Z_\alpha}{V-Z\dot{\alpha}} & \frac{V+Z_q}{V-Z\dot{\alpha}} & 0 \\ VM_u + \frac{VZ_u M_{\dot{\alpha}}}{V-Z\dot{\alpha}} & M_\alpha + \frac{Z_\alpha M_{\dot{\alpha}}}{V-Z\dot{\alpha}} & M_q + M_{\dot{\alpha}} \frac{V+Z_q}{V-Z\dot{\alpha}} & 0 \\ 0 & 0 & 1 & 0 \end{bmatrix}, \quad (5.17)$$

$$x_{long} = \begin{bmatrix} \Delta u \\ \Delta \alpha \\ \Delta q \\ \Delta \theta \end{bmatrix}, B_{long} = \begin{bmatrix} \frac{X_\delta}{V} \\ \frac{Z_\delta}{V-Z\dot{\alpha}} \\ M_\delta + \frac{Z_\delta M_{\dot{\alpha}}}{V-Z\dot{\alpha}} \\ 0 \end{bmatrix}, u_{long} = \Delta \delta_e$$

For both longitudinal modes, the natural frequency ω_n and the damping ratio ξ are estimated from the characteristic equation $|\lambda I - A_{long}| = 0$ as functions of the eigenvalues $\lambda_1, \lambda_2, \lambda_3$ and λ_4 (eq.(5.18)), with the specification that $\lambda_{1,2}$ correspond to short-period and $\lambda_{3,4}$ correspond to phugoid motions.

$$\begin{cases} \zeta \omega_n = |\operatorname{Re}(\lambda_{1,2})| \\ \omega_n \sqrt{1 - \zeta^2} = |\operatorname{Im}(\lambda_{1,2})| \end{cases}, \quad \begin{cases} \zeta \omega_n = |\operatorname{Re}(\lambda_{3,4})| \\ \omega_n \sqrt{1 - \zeta^2} = |\operatorname{Im}(\lambda_{3,4})| \end{cases} \quad (5.18)$$

The natural frequencies ω_n and the damping ξ of short-period and phugoid modes verify the next eq.(5.19).

$$\left(\zeta_p^2 + 2\zeta_p \omega_{np} + \omega_{np}^2 \right) \left(\zeta_{sp}^2 + 2\zeta_{sp} \omega_{nsp} + \omega_{nsp}^2 \right) = 0 \quad (5.19)$$

The imaginary parts of the eigenvalues are presented as functions of their real parts in Figure 5.8, where it can be observed that all the real parts of the eigenvalues are negative, which means that, in terms of stability, the aircraft longitudinal mode is stable in both short-period and phugoid modes. For the phugoid mode, the real parts of eigenvalues are negative, but they are very close to positive values if the limits are increased, which means pitch angles θ that are greater than 20° or smaller than -20° and pitch rates q less than $-3.5^\circ/\text{s}$ or greater than $3.5^\circ/\text{s}$.

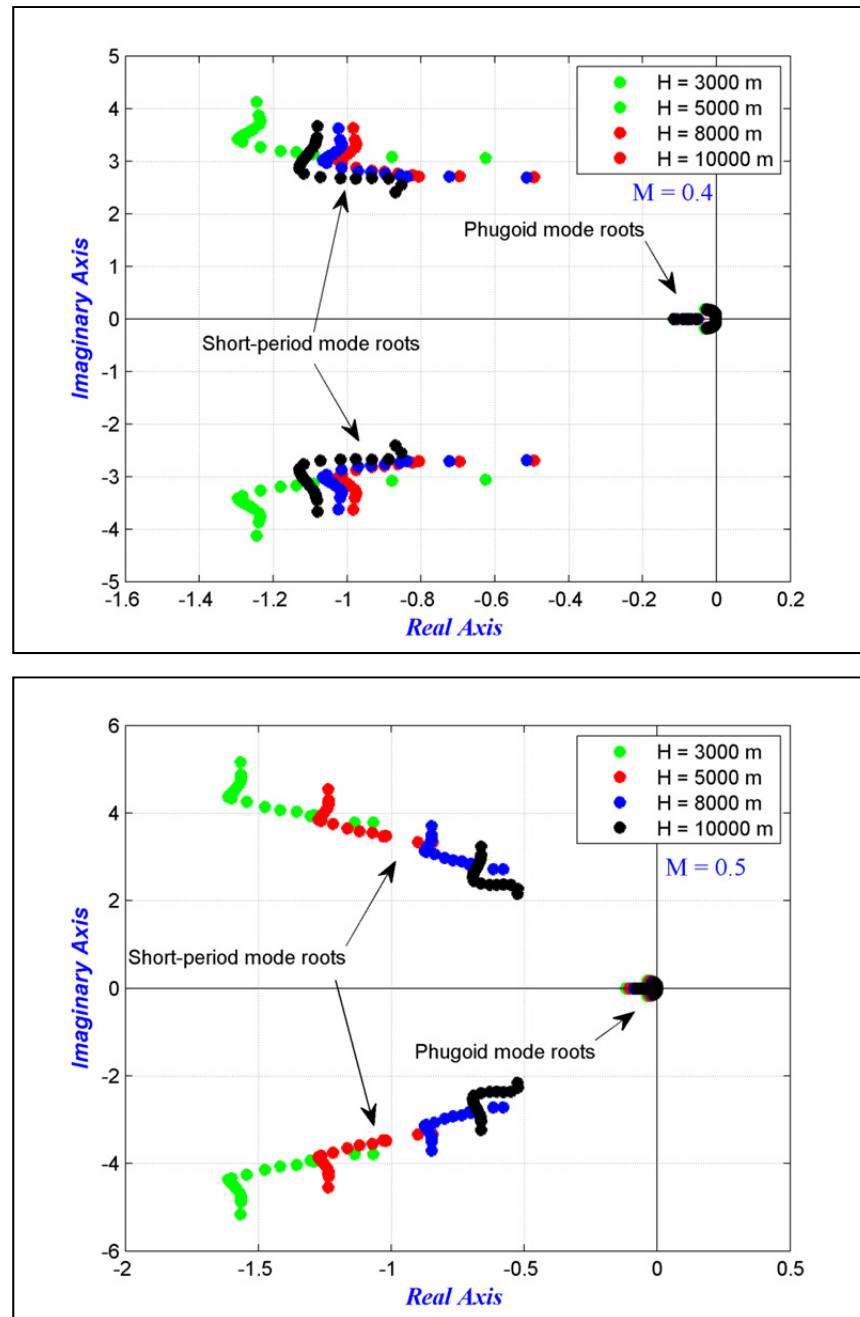


Figure 5.8 Root locus plot (Imaginary vs. Real eigenvalues) longitudinal motion representation for $M = 0.4$ and 0.5

5.5.2 Lateral motion results

Based on eq. (5.1) and (5.2) the system can be written in the following form (Hodgkinson, 1999):

$$A_{lat} = \begin{bmatrix} \frac{Y_\beta}{V} & \frac{Y_p}{V} & \frac{Y_r - V}{V} & \frac{g}{u_0} \cos \theta_0 \\ G \left(L_\beta + N_\beta \frac{I_{xz}}{I_x} \right) & G \left(L_p + N_p \frac{I_{xz}}{I_x} \right) & G \left(L_r + N_r \frac{I_{xz}}{I_x} \right) & 0 \\ G \left(N_\beta + L_\beta \frac{I_{xz}}{I_z} \right) & G \left(N_p + L_p \frac{I_{xz}}{I_z} \right) & G \left(N_r + L_r \frac{I_{xz}}{I_z} \right) & 0 \\ 0 & 1 & 0 & 0 \end{bmatrix}, x_{lat} = \begin{bmatrix} \Delta\beta \\ \Delta\phi \\ \Delta r \\ \Delta\varphi \end{bmatrix},$$

$$B_{lat} = \begin{bmatrix} \frac{Y_\delta}{V} \\ G \left(L_\delta + N_\delta \frac{I_{xz}}{I_x} \right) \\ G \left(N_\delta + L_\delta \frac{I_{xz}}{I_z} \right) \\ 0 \end{bmatrix}, u_{lat} = \Delta\delta_a$$
(5.20)

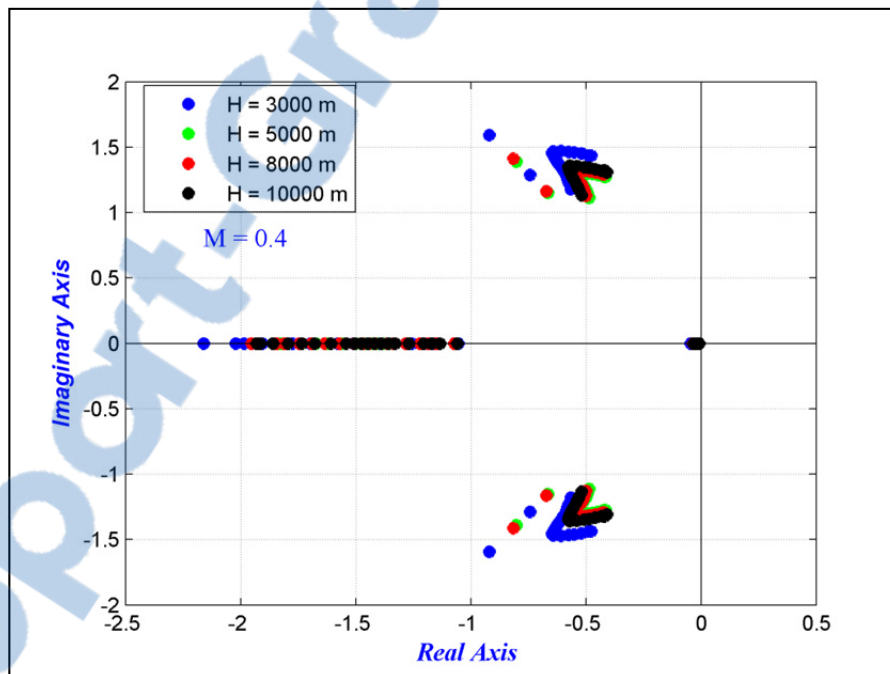
Generally, the eigenvalues λ_1 , λ_2 , λ_3 and λ_4 of the characteristic equation $|\lambda I - A_{lat}| = 0$ for lateral motion are composed of two real eigenvalues and a pair of complex eigenvalues. The eigenvalues are chosen so that the response of the aircraft is characterized by the following modes:

- A *Spiral* mode characterized by convergent or divergent motions;
- A *Roll* mode characterized by fast convergent motion; and
- A *Dutch Roll* mode characterized by lightly damped oscillatory motion with a low frequency.

The rolling motion is generally quite damped, and reaches the steady state in a very short time. In the case of a roll mode, the desired roll rates and angles can be obtained. The

rapidity with which the commanded roll rate is reached influences the response to the inputs as well as the ability to achieve and maintain the roll angle ϕ .

Dutch roll motion is a combination of yaw and roll motions, and is a lateral-directional short period oscillatory mode. The Dutch roll is a nuisance mode that appears in the roll response to lateral control and it can introduce uncontrolled and undesired roll and yaw motion. These motions can significantly influence the ability of the pilot to precisely control lateral-directional motions. Figure 5.9 shows the eigenvalues' (imaginary versus real parts) variations for the lateral aircraft analysis. It can be concluded that the Hawker 800XP is a stable aircraft in its lateral motion for all three motions (roll, spiral and Dutch roll).



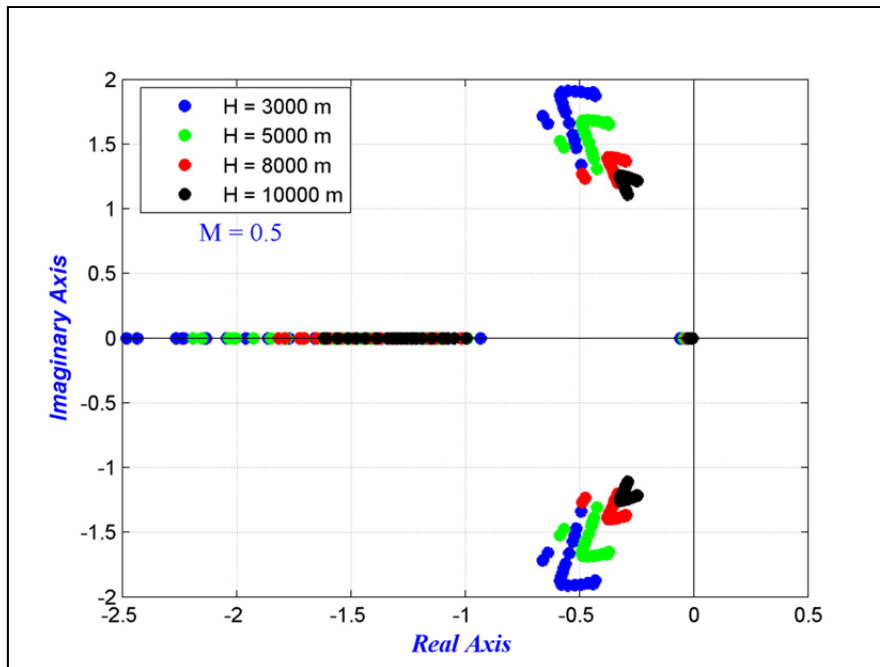


Figure 5.9 Root locus plot (Imaginary vs. Real eigenvalues) lateral directional motion representation for $M = 0.4$ and 0.5

We can see that for the highest altitude the stability field is close to instability, meaning that any change of limits defined as roll rate $p = [-6 \text{ to } 6]^0/\text{s}$, yaw rate $r = [-2 \text{ to } 2]^0/\text{s}$, sideslip angle $\beta = [-5 \text{ to } 5]^0$ and roll angle $\Phi = [-15 \text{ to } 15]^0$ could induce instability.

5.6 Conclusions

The main objective of this study was to determine, as a design tool, the positive weight functions by the Weight Functions Method as a means to analyze the stability fields of a Hawker 800XP configuration. eigenvalues stability analysis of linear small-perturbation equations was the selected validation method since eigenvalues can be determined quickly for any flight condition as well as from the stability derivatives for a particular flight case. The aerodynamic coefficients and their stability derivatives were found with our new in-house FDerivatives code.

Based on the aircraft's aerodynamic model calculated with the WFM, three functions were defined in terms of stability derivatives terms, and the last function was considered to be

positive and chosen to be 1 or 100. The WFM was applied for longitudinal and lateral motion studies.

For all four altitudes, considered at two Mach numbers, the longitudinal dynamics of the Hawker 800XP remains stable for any combination of pitch angle/pitch rate θ/q . It was determined that the Hawker 800XP aircraft has a stable lateral dynamic in climb or in descent for roll, Dutch roll and spiral motions, as the total weight function W variation with the angle of attack is negative for the subsonic regime characterized by Mach numbers 0.4 and 0.5 and at four altitudes, for combinations of p , r , β and φ .

Both methods indicate a stability field and that, for certain combinations, instability can occur if the limits are exceeded:

- longitudinal motion at $M = 0.5$:
 - θ smaller than -20° with $q = 0^\circ/\text{sec}$;
 - θ smaller than -20° and q smaller than $-3.5^\circ/\text{sec}$
- lateral motion for high angles of attack at $M = 0.4$:
 - p smaller than $-6^\circ/\text{s}$, with $\beta = 0^\circ$, $r = 0^\circ/\text{s}$ and $\varphi = 0^\circ$;
 - p greater than $-6^\circ/\text{s}$, with $\beta = 0^\circ$, $r = 0^\circ/\text{s}$ and $\varphi = 0^\circ$;
- lateral motion for high angles of attack at $M = 0.5$:
 - p smaller than $-6^\circ/\text{s}$, with $\beta = 0^\circ$, $r = 0^\circ/\text{s}$ and $\varphi = 0^\circ$;
- lateral motion for small angles of attack at $M = 0.4$:
 - r smaller than $-2^\circ/\text{s}$, β smaller than -5° with $p = 0^\circ/\text{s}$ and $\varphi = 0^\circ$;
 - r greater than $-2^\circ/\text{s}$, β greater than -5° with $p = 0^\circ/\text{s}$ and $\varphi = 0^\circ$;
 - r smaller than $-2^\circ/\text{s}$ or β smaller than -5° or p smaller than $-6^\circ/\text{s}$ or φ smaller than -15° ;
- lateral motion for small angles of attack at $M = 0.5$:
 - r smaller than $-2^\circ/\text{s}$, β smaller than -5° with $p = 0^\circ/\text{s}$ and $\varphi = 0^\circ$;
 - r greater than $-2^\circ/\text{s}$, β greater than -5° with $p = 0^\circ/\text{s}$ and $\varphi = 0^\circ$.

CHAPTER 6

APPLICATION OF THE WEIGHT FUNCTIONS METHOD ON A HIGH INCIDENCE RESEARCH AIRCRAFT MODEL

Nicoleta Anton and Ruxandra Mihaela Botez

École de Technologie Supérieure, Montréal, Canada

Laboratory of Research in Active Controls, Aeroservoelasticity and Avionics

This article was accepted to be published in The Aeronautical Journal, Paper 3921

Résumé

Ce document évalue l'application d'une nouvelle méthode d'analyse de la stabilité du système, la méthode des fonctions du poids, pour les mouvements longitudinaux et latéraux d'un modèle d'aéronef qui s'appelle HIRM (High Incidence Research Aircraft Model). Le procédé consiste à trouver le nombre de fonctions de poids qui est égal au nombre d'équations différentielles nécessaires à la modélisation du système. La stabilité de l'aéronef est déterminé à partir du signe de la fonction de poids total, qui doit être négatif pour un modèle stable. Le modèle Aero-Data Model In Research Environment (ADMIRE), développé par l'Agence suédoise de recherche pour la défense, a été utilisé pour la modélisation aérodynamique de l'avion, avec les configurations suivantes: nombre de Mach = 0.25, altitude = 500 m, l'angle d'attaque $[-10 \text{ à } 30]^\circ$, angle de déflexion élevo $[-30 \text{ à } 30]^\circ$, déviation canard $[0^\circ \text{ et } 25^\circ]$ et les angles de déviation du gouvernail $[-30^\circ \text{ et } 30^\circ]$. Ces configurations de vol ont été choisies parce qu'elles sont parmi les conditions de vol pour Cat. II Oscillations Induites par le Pilote (PIO) critères de validation, effectuées sur le modèle des avions accès à l'information présentée dans le PIO Handbook by the Group for Aeronautical Research and Technology in Europe, Flight Mechanics/Action Group 12. Ce modèle d'avion a une instabilité connue pour des mouvements longitudinaux et latéraux et ainsi une loi de commande a été introduit pour stabiliser son vol.

Abstract

This paper assesses the application of a new method for system stability analysis, the weight functions method, to the longitudinal and lateral motions of a High Incidence Research Aircraft Model. The method consists of finding the number of weight functions that is equal to the number of differential equations required for system modelling. The aircraft's stability is determined from the sign of the total weight function; which should be negative for a stable model. The Aero-Data Model In Research Environment (ADMIRE), developed by the Swedish Defense Research Agency, was used for the aerodynamic aircraft modelling, with the following configurations: Mach number = 0.25, altitude = 500 m, angle of attack $[-10$ to $30]^\circ$, elevon deflection angle $[-30$ to $30]^\circ$, canard deflection $[0^\circ$ and $25^\circ]$ and rudder deflection angles $[-30^\circ$ and $30^\circ]$. These flight configurations were selected because they are among the flight conditions for Cat. II Pilot Induced Oscillation (PIO) criteria validation, performed on the FOI aircraft model presented in the PIO Handbook by the Group for Aeronautical Research and Technology in Europe, Flight Mechanics/Action Group 12. This aircraft model has a known instability for longitudinal and lateral motions and so a control law was introduced to stabilize its flight.

6.1 Introduction

The Weight Function Method (WFM) has been applied in various engineering fields. For example, it has been used to determine stress factors for crack problems. The WFM was applied by Yoichi et al. (2003) to solve two- and three-dimensional crack problems and to calculate stress intensity factors for arbitrary loading conditions. Their application has been generalized to calculate the response analysis of structures and to solve two-dimensional elasticity and plate bending problems. The weight function method was found to be useful for analyzing structures subjected to a variety of loading conditions because the responses expressed in terms of displacements and stresses may be calculated by integrating the inner product of a universal weight function and a load vector. The stress intensity factor for a

patched crack within an infinite plate was successfully numerically validated using the WFM (Kim et al., 2000).

Paris et al. (1976) presented an alternate method of Bueckner and Rice for the deviation of a two-dimensional weight function to eliminate crack tip stress intensity factors. A generalised weight function method was developed by Wu et al. (1983), based on Betti's reciprocal theorem application to the equivalent cracks problem involving mixed boundary conditions. Fett (1991) contributed an analytical solution for determining stress distribution using a weight function based on the Boundary Collocation Method. Schneider et al. (1989) used a closed-form weight function formula to calculate the stress intensity factor of an edge crack for an elastic disc. A three-dimensional linear elastic fracture mechanics (LEFM) problem was also solved using the WFM (Vainshtok et al., 1987).

Stroe (2008) solved the Lurie-Postnikov problem using general vibration equations involving linear transformations. Stroe also analyzed a holonomic system with dependent variable equations in (Stroe et al., 2008), where the WFM was applied to vibration and stability studies in cases of damped holonomic systems.

The selections of H_∞ weighting functions were presented for practical applications by Jiankun et al. (2000), where the authors showed that an H_∞ weighting function for a single-input single-output system could be obtained by considering it as a series of connections of elementary low-order systems. For a constrained control effort, an explicit weighting function was obtained. They proposed a novel method for the selection of weighting functions in an H_∞ mixed sensitivity design to directly control the percentage overshoot. Real-time experimental results were presented for the roll-angle control of a laboratory scale model of a vertical take-off aircraft (Jiankun et al., 2000).

Our analysis of longitudinal and lateral motions using the WFM was performed on the Aero-Data Model In Research Environment model (ADMIRE) developed by the FOI (Admirer4p1), based on the Generic Aerodata Model (GAM) developed by SAAB AB in the framework of the GARTEUR Group (GARTEUR FM(AG12), 2001). « The ADMIRE

describes a generic small-single seated, single-engine fighter aircraft with a delta-canard configuration, implemented in MATLAB/SIMULINK Release 13 » (Lars et al., 2005, pp iii). The stability domains were determined for each flight case for the given configurations.

This paper is part of a project developed at LARCASE laboratory to perform a more complete analysis of an aircraft in subsonic regime as a design tool, based on geometrical parameters. Three real different configurations were analyzed and HIRM model was chosen for its instability well known. The WFM was applied to the original non-linear aerodynamics model implemented in ADMIRE simulation, as well as for the model stabilized with control laws, in order to stabilize its flight.

6.2 The HIRM: Model Description and its Implementation in Admire Code

The HIRM (High Incidence Research Model) (Admirer4p1), (Lars et al., 2005), (Terlouw, 1996) of a generic fighter aircraft was used in this study. This aircraft model has an envelope defined by a Mach number between 0.15 and 0.5 and altitude of between 100 and 20,000 ft for the following angles: the angle of attack $\alpha = [-10 \text{ to } 30]$ degrees, sideslip angle $\beta = [-10 \text{ to } 10]$ degrees, elevon angle $\delta_e = [-30 \text{ to } 30]$ degrees, canard angle $\delta_c = [-55 \text{ to } 25]$ degrees, and rudder angle $\delta_r = [-30 \text{ to } 30]$ degrees.

The aerodynamics coefficients were obtained based on wind tunnel and flight tests for a model « ... originally designed to investigate flight at high angles of attack ... but [that] does not include compressibility effects resulting from high subsonic speeds. » (Terlouw, 1996, p 21). These coefficients were further implemented in the ADMIRE model using the main graphical window simulation presented in Figure 5.1, which also shows the response of the aircraft model. The tests and analyses provided in the GARTEUR program were focused on PIO detection, while this paper evaluates a new method to investigate the model's stability.

« The ADMIRE contains twelve states ($V_T, \alpha, \beta, p_b, q_b, r_b, \psi, \theta, \varphi, x_v, y_v, z_v$) plus additional states due to actuators and Flight Control System (FCS). Available control effectors are left- and right canard, leading edge flap, four elevons, rudder and

throttle setting. The model is also equipped with thrust vectoring capability and an extendable landing gear. The model is prepared for the use of atmospheric turbulence as external disturbance. The ADMIRE is augmented with an FCS in order to provide stability and sufficient handling qualities within the operational envelope (altitude <6 km, Mach < 1.2). The FCS contains a longitudinal and a lateral part. ... The lateral controller enables the pilot to perform roll control where the roll motion is initiated around the velocity vector of the a/c, and angle of sideslip control. Sensor models are incorporated. The 20 ms flight computer delay on the actuator inputs that is implemented in other versions of ADMIRE was not used here. The model has the facility to define model uncertainties, but this was not used. ADMIRE is implemented in MATLAB and SIMULINK using a combination of standard SIMULINK blocks and S-functions written in C. » (GARTEUR FM(AG12), 2001, p 36).

Figure 6.1 is a screenshot of the ADMIRE window simulation and it is presented here to understand how this model works. Each block is define on different level and for Aircraft Response a screen shot was considered necessary, because of the ADMIRE_main block which contains the non-linear coefficients given as tables.

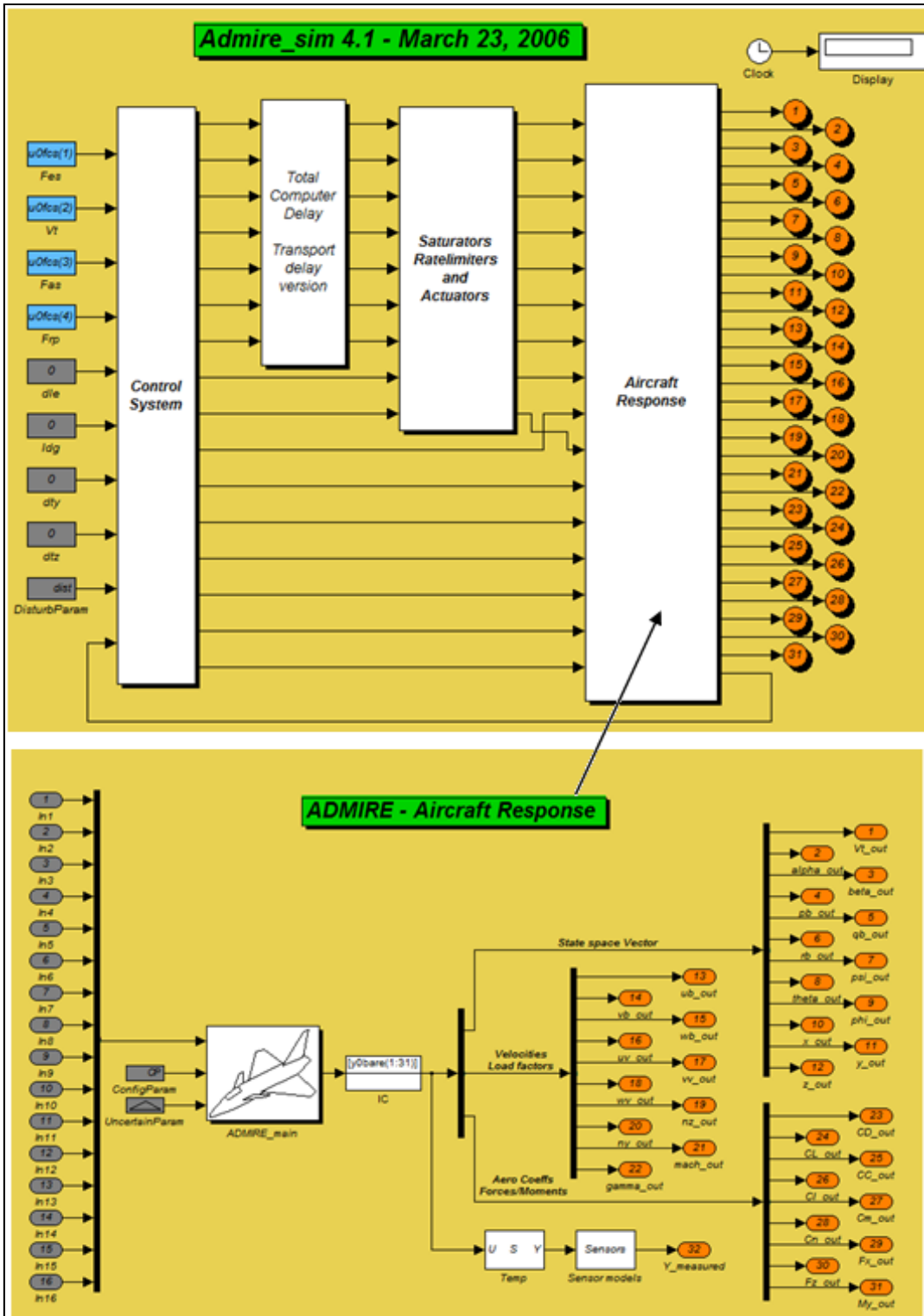


Figure 6.1 ADMIRE: Main graphical window simulation and Aircraft response
 Source: Screenshot from graphical interface (Admirer4p1)

The following table contains a summary of the aircraft geometrical data, along with aircraft mass and mass distribution data (Lars et al., 2005).

Table 6.1 HIRM geometrical data

Parameters	Numerical values [Units]
Wing area S	45 m ²
Wing span b	10 m
Wing Mean Aerodynamic Chord \bar{c}	5.2 m
Mass m	9100 kg
x-body axis moment of inertia I_x	21000 kgm ²
y-body axis moment of inertia I_y	81000 kgm ²
z-body axis moment of inertia I_z	101000 kgm ²
xz-body axis product of inertia I_{xz}	2500 kgm ²
z_{eng}	-0.15 m
x_{cg}	0.25 \bar{c}

Let us consider a model defined by a nonlinear autonomous system of equations for the longitudinal motion and for its lateral motion, given below as (6.1) and (6.2), respectively (Lars et al., 2005), (Terlouw, 1996), (Schmidt, 1998).

$$\begin{cases} \dot{V} = -\frac{\tilde{q}S}{m}C_D + \frac{1}{m}T \cos \alpha - g \sin \gamma \\ \dot{\gamma} = \frac{\tilde{q}S}{mV}C_L + \frac{1}{mV}T \sin \alpha - m\frac{g}{V}\cos \gamma \\ \dot{q} = \frac{1}{I_y}[\tilde{q}S\bar{c}C_m + x_{CG}\tilde{q}SC_T + z_eT] \\ \dot{\theta} = q \end{cases} \quad (6.1)$$

$$\begin{cases} \dot{\beta} = p\alpha - r - \frac{\tilde{q}S}{mV}C_y + \frac{g}{V}\sin\phi \cos\theta \\ \dot{p} = -\frac{1}{I_x}[(I_z - I_y)qr + \tilde{q}SbC_l] \\ \dot{r} = -\frac{1}{I_z}[(I_y - I_x)pq + \tilde{q}S(\bar{c}C_n - x_{cg}C_y)] \\ \dot{\phi} = p \end{cases} \quad (6.2)$$

The aerodynamic force and moment coefficients contain degrees of non-linearities, as shown in the next eq.(6.3). Their values were obtained from the ADMIRE simulation (Admirere4p1):

$$\begin{cases}
 C_N = C_{N1}(\alpha) + C_{N2}(\alpha, \delta_e) + C_{N3}(\alpha, \delta_c) + C_{N4}(\alpha, \beta, \delta_e) \\
 C_T = C_{T1}(\alpha) + C_{T2}(\alpha, \delta_e) + C_{T3}(\alpha, \delta_c) \\
 C_m = C_{m1}(\alpha) + C_{m2}(\alpha, \delta_e) + C_{m3}(\alpha, \delta_c) + C_{m4}(|\alpha|)\dot{\alpha} + C_{m5}(\alpha, \delta_c)q + \\
 \quad + C_{m6}(\alpha, |\beta|, \delta_c) + C_{m7}(\alpha, \delta_a) \\
 C_D = C_N \sin \alpha + C_T \cos \alpha \\
 C_L = C_N \cos \alpha - C_T \sin \alpha \\
 C_y = C_{y1}(\alpha, |\beta|) + C_{y2}(\alpha, |\beta|, \delta_r) + C_{y3}(\alpha, \delta_a) + C_{y4}(\alpha) \delta_{ca} + C_{y5}(\alpha, |\beta|)p + C_{y6}(\alpha, |\beta|)r \\
 C_l = C_{l1}(\alpha, |\beta|) + C_{l2}(\alpha, |\beta|, \delta_r) + C_{l3}(\alpha, \delta_a) + C_{l4}(\alpha, \delta_c) \delta_{ca} + C_{l5}(\alpha, |\beta|)p + C_{l6}(\alpha, |\beta|)r \\
 C_n = C_{n1}(\alpha, |\beta|) + C_{n2}(\alpha, |\beta|, \delta_r) + C_{n3}(\alpha, |\beta|, \delta_a) + C_{n4}(\alpha, \delta_c) \delta_{ca} + C_{n5}(\alpha, |\beta|)p + C_{n6}(\alpha, |\beta|)r
 \end{cases}
 \quad (6.3)$$

6.3 The Weight Functions Method

The main objective of this paper is to study, based on the above eq.(6.1) and (6.3), the HIRM stability when the Weight Function Method (WFM) is applied. The WFM is based on the following theorem:

Theorem (Stroe et al., 2008): Given the autonomous system $\dot{x} = f(x)$, $x \in R^n$, if $w_k(x_1, x_2, \dots$

$x_n)$ exists such that $dV = \sum_{k=1}^n x_k w_k dx_k$ is a total exact differential, then its stability is given by

$W = \sum_{k=1}^n x_k w_k f_k$ as follows:

- if W is negative-definite, the solution is asymptotically stable;
- if W is the null function, the solution is neutrally stable; or
- if W is positive-definite, the solution is unstable.

The WFM replaces the classical Lyapunov function by finding a problem with a method which obtains a number of weight functions equal to the number of the first-order differential equations modelling the system (Stroe, 2008), (Stroe et al., 2008). The difference between these two methods is that the weight functions method finds one function at a time, with their number equal to the number of the first-order differential equations.

The WFM's basic principle is to find three positive weight functions for a system with four first-order differential equations, where the fourth weight function is a constant, imposed by the author. The total weight function $W = \sum_{k=1}^4 w_k x_k f_k$ is defined, and its sign should be negative to ensure the stability of the aircraft.

6.3.1 Longitudinal aircraft model

For longitudinal aircraft modeling, it was assumed that $\gamma = 0$, $V = const$ and $h = const$; with these conditions, the first two equations of eq.(6.1) become equivalent to

$$T = mg \sin \alpha + \tilde{q}S(C_D \cos \alpha - C_L \sin \alpha) = mg \sin \alpha + \tilde{q}SC_T \quad (6.4)$$

and the longitudinal model is described by .

$$\left\{ \begin{array}{l} \dot{\alpha} = q \\ \dot{q} = \frac{\tilde{q}S}{I_y} \left[(x_{cg} + z_e)(C_{T1}(\alpha) + C_{T2}(\alpha, \delta_e) + C_{T3}(\alpha, \delta_c)) + \frac{mg}{\tilde{q}S} z_e \sin \alpha \right] + \\ \quad + \frac{\tilde{q}S\bar{c}}{I_y} \left[C_{m1}(\alpha) + C_{m2}(\alpha, \delta_e) + C_{m3}(\alpha, \delta_c) + C_{m4}(|\alpha|)\dot{\alpha} + C_{m5}(\alpha, \delta_c)q + \right. \\ \quad \left. + C_{m6}(\alpha, |\beta|, \delta_c) + C_{m7}(\alpha, \delta_a) \right] \end{array} \right. \quad (6.5)$$

or

$$\left\{ \begin{array}{l} \dot{\alpha} = q \\ \dot{q} = \frac{\bar{q}S}{I_y} \left[\bar{c}C_{M1} + (x_{cg} + z_e)C_T + \frac{mg}{\bar{q}S} z_e \sin \alpha \right] + \frac{\bar{q}S}{I_y} \bar{c}C_{M2}q \end{array} \right.$$

where C_{M1} is the sum of C_{m1} , C_{m2} , C_{m3} , C_{m6} and C_{m7} , and $C_{M2} = C_{m4} + C_{m5}$.

The total weight function W_{long} is given by eq.(6.6), where $f_1 = \dot{\alpha}$, $f_2 = \dot{q}$:

$$\begin{aligned}
 W_{long} &= \sum_{k=1}^2 w_k x_k f_k = w_{long1} \alpha f_1 + w_{long2} q f_2 = \\
 &= w_{long1} \alpha q + w_{long2} q \left[\frac{\bar{q}S}{I_y} \left(\bar{c}C_{M1} + (x_{cg} + z_e)C_T + \frac{mg}{\bar{q}S} z_e \sin \alpha \right) + \frac{\bar{q}S}{I_y} \bar{c}C_{M2} q \right] = \\
 &= \alpha q \left(w_{long1} + w_{long2} \frac{mg}{I_y} z_e \frac{\sin \alpha}{\alpha} \right) + w_{long2} q \left[\frac{\bar{q}S}{I_y} \left(\bar{c}(C_{M1} + C_{M2}q) + (x_{cg} + z_e)C_T \right) \right]
 \end{aligned} \tag{6.6}$$

In the first parenthesis of eq.(6.6) that multiplies the term αq , the first weight function w_{long1} is defined as $w_{long1} = -w_{long2} \frac{mg}{I_y} z_e \frac{\sin \alpha}{\alpha} > 0$, for any positive value of w_{long2} , because $z_e = -0.15$ m is negative from the aircraft geometry, a value implemented in the ADMIRE simulation.

The next step consists of replacing w_{long1} in eq.(6.6) and obtaining the total longitudinal weight function W_{long} , as defined in eq.(6.7), where its sign depends on the sign of q .

$$W_{long} = w_{long2} q \left[\frac{\bar{q}S}{I_y} \left(\bar{c}(C_{M1} + C_{M2}q) + (x_{cg} + z_e)C_T \right) \right] \tag{6.7}$$

6.3.2 Lateral aircraft model

The lateral model was given in eq.(6.2), and using the following notations: $i_1 = \frac{(I_z - I_y)}{I_x}$,

$i_3 = \frac{(I_y - I_x)}{I_z}$, eq. (6.2) is written in the form:

$$\begin{cases} \dot{\beta} = p\alpha - r - \frac{\tilde{q}S}{mV} C_y \\ \dot{p} = -i_1 q r + \frac{\tilde{q}Sb}{I_x} C_l \\ \dot{r} = -i_3 p q + \frac{\tilde{q}S}{I_z} [\bar{c}C_n - x_{cg} C_y] \\ \dot{\phi} = p \end{cases} \quad \text{or} \quad (6.8)$$

$$\begin{cases} \dot{\beta} = y_\beta \beta + (y_p + \alpha) p + (y_r - 1) r + y_{\delta_a} \delta_a + y_{\delta_r} \delta_r \\ \dot{p} = (l_\beta + l_{\alpha\beta} \alpha) \beta + l_p p + (l_r - i_1 q) r + l_{\delta_r} \delta_r + (l_{\delta_a} + l_{\alpha\delta_a} \alpha) \delta_a \\ \dot{r} = n_\beta \beta + (n_p + n_{\alpha p} \alpha + i_3 q) p + n_r r + n_{\delta_r} \delta_r + (n_{\delta_a} + n_{\alpha\delta_a} \alpha) \delta_a \\ \dot{\phi} = p \end{cases}$$

The system of eq.(6.8) can be simplified as follows:

$$\begin{cases} f_1 = y_\beta \beta + Y_p p + Y_r r + y_{\delta_a} \delta_a + y_{\delta_r} \delta_r \\ f_2 = L_\beta \beta + l_p p + L_r r + l_{\delta_r} \delta_r + L_{\delta_a} \delta_a \\ f_3 = n_\beta \beta + N_p p + n_r r + n_{\delta_r} \delta_r + N_{\delta_a} \delta_a \\ f_4 = p \end{cases} \quad (6.9)$$

where $f_1 = \dot{\beta}$, $f_2 = \dot{p}$, $f_3 = \dot{r}$, $f_4 = \dot{\phi}$, and

$$\begin{aligned} Y_p &= (y_p + \alpha), \quad Y_r = (y_r - 1) \\ L_\beta &= (l_\beta + l_{\alpha\beta} \alpha), \quad L_r = (l_r - i_1 q), \quad L_{\delta_a} = (l_{\delta_a} + l_{\alpha\delta_a} \alpha) \\ N_p &= (n_p + n_{\alpha p} \alpha + i_3 q), \quad N_{\delta_a} = (n_{\delta_a} + n_{\alpha\delta_a} \alpha) \end{aligned} \quad (6.10)$$

By denoting the state vector $x_k = [\beta \quad p \quad r \quad \phi]^T$, the lateral weighting function is then given as:

$$\begin{aligned} W_{lat} &= \sum_{k=1}^4 w_{latk} x_k f_k = w_{lat1} \beta f_1 + w_{lat2} p f_2 + w_{lat3} r f_3 + w_{lat4} \phi f_4 = \\ &= w_{lat1} \beta (y_\beta \beta + Y_p p + Y_r r + y_{\delta_a} \delta_a + y_{\delta_r} \delta_r) + w_{lat2} p (L_\beta \beta + l_p p + L_r r + l_{\delta_r} \delta_r + L_{\delta_a} \delta_a) + \\ &+ w_{lat3} r (n_\beta \beta + N_p p + n_r r + n_{\delta_r} \delta_r + N_{\delta_a} \delta_a) + w_{lat4} \phi p \end{aligned} \quad (6.11)$$

$$\begin{aligned} W_{lat} &= [w_{lat1} \beta Y_r + w_{lat3} (N_p p + n_r r + n_{\delta_r} \delta_r + N_{\delta_a} \delta_a)] r + \beta (w_{lat1} y_\beta \beta + w_{lat3} n_\beta r) + \\ &+ w_{lat1} \beta (Y_p p + y_{\delta_a} \delta_a + y_{\delta_r} \delta_r) + w_{lat2} p (L_\beta \beta + l_p p + L_r r + l_{\delta_r} \delta_r + L_{\delta_a} \delta_a) + w_{lat4} \phi p \end{aligned}$$

To solve the stability analysis problem, the first weight function is defined from the third term of the lateral weighting function, eq.(6.11), where w_{lat3} is a constant defined by the authors as equal to 1 in this paper, so that:

$$w_{lat1} = -w_{lat3} \frac{n_\beta r}{y_\beta \beta} \quad (6.12)$$

Equation (6.12) is replaced in eq.(6.11), to obtain:

$$\begin{aligned} W_{lat} = & \left[w_{lat3} r \left(N_p - \frac{n_\beta}{y_\beta} Y_p \right) + w_{lat2} l_p p + w_{lat4} \phi \right] p + \\ & + \left[-w_{lat3} \frac{n_\beta}{y_\beta} (Y_r r + y_{\delta_a} \delta_a + y_{\delta_r} \delta_r) + w_{lat2} L_r p \right] r + \\ & + w_{lat2} p (L_\beta \beta + l_{\delta_r} \delta_r + L_{\delta_a} \delta_a) + w_{lat3} (n_r r + n_{\delta_r} \delta_r + N_{\delta_a} \delta_a) r \end{aligned} \quad (6.13)$$

The second weight function, w_{lat2} , can be defined as a function of the w_{lat3} positive function:

$$w_{lat2} = w_{lat3} \frac{n_\beta}{y_\beta L_r p} (Y_r r + y_{\delta_a} \delta_a + y_{\delta_r} \delta_r) \quad (6.14)$$

The last step in our analysis is to find the total W_{lat} lateral weight function, defined in eq.(6.15), so that the w_{lat4} function can be given in eq.(6.16) as a function of w_{lat3} .

$$\begin{aligned} W_{lat} = & \left[w_{lat3} \frac{n_\beta l_p}{y_\beta L_r r} (y_{\delta_a} \delta_a + y_{\delta_r} \delta_r) + w_{lat4} \phi \right] p + \\ & + w_{lat3} \left[\frac{n_\beta}{y_\beta L_r} (Y_r + y_{\delta_a} \delta_a + y_{\delta_r} \delta_r) (L_\beta \beta + l_{\delta_r} \delta_r + L_{\delta_a} \delta_a) + \right. \\ & \left. (n_r r + n_{\delta_r} \delta_r + N_{\delta_a} \delta_a) r + N_p r p + \frac{n_\beta}{y_\beta} p \left(\frac{l_p}{L_r r} - Y_p \right) \right] \end{aligned} \quad (6.15)$$

$$w_{lat4} = -w_{lat3} \frac{n_\beta l_p}{y_\beta L_r r \phi} (y_{\delta_a} \delta_a + y_{\delta_r} \delta_r) \quad (6.16)$$

Finally, the final weight function W_{lat} is determined from w_{lat1} , w_{lat2} and w_{lat4} , given by eq.(6.12), (6.14) and (6.16) as a function of w_{lat3} ,

$$W_{lat} = w_{lat3} \left[\begin{array}{l} \frac{n_\beta}{y_\beta L_r} (Y_r + y_{\delta_a} \delta_a + y_{\delta_r} \delta_r) (L_\beta \beta + l_{\delta_r} \delta_r + L_{\delta_a} \delta_a) + \\ + (n_r r + n_{\delta_r} \delta_r + N_{\delta_a} \delta_a + N_p p) r + \frac{n_\beta}{y_\beta} p \left(\frac{l_p}{L_r r} - Y_p \right) \end{array} \right] \quad (6.17)$$

6.4 Results

The longitudinal motion's results are presented for a range of angles of attack, elevon angles and canard angles defined as $\alpha = [-10 \text{ to } 30]^\circ$, $\delta_e = [-30 \text{ to } 30]^\circ$, $\delta_c = 0^\circ$, and sideslip angle $\beta = 2^\circ$. For the lateral motion, the roll rate $p = [-10 \text{ to } 10]^\circ/\text{s}$, the yaw rate $r = [-5 \text{ to } 5]^\circ/\text{s}$, the sideslip rate $\beta = [0 \text{ to } 10]^\circ$ and the bank angle $\Phi = [-20 \text{ to } 20]^\circ$.

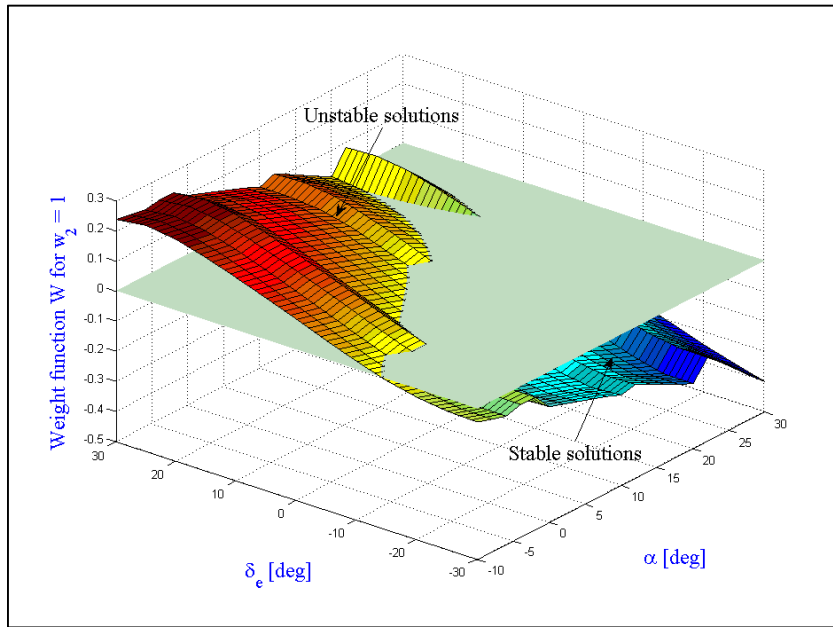
The system defined by eq.(6.1) and (6.2) is linearized about a specific equilibrium point, and the results are presented for longitudinal and lateral motions with and without control laws in Figures 6.5 and 6.8, respectively. In this context, investigations based on the HIRM database and using the WFM have shown the stability and instability fields and the simple stable solutions for the different system configurations.

6.4.1 Longitudinal motion

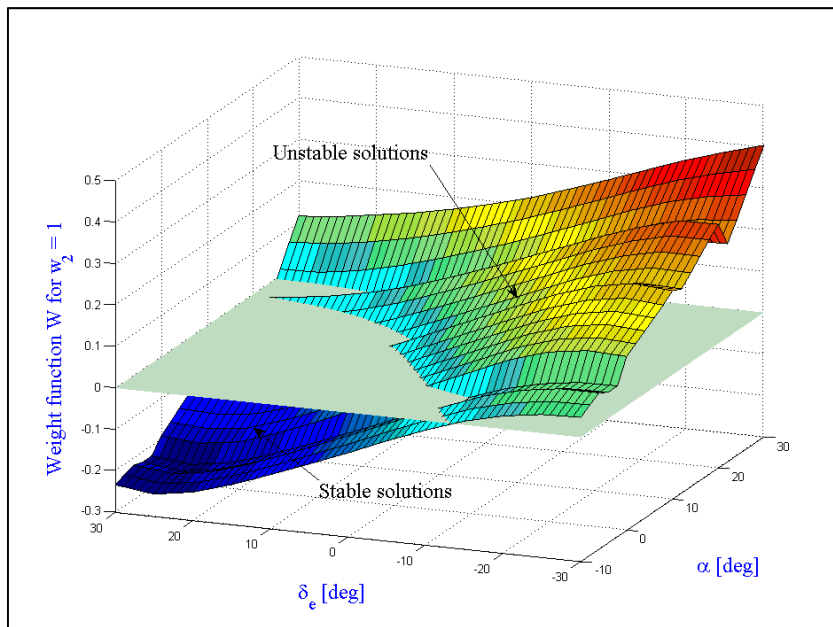
An analysis of the mathematical model was performed, based on the weight function w_{long1} given by eq. (6.6) and with w_{long2} positively defined. The results are for a system with Mach number $M = 0.25$, an altitude of 500 m, a null canard angle, sideslip angle $\beta = 1^\circ$, and for the same variation of angle of attack and elevon deflection as presented for the equilibrium solution.

In this case, based on eq. (6.7), a dependence on the sign of q can be observed. The weight function w_{lon2} is equal to 1, the smallest integer. The variation of the total weight function W versus the angle of attack and elevon deflection are given in Figure 6.2 (a) for negative values, $q = -5^\circ/\text{s}$ and in Figure 6.2 (b) for positive values, $q = 5^\circ/\text{s}$. The sign of q changes

when the stability field is unstable, and vice versa. The aircraft is simple stable for the pairs of angle of attack and elevator angle given in Figure 6.3.



a)



b)

Figure 6.2 Total weight function W for a complete range angle of attack/elevon deflection, with a null canard deflection for longitudinal motion.

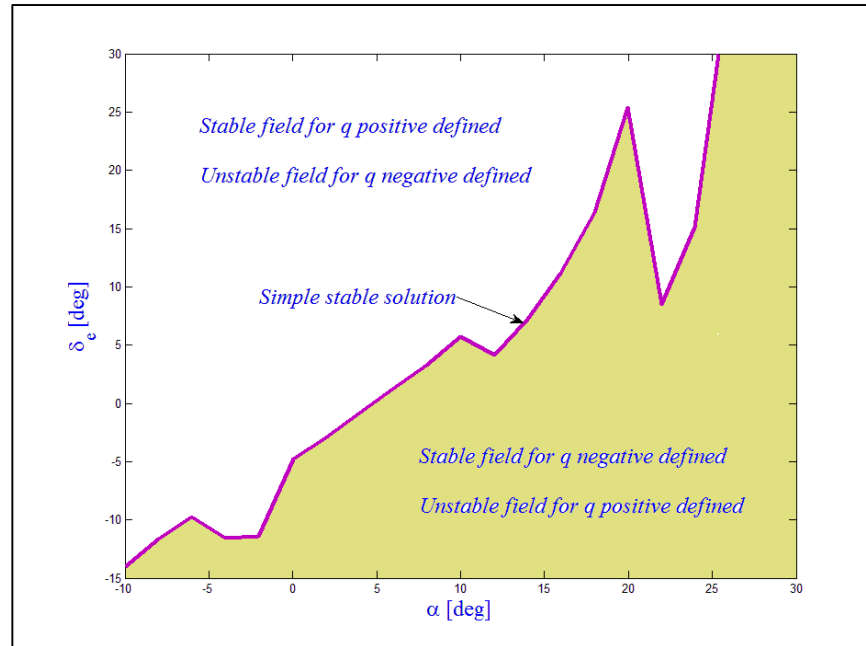


Figure 6.3 Stability/instability fields for longitudinal motion using the Weight Functions Method with $w_2 = 1$

The simple stable solution varies between $(\alpha = -10^0, \delta_e = -14^0)$ and $(\alpha = 25.4^0, \delta_e = 29.93^0)$, as shown in Figure 6.3.

The two equilibrium curves for elevon and canard deflection angles versus angle of attack are shown in Figure 6.4, for an altitude of 500 m and Mach number $M = 0.25$. The symmetrical elevon deflection angle was estimated using eq.(6.18) and (6.19):

$$\delta_e = \frac{\delta_{ei} - \delta_{ey}}{2}, \quad \begin{cases} \delta_{ei} = \delta_{lie_in} + \delta_{rie_in} \\ \delta_{ey} = \delta_{loe_in} + \delta_{roe_in} \end{cases} \quad (6.18)$$

where :

$$\begin{aligned} \delta_{lie_in} & \text{-- left outboard elevon angle} \\ \delta_{rie_in} & \text{-- right outboard elevon angle} \\ \delta_{loe_in} & \text{-- left inboard elevon angle} \\ \delta_{roe_in} & \text{-- right inboard elevon angle} \end{aligned} \quad (6.19)$$

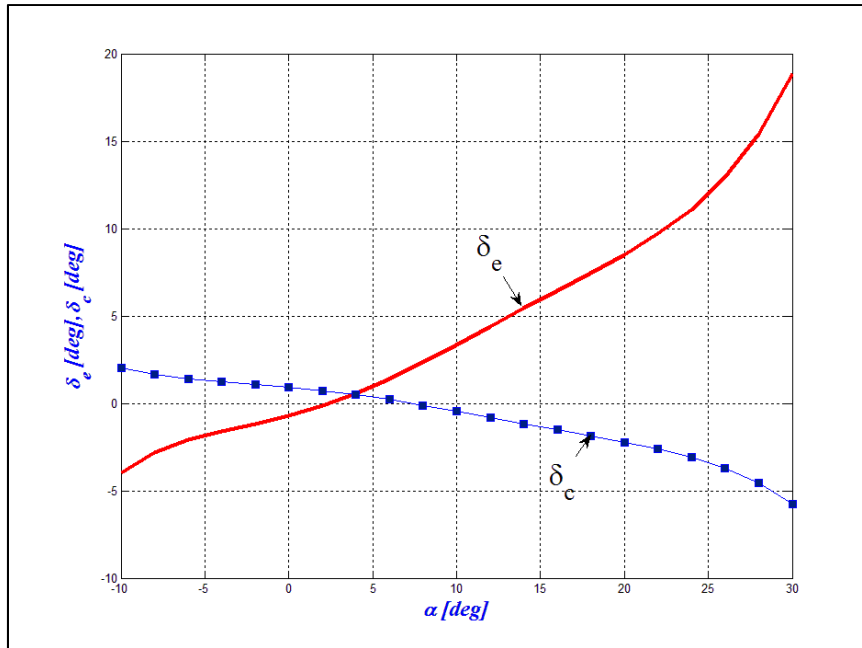


Figure 6.4 Equilibrium curves for elevon and canard deflection angles versus angle of attack

The total weight function variation with α for the longitudinal motion, for $w_{long2} = 1$, is given by eq.(6.7) and is shown in Figure 6.5. The smallest integer 1 was used for w_{long2} , which multiplies a term whose sign is analyzed here (w_1), so that for any higher value of the constant w_{long2} , the variation of W is the same only its value increases. The red curve shows the variation of the total weight function with α in Figure 6.5, where it can be seen that for:

- $\alpha = [-10^0 \div 10.8776^0)$ and $\delta_e = (-4^0 \div 3.585^0)$ the aircraft is *asymptotically stable*;
- $\alpha = 10.8776^0$ and $\delta_e = 3.585^0$ the aircraft is *simple stable*;
- $\alpha = (10.8776^0 \div 30^0]$ and $\delta_e = (3.585^0 \div 19^0)$ the aircraft is *unstable*;

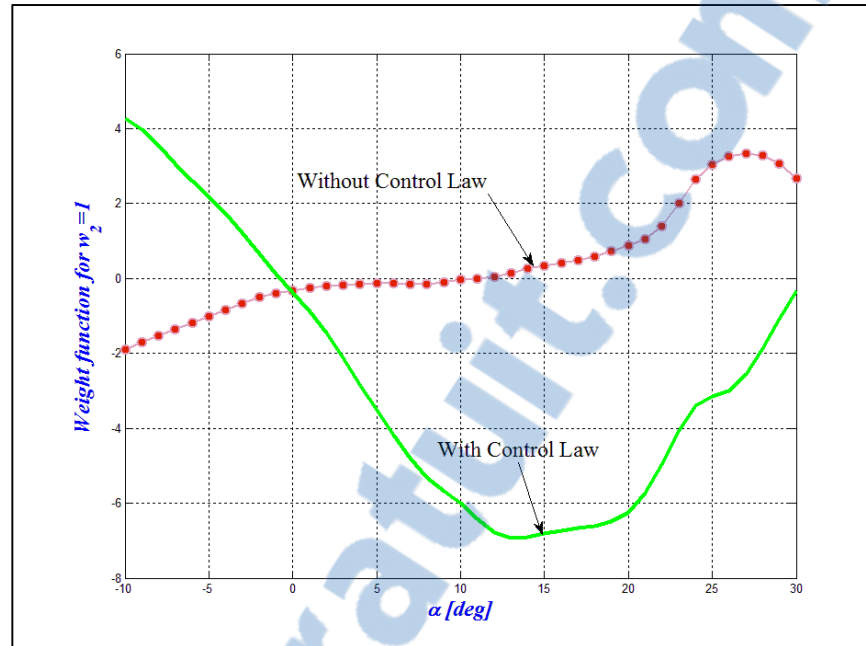


Figure 6.5 Weight function W without/ with a control law at equilibrium for longitudinal motion

To stabilize the model, a control law was used for the longitudinal aircraft motion, given by:

$$\delta_e = \delta_{e0} + k_\alpha \alpha + k_q q \quad (6.20)$$

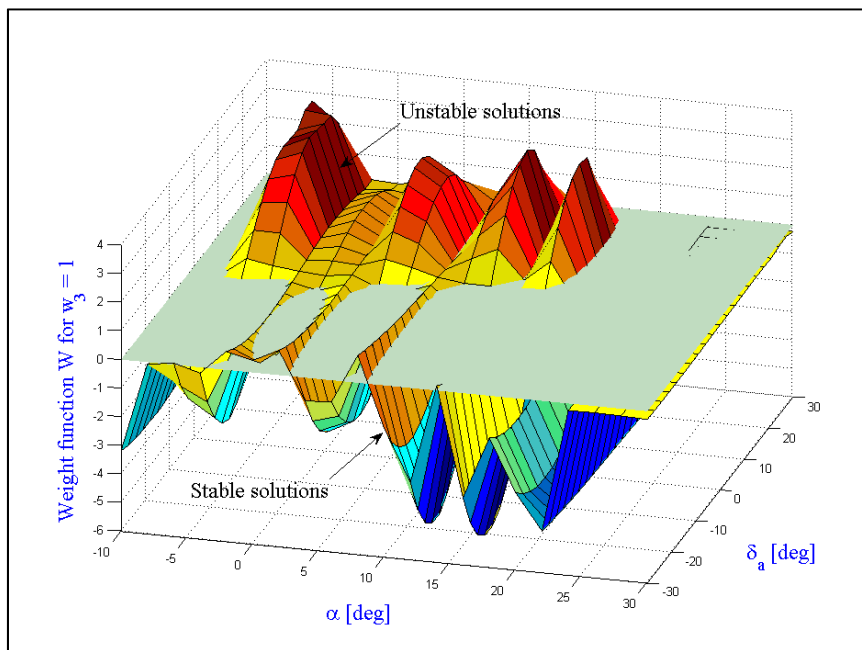
Using this control law with the regulator gains $k_\alpha = 0.4$ and $k_q = 1.284$ (Admirer4p1), the stability field increases, as shown by the total weight function W , represented by the green curve in Figure 6.5. In order to analyze aircraft's stability as function of α and δ_e , the value of δ_e at equilibrium corresponding to the angle of attack α was obtained from Figure 6.4. It was concluded that, with aircraft longitudinal motion, for:

- $\alpha = (-0.64^0 \div 30^0]$ and $\delta_e = (-1.063^0 \div 26^0)$ the aircraft is asymptotically stable;
- $\alpha = -0.64^0$ and $\delta_e = -1.063^0$ the aircraft is simple stable;
- $\alpha = [-10^0 \div -0.64^0]$ and $\delta_e = (-10^0 \div -1.063^0)$ the aircraft is unstable.

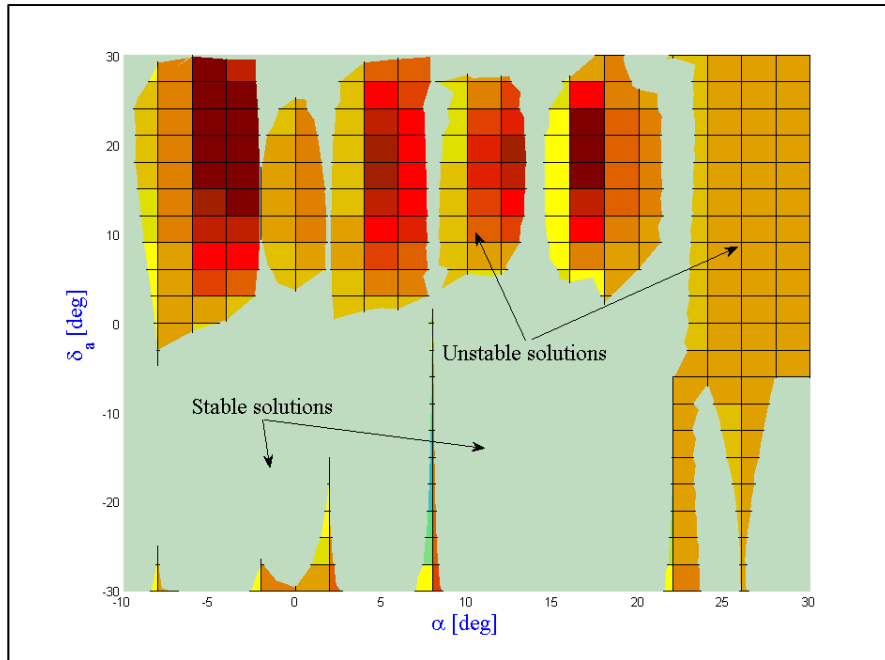
6.4.2 Lateral motion

Based on the weight functions w_{lat1} , w_{lat2} and w_{lat4} given in eq.(6.12), (6.14), (6.16) and with w_{lat3} positively defined by the authors, results are presented for a Mach number $M = 0.25$, altitude $H = 500$ m, sideslip angle $\beta = 2^\circ$, roll rate $p = [-10 \text{ to } 10]^0/\text{s}$, yaw rate $r = [-5 \text{ to } 5]^0/\text{s}$, bank angle $\Phi = [-20 \text{ to } 20]^0$, and the same variation of angle of attack and elevon deflection presented for longitudinal motion in this paper. The sign of eq.(6.17) depends on the signs of p , r and ϕ .

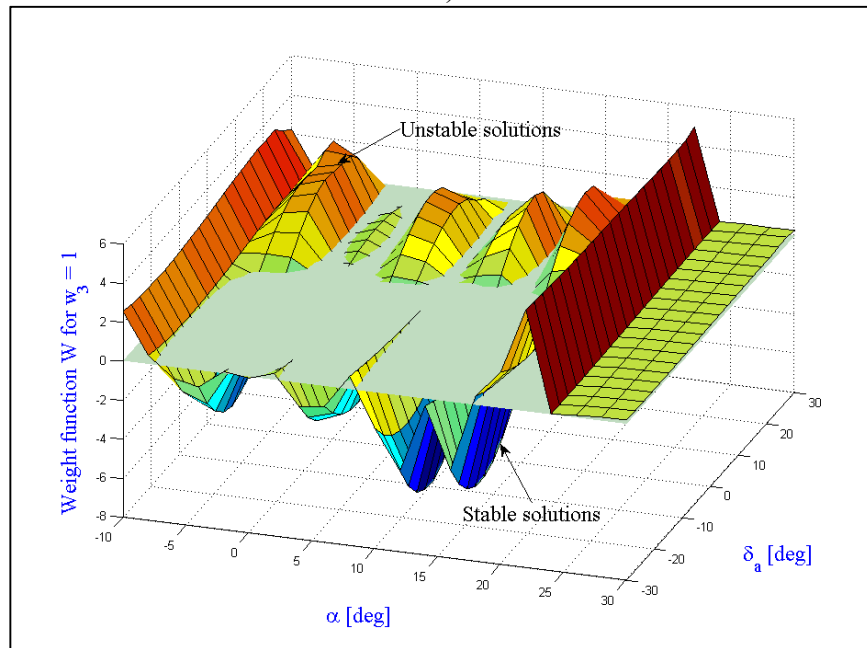
The weight function w_{lat3} has the same value as that of the longitudinal motion, the smallest integer equal to 1, and the variations of the total weight function W versus angle of attack and elevon deflection are given in Figure 6.6 ((a) for negative value $p = -10^0/\text{s}$, $r = -5^0/\text{s}$, $\Phi = -20^0$, (b) for null values $p = 0^0/\text{s}$, $r = 0^0/\text{s}$, $\Phi = 0^0$ and (c) for positive values $p = 10^0/\text{s}$, $r = 5^0/\text{s}$, $\Phi = 20^0$). Figure 6.6 (b) is a section with the plane, i.e. $W = 0$.



a)



b)



c)

Figure 6.6 Total weight function W for a complete range of angle of attack/elevon deflection, for lateral motion

It is not easy to detail all the stability/instability fields concerning the lateral motion. Figure 6.6 (a), (b) and (c) shows the variation of the weight function with angle of attack and elevon/rudder deflection.

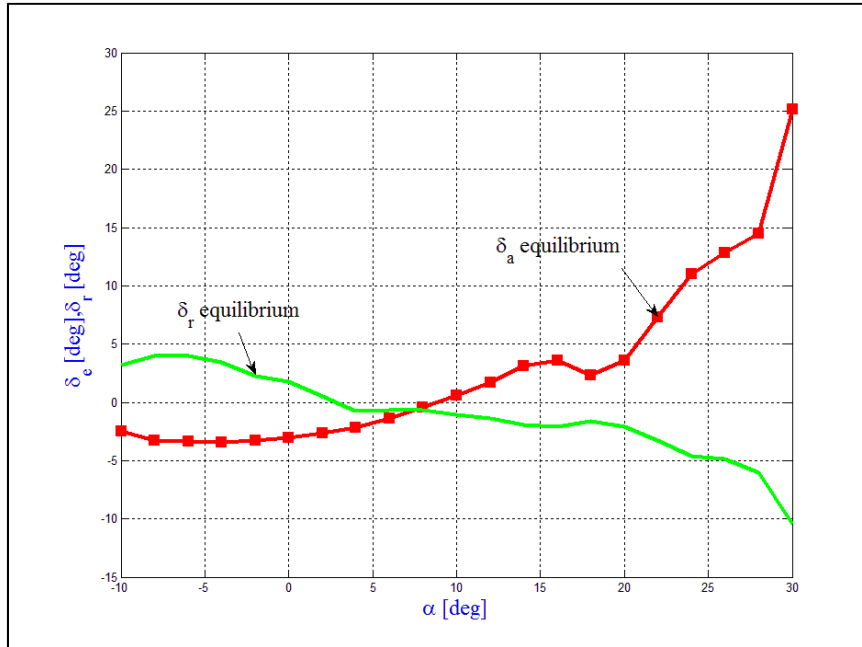


Figure 6.7 Equilibrium curves for elevon and rudder deflection angles versus angle of attack

The two equilibrium curves for elevon and rudder deflection angles versus angle of attack are shown in Figure 6.7. The asymmetrical elevon deflection angle was estimated based on the notations used in eq.(6.19):

$$\delta_a = \frac{\delta_{ai} - \delta_{ay}}{2}, \quad \begin{cases} \delta_{ai} = \delta_{lei_in} - \delta_{rei_in} \\ \delta_{ay} = \delta_{loe_in} - \delta_{roe_in} \end{cases} \quad (6.21)$$

The total lateral weight function is given by eq.(6.17), in which $w_{lat3} = 1$, and is plotted in Figure 6.8 where the red curve represents the solution without a control law, and the stability and instability fields are the following for various values of α and δ_a :

- the aircraft is asymptotically stable for
 - $\alpha = [-10^0 \div -8.046^0]$ and $\delta_a = (-2.55^0 \div -3.272^0)$;
 - $\alpha = (4.996^0 \div 8.362^0)$ and $\delta_a = (-1.754^0 \div -0.244^0)$;

- $\alpha = (12.29^0 \div 19.389^0)$ and $\delta_a = (1.924^0 \div 3.201^0)$;
- $\alpha = (22.97^0 \div 30^0)$ and $\delta_a = (9.07^0 \div 25.15^0)$;
- the aircraft is simple stable for:
 - $\alpha = -8.046^0$ and $\delta_a = -3.272^0$;
 - $\alpha = 4.996^0$ and $\delta_a = -1.754^0$ / $\alpha = 8.362^0$ and $\delta_a = -0.244^0$;
 - $\alpha = 12.29^0$ and $\delta_a = 1.924^0$ / $\alpha = 19.389$ and $\delta_a = 3.201^0$;
 - $\alpha = 22.97^0$ and $\delta_a = 9.07^0$;
- the aircraft is unstable for:
 - $\alpha = (-8.046^0 \div 4.996^0)$ and $\delta_a = (-3.272^0 \div -1.754^0)$;
 - $\alpha = (8.362^0 \div 12.29^0)$ and $\delta_a = (-0.244^0 \div 1.924^0)$;
 - $\alpha = (19.389^0 \div 22.97)$ and $\delta_a = (3.201^0 \div 9.07^0)$;

A control law was used to stabilize the model, given by:

$$\begin{aligned}\delta_a &= \delta_{a0} + k_p p + k_\phi \phi \\ \delta_r &= \delta_{r0} + k_\beta \beta + k_{\dot{\beta}} \dot{\beta}\end{aligned}\tag{6.22}$$

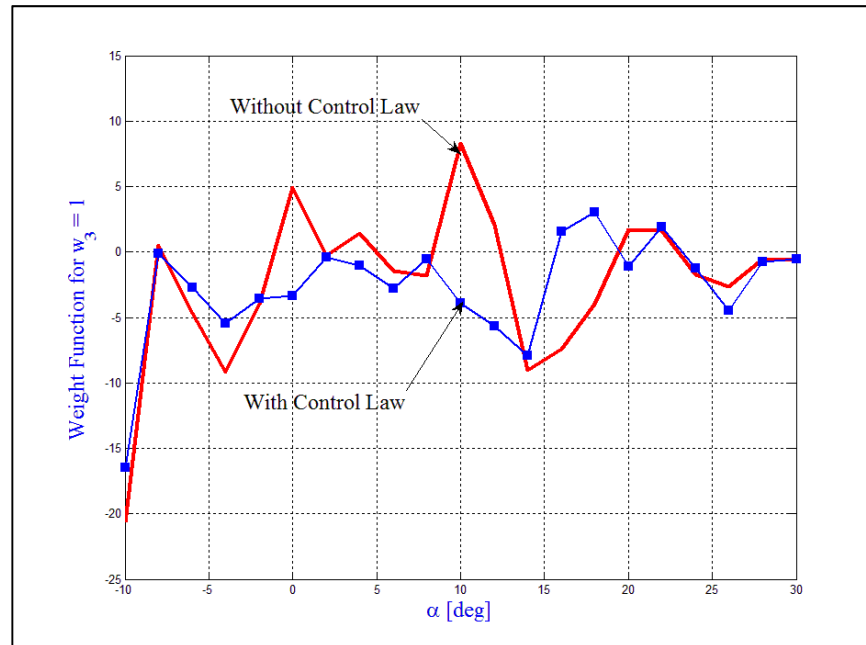


Figure 6.8 Weight function W with and without a control law at equilibrium for lateral motion

This control law was used with the regulator gains given as $k_p = 0.52106$, $k_\phi = -0.27704$, $k_\beta = 7.6727$, and $k_{\beta\dot{\sigma}} = -4.9301$ (Admirer4p1); the field of stability increases for the range of angles of attack from -10 to 15.67 degrees (see the blue curve in Figure 5.8), as shown next for different values of α and δ_a :

- *asymptotically stable* for:
 - $\alpha = (-10^0 \div 15.67^0)$ and $\delta_a = (-2.551^0 \div 3.47^0)$
 - $\alpha = (19.45^0 \div 20.73^0)$ and $\delta_a = (3.186^0 \div 4.894^0)$
 - $\alpha = (23.21^0 \div 30^0)$ and $\delta_a = (9.712^0 \div 25.15^0)$;
- *simple stable* for:
 - $\alpha = 15.67^0$ and $\delta_a = 3.47^0$;
 - $\alpha = 19.45^0$ and $\delta_a = 3.186^0$;
 - $\alpha = 20.73^0$ and $\delta_a = 4.894^0$;
 - $\alpha = 23.31^0$ and $\delta_a = 9.712^0$;
- *unstable* for:
 - $\alpha = (15.67^0 \div 19.45^0)$ and $\delta_a = (3.47^0 \div 3.186^0)$;
 - $\alpha = (20.73^0 \div 23.21^0)$ and $\delta_a = (4.894^0 \div 9.712^0)$.

6.5 Conclusions

The maneuverability of an aircraft is determined by its ability to change its attitude and speed about three axes (longitudinal, lateral and vertical). The main aim of this paper was to determine the positive weight functions by using the Weight Functions Method to analyze the stability/instability fields of an HIRM model and to stabilize this model using control laws.

For the autonomous system of differential equations used in this paper, the WFM gives the stability and instability fields. Based on the analysis presented above for the nonlinear model, the oscillatory behavior was observed for the lateral motion, equivalent to an unstable one, and for longitudinal motion it could be seen that the sign of q changes the stability field to unstable and vice versa.

The HIRM is an unstable model and the control law introduced for each motion, longitudinal and lateral, was used to stabilize its flight in the range of $\alpha = (-0.64^0 \div 30^0]$ and $\delta_e = (-1.063^0 \div 26^0)$ for longitudinal motion, and $\alpha = (-10^0 \div 15.67^0)$ and $\delta_a = (-2.551^0 \div 3.47^0)$ for lateral motion.

GENERAL CONCLUSION

In this thesis, a new code FDerivatives was used to determine the aerodynamic coefficients and their derivatives. Utilizing those derivatives, a new method, called the Weight Functions Method, was applied for stability analysis of three aircrafts. In addition, a continuity algorithm was used to define the minimum airspeed of flight envelope. The main contribution of this thesis consisted on the application of these approaches to define a new stability analysis design tool, a lower cost paid to defined the stability fields for an aircraft versus a CFD method.

Based on the DATCOM method and using the geometrical parameters of two real aircraft as input, a new code called FDerivatives was developed at the LARCASE laboratory. FDerivatives is an in-house code developed for the subsonic regime for classical Wing-Body-Tail configurations and applied on the Hawker 800XP aircraft and a delta-wing configuration, tested on X-31 aircraft. The work developed and validated for the X-31 was part of a major project funded by NATO in the framework of NATO RTO AVT-161 « Assessment of Stability and Control Prediction Methods for NATO Air and Sea Vehicles », This project was awarded with the « RTO Scientific Achievement Award 2012 », that is the most prestigious award given to NATO's AVT-161 research team .

Compared to the applicability limits of the Digital DATCOM, the FDerivatives code adds several enhancements by taking into account a smaller number of the geometrical parameters of an airplane, with the fuselage modeled as a body of revolution and using the real airfoil coordinates. In the new code, the calculation possibilities have been extended to wings with variable airfoils along the span and with negative sweepback. Different approaches to calculate the drag and pitching moment must still refine the results for the drag coefficient and to significantly improve those of the coefficient of pitching moment. Presagis gave the « Best Simulation Award » to the LARCASE laboratory for FDerivatives and data FLSIM applications.

The results for both aircraft are presented in Chapter 2 and in Chapter 3, validated with flight test data provided by CAE Inc. for Hawker 800XP business aircraft and with the experimental data provided in the Low-Speed Wind Tunnel of the German-Dutch Wind Tunnels (DNW-NWB) for the X-31 model.

Proper geometric modelling is essential to correctly obtain aerodynamic coefficients and their derivatives. Pitching moment coefficient analysis demonstrated how a correct approximation of an aircraft's geometry can be obtained. Lift, drag and pitching moment coefficients, for angles of attack between -2 and 20 degrees, were calculated with very good accuracy by the FDerivatives code. In addition, rolling and yawing moment coefficients and side force coefficients were well-estimated.

The weight functions method (WFM) was chosen as the means to study the airplane's stability for longitudinal and lateral motions. This new method determines a number of weight functions that are equal to the number of first-order differential equations. The WFM was selected because this thesis serves as a summary of the code(s) and methods needed to perform a complete aircraft analysis at the design phase, based only on its geometrical parameters. A stability analysis based on the null solutions stability studies for differential equation systems was presented in Chapters 4, 5 and 6. The main aim was to find the positive weight functions in order to analyze aircraft stability, considering the negative sign of the total weight function. Hawker 800XP and X-31 aircraft were determined to be stable for the configurations considered. The weight functions method was validated with the root locus method.

A third model was analyzed to validate the new method and the continuity algorithm. The High Incidence Research Aircraft Model (HIRM) developed by the Swedish Defense Research Agency and implemented in Aero-Data Model In Research Environment (ADMIRE) code was chosen because it is known to be an instable model. Its stability and instability fields have been determined, as well as an equilibrium configuration for

longitudinal and lateral motions. Control laws, introduced in Chapter 5, were utilized to stabilize the aircraft and to determine the new stability fields.

These fields are for:

- angle of attack $\alpha = (-0.64^{\circ} \div 30^{\circ})$ and elevon angle $\delta_e = (-1.063^{\circ} \div 26^{\circ})$ for longitudinal motion; and
- angle of attack $\alpha = (-10^{\circ} \div 15.67^{\circ})$ and aileron angle $\delta_a = (-2.551^{\circ} \div 3.47^{\circ})$ for lateral motion.

The continuity algorithm was presented in Section 0.6. This method was used to define the new minimum airspeeds of the flight envelope for the HIRM model stabilized with a control laws and validated with numerical results. The initial conditions were calculated for three Mach number/Altitude pairs: $(M = 0.22, H = 20\text{m})$, $(M = 0.22, H = 3000\text{m})$ and $(M = 0.55, H = 6000\text{m})$. For smaller Mach numbers and altitudes less than or equal to 3000 m we have improved the flight envelope, up to Mach number $M = 0.182$. For altitudes values situated between 3000 m and 6000 m the flight envelope the improvement was considerable.

The most important steps of this thesis are found in the journal publications as follows:

- The development and use of a new code, FDerivatives, to estimate aerodynamic coefficients and their derivatives, based on the geometrical parameters presented in the first two papers;
- The identification and use of the weight functions method for the longitudinal and lateral stability of three real aircraft in the third, fourth and fifth papers;
- The continuity algorithm presented in section 0.6.

RECOMMANDATIONS

The research presented in this thesis could be improved in many ways or be used as a starting point to undertake many other research projects:

1. Complete the FDerivatives code with the stability derivatives related to control surfaces;
2. The weight functions defined for a typical aircraft configuration could be further generalized by use of new similar configurations. The Weigh Function Method was never used for aircrafts stability and for this reason a general model can be useful. It would be suitable to keep or modify and validate this method with the aim of model generalization;
3. Define a new code to implement all methods and the code FDerivatives presented in this thesis into a single code, based only on the geometrical parameters of an aircraft, completed by the airfoils coordinates.

APPENDIX A: GEOMETRICAL PARAMETERS OF THE AIRCRAFT

PRESENTED IN REFERENCE NACA-TN-4077

<i>Fuselage</i>	
Length, [ft]	3.750
Finesse ratio	7.50
Mounting point, distance measured from nose of fuselage parallel to the fuselage reference line, [ft]	2.125
Diameter at $c/4$ of tail group, [ft]	0.170
<i>Vertical tail</i>	
Aspect ratio	1.4
Sweep angle of quarter-chord line, [deg]	45
Taper ratio	0.6
Span, [ft]	0.688
Root chord, [ft]	0.614
Tip chord, [ft]	0.368
Mean aerodynamic chord, c_V , [ft]	0.502
x_V , [ft]	0.468
z_V , [ft]	0.315
Area ratio, S_V / S_W	0.15
NACA airfoil section in planes parallel to the fuselage centre line	65 _A 008
<i>Horizontal tail</i>	
Aspect ratio	2.77
Sweep angle of quarter-chord line, [deg]	45
Taper ratio	0.60
Span, [ft]	1.117
Root Chord, [ft]	0.504
Tip chord, [ft]	0.303
Mean aerodynamic chord, c_H , [ft]	0.412

x_H , [ft]	0.382
y_H , [ft]	0.256
Area ratio S_H/S_W	0.20
NACA airfoil section in planes parallel to the plane of symmetry	65 _A 008
<i>Wings</i>	
Aspect ratio	4
Sweep angle of quarter chord line, [deg]	45
Taper ratio	0.60
Span, [ft]	3.000
Area	2.250
Root chord, [ft]	0.938
Tip chord, [ft]	0.563
Mean aerodynamic chord, c_W , [ft]	0.766
x_W , [ft]	0.922
y_W , [ft]	0.688
Dihedral angle, [deg]	0
Twist, [deg]	0
NACA airfoil section in planes parallel to the plane of symmetry	65 _A 008

APPENDIX B: LONGITUDINAL AND LATERAL AERODYNAMIC DERIVATIVES

The non-dimensional aerodynamic derivatives for conventional aircraft are next presented, divided into two groups, longitudinal and lateral (Schmidt, 1998).

There are three categories of derivatives: static, dynamic and control.

- Static derivatives include all those derivatives concerned with the angle of attack α and the sideslip angle β ; they give the force and moment variations with respect to changes in the aircraft position.
- Dynamic derivatives include the force and moment derivatives, with respect to time, of the change of angle of attack α , of sideslip angle β and of roll rate p , pitch rate q and yaw rate r .
- Control derivatives result from the control actuation.

B.1 Longitudinal parameters

Short-period derivatives

Heavy damping lift curve slope

$$Z_w = \frac{Z_\alpha}{V} = -\frac{\rho S}{mV} (C_D + C_{L\alpha})$$

Longitudinal static stability

$$M_\alpha = \frac{\rho S \bar{c}}{I_y} C_{m\alpha}$$

Pitch damping /pitching moment due to pitch rate

$$M_q = \frac{\rho S \bar{c}}{I_y} \frac{\bar{c}}{2V} C_{mq}$$

Pitching moment due to angle of attack rate

$$M_{\dot{\alpha}} = \frac{\rho S \bar{c}}{I_y} \frac{\bar{c}}{2V} C_{m\dot{\alpha}}$$

Phugoid derivatives

Phugoid damping parameters

$$X_u = -\frac{\partial \mathcal{S}}{mV} 2C_D$$

Vertical speed stiffness parameters

$$Z_u = -\frac{\partial \mathcal{S}}{mV} 2C_L$$

B.2 Lateral directional derivatives

Roll mode derivatives

Roll damping

$$L_p = \frac{\partial \mathcal{S} b}{I_x} \left(\frac{b}{2V} \right) C_{lp}$$

Lateral control effectiveness

$$L_{\delta a} = \frac{\partial \mathcal{S} b}{I_x} C_{l\delta a}$$

Dutch roll derivatives

The weathercock

$$N_v = \frac{N_\beta}{V} = \frac{\partial \mathcal{S} b}{VI_z} C_{n\beta}$$

Yaw damping

$$N_r = \frac{\partial \mathcal{S} b}{I_z} \left(\frac{b}{2V} \right) C_{nr}$$

Side force due to velocity

$$Y_v = \frac{\partial \mathcal{S}}{m} C_{y\beta}$$

The directional control

$$N_{\delta r} = \frac{\partial \mathcal{S} b}{I_z} C_{n\delta r}$$

Lateral-directional cross derivatives

Dihedral effect

$$L_v = \frac{L_\beta}{V} = \frac{\partial \delta b}{V I_x} C_{l\beta}$$

Rolling due to yawing

$$L_r = \frac{\partial \delta b}{I_x} \left(\frac{b}{2V} \right) C_{lr}$$

Yawing due to rolling

$$N_p = \frac{\partial \delta b}{I_z} \left(\frac{b}{2V} \right) C_{np}$$

BIBLIOGRAPHY

- Abbot, Ira H. and A.E. von Doenhoff. 1959. *Theory of wing sections, Including a Summary of Airfoil Data*, New York: Dover Publication Inc.
- Admirer4p1. Online < [http://www.foi.se/en/Our-Knowledge/Aeronautics Admirer/Downloads](http://www.foi.se/en/Our-Knowledge/Aeronautics%20Admirer/Downloads) >. Verified March, 29 2013.
- Advanced Aircraft Analysis 3.3 code. Online < <http://www.darcorp.com/Software/AAA/> >. Verified April, 04 2013.
- Alley, N.R., Phillips, W.F. and Spall, R.E. 2007. « Predicting Maximum Lift Coefficient for Twisted Wings Using Computational Fluid Dynamics ». *Journal of Aircraft*, Vo.44, No 3.
- Anscombe, A. and Raney, D.J. 1950. *Low-speed tunnel investigation of the effect of the body on C_{m0} and aerodynamic centre of unswept wing-body combinations*. (ARC)/CP-16, Aeronautical Research Council.
- Anton, Nicoleta. 2005. « Analiza miscarii longitudinale a unui avion de mare manevrabilitate prin metoda bifurcatie ». "AEROSPACE 2005" Conference, October 11–12, Bucharest.
- Anton, Nicoleta, Botez, Ruxandra Mihaela and Popescu, Dumitru. 2011. « Stability derivatives for X-31 delta-wing aircraft validated using wind tunnel test data ». *Proceeding of the Institution of Mechanical Engineers*, Vol. 225, Part G, *Journal of Aerospace Engineering*, pp 403-416.
- Anton, Nicoleta, Botez, Ruxandra Mihaela and Popescu, Dumitru. 2010. « New methodology and code for Hawker 800XP aircraft stability derivatives calculations from geometrical data ». *The Aeronautical Journal*, Vol. 114, No. 1156, Paper No. 3454.
- Anton, Nicoleta, Botez, Ruxandra Mihaela and Popescu, Dumitru. August 10-13, 2009. « New methodologies for aircraft stability derivatives determination from its geometrical data ». *AIAA Atmospheric Flight Mechanics Conference*. AIAA 2009-6064, Chicago, Illinois.
- Babcock, D.A. and A.S. Arena Jr., 2004. « Estimating Aircraft Stability Derivatives through Finite Element Analysis ». *AIAA 2004-5174*.
- Bihrlé, W. 1965. *A Handling Qualities Theory for Precise Flight Path Control*, Tech. Rep. AFFDL-TR-65-195, AFRL, Wright Patterson AFB, OH.

Blake, William B. and Etan D. Karni. June, 2005. « A Cambered Body Method for Missile DATCOM ». *23rd AIAA Applied Aerodynamics Conference*, Toronto, Ontario Canada. p. 11.

Boelens, O.J. June 22 – 25, 2009. « CFD Analysis of the Flow around the X-31 Aircraft at High Angle of Attack ». *27th AIAA Applied Aerodynamics Conference. AIAA 2009–3628–968*, San Antonio, Texas.

Botez, Ruxandra. 2004. *Notes de cours GPA740: Système informatique embarqués*, École de Technologie Supérieure, Montréal.

Bryson, A.E. Jr. 1953. « Stability Derivatives for a Slender Missile with Application to a Wing Body Vertical Tail Configuration ». *Journal of the Aeronautical Sciences*, Vol. 20, No. 5.

Champigny, P. and P. Denis. 2004. *The ONERA aero prediction code « MISSILE »*, ONERA–TP–04–112, France.

Chang Byeong-Hee, Cho Sang-Oh, Cho Tae-Hwan. January 2004. « Development of dynamic stability derivatives of an airplane from static wind tunnel tests ». *AIAA 2004–1142*.

Christoffer M. Cotting, 2010. « Evolution of flying qualities analysis: Problems for the new generation of aircraft ». PhD Thesis, Faculty of the Virginia Polytechnic Institute and State University, Blacksburg, Virginia.

Cobleigh, B.R. 1994. « High-Angle-of-Attack Yawing Moment Asymmetry of the X-31 Aircraft from Flight Test ». *AIAA 94–1803–735*.

Croom, M.A., Fratello, D.J. and Whipple, R.D. 1993. « Dynamic Model Testing of the X-31 Configuration For High-Angle-of-Attack Flight Dynamics Research ». *AIAA–93–3674–CP*.

Cooper, G.E. and Harper, R.P. April 1969. *The Use of Pilot Rating in the Evaluation of Aircraft Handling Qualities*. NASA TN D5153.

DARcorporation. online < <http://www.darcorp.com> >, Verified April, 04 2013.

Davidenko, F. 1953. *On a New Method of Numerical Solution of Systems of Nonlinear Equations*. (in Russian), Dokl. Akad. Nauk SSSR 88, 601-602.

Digital DATCOM, online < <http://www.pdas.com/datcom.htm> >, Verified April, 04 2013.

Etkin, Bernard and Lloyd D. Reid. 1996. *Dynamics of Flight, Stability and Control (3rd edition)*, Third Edition, John Wiley & Sons. Chapter 2, p. 25.

- Fett, T. 1991. « An analysis of the three-point bending bar by use of the weight function method ». *Engineering Fracture Mechanics*, Vol. 40, Issue 3, pp. 683-686.
- Finck, R.D. et al. April 1978, updated December 1999. *The USAF Stability and Control DATCOM (Data Compendium)*, AFWAL-TR-79-3032. Air Force Wright Aeronautical Laboratories, 3200 p.
- Fitzgibbon, A., Pilu, M. and Fisher, R. 1996. « Direct least-square fitting of ellipses ». International Conference on Pattern Recognition, Vienna, august 1996.
- Galbraith, Bill. *DATCOM+ Pro version 3.0*. Online < <http://www.holycows.net/datcom/> >. Verified April, 04 2013.
- GARTEUR FM(AG12), 2001. *PIO Analysis of a Highly Augmented Aircraft*, GARTEUR/TP-120-07.
- Grasmeyer, Joel. 1998. « Stability and Control derivative Estimation and Engine-Out Analysis ». Ph.D. Thesis. Faculty of the Virginia Polytechnic Institute, *VPI-AOE-254*.
- Green, L.L. and Spence, A.M. 2004. « Applications of computational methods for dynamic stability and control derivatives ». *AIAA 2004-0377*.
- Hacker T. 1992. *Studii privind bazele teoretice ale dinamicii zborului: stabilitate, comandă, optimizare, robustețe*, (in Romanian) Contract 711/IS.
- Hahn, H. and Herz, B. 1981. *Higher Order Root-Locus Technique with Applications in Control System Design*, International Publishers Service, Incorporate.
- Hallíř, R. and Flusser, J. 1998. « Numerically Stable Direct Least Squares Fitting of Ellipses ». *Proceedings of the 6th International Conference in Central Europe on Computer Graphics and Visualization*. Plzen, Czech Republic.
- Henne, U., Höhler, G., Klein, Chr., Rein, M., Sachs, W. and Schütte, A. 23.09.2005. *Steady state pressure measurements using PSP – « Pressure Sensitive Paint » and PSI pressure tubes, as well as forces and moments measurements of the X-31 configuration in the low speed wind tunnel Braunschweig DNW-NWB*. DLR IB_224-2005_A16, DLR.
- Hodgkinson, J. 1999. *Aircraft Handling Qualities*, AIAA Education Series.
- Hoffman, J.D. 2001. *Numerical methods for engineers and scientists*, Second Edition .
- Jiankun, H., Bohn, C., and Wu, H.R. 200. « Systematic H_∞ weighting function selection and its application to the real-time control of a vertical take-off aircraft ». *Control Engineering Practice*, Vol. 8, pp. 241-252.

- Jorgensen, L.H. 1978. *Prediction of Aerodynamic Characteristics for Slender Bodies Alone and Width Lifting Surfaces to High Angles of Attack*. AGARD–CP–247.
- Kim, J.H., and Lee, S.B. 2000. « Calculation of stress intensity factor using weight function method for a patched crack with debonding region ». *Engineering Fracture Mechanics*, Vol. 67, pp. 303–310.
- Lan, C.E. and Roskam, Jan. 1981. *Airplane aerodynamics and performance*, Roskam Aviation and Engineering Corporation, Ottawa, Kansas.
- Lars, F. Ulrik, N. 2005. *ADMIRE The Aero-Data Model In a Research Environment Version 4.0, Model Description*. FOI-R-1624-SE, ISSN-1650-1942.
- Letko, William and Donald R. Riley. August, 1950. *Effect of an unswept wing on the contribution of unswept-tail configurations to the low-speed static- and rolling-stability derivatives of a midwing airplane model*. NACA TN 2175, Washington, pp 25–26.
- Limache, A.C. 2000. « Aerodynamic Modeling Using Computational Fluid Dynamics and Sensitivity Equations ». Faculty of the Virginia Polytechnic Institute.
- MacMillin, P.E., Golovidov, O.B., Mason, W.H., Grossman, B. and Haftka, R.T. 1996. *Trim, Control, and Performance Effects in Variable-Complexity High-Speed Civil Transport Design*. MAD 96-07-01.
- Multhopp, H. December 1942. *Aerodynamics of the Fuselage*. NACA–TM–1036. Washington. 47 p.
- Murman, S.M. 2005. *A Reduced–Frequency Approach for Calculating Dynamic Derivatives*. AIAA 2005–0840.
- Nakamura, Y., Muramatsu, E., Okubo, H. and Tokutake, H. 2002. *Adaptive Estimation of Stability Derivatives via Multiple Observers*. TEA18–2.
- Nelly, Robert H. and Thomas V. Bollech. May, 1947. *Experimental and calculated characteristics of several NACA 44–series wings with aspect ratios of 8, 10, and 12 and taper ratios of 2.5 and 3.5*. NACA–TN–1270, Washington.
- Olson, L. 2006. « Lecture 8 Gaussian Elimination with Pivoting ». Online < <http://www.cs.uiuc.edu/class/fa06/cs257/lecture/lecture08.pdf> >. Verified April, 04 2013.
- Paris, P.C, McMeeking, R.M and Tada, H. 1976. « The Weight Function Method for Determining Stress Intensity factors ». *Cracks and Fracture - Proceedings of the Ninth national Symposium on Fracture Mechanics*, 76–1712, pp. 471–489.

- Phillips, W.F. and Alley, N.R. May/June 2007. « Predicting Maximum Lift Coefficient for Twisted Wings Using Lifting-Line Theory ». *AIAA Journal of Aircraft*, Vol. 44, No. 3.
- Phillips, W.F., Fugal, S.R. and Spall, R.E. 2006. « Minimizing Induced Drag with Wing Twist, Computational-Fluid-Dynamics Validation ». *Journal of Aircraft*, Vo.43, No 2.
- Popescu, Dumitru. 2009. « Nouvelle implémentation de la procédure DATCOM pour le calcul des coefficients aérodynamiques et des dérivées de stabilité dans le domaine subsonique de vol ». Thesis M. Eng., Montréal, École de Technologie Supérieure.
- Rao, S.S. 1996. *Engineering Optimization: Theory and Practice*, 3rd Edition, New York.
- Rein, M., Höhler, G., Schütte, A., Bergmann, A. and Löser, T. January/February 2008. « Ground-Based Simulation of Complex Manoeuvres of a Delta-Wing Aircraft ». *Journal of Aircraft*, Vol. 45, No. 1.
- Rice, J.R. 1972. « *International Journal of Solids and Structures* ». Vol. 8, pp. 751-756.
- Roskam, Jan. 1973. *Methods for Estimating Stability and Control Derivatives for Conventional Subsonic Airplane*, Lawrence, Kansas.
- Roskam, Jan. 1995. *Airplane Flight Dynamics and Automatic Flight Controls*, Lawrence, Kansas: DARcorporation.
- Roskam, Jan. and Lan, C.T.E. 1997. *Airplane Aerodynamics and Performances*, Lawrence, Kansas: DARcorporation.
- Roskam, Jan. 2000. *Airplane design Part VI: Preliminary Calculation of Aerodynamic, Thrust and Power Characteristics*, Lawrence, Kansas: DARcorporation.
- Roskam, Jan. 1973. *Methods for Estimating Stability and Control Derivatives for Standard Subsonic Airplanes*, Lawrence, Kansas.
- RTO Technical Report 61. 2002. *Collaboration for Land, Air, Sea and Space Vehicles: Developing the Common Ground in Vehicle Dynamics, System Identification, Control and Handling Qualities*. RTO-TR-061 AC/323(SCI-053) TP/51, North Atlantic Treaty Organization, Research and Technology Organization.
- Schmidt, L.V. 1998. *Introduction to Aircraft Flight Dynamics*, AIAA Education Series, Reston, Virginia.
- Schneider, G.A. and Danzer, R. 1989. « Calculation of stress intensity factor of an edge crack in a finite elastic disc using the weight function method ». *Engineering Fracture Mechanics*, Vol. 34, Issue 3, pp. 547-552.

- Schütte, A. 2009. *X-31 Integral PSI Steady State Plots*. DLR, Braunschweig, pp 25–121.
- Sivells, James C. and Neely, R.H. April 1947. *Method for calculating wing characteristics by lifting-line theory using nonlinear section lift data*. NACA–TN–1269, Washington.
- Speyer, J.L. and Crues, E.Z. 1987. « On–line Aircraft State and Stability Derivatives Estimation Using the Modified–Gain Extended Kalman Filter ». *Journal of Aircraft*, Vol. 10, No. 3
- Stroe, Ion. 2008. « Weight Functions Method in stability study of vibrations ». *SISOM 2008 and Session of the Commission of Acoustics*, Bucharest 29–30 May, 2008.
- Stroe, Ion., and Parvu, Petrisor. 2008. « Weight Functions Method in Stability Study of Systems ». *PAMM, Proc. Appl. Math. Mech.* 8, 10385 – 10386 (2008) / DOI 10.1002/pamm.200810385.
- Terlouw, J.C. et al. 1996. *Robust flight control design challenge. Problem formulation and manual: The high incidence research model (HIRM)*. GARTEUR/FM/AG-08 TP-088-4.
- Thomas, David F. Jr. and Wolhart, Walter D. 1957. *Static longitudinal and lateral stability characteristics at low speed of 45 degree sweptback-midwing models having wings with an aspect ratio of 2, 4, or 6*, NACA-TN-4077. Langley Research Centre.
- Torenbeek, Egbert. 1976. *Synthesis of subsonic airplane design. An introduction to the preliminary design of subsonic general aviation and transport aircraft, with emphasis on layout, aerodynamic design, propulsion and performance*. Delft, Holland, Delft University Press, 598 p.
- MIL-F-8785C .United States Air Force. 1996. *MIL-F-8785C Notice 2 – Military Specification Flying Qualities of Piloted Airplanes*.
- Vainshtok, V.A. amd Varfolomeyev, I.V. 1987. « Application of the weight function method for determining stress intensity factors of semi-elliptical cracks ». *International journal of Fracture*, Vol. 35, Number 3, pp. 175-186, DOI: 10.1007/BF00015587.
- Vorstab95, Online < <http://archive.nrc-cnrc.gc.ca/eng/programs/iar/parameter-estimation.html> >http://iar-ira.nrc-cnrc.gc.ca/flight/flight_6b_e.html, Verified April, 05 2013
- Yeh, D.T., George, M.W., Clever, W.C., Tam, C.K. and Woan, C.J. June 24–26, 1991. « Numerical Study of the X-31 High Angle-of-Attack Flow Characteristics ». *AIAA 22nd Fluid Dynamics, Plasma Dynamics & Lasers Conference*. AIAA–91–1630, Honolulu, Hawaii.

- Yoichi, S., and Yasumi, K. 2003. « Numerical Weight Function Method for Structural Analysis Formulation for two– dimensional elasticity and plate structures ». *Journal of the Society of Naval Architects of Japan*, ISSN 0514–8499, Vol. No. 193, pp. 33–38.
- Weber, J. June 1955. *The calculation of the pressure distribution on the surface of thick cambered wings and the design of wings with given pressure distribution*. Royal Aircraft Establishment, Report No. AERO 2548.
- Wilde, J. August 26, 2011. « Linear Algebra II: Quadratic Forms and Definiteness ». Online < http://www.econ.brown.edu/students/Takeshi_Suzuki/Math_Camp_2011/LA2-2011.pdf > Verified April, 04 2013.
- Williams, John E. and Vukelich, Steven R. 1979a. *The USAF Stability and Control Digital DATCOM, Volume I. Users Manual, AFFDL-TR-79-3032*, St. Louis, Missouri: McDonnell Douglas Astronautics Company, St. Louis Division, Wright – Patterson Air Force Base, 1979a, 317 p.
- Williams, John E. and Vukelich, Steven R. 1979b. *The USAF Stability and Control Digital DATCOM, Volume II. Implementation of DATCOM Method, AFFDL-TR-79-3032*. 155. St. Louis, Missouri: McDonnell Douglas Astronautics Company, St. Louis Division, Wright - Patterson Air Force Base.
- Williams, D.L.II and Nelson, R.C. January 10–13, 1994. « An investigation of X-31 Roll Characteristics at High Angle-of-Attack Through Subscale Model Testing ». *32nd Aerospace Sciences Meeting & Exhibit. AIAA 94–0806*, Reno, NV.
- Wu, X.R. and Carlsson, J. 1983. « The generalised weight function method for crack problems with mixed boundary conditions ». *Journal of the Mechanics and Physics of solids*, Vol. 31, Issue 6, pp. 485–497.